THE EQUILIBRIA AND KINETICS OF CERTAIN ION EXCHANGE SYSTEMS

by

PAUL CHARLES KENNET

Submitted to the University of Cape Town in fulfilment of the requirements for the degree of Master of Science in Engineering

July 1980

ABSTRACT

Fresh water is becoming increasingly scarce in the modern technological world, and thus alternative sources of potable water must be found. One possible source of water of relatively low total dissolved salt content is municipal effluent. This has been successfully desalinated using continuous countercurrent ion exchange systems, the design and structure of which depend largely on the resin types used, and in particular on their equilibrium and kinetic properties. In recent years new and improved resins, such as macroporous and high density resins, have come onto the market, and the vital properties of these have not been well investigated.

With this in mind, the H^+, Na^+ and Ca^{2+} equilibria and kinetics of both a gel type strong acid cation resin (Cation Fort) and a macroporous strong acid cation resin (Zerolit 625) were investigated and compared, as well as the Cl^-, SO_4^{2-} and artificial COD kinetics of a macroporous normal density weak base anion resin (Zerolit MPH) and a high density macroporous weak base anion resin (Senbrix). The COD kinetic tests were performed using a conductiometric apparatus, while all the inorganic ion studies were performed on a fractional sampling apparatus. The equilibrium isotherms were obtained using batch tests.

The macroporous Zerolit 625 resin displayed greater film-diffusion controlled kinetic properties (even at 0,5ON concentration) than those of the gel resin. Further, the gel resin kinetics were found to be consistently faster than those of the macroporous resin. Both these properties were attributed to the resins' respective pore structure. In general, the counter-ion with the highest charge density (Ca^{2+} in the case of cation studies) loaded faster and stripped slower than the other ions, and this resulted in an "overshoot" of the equilibrium value in the ternary loading systems of both resins, but not in the regeneration systems.

The anion kinetics were found to be film-diffusion

controlled (since they were performed at low concentrations of 0,01N and 0,05N). This resulted in the kinetics being governed not only by the charge density of the counter-ion, but also the resin selectivity. Thus the Cl^- (although having a higher mobility than the SO_4^{2-}) did not always exhibit faster kinetics, since the resin selectivity for SO_4^{2-} is higher than for Cl^-. The larger monocarboxylic acids used as artificial COD material were found to load slower than the smaller acid molecules. The pore size distribution was found to have a marked effect on the COD kinetics because of the hindrance of the smaller pores on the larger organic molecules. Senbrix resin was found to have faster kinetics for organic loading and Cl^- loading at low concentrations, but Zerolit MPH was found to have faster kinetics for SO_4^{2-} loading and Cl^- loading at high concentrations.

For both cation and anion resins the higher the degree of crosslinking the slower the kinetics become.

ACKNOWLEDGEMENTS

The author wishes to express his sincere appreciation and gratitude to Professor A.D. Carr for valuable guidance, advice and encouragement during the course of this work. Also to Professor G.S. Hansford, Dr. T.B.S. Giddey, Mr. B.A. Hendry and Mr. E.W. Randall for their valuable help.

Thanks are also expressed to Mr. E.T. Reyneke for construction and maintenance of the equipment, to Mrs. S. Broekhuysen and Mrs. J. Dold for their help with the laboratory work, and to Miss L.J. Jennings for efficient typing.

The financial assistance of the Sentrachem group is gratefully acknowledged.

Finally, the author wishes to express his most sincere gratitude to his parents for their untiring support and encouragement during his undergraduate studies, and during the course of this work.

TABLE OF CONTENTS

Page

Page

Page

Page

Page

Page

TABLE OF FIGURES

Page

Page

Page

Page

Page

TABLE OF TABLES

Page

NOMENCLATURE

A	=	Amps.
$\mathring{A}$	=	Angström unit (10^{-10} m).
a	=	Area through which exchange occurs.
C	=	Concentration in liquid in equivalents per unit volume.
$\overline{C}$	=	Concentration in resin in equivalents per unit volume or molality.
$C_A(t)$	=	Liquid concentration of ion A at time t after commencement of run.
$D; D_L$	=	Diffusivity coefficient.
D_i	=	Distribution coefficient.
F	=	Capacitance (farads).
F(t)	=	Fractional approach to equilibrium based on liquid concentration.
F'(t)	=	Fractional approach to equilibrium based on resin ionic fraction.
F''(t)	=	Fractional approach to equilibrium based on liquid ionic fraction.
h	=	Planck's constant ($6{,}6262 \times 10^{-34}$ J s^{-1}).
k	=	Mass transfer coefficient.
K	=	Equilibrium constant.
L	=	Equivalents in liquid phase.
M	=	Concentration of solution in molality.
$\overline{M}$	=	Concentration of fixed ionic groups on the resin in equivalents per unit volume.
m	=	Slope of operating line.
N	=	Flux.
Q	=	Concentration in the resin.
r	=	Radius of resin bead.
R	=	Rate of exchange.
R	=	Equivalents in the resin.

R	=	Universal gas constant.
t	=	Time from commencement of run.
$t_{\frac{1}{2}}$	=	Time to reach an F(t) value of 0,5.
T	=	Temperature.
V	=	Volume of solution.
x	=	Ionic fraction in resin.
X	=	Concentration in unit volume of packed bed.
$\overline{X}$	=	Concentration in resin in moles per unit bed volume.
y	=	Ion fraction in liquid.
z	=	Valency.
Z	=	Length parameter.

Greek Symbols

α	=	Separation factor.
δ	=	Film thickness.
ΔG^{o}	=	Standard free energy.
κ	=	Selectivity coefficient.
τ_{max}	=	Time taken to reach the maximum F(t) "overshoot" value.
μ	=	Micro (10^{-6}).
Ω	=	Resistance (Ohms).

Subscripts

o	=	At time zero.
∞	=	At time infinity (equilibrium).
A	=	Of or with reference to counter-ion A.
B	=	Of or with reference to counter-ion B.
i	=	With reference to the total system.
1,2	=	Different sides of a membrane.
L	=	Liquid side.

Superscripts

*	=	At equilibrium.
A	=	With reference to counter-ion A.
B	=	With reference to counter-ion B.

Abbreviations

CCIX	=	Continuous countercurrent ion exchange.
COD	=	Chemical oxygen demand.
DVB	=	Divinylbenzene.
f.s.	=	Free-settled.
IC	=	Integrated circuit.
I.D.	=	Internal diameter.
LED	=	Light emitting diode.
ℓ	=	Litres.
meq	=	Milliequivalents.
mg	=	Milligrams.
ml	=	Millilitres.
MRC	=	Moisture retention capacity.
MW	=	Molecular weight.
N	=	Normality (equivalents per litre).
R/L	=	Stoichiometric ratio.

CHAPTER 1

INTRODUCTION

1.1 BACKGROUND AND USES OF ION EXCHANGE

The phenomenon of ion exchange was first recognised (on naturally occurring clays and zeolites) in 1845 by Thompson and Way in England [1], and since then has been used increasingly in many diverse applications. Its history is well documented in the literature [1,2,3,4,5], but it is the present-day uses of this versatile process that is of interest and relevance to this project.

Of the common modern uses of ion exchange, water treatment was the first to develop, and is today the most important [6]. It covers several treatment processes, these being:

i) Water softening, which involves the exchange of Mg^{2+} and Ca^{2+} for Na^{+}, producing high purity water required for modern boilers;

ii) Desalination, which involves either the partial (carbonate hardness) or total removal of ions from the raw water by applying either separate cation and anion exchangers or a mixed bed exchanger containing both cation and anion resins; and finally

iii) Wastewater and effluent treatment, which is the most recent of the ion exchange applications, used to treat valuable or toxic effluents from diverse fields such as mining industries, atomic power plants and food processing factories [7,8,9].

The more recent industries that, within the last 15 years [10], have found applications for ion exchange, include mining [11] (particularly the recovery of uranium, gold,

platinum and silver), food processing (particularly sugar refining and wine production) and pharmaceutical and medical (for the production of drugs, as well as for uses in chromatographic and other analytical fields). It is, however, another water treatment process - that of wastewater reclamation and re-use, that is receiving increasingly more attention and research (including work at the Department of Chemical Engineering, U.C.T.) [12].

1.2 THE NEED FOR WATER RECLAMATION AND RE-USE

In the modern, technological world, fresh water is becoming increasingly scarce. Rapid population growth and industrial expansion are putting ever increasing demands on local and traditional water supplies. It is sufficient to point to the fact that over two million people are added to the world's population every week, increasing exponentially the demand for food, water, fuel and other commodities. For example, one ton of petroleum or sulphuric acid requires 20 tons of water, while 250 tons of water is required per ton of steel [13]. Yet the world's water supply remains constant - it only becomes more polluted as domestic and industrial effluent is discharged, without treatment, into rivers, lakes and seas [14].

Natural water supplies in many countries will be insufficient, in the near future, to meet the ever growing demand [15]. It has been estimated that, by the early 1980's, the withdrawal of waters in the United States will approximately equal the recoverable streamflow and ground water supply [16]. Thus man must turn more and more to the reclamation of brack, sea and waste waters. Many desalting processes have been developed, including distillation, freezing, electrodialysis, reverse osmosis and ion exchange. It is, however, less costly to desalinate waters of a relatively low total dissolved salt (TDS) content (< 500 mg/ℓ). One possible source of such low TDS water is municipal effluent, and ion exchange is ideal for upgrading sewage water for, even, domestic re-use.

Another recent innovation in the ion exchange field is the development of continuous ion exchange (CIX) systems, which solve many of the problems associated with the older, fixed bed type systems [22]. Of the CIX processes developed, continuous counter-current ion exchange (CCIX) is the most suitable for wastewater treatment, since it can accommodate particulate matter in the feed and columns, and it offers the facility of accurately controlling the final resin and liquid compositions by simply altering the resin to liquid (R/L) ratio in the columns. A description of the CCIX columns, and their uses in the desalination of municipal effluents, was given by Giddey [18].

It is, in particular, the equilibrium and kinetic properties of the resins used that determine the ease of exchange, and thus the physical makeup, of each column. The equilibrium largely determines the number of stages for a particular conversion - the less favourable the exchange, the more stages will be required for a given conversion. The resin kinetics, on the other hand, affect the contact time, and thus the efficiency, of a stage. A more detailed description of the relationship between resin properties and column design is given in Chapter 7.

1.4 AIMS AND OBJECTIVES OF THE PRESENT WORK

Despite the importance of the resin equilibrium and kinetic properties in the design of CCIX systems, very little information is available on the properties of the newer resin types.

Thus the aim of this thesis was to determine and compare the kinetic and equilibrium properties of four resin types for the most common exchange reactions encountered in water desalination processes.

The Na^+, Ca^{2+} and H^+ exchanges were studied on a macroporous strong acid resin and a gel strong acid resin, while the Cl^-, SO_4^{2-} and artificial COD loading kinetics were

studied on a macroporous weak base resin and a gel weak base resin. The kinetic behaviours were compared and explained in terms of diffusion effects, in order to attempt to predict kinetic behaviours of exchange reactions using similarly structured resins.

CHAPTER 2

THEORY OF ION EXCHANGE

2.1 INTRODUCTION

Ion exchange is the reversible exchange of cations or anions from a liquid to a solid phase, and vice versa, according to the following simple reactions [18]:

$$R^- - A^+ + B^+Y^- \rightleftharpoons R^- - B^+ + A^+Y^- \qquad \text{(cation exchange)} \qquad (2.1)$$

$$R^+ - X^- + A^+Y^- \rightleftharpoons R^+ - Y^- + A^+X^- \qquad \text{(anion exchange)} \qquad (2.2)$$

where R represents the solid, or resin, phase.

Ions of similar charge to that of the exchanger are called co-ions (Y for cation and A for anion in equations (2.1) and (2.2)), while ions of opposite charge to that of the exchanger are called counter-ions (A and B in cation exchange (equation (2.1)), and X and Y in anion exchange (equation (2.2))).

Most modern ion exchange resins are porous polymer spheres of varying diameter, the characteristics of which are dependent on the pore size distribution, percent crosslinking within the beads, and the functional group(s) introduced by reaction techniques.

2.2 ION EXCHANGE RESINS

2.2.1 Resin Types

There are four fundamental resin types available on the market [23]. They are:

i) strong acid cation resin;

ii) weak acid cation resin;
iii) strong base anion resin; and
iv) weak base anion resin.

Each of these shall be discussed in turn.

In addition, special resins are available for selective removal of substances (e.g. nitrate [24]), but these will not be discussed here in any detail.

2.2.1.1 Strong Acid Cation Resins

These are made by sulfonation of a styrene-divinylbenzene matrix [23]. As the synthesis implies, these beads are crosslinked polymers, with SO_3^- groups attached. However, other groups are also available in varying acid strengths [25] and include PO_3^{2-}, HPO_2^- and SeO_3^-. Many resins contain two or more types of fixed ionic groups and are called "bifunctional".

Other methods used for synthesizing acid resins are condensation with phosphoric acid groups ($PO_3^{2-}(H^+)_2$), and the alkali condensation of phenolate, sodium sulfate and formaldehyde. Since the pK of the functional groups is low, these resins have the ability to exchange under either high or low solution pH conditions (provided that the pH of the solution remains above the pK of the functional group). For regeneration, the pH of solution must be maintained below the pK of the functional group, and thus strong acid resins are only able to be regenerated with strong acids (HCl, H_2SO_4, etc.).

2.2.1.2 Weak Acid Cation Resins

These resins contain carboxylic acid functional groups and are analogous to weak base resins in most respects (see Section 2.2.1.4). They can also exist as bifunctional resins, and are able to be regenerated with both strong or weak acid solutions. However, for exchange to take place, the pH of the external solution must be above the pK of the

carboxyl group, and thus weak acid resins are only effective at high solution pH [26].

A typical cation exchange would be of the form:

$$2(R^- - Na^+) + Ca^{2+} - Cl_2^- \rightleftharpoons R_2^+ - Ca^{2+} + 2(Na^+ - Cl^-) \qquad (2.3)$$

2.2.1.3 Strong Base Anion Resins

Anion exchange resins were not available in the old zeolite forms (see Chapter 1). It was only with the advent of modern polymerisation techniques that they became commercially available.

Strong base anion resins are those with a quaternary amine functional group (NH_4^+). They behave in a similar fashion to strong acid resins in that they exhibit a high degree of dissociation. They are capable of "splitting" a neutral salt in the exchange of an hydroxyl ion for another ion and are able to load under high solution pH conditions while also requiring a strong base for regeneration.

A typical exchange reaction would be:

$$2(R^+ - Cl^-) + Na_2^+ - SO_4^{2-} \rightleftharpoons R_2^+ - SO_4^{2-} + 2(Na^+ - Cl^-) \qquad (2.4)$$

More recently P^+- and S^+- groups have been added in place of the amine group. Methods used for producing these resins include condensation of aromatic amines with formaldehyde; condensation of aliphatic polyamines; condensation of anhydrous ammonia with dihaloparafins under pressure; and the chloromethylation of polystyrene [27] Most of these techniques involve two reaction steps - chloromethylation and amination. The former step does not have well defined limits, resulting in possible methylene bridging occurring [28]. This alters the topology of the polymer, and thus resins of a wide range of properties can be made from a given copolymer composition. In addition, resins exhibiting similar properties can be made from copolymers of widely different crosslinking.

2.2.1.4 Weak Base Anion Resins

Those resins containing primary, secondary and tertiary amine groups fall into this category. They are only able to load under low pH conditions since hydrogen ions are involved in the exchange, which occurs in two distinct steps, as follows:

(a) Protonation of the amine group:

$$R - NH_2 + H^+ \rightarrow R - NH_3^+ \qquad (2.5)$$

(b) Association:

$$R - NH_3^+ + Cl^- \rightarrow R - NH_3^+ - Cl^- \qquad (2.6)$$

The above mechanism is generally accepted, and is described by Helfferich [25], although Kunin [3] suggests that this is not necessarily true, and that it is quite possible that weak base anion exchange is similar to weak acid cation exchange. However, the mechanism given by Helfferich is the more generally accepted one, and will be used in these discussions. The loading exchanges involving weak base anion resins are unique in the fact that an entire molecule (e.g. HCl) is absorbed into the pore and reacts with the active site, as compared with only the counter-ion being involved in other exchanges.

Regeneration (i.e. the conversion to free base form) is accomplished in any solution which is able to raise the pH above that of the amine group.

2.2.2 Resin Structure

Resins are broadly available in two physical structure types. The gel type resins and the macroporous (macroreticular) types [20,29,30].

2.2.2.1 Gel Resins

All resins prior to 1966 belong to this category. They

consist of crosslinked polyelectrolytic gel-type polymer with no defined internal structure [20]. The pore structure of any resin depends on six parameters:

i) the nature of the ions involved in the exchange;
ii) the ionic strength of the solutions (due to swelling);
iii) the temperature;
iv) the number of fixed ionic charges in the exchanger;
v) the degree of crosslinking; and
vi) the polarity of the solvent.

Thus, gel-type exchangers have ill-defined pore structures with the pores generally < 30 Å [20,29] , the average surface area being $< 0,1$ m^2/gm resin and the porosity approximately 0,003 ml pores/ml resin. They are usually translucent in appearance.

This typical structure may disappear on drying [31] and may show practical disadvantages such as poisoning by colloidal material [32] and fracture due to osmotic shock.

2.2.2.2 Macroporous Resins

These resins consist of a polystyrene polymer base with divinylbenzene crosslinking. As polymerization proceeds, phase separation occurs, leading to polymer beads containing microspheres cemented together at points of contact which, in turn, form larger pores (see Fig. 2.1).

Typically, the pore size of a macroporous resin would be 60 - 400 Å for a cation resin, and 200 to 2000 Å for an anion resin [20], their surface area 100 m^2/gm and their porosity approximately 0,35 ml pores/ml resin. They are opaque in colour.

Fig. 2.2 shows a schematic comparison between the two resin types.

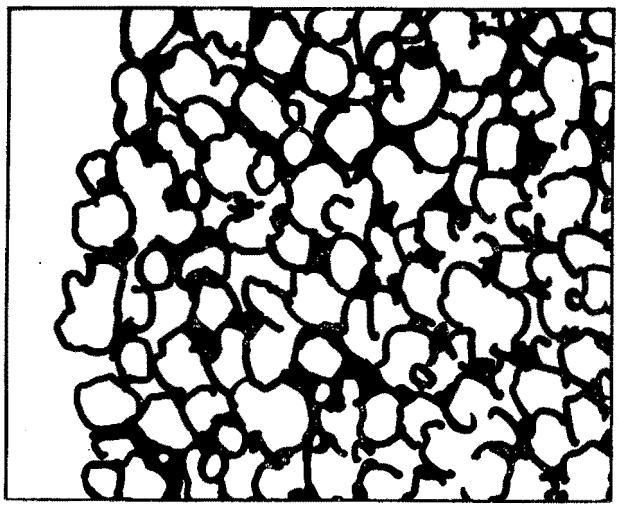

Fig. 2.1: Hypothetical Structure of Macroporous Ion Exchange Resin Bead [20].

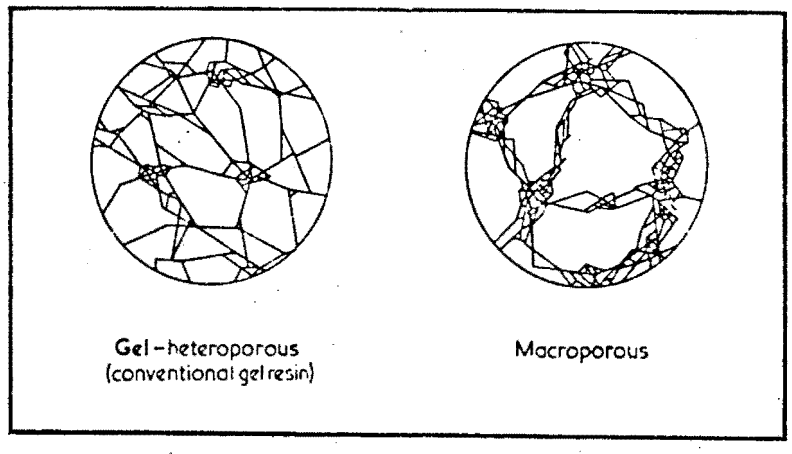

Fig. 2.2: Schematic Representation of Gel and Macroporous Resin Structures [18].

2.2.3 Resin Properties

These are extremely important, and within a resin type determine, to a large extent, the kinetic and equilibrium characteristics of the resin.

2.2.3.1 Capacity

The capacity, or potential for taking up counter-ions, is one of the most important properties of a resin, since it

determines its "workability". Capacity is defined as the number of ionogenic sites per volume (or weight) of resin [25,6] and is a measure of the quantity of ions it is capable of exchanging per unit volume or mass.

A number of different definitions and units apply:

i) weight capacity: milliequivalents per gram of dry resin in the H^+ or Cl^- form.

ii) volume capacity: milliequivalents per litre of packed bed of resin in the H^+ or Cl^- form and fully water swollen.

iii) apparent capacity: number of exchangable counter-ions per specified amount of resin.

2.2.3.2 Particle Size

Most resins vary in diameter between 0,3 mm and 1,5 mm. The particle size has a marked effect on the kinetics of ion exchange systems, and thus should be stated in all work of this nature (see Section 2.5.4). It can be measured by either microscopic techniques or by screen analysis [6] The latter is more common.

2.2.3.3 Degree of Crosslinking

The degree of crosslinking in a polymer resin is varied by adjusting the percentage divinylbenzene present during manufacture. It is usually expressed as "% DVB".

The degree of crosslinking determines the mesh width of the matrix, and thus the resin's swelling ability and a major part of its performance characteristics [25,33]. Fig. 2.3 shows how the resin diameter varies with the % DVB in typical cation and anion resins.

A resin with high DVB content is very rigid and thus resistant to osmotic shock; but its inability to swell to any appreciable extent results in low diffusion coefficients

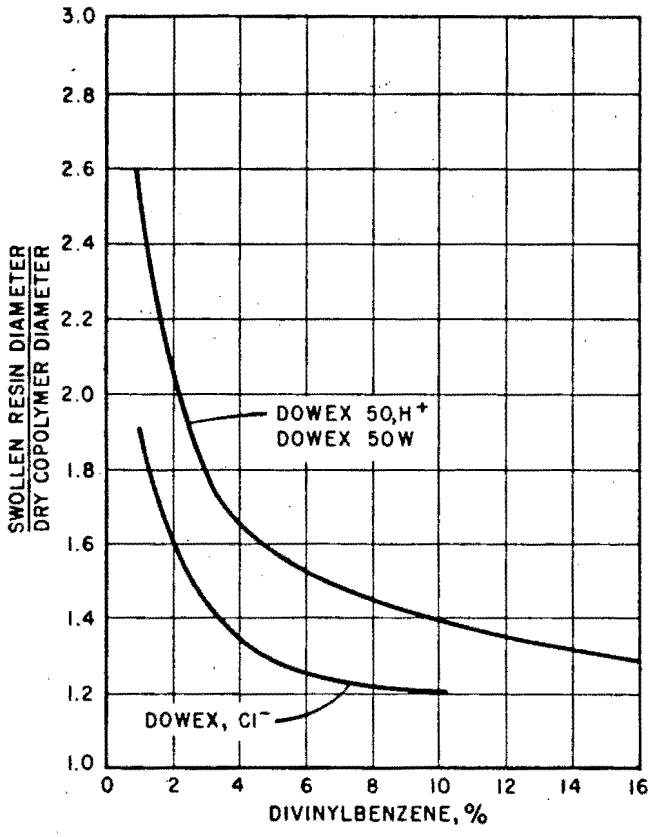

Fig. 2.3: Variation of Resin Diameters with % DVB [23].

[25,33] and thus slower kinetics as well as an increase in the effect of sieve action (see Section 2.4.2.3). A resin of low DVB content, however, will have relatively faster kinetics and be less affected by sieve action, but will be physically weaker and thus more susceptible to breaking and fractioning. By varying the degree of crosslinking, therefore, the physical properties of a resin can be appreciably changed. Fig. 2.4 shows how the average pore diameter varies with % DVB.

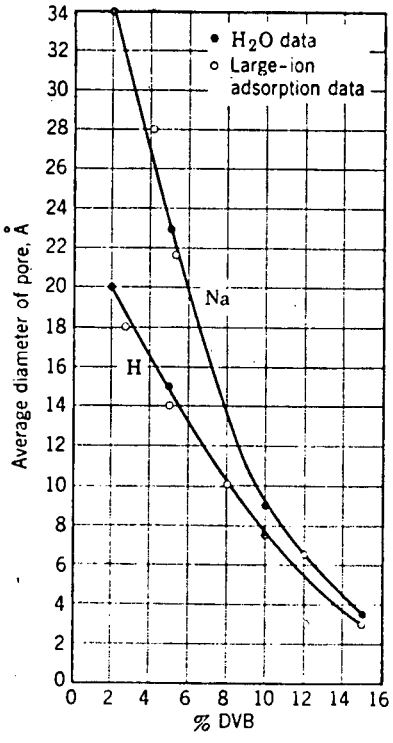

Fig. 2.4: Variation of Pore Diameter with % DVB [3].

2.3 THEORY AND MECHANISM OF ION EXCHANGE

Although many different theories have been postulated with respect to mechanisms of ion exchange, these can all be grouped together under three major headings [34].

2.3.1 Crystal Lattice Theory

This theory, postulated by Panting and Bragg [3], states that there is a fixed number of ions of opposite charge surrounding each ion of a crystal of an ionic solid. These are subject to certain coulombic attractive forces that are dependent upon the relative charges of the ions and the distances between them. If placed in a highly polar medium, the nett attractive force binding the ion to the crystal is diminished to the extent that an exchange of this ion for another ion is possible.

The ease of exchange depends on:

sides of a membrane [3] , one side containing ions not able to diffuse through the membrane. Applying this theory to Na^+ and Cl^-, we get:

$$(Na^+)_1(Cl^-)_1 = (Na^+)_2(Cl^-)_2 \tag{2.7}$$

where 1 and 2 refer to opposite sides of the membrane. Since electroneutrality must hold,

$(Na^+)_1 = (Cl^-)_2$ and $(Na^+)_1 = (Cl^-)_1 + (An^-)_1$
$(Na^+)_2(Cl^-)_2 = (Cl^-)_2^2$ and (Na^+) must be greater than $(Cl^-)_1$.

Since:

$$(Cl^-)_2^2 = (Cl^-)_1(Na^+)_1 \tag{2.8}$$

then:

$$(Cl^-)_2 > (Cl^-)_1$$

or the concentration of NaCl is greater on the side that is free of the non-diffusible ion.

If we let:

$(Na^+)_2 = (Cl^-)_2 = X$ and $(Cl^-)_1 = Y$
and $(An^-)_1 = Z$,

$$\therefore \quad X^2 = Y(Y+Z) \ . \tag{2.9}$$

If K^+ is added,

$$(Na^+)_1(Cl_1^-) = (Na^+)_2(Cl^-)_2 \tag{2.10}$$

$$(K^+)_1(Cl^-)_1 = (K^+)_2(Cl_2^-) \ . \tag{2.11}$$

Dividing, we get:

$$\frac{(Na^+)_1}{(K^+)_1} = \frac{(Na^+)_2}{(K^+)_2} \qquad (2.12)$$

For pairs of ions of unequal valence (e.g. Na^+ and Ca^{2+}) equation (2.12) becomes:

$$\frac{(Na^+)_1}{\sqrt{(Ca^{2+})_1}} = \frac{(Na^+)_2}{\sqrt{(Ca^{2+})_2}} \qquad (2.13)$$

Equations (2.12) and (2.13) state that an exchange of ions must take place until concentration ratios are equal in both phases. This is the basis of the Donnan theory, which explains:

i) the inability of free electrolyte to enter the resin phase of resins having a high exchange capacity;

ii) the effect of valency;

iii) the effects of solution volume and electrolyte concentration; and

iv) the effect of the fixed ion concentration of the resin phase.

The assumption is made that the colloidal micelle, to which is attached the exchangable ion, is considered to be the non-diffusable membrane. The interface between the solid and liquid phases may be considered to be the membrane.

All the above theories must satisfy the electroneutrality law - the only difference being the origin and position of the exchange site.

2.4 ION EXCHANGE EQUILIBRIUM

2.4.1 Introduction - Selectivity and Equilibrium

Capacity alone is not sufficient to characterise a resin.

It is also necessary to obtain sufficient information on the exchange equilibria. An equilibrium condition is attained when an ion exchanger is placed in an electrolyte solution containing a counter-ion which is different from that within the exchanger.

This can be expressed as follows:

$$\overline{A} + B \rightleftharpoons \overline{B} + A \qquad (2.14)$$

where $\overline{A}$ and $\overline{B}$ indicate solid state.

With the exception of very few special cases, all equilibrium reactions are reversible.

The concentration distribution of the two (or more) competing counter-ion species in the liquid is usually different from that of the ion exchanger; as a rule the ion exchanger selects one species in preference to another. This phenomenon is termed selectivity, and is an integral part of equilibrium as a whole.

In the following section, some definitions used in relation to equilibria are given.

2.4.1.1 Definitions

The ion exchange equilibrium can be characterised by means of the isotherm or "equilibrium curve". This gives an indication of the ease of separation of ions in solution by an ion exchanger in a similar fashion to the way the equilibrium line in distillation relates the mole fraction of a component in the gas with the mole fraction of the component in the liquid at steady state conditions [32]. As a rule, the equivalent ionic fraction of A in the liquid (y_A) is plotted against the equivalent ionic fraction of A in the resin (x_A), and this produces a graphical representation of the ionic compositions of the ion exchanger as a function of the experimental conditions (see Fig. 2.5). (The equivalent ionic fraction is expressed as:

$$x_A = \frac{Z_A M_A}{\Sigma Z_i M_i} \qquad (2.15)$$

where Z is the valency and M the concentration (in molality).)

Selectivity (the preference of the resin for one ionic species over another) produces a non-linear equilibrium line, which may be conveniently expressed in terms of one of the following parameters:

(a) The Separation Factor:

This is used mainly in calculations of column performance and is given the symbol α_B^A, defined as:

$$\alpha_B^A = \frac{\bar{m}_A \cdot m_B}{\bar{m}_B \cdot m_A} = \frac{\bar{C}_A \cdot C_B}{\bar{C}_B \cdot C_A} = \frac{x_A \cdot y_B}{x_B \cdot y_A} \qquad (2.16)$$

where m = the concentration in molality;
C = the concentration in equivalents per unit volume;
and x,y = the ionic fractions in the resin and liquid, respectively.

If ion A is preferred, α_B^A will be larger than unity, and if ion B is preferred, α_B^A will be smaller than unity. A simple relationship exists between the separation factor and the equilibrium isotherm, shown in Fig. 2.5. α is equivalent to the ratio of the two rectangles I and II.

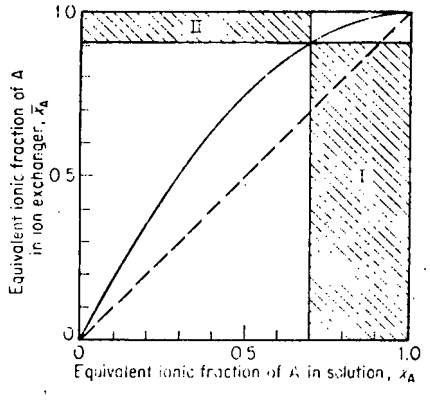

Fig. 2.5: Schematic Representation of Ion-Exchange Isotherms and Separation Factor [25].

(b) The Selectivity Coefficient:

This is often used for theoretical studies. The molal selectivity coefficient is defined by:

$$K_B^A = \frac{\bar{M}_A^{|Z_B|} \cdot M_B^{|Z_A|}}{\bar{M}_B^{|Z_A|} \cdot M_A^{|Z_B|}} \quad . \tag{2.17}$$

Molarities, or equivalent ionic fractions, may be used instead of molalities, and result in similar equations. For counter-ions of equal valence, K_B^A is independent of concentration units, whereas for differing valence counter-ions, the value K_B^A depends on the concentration units chosen.

The essential difference between the separation factor and the selectivity coefficient is that the latter contains the ionic valencies as exponents, and, as such, when the valencies of the ionic species are not equal (in which case the separation factor and selectivity coefficient will differ), the selectivity coefficient is used, since it is not as sensitive to experimental conditions.

(c) The Distribution Coefficient:

This is used in certain practical applications. It is defined as:

$$D_i = \frac{\bar{M}_i}{M_i} = \frac{\bar{X}_i \bar{M}}{X_i M} \tag{2.18}$$

$$\text{or} \quad D_i' = \frac{\bar{C}_i}{C_i} = \frac{\bar{X}_i \bar{C}}{X_i C} \tag{2.19}$$

where M_i = the concentration of species i (in molality);

$\bar{M}$ = the concentration of fixed ionic groups (e.g. per unit weight);

X_i = the amount of species i in unit volume of packed bed;

$\bar{X}_i$ = the concentration of species i in resin in moles per unit bed volume;

C_i = the concentration of species i in molality;
$\bar{C}_i$ = the resin concentration of species i in molality.
Symbols with subscript i refer to the total system.

The coefficients increase with an increase in dilution, and for non-linear isotherms, the coefficients depend on the equivalent fraction X_i. This distribution coefficient is used mostly in systems with a trace component present, since under these circumstances the section of the isotherm of interest is that part near the origin which is usually linear and thus independent of X_A.

(d) The Thermodynamic Equilibrium Constant:

This is used occasionally in theoretical studies, and is defined as:

$$\Delta G^{\circ} = -RT \ln \kappa_B^A \qquad (2.20)$$

where ΔG° = the standard free energy; and
κ_B^A = the equilibrium constant.

In contradiction to the previous three parameters, κ_B^A is an integral quantity of the whole isotherm surface.

2.4.2 Causes of Selectivity

The selectivity of ion exchangers, which results in non-linear equilibrium isotherms, is well understood and, in general, a result of various physical properties [25]. Some of the more important of these are described in this section.

2.4.2.1 The Effect of Counter-Ion Valency and Solution Concentration

The counter-ion valencies have a marked effect on the equilibrium isotherm of even ideal systems linked to the solution concentration. In general, the ion exchanger prefers the ion of higher valency, and this preference increases with dilution of the bulk solution. Fig. 2.6 shows

the concentration effect for the system Cu^{2+}/Na^{+}. As the solution concentration decreases, the preference of the resin for the divalent Cu^{2+} counter-ion increases (represented by the isotherm moving further from the diagonal) [35].

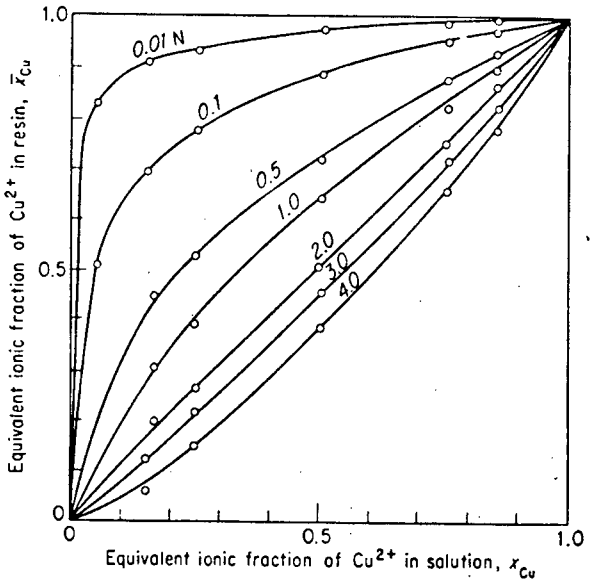

Fig. 2.6: Effect of Concentration on Cu^{2+}/Na^{+} Exchange Equilibrium [25].

In systems with counter-ions of the same valency, there is no concentration effect.

These observations can be explained in terms of the Donnan potential in which the force of attraction on an ion is proportional to its charge, and hence more strongly charged ions, i.e. of higher valency, are attracted the strongest. Furthermore, the absolute value of the Donnan potential increases with dilution of the bulk liquid.

2.4.2.2 Solution and Swelling Pressure

It has been shown that large solvated counter-ions in exchangers cause stronger swelling and higher swelling pressures than smaller ones [25]. This can be explained by the fact that, as the exchanger is solvated and swells, the matrix will tend to relax to counteract the swelling. It can do so by exchanging a larger counter-ion for a smaller

one, and thus the ion exchanger prefers the counter-ion of smaller solvated volume. The selectivity should increase, therefore, with (1) dilution of the solution; (2) decreasing equivalent fraction of the smaller ion; and (3) with degree of crosslinking.

The selectivity sequence of the alkali ions follows the series $Li^+ < Na^+ < K^+ < Rb^+ \leq Cs^+$ [6]. It must be borne in mind, however, that this phenomenon is outweighed in many systems by some of the other effects.

2.4.2.3 Sieve Action

Very large counter-ions may be excluded from the matrix by sieve action. Such an exclusion occurs if the meshes of the matrix are too narrow to accommodate the ion. This phenomenon is most marked in the zeolites since, in ion exchange resins, the non-uniform pore structure decreases the occurrence of sieve action. In resins of very high degree of crosslinking, sieve action may also become pronounced.

2.4.2.4 Specific Interactions in the Ion Exchanger

Specific interactions may occur in the exchanger or in solution, and some important examples are:

(a) Ion pair formation and association, the most important of which is between the counter-ions and the fixed ionic groups. It has been found that the ion exchanger prefers the counter-ion which forms the stronger ion pair with fixed groups. This can be explained by La Chatalier's principle in the exchange in equation (2.21):

$$\overline{A} + B \rightleftharpoons \overline{B} + A \qquad (2.21)$$

The reverse process is favoured if A is sequestered in the exchanger by fixed ionic groups. For example, resins with groups resembling dipicrylamine are highly selective for K^+.

(b) Electrostatic attraction, which depends on the ionic charge and the distance of closest approach between counter-ion and the fixed ionic group. The electrostatic effect thus favours preference for the counter-ion of higher valency and, in many cases, preference for the smaller counter-ion.

In the case of the alkali ions, most cation exchangers prefer the smaller ion, which is well explained by both electrostatic forces and swelling pressure.

(c) London interactions, which do not necessarily involve the fixed ionic groups. Selectivity may arise from London forces between the counter-ion and the matrix and from interactions of the solvent molecules with one another. These forces become important if one or both ions are organic. The ion exchanger prefers counter-ions with organic groups which resemble the components of a matrix. The strength of the interaction increases with the size of the molecule, but since these forces are small, they are often outweighed by sieve action and swelling pressure.

2.4.2.5 Associating and Complex Formation in Solution

Equilibria are strongly affected by associations of ions in the external solution. Application of La Chatalier's principle to the equilibria shows that the reverse exchange is favoured when species B is sequestered by reaction with the co-ion. The ion exchanger prefers the counter-ion which associates less strongly with the co-ion.

2.4.2.6 Formation of Precipitates

The removal of the counter-ion can be made easier by extracting it from solution by precipitation. The exchanger reduces the concentration of the competing species from solution, thus causing the ion exchanger to release this species. In practice, this is avoided as it tends to clog up the pores of the resin.

2.4.2.7 Temperature and Pressure

The temperature dependence of equilibrium is related to the standard enthalpy change. High temperatures discourage the reaction which is exothermic. Since ion exchange is not a chemical reaction, it occurs with very little heat change, and thus temperature has little effect on the exchange equilibrium (excluding thermally regeneratable resins).

The exchange itself, however, may be followed by reactions with significant energy changes, e.g.:

$$\overline{H^+} + Na^+ \rightarrow \overline{Na^+} + H^+ \qquad (2.22)$$

$$H^+ + OH^- \rightarrow H_2O \qquad (2.23)$$

In the reaction given by equation (2.23), the heat of neutralization is liberated, and systems such as this are far more likely to be affected by temperature changes. (Selectivity decreases with increase in temperature.)

The pressure dependence of equilibria is a function of the volume change. High pressure favours the reaction which results in a volume decrease, and vice versa. In ion exchange, very little volume change occurs, and therefore external pressure has minimal effect.

2.4.3 Systems With More Than Two Counter-Ions

The general qualitative rules for the selectivity of ion exchangers are usually valid for systems with more than two counter-ions. The ability of the ion exchanger to discriminate between the two species is affected by the presence of other species which alters the Donnan potential and the swelling pressure; also, direct interaction between the counter-ion may occur.

Systems with three counter-ions may be conveniently expressed on a triangular system [36] (example for Cu^{2+}, Ag^+ and H^+ is given in Fig. 2.7).

It may occur that one species is predominant, and this simplifies the overall situation.

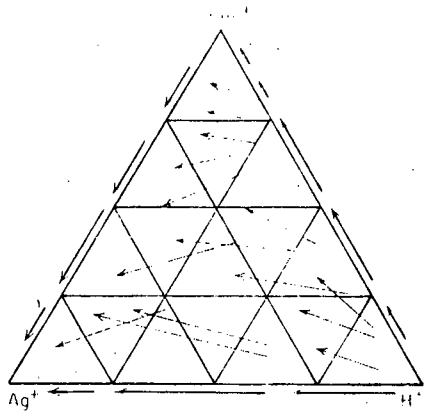

Fig. 2.7: Example of Triangular Representation in a Ternary System [25].

2.5 ION EXCHANGE KINETICS

2.5.1 Introduction

Kinetics have not been as well investigated, and are not as well understood, as equilibria [25]. The kinetics of a system pose the following questions:

i) What is the mechanism?
ii) What is the rate-determining step?
iii) What rate laws are obeyed?
iv) How can rate be predicted?

Only the first two questions are well understood, and their discussion follows below.

2.5.2 Mechanism of Ion Exchange

Assume a spherical resin bead of uniform size containing ion A in a well stirred solution of BY (electrolyte), where B is the counter-ion. As equilibrium is approached, ion A diffuses out of the bead into solution, and ion B diffuses from the bulk solution into the bead (ion exchange). It has been shown that the process is primarily one of diffusion and

not of chemical reaction. Because of the law of electroneutrality (already discussed) any counter-ions which leave the resin are replaced by an equivalent number of other counter-ions; when the counter-ion moves out into the solution, the ion exchanger is left with an electrical surplus, which must be compensated for by taking up another counter-ion. Under normal conditions, Donnan exclusion keeps the co-ion content at a very low level, resulting in few deviations from stoichiometry. The co-ion, therefore, does not participate in the exchange and has little effect on the rate [25].

A satisfactory method for explaining kinetics was proposed by Nernst, cited by Kitchener [2]. This proposes that the bulk of the solution is being instantaneously mixed by stirring, but in the vicinity of the solid surface (ion exchange resin bead) there is a thin film of immobile solution in which diffusion is the only transport process (Fig. 2.8).

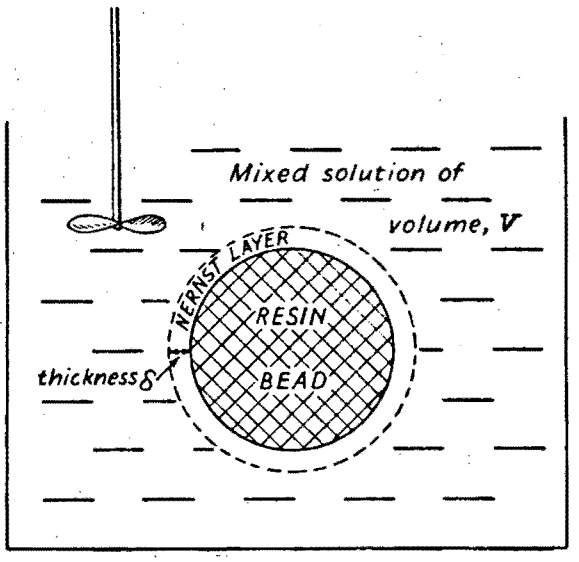

Fig. 2.8: Representation of Nernst Layer Theory of Kinetics [2].

This is a simplification, since it is impossible to perfectly mix a liquid, but the theory has been shown to work reasonably well.

2.5.3 The Rate Determining Step

Boyd cited by Miller [5] postulated the following five steps for the exchange reaction $R^- - B^+ + A^+ \rightleftharpoons R^- - A^+ + B^+$:

i) Diffusion of A^+ through the Nernst layer up to the particles of exchanger;

ii) Diffusion of A^+ through the exchanger;

iii) Chemical exchange of A^+ and B^+ at the ion exchange site;

iv) Diffusion of B^+ out through the particles of exchanger;

v) Diffusion of B^+ away from the exchanger into solution through Nernst layer.

It is generally accepted that the chemical exchange is almost instantaneous, and therefore two general rate controlling mechanisms exist:

i) Counterdiffusion of counter-ions within the exchanger itself (pore diffusion); and

ii) Counterdiffusion of counter-ions in the adherent film surrounding the resin bead (film diffusion).

These are shown diagrammatically in Fig. 2.9.

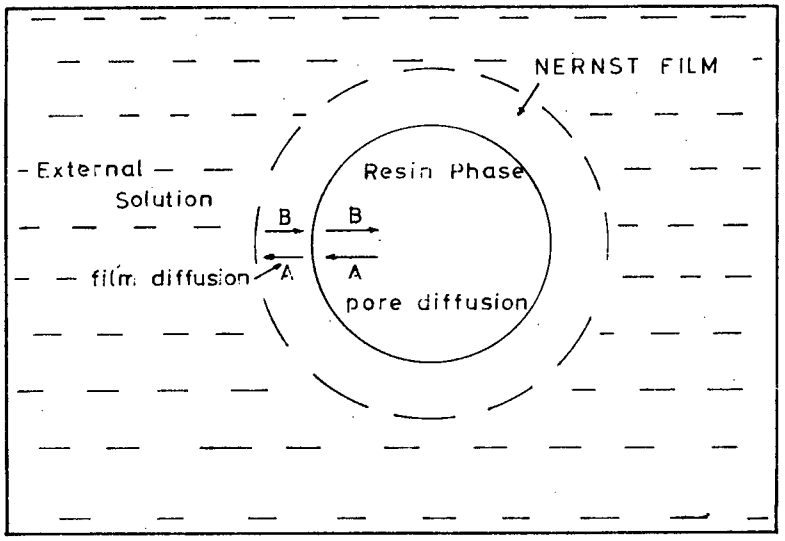

Fig. 2.9: Diagrammatic Representation of Diffusion in Ion Exchange Bead [18].

LIQUID FILM CONTROLLING

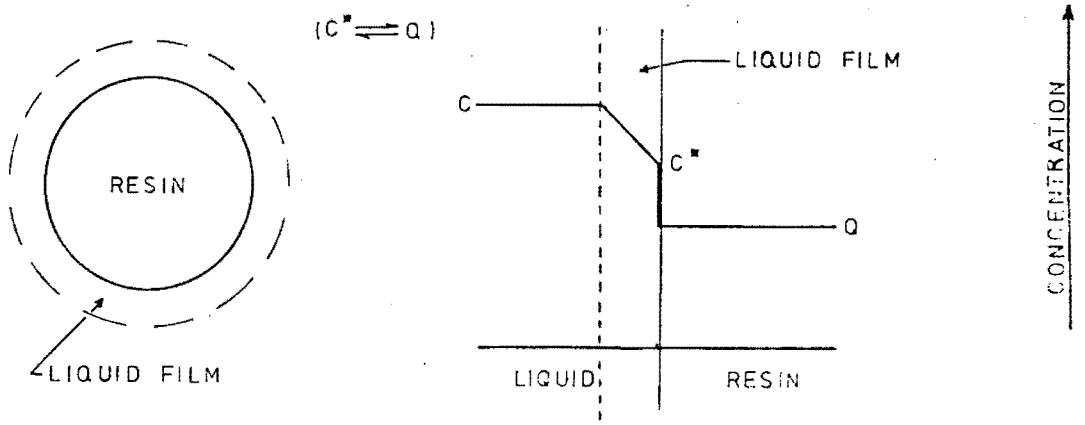

PORE CONTROLLING

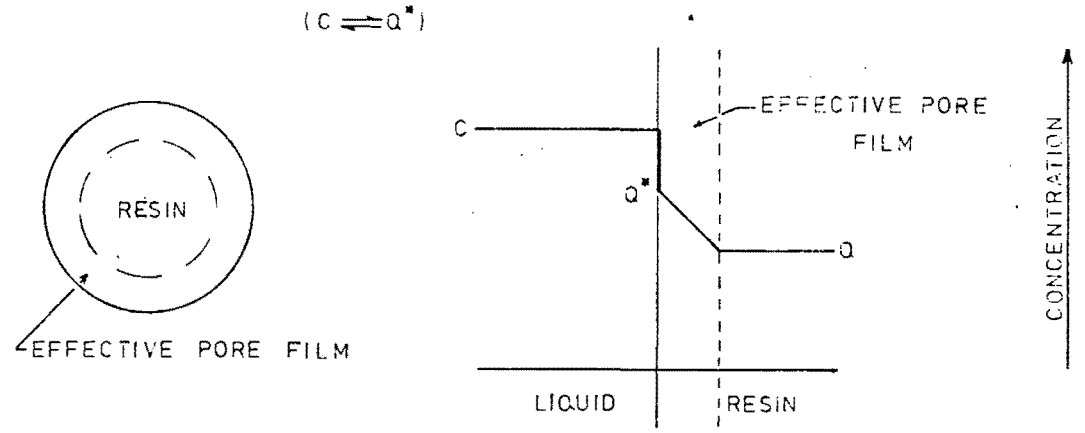

COMBINED LIQUID FILM & PORE CONTROLLING

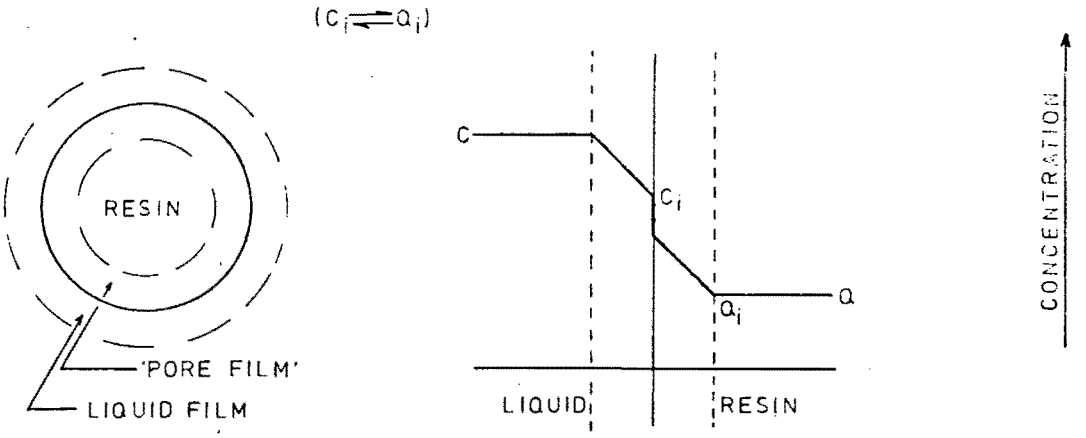

Fig. 2.10: Schematic Representation of Controlling Mechanisms [13].

In practice, either one mechanism or the other can occur, or both mechanisms can apply simultaneously, as is represented schematically in Fig. 2.10.

Considering each case separately, if particle diffusion controls, film diffusion is so much faster that concentration differences in the films are levelled out instantaneously. Fig. 2.11 shows the radial concentration profiles of the exchanging species. The local interdiffusion flux is proportional to the steepness of the profile and to the interdiffusion coefficient.

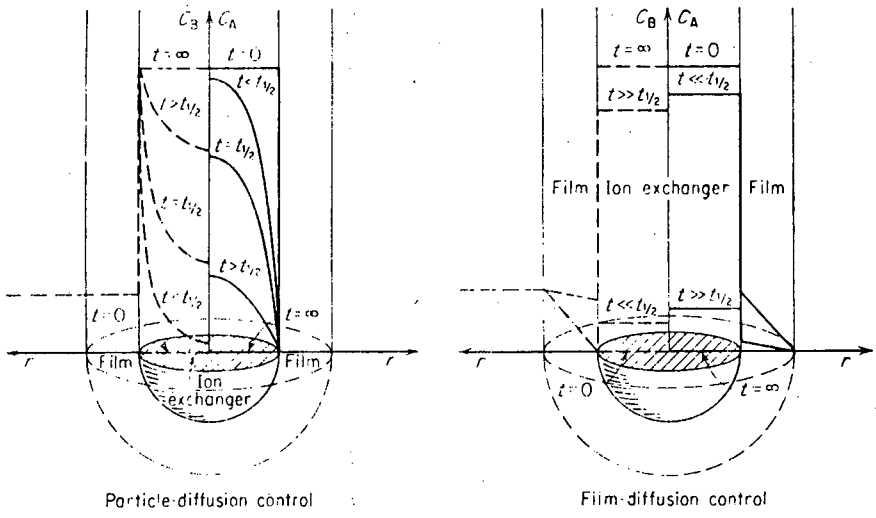

Fig. 2.11: Radial Concentration Profiles for the Two Diffusion Control Cases [25].

For film-diffusion control, particle diffusion is much faster than film diffusion and thus concentration gradients exist only in the film. Hence, the flux is proportional to the solution concentration and to the interdiffusion coefficient in the film and inversely proportional to the film thickness.

Film-diffusion control tends to exist in systems (1) with ion exchangers of high concentration of fixed ionic groups; (2) low degree of crosslinking and small particle size; (3) with dilute solutions; and (4) with inefficient agitation [25].

quadratic expression for the driving force [18]. Later attempts at deriving a generalised expression for diffusion in a resin bead used Fick's Law, which expresses the flux of ion A as follows:

$$N_A = -D \frac{d\overline{C_A}}{dZ} \tag{2.24}$$

where N_A = flux of A;
D = diffusivity coefficient of A in the bead;
$\overline{C_A}$ = concentration of A at some point in the bead;
Z = length parameter.

Incorporating material balance considerations and converting to spherical geometry, the following rate expression was derived [18]:

$$\frac{\partial \overline{C_A}}{\partial t} = \overline{D} \left(\frac{\partial^2 \overline{C_A}}{\partial r^2} + \frac{2}{r} \frac{\partial \overline{C_A}}{\partial r} \right) \tag{2.25}$$

where r = the distance from centre of bead.

This equation (known as Fick's Second Law) formed the basis of all the kinetic studies until the late 1950's, when it was found that this did not adequately describe the rate of exchange in certain common systems and with certain new resin types. Two major new models were developed, namely the "Homogeneous Sphere Model" and the "Bi-disperse Model", and these are described in more detail below:

i) Homogeneous Sphere Model:

Schlogl and Helfferich [39] first raised doubts about the ability of Fick's Second Law (Equation (2.25)) to adequately describe the kinetics of two-counter-ion systems. It was felt that the exchange flux for the two counter-ions was not identical, since they have different mobilities. This phenomenon produced an electric potential gradient, and thus the overall flux for each counter-ion is equal to the

sum of the fluxes due to Fickian diffusion and the electrochemical gradient.

Various workers in the field [18] have solved Schlogl's equations for specific systems using finite difference.

ii) Bi-disperse Pore Model:

Weatherley and Turner [40] found that the homogeneous sphere model did not adequately describe the kinetics of a macroporous resin. They predicted that a macroporous resin could be considered to consist of two pore types - the microspheres and the macrospheres (see Fig. 2.12).

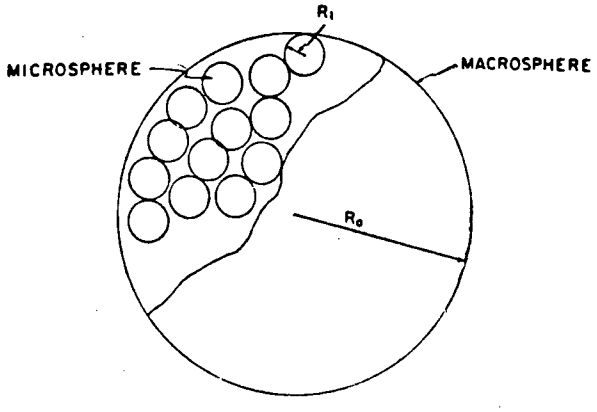

Fig. 2.12: Schematic Representation of Weatherley's Macroporous Resin Bead [18].

This bi-disperse pore size distribution meant that counter-ion diffusivities could be different at different parts of the bead. Further, the macropores, due to their larger size, would not necessarily exclude bulk solution electrolyte via Donnan exclusion as efficiently as a gel resin might. (These considerations are discussed in Section 5.2.2.2 with reference to cation exchange kinetics.)

Weatherley derived new equations, analogous to those of the homogeneous sphere model, and his solution is given in Fig. 2.13, which also compares results of the two different models.

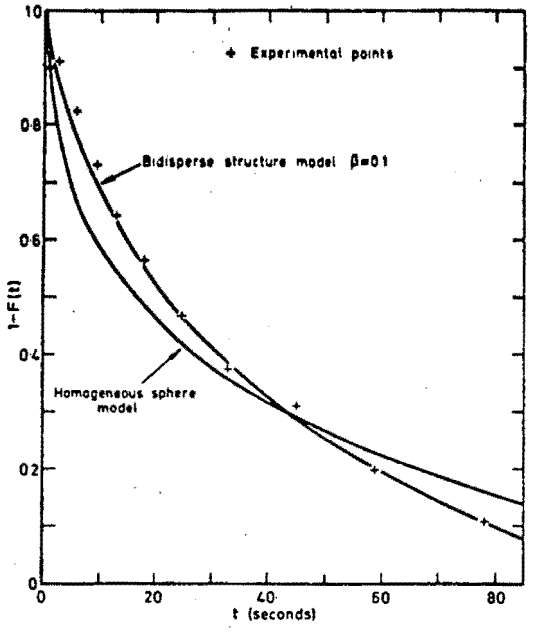

Fig. 2.13: Comparison of Diffusion Rate Models [40].

2.5.4.2 Film Diffusion

(a) Factors Affecting Film Diffusion:

With film-diffusion controlled kinetics, it is usually the solution properties which dictate the control. Of these, two are generally responsible - the "film thickness" and the solution concentration.

If the "film thickness" decreased (due to increased shear forces), the rate of mass transfer through the film would increase. If this were continued, diffusion through the film would eventually offer less resistance to transfer than the diffusion through the pore, and the system would become pore-diffusion controlled.

Secondly, the solution concentration has a marked effect on the rate of exchange. Since an exchange occurs because of the concentration gradient between the bulk solution and the equilibrium at the bead surface, an increase in solution concentration would result in a proportional increase in diffusion rate. Helfferich [25] states that, at concentrations

exceeding approximately 0,05N, pore diffusion becomes controlling since the higher concentration gradient makes the film diffusion more rapid than the pore diffusion (see Section 5.2.2.2(c)).

Further, two resin properties affect the film diffusion rate - the bead diameter and the resin capacity [18,25,34]. As the bead radius increases, so the area per unit volume of resin through which transfer can take place decreases, and so does the rate.

(b) Rate Theories:

The initial theories on film-diffusion controlled mass transfer were based on the "double layer theory" (see Section 2.3.2) [41]. On the assumption that:

i) the bulk solution is perfectly mixed, and
ii) equilibrium exists at the resin surface,

the following rate expression was postulated:

$$R = k_L a (C_A - C_A^*) \qquad (2.26)$$

where R = rate of exchange;
k_L = mass transfer coefficient;
a = area through which exchange can occur;
C_A = concentration of A in bulk solution;
C_A^* = equilibrium concentration of A at resin surface.

This theory, which postulates a linear concentration gradient across the film, has been shown to be in good agreement with experimental data [41].

Glaski and Smith and Dranoff (cited by Giddey [18]) used another approach, based on Fick's law:

$$N_A = -D \frac{dC_A}{dZ} \qquad (2.27)$$

where Z = film thickness.

The results of this equation, adapted to include the electrostatic potential gradients (suggested by Schlogl - see Section 2.5.4.1(b)(i)), when compared with the results of equation (2.24), show that both models adequately describe film diffusion kinetics [18].

CHAPTER 3

EXPERIMENTAL

3.1 TYPES AND MAKES OF RESINS

Two different cation and anion resins were used in the course of this project.

The cation resins were, firstly, Zerolit 625, a macroporous, sulphonated polystyrene, strong acid cation exchange resin, of approximately 8% DVB content, manufactured and supplied by the Permutit Company, England, and secondly, Cation Fort, a gel type, sulphonated polystyrene, strong acid cation exchange resin manufactured by Dia-Prosim, France, and supplied by Sentrachem Ltd., South Africa. This latter resin was supplied with five different crosslinkings, namely 4,5%, 5,5%, 6,75%, 7,6% and 8,5% DVB.

The two anion resins used were Zerolit MPH, a macroporous weak base crosslinked polystyrene anion exchange resin, manufactured and supplied by the Permutit Company, England, and Senbrix, a high density, macroporous crosslinked polystyrene weak base anion exchange resin with certain isoporous character, manufactured by Dia-Prosim, France, and supplied by Sentrachem Ltd., South Africa. Again, this latter resin was supplied with three different crosslinkings, namely 6,5%, 8% and 12% DVB.

3.2 THE EXPERIMENTAL APPARATUS

3.2.1 The Fractional Sampling Device

As is shown in the photographs (page 39), this apparatus consists of five basic items, namely (a) the reaction vessel and stirrer; (b) the pump; (c) the three way valve; (d) the sample tray; and (e) the timer. During operation,

solution in the reaction vessel, which is stirred continuously at 2900 r.p.m., is drawn up the sampling tube (equipped with a wire mesh screen to prevent resin being drawn up) by means of the peristaltic pump (see photograph 4) into the three way valve. This device directs the flow either via the delivery tube into a sample cup (see photograph 1), or back into the reaction vessel via the recycle pipe (see photograph 4). A flow rate of 25 ml/min was used, which resulted in minimal mixing in the tube (tested by means of a dye solution) as well as a relatively short recycle time (approximately 10 seconds). At the completion of each sampling operation the tray rotation solenoid would be activated, placing another sample cup in position below the delivery tube (see photograph 3). The frequency of sampling and volume of sample were controlled by the multiple timing unit, full details of which are given in Appendix A, Section A.1. The timer also activates the rotation solenoid, which results in the pin retracting from its slot and penetrating the next slot as the tray rotates (see photograph 3). Gravitational torque is provided by means of a string wound around the lower tray, over a pulley and connected to a 100 gm weight.

The entire system, with the exception of the pump and pump control, as shown in Fig. A-2 (Appendix A), is secured to a wooden base. The valve and tray are constructed of perspex.

3.2.2 Conductiometric Apparatus

This apparatus consists of seven basic units, namely (a) the reaction vessel and stirrer; (b) the oscilloscope; (c) the variable resistor; (d) the sine-wave generator; (e) the amplifier; (f) the pen recorder; and (g) the power supply. These are all shown in the photographs of this equipment on page 40.

The system relies on the changing conductivity of the bulk solution with progressing exchange. The conductivity probe (see photograph B) is immersed in the stirred solution

1. 3-WAY VALVE

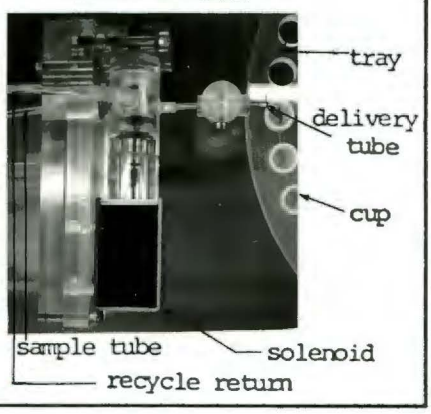

2. SAMPLE TRAY

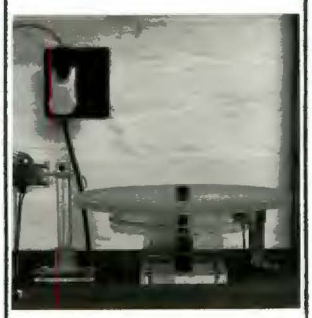

3. TRAY ROTATION SYSTEM

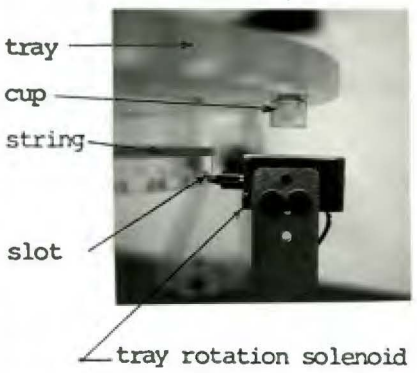

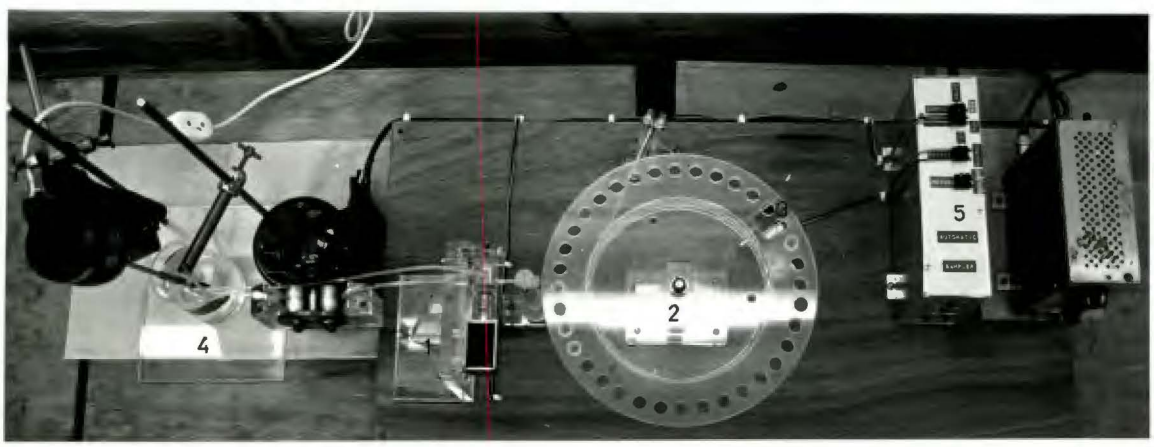

PLAN VIEW OF FRACTIONAL SAMPLING DEVICE FOR ION EXCHANGE KINETIC STUDIES

4. REACTOR VESSEL SYSTEM

5. CONTROL SYSTEMS

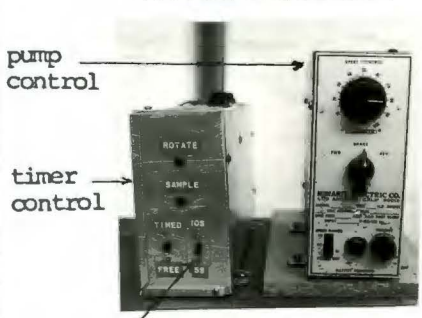

A.

REACTOR VESSEL SYSTEM

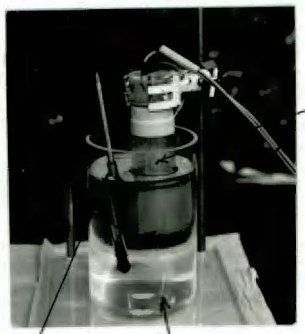

B.

CONDUCTIVITY PROBE

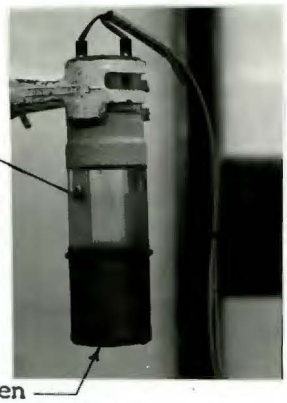

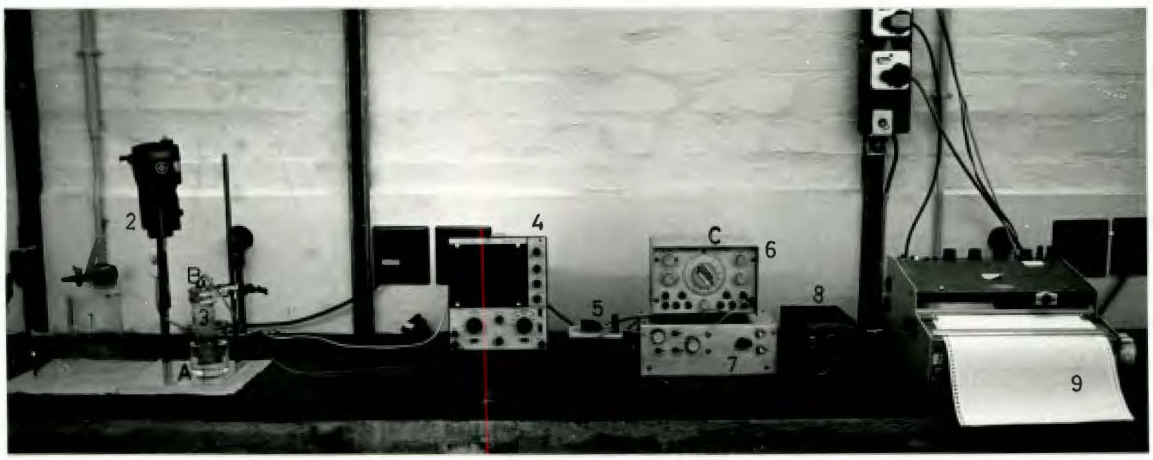

CONDUCTIVITY EQUIPMENT FOR ION EXCHANGE KINETIC STUDIES

C.

AMPLIFICATION SYSTEM

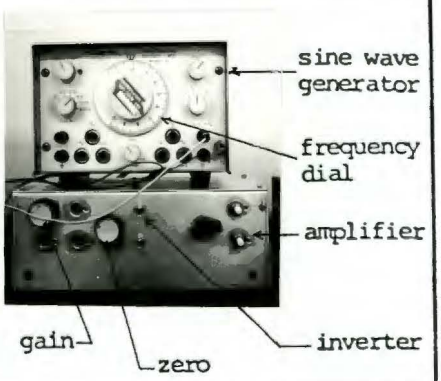

KEY

1. Reaction Vessels
2. Stirrer
3. Conductivity Probe
4. Oscilloscope
5. Variable Resistor
6. Sine Wave Generator
7. Amplifier
8. Power Supply
9. Chart Recorder

(see photograph A), and the resulting electrical signal is fed into the amplifier where it is compared with a standard signal produced by the sine wave generator (see photograph C). The difference between the two signals produces an offset on the pen recorder. The pen position can be adjusted by the zero knobs on the amplifier and recorder, as well as by the variable resistor which, together with a knob on the amplifier, adjusts the gain of the system, setting the sensitivity of the equipment.

The conductivity probe signal is also displayed on an oscilloscope screen.

3.2.3 Resin Handling Equipment

Three sets of equipment used in the handling of resin are discussed in this section. These are the resin screening apparatus (see Fig. 3.1), the centrifuge holder (see Fig. 3.2) and the resin elution column (see Fig. 3.3).

3.2.3.1 Resin Screening Apparatus

This apparatus was devised in order to wet screen the Zerolit resin samples between 0,852 and 0,60 mm. As is shown in Fig. 3.1, it consists of two standard 210 mm diameter copper sieves of 0,852 mm and 0,60 mm mesh size respectively, clamped together (with a top and bottom plate) by spring-iron clamps, and suspended in a bucket of water which is placed on a Labotec flat bed shaker. The bucket is held in position by two supporting bars. Nylon cord is used to suspend the sieve arrangement in order to allow a swaying action when the shaker is in motion.

3.2.3.2 Resin Centrifuge Holder

This item of equipment consists of a perspex inner resin basket of 38 mm I.D., with a wire screen at the bottom and a lip on the top, designed to fit into a standard plastic centrifuge tube (see Fig. 3.2). The inner basket is 58 mm long with 3 mm walls, and the plastic centrifuge tube 110 mm long.

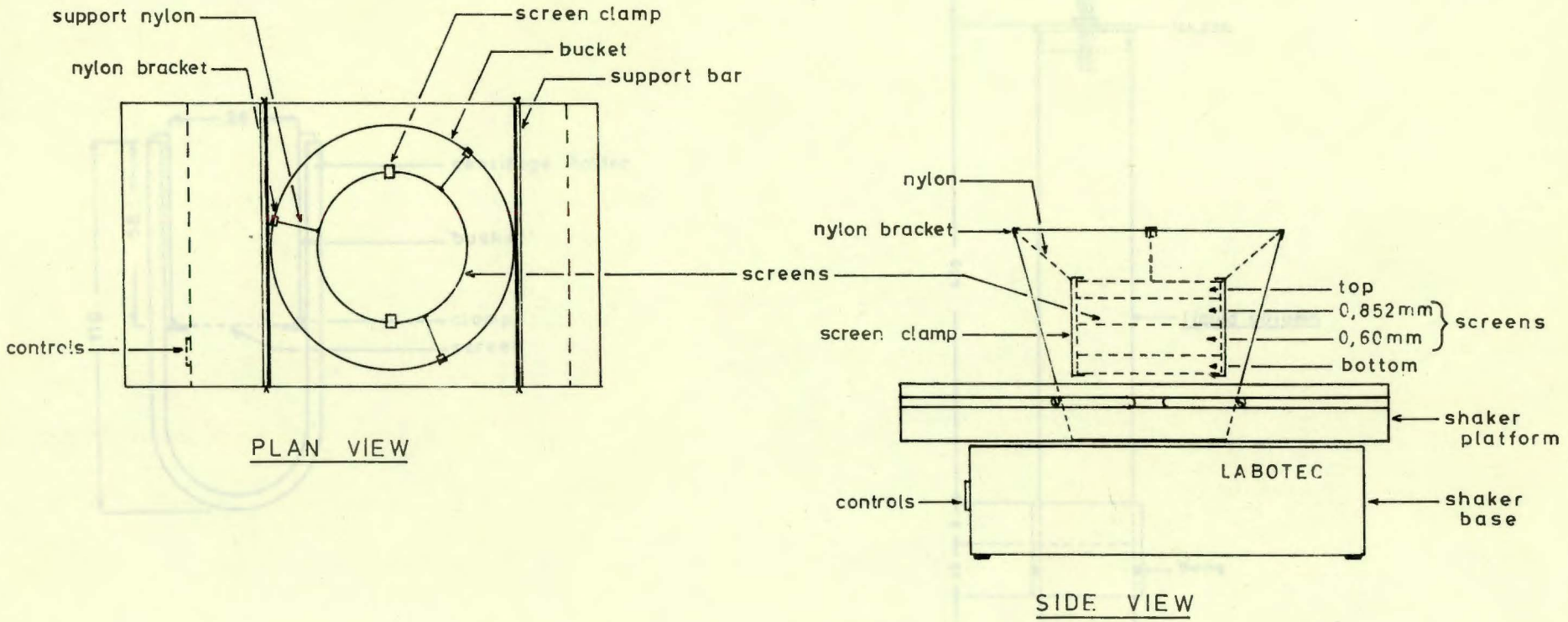

FIG. 31: SCHEMATIC VIEWS OF RESIN SCREENING APPARATUS

3.2.3.3 Resin Elution Column

This item of equipment consists of a 25 mm I.D. perspex liquid column (see Fig. 3.3), approximately 460 mm long, with an "O-ring flange" at the bottom. Into this flange is connected a 60 mm perspex resin container, with a removable bottom cap covered with wire screening, to avoid resin loss from its centrally positioned rubber exit tube. At the top of the liquid column is attached a similar cap into which is positioned a 500 mm thin bore glass tube which controls the liquid flow rate by means of a length of wire placed in its bore. The position of the wire controls the entry of air into the column, and thus the liquid flow rate out. A clamp is used on the rubber exit tube for filling the column. "O" rings are also used on the top and bottom caps, to ensure air-tight seals.

3.3 EXPERIMENTAL METHODS AND PROCEDURES

3.3.1 Resin Screening

Resin kinetics are sensitive to resin bead size, and thus, in order to obtain compatible kinetic results, the Zerolit resins were screened between 0,60 mm and 0,852 mm diameter.

The resin was soaked in distilled water overnight (to ensure that it was in the fully water-swollen form) and then loaded into the required form (H^+ form for cation resin and OH^- form for anion resin - see Section 3.3.2 below). Once the resin was entirely in this form, it was washed with distilled water. 500 cm^3 samples were placed onto the 0,822 mm screen, the screen assembly clamped together and the entire arrangement suspended in the bucket which was secured onto the shaker (see Fig. 3.1). Water was added to a level just above the screen cover, and the shaker operated at approximately 100 r.p.m. for 10 minutes. On completion of the cycle, the 0,60 mm screen was removed and the required

resin fraction on it decanted. The remainder of the resin was discarded before a new batch was started.

3.3.2 Resin Preparation

3.3.2.1 Loading

The loading of a resin into a specific ionic form was achieved by allowing a resin sample to equilibrate with a 2N solution of the required acid or alkali. The solution and resin were agitated for a ½-hour on the Labotec shaker, after which the solution was discarded and fresh solution poured in and again agitated for a ½-hour. This process was repeated three times in the case of cation resins, and six times in the case of anion resins.

Table 3.1 gives the solutions used to load both the cation and anion resins into various ionic forms.

TABLE 3.1

SOLUTIONS USED FOR SPECIFIC IONIC RESIN LOADING

Resin Type	Ionic Form	Loading Solution
Cation	H^+	HCl
	Na^+	NaCl
	Ca^{2+}	$CaCl_2$
Anion	OH^-	NaOH
	Cl^-	HCl
	SO_4^{2-}	H_2SO_4

In the case of a preloaded or mixed loaded resin, a similar procedure was followed, using the quantities of solution(s) calculated from equilibrium data to give the required final degree of preloading.

3.3.2.2 Centrifuging

Before loaded resin samples were used for kinetic studies, they were centrifuged at 2400 r.p.m. for 10 minutes in order to remove as much surface and pore liquid as possible.

A resin sample was placed in the centrifuging "basket" (see Fig. 3.2), and rinsed with 100 ml of distilled water to remove excess loading solution. (Although Giddey [18] reported that anion resin can lose loaded ions by an hydrolysis reaction during washing, there was no evidence that this occurred with the resins used in this study.) The basket was then hand-shaken to remove free water, and the resin centrifuged using an MSE Super Minor Centrifuge to remove the largest quantity of pore liquid possible.

3.3.2.3 Elution

Elution of resin samples was required for capacity and equilibrium determinations. Fig. 3.3 shows details of the perspex elution column used (see Section 3.2.3.3 for detailed apparatus description).

The resin sample was placed in the resin column which was then positioned with a clamp onto the bottom of the liquid column. 100 ml of distilled water were poured into the top of the liquid column, and the top cap secured in place. The rubber exit hose clamp was released, allowing the water rinse to run to waste. The rate of liquid flow was controlled (by means of the position of the control wire in the glass control rod - see Fig. 3.3) at approximately 10 ml/minute.

On completion of the first rinse, the exit tube clamp was closed, the top cover removed, and 100 ml of eluting solution poured in (see Table 3.2). This solution was allowed to run into a 250 ml volumetric flask and, once completed, the rinsing procedure was repeated with a final 100 ml distilled water aliquot (run into the volumetric flask, which was finally topped up to the mark with distilled water). The solution in the flask was analysed for the specific ions.

Table 3.2 gives the concentration and nature of solution used for eluting different resin samples.

TABLE 3.2

CONCENTRATION AND NATURE OF RESIN ELUTING SOLUTIONS

Resin Type	Loaded Ion to be Analysed	Solution Type	Concentration (N)
Cation	H^+	$CaCl_2$	2,0
	Na^+	HCl and $CaCl_2$	5,0
	Ca^{2+}	HCl and $MgCl_2$	5,0
Anion	Cl^-	H_2SO_4	5,0
	SO_4^{2-}	HCl	5,0

In order to determine the efficiency of the elution process, a repeat elution (with solution and final rinse) was performed on about five resin samples (see Chapter 5, Table 5.2 for an example).

3.3.3 Initial Resin Tests

3.3.3.1 Volume Capacity Determinations

Cation and anion resins each require different methods for the determination of capacity. These are described separately below.

(a) Cation Resin:

The capacity of cation resins was determined in both the Na^+ and Ca^{2+} forms.

The method used to determine the volume capacity involved the initial loading of the screened resin into the required form (see Section 3.3.2.1) and the subsequent elution of a

known resin volume (see Section 3.3.2.3). A glass scoop was used to measure out a constant resin volume of 14,65 ml, and this was used as the standard. Where repeat determinations were performed, a different resin volume of 20 ml was measured and used.

The concentration of the required ion in the 250 ml volumetric flask was measured (see Section 3.4 and Appendix E) and this value (in ppm) used to calculate the volume capacity according to equation (5.1).

(b) Anion Resin:

The capacity of anion resins was determined in the Cl^- form only.

The method involved the back titration of a known quantity of 0,05N HCl, with 0,05N Na_2CO_3, using screened methyl orange as indicator. A volume of resin was regenerated into the OH^- form (see Section 3.3.2.1) and a 14,65 ml aliquot was rinsed well with 0,05N NaOH, centrifuged and added to a known quantity of the 0,05N HCl loading solution. After approximately 16 hours, during which time the system was allowed to equilibrate with intermittent agitation, the excess HCl was back titrated and the capacity calculated using equation (3.1).

$$\text{Vol. Capacity (meq/ml)} = \frac{(\text{ml HCl} \times 0{,}05) . (\text{ml } Na_2CO_3 \times 0{,}05)}{(\text{ml resin})} \qquad (3.1)$$

3.3.3.2 Moisture Retention Capacity Determinations

The moisture retention capacity (MRC) value gives a measure of the total internal pore volume of the resin beads.

The resin was initially loaded into the required form (see Section 3.3.2.1) and a 50 ml sample was placed in a Buchner funnel. After rinsing with 250 ml of distilled water, the resin was air dried for 5 minutes through a damp cloth placed over the top of the funnel. A 3-5 gm sample of this prepared resin was placed in a dried and weighed sample

tube, reweighed, and then dried at 105-110°C for 16 hours. The sample and tube were finally reweighed, and the MRC value calculated from equation (5.2). MRC values were usually determined in duplicate.

3.3.4 Equilibrium Studies

Equilibrium isotherms of a system are determined by a series of experiments in which solution and resin are contacted together for a sufficiently long period to ensure equilibrium is attained. The resin samples are then eluted and analysed together with the liquid.

The anion and cation experimental procedures are similar, except for the length of time each experiment is left to equilibrate. Because the anion kinetics are significantly slower than those of the cation resins, the anion equilibrium tests were left overnight while the cation tests were left for only an hour.

The steps involved in a typical equilibrium determination are given below. This 0,125N Na^+/H^+ equilibrium is used as an example. The aim of these tests was to obtain an even spread of data points to produce an accurately plotted isotherm.

i) Two 14,65 ml aliquots of screened and centrifuged (see Sections 3.3.1 and 3.3.2.2) Na^+ form resin were placed in separate 400 ml glass stoppered bottles with 100 ml of 0,125N HCl and 100 ml of 0,125N NaCl. These bottles were placed on a flat bed shaker and allowed to equilibrate for two hours with gentle agitation.

ii) The two resin samples were eluted with $CaCl_2$ and this elutant solution and equilibrated liquid were analysed for Na^+ and H^+ (titration). A separation factor ($\alpha_{Na^+}^{H^+}$) was calculated from these results, using equation (2.16).

iii) From this initial $\alpha_{Na^+}^{H^+}$ value, liquid and resin volumes, which would result in an even spread of data points, were calculated, using equation (4.1). The required

resin and liquid quantities (taken in duplicate) were placed in glass bottles and again allowed to equilibrate for two hours. These samples were then analysed, and the respective ion fractions (x and y) and separation factors calculated from the number of equivalents of each species present. An average separation factor ($\alpha^{H^+}_{Na_{ave}}$) was worked out, and from this, intermediate points on the isotherm could be calculated to give an even spread of data points over the whole concentration range, and hence achieve a more accurate plot.

iv) For the remaining equilibrium tests performed, the only change in the technique was the solution concentration and the form in which the resin was initially loaded.

3.3.5 Kinetic Studies

Kinetic runs were performed in order to determine the rate of specific ion exchange in simple binary, as well as ternary, ionic systems. Both the fractional sampling apparatus and the conductiometric apparatus were used for these studies, and the methods and procedures of both are discussed in turn in Sections 3.3.5.1 and 3.3.5.2 respectively.

Both regeneration and loading kinetic studies were performed on this apparatus. The only difference between the two systems was the ionic form of the resin and the solution type. For example, Na^+ loading involved H^+ form resin and NaCl solution, while the equivalent Na^+ regeneration involved Na^+ form resin and HCl solution. The experimental techniques and methods remained the same.

3.3.5.1 Cation and Anion Studies on the Fractional Sampling Apparatus

All the binary and ternary inorganic counter-ion kinetic studies were performed on this apparatus. The steps that were followed in a typical run are outlined below. The only difference between the cation and anion studies was the length of time between samples (see points ii) and iv) below).

i) A screened, centrifuged and preloaded resin sample (of the correct, measured volume to give the required R/L ratio) was placed in a 50 ml plastic syringe. This was used to instantaneously start the reaction by "injecting" the sample into the reaction vessel at the initiation of a run.

ii) The sample tray was loaded with cups, and cup number 34 (see Fig. 3.4) (in the case of cation studies, and cup number 35 in the case of anion studies) was placed under the delivery tube. This ensured sufficient time for the reaction liquid to be pumped through the tubing, such that the sample that was delivered into cup 1 (see Fig. 3.4) corresponded to the start of the run (t=0). The time delay switch was set at 5 seconds for cation studies (or 30 seconds in the case of anion studies) and the correct quantity of solution (minimum of 400 ml) was placed in the reaction vessel. The stirrer was activated and the sampling tube was positioned.

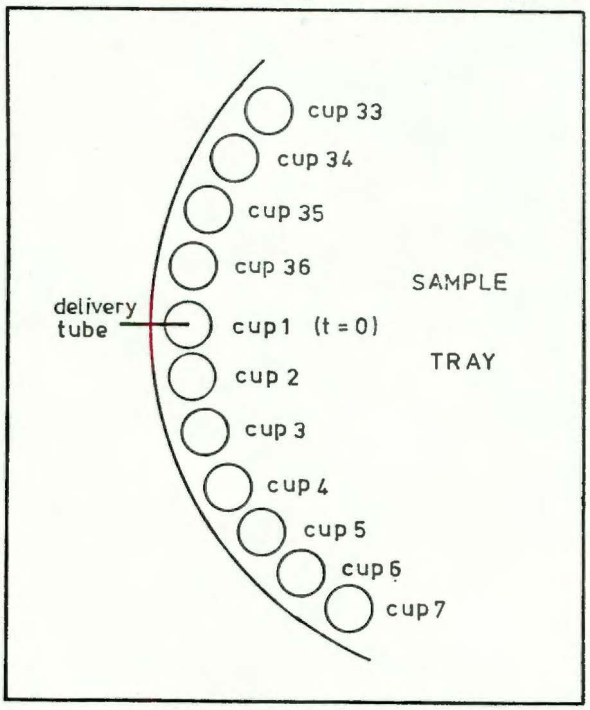

Fig. 3.4: Schematic Representation of the Fractional Sampler Tray Showing the Cup Numbers.

iii) The run was initiated by simultaneously "injecting" the resin, and switching on the multiple timer.

iv) The time selector switch was set to 10 seconds (1 minute for anion studies) as cup 6 (see Fig. 3.4) moved into position below the delivery tube. This convenient point of switch-over resulted in longer time periods between successive samples, ensuring a relatively larger number of data points at the beginning of the run where the exchange was most rapid, while allowing sufficient time for the end of the run to be accurately plotted.

v) The full cups (see ii) above) were replaced, and at the end of the run (315 seconds for cation runs and 33 minutes for anion runs) the multiple timer was switched off and the 36 cups were loaded onto a wooden holder and analysed for the required ions.

vi) The sampling tube was removed from the solution and the tubes pumped empty. The reaction vessel was continually stirred until equilibrium had been attained (30 minutes for cation runs and 2½ hours for anion runs), after which a sample was taken and analysed in order to obtain the C_{A_∞} value.

vii) The reaction vessel and tubes were rinsed with distilled water before re-use.

3.3.5.2 Anion COD Studies on the Conductiometric Apparatus

The formic, propionic and butyric acid artificial COD anion kinetic runs were performed on this apparatus. The steps involved in a typical run are outlined below.

i) A screened, centrifuged and preloaded resin sample was loaded into a 50 ml plastic syringe in the same way as for the run on the fractional sampling device described in Section 3.3.5.1(i) above.

ii) Two beakers, containing samples of the maximum and minimum expected acid concentrations, were prepared. The sine wave generator was set at 1800 Hz, and the conductivity of each solution was measured, using the conductivity

probe. The required displacement of the recorder pen was set, using the variable resistor and the zero and gain controls on the amplifier and recorder.

iii) The correct volume and concentration of the exchanging solution was placed in the reaction vessel, and the stirrer inserted and activated. The chart speed of the Heathkit pen recorder was set at 1 inch/minute, and the conductivity probe placed in the exchanging solution. The zero on the recorder was then checked and the chart set in motion in order to obtain a base line.

iv) At a convenient point on the chart paper, the run was initiated by "injecting" the resin sample into the stirred reaction vessel. The system was left to run until the pen recorded a near horizontal line (equilibrium condition - approximately 30 minutes for cation studies and 2 hours for anion studies). The recorder and instruments were switched off and the probe removed from the reaction vessel.

v) A sample of solution was taken and the vessel left stirring for a further two hours, after which time another sample was taken. These two samples, as well as one of the initial, unreacted solution, were analysed, and the results compared with the calibration of the plot. In this way, the C_{A_o} and C_{A_∞} values were determined.

vi) Calibration of the recorder plot was achieved by measuring the pen deflection at four or five known, intermediate acid concentrations, and curve fitting the results. In this way, a correlation of displaced height against concentration was obtained (usually not linear) and thus concentration data at fixed time intervals could be calculated by measuring the graph height and the corresponding distance from the beginning of the run.

3.4 PRESENTATION OF RESULTS

The kinetic results are presented in the form of a fractional approach to equilibrium (designated by the symbol F(t)) versus time (in seconds) plot. Equation (5.3) was used to calculate cation F(t) values, and equation (6.1) used to calculate anion and COD F(t) values from the concentration data obtained from the results of the fractional sampling (see Section 3.3.5.1) and conductiometric (see Section 3.3.5.2) apparatus. These detailed results are tabulated in Appendices C and D for cation and anion studies respectively.

In all kinetic presentations and discussions the word "kinetics" is used to describe the kinetic rate of an exchange or system. Further, for ease of reference, in addition to the contents page at the beginning of this thesis, a detailed contents description is included at the beginning of each of the three result chapters (4, 5 and 6). The % ratios in the figure captions refer to Na^+ and Ca^{2+} respectively.

The equilibrium isotherms are plotted on the standard liquid ion fraction (y) versus resin ion fraction (x) plots. The detailed results of this work are tabulated in Appendix B.

3.5 METHODS OF ANALYSIS

3.5.1 Cation Analyses

The analysis of Na^+ and Ca^{2+} was performed on a Varian Techtron Model 1000 atomic absorption spectrophotometer. Standard solutions of known concentration were prepared, the concentration range of these standards being dependent on the sensitivity of the apparatus for the particular ion being measured.

The atomic absorption spectrophotometer was calibrated with these solutions, and the concentration of the samples to be analysed was then compared with those of the standards.

It was found that the readings were reproducible to

within 3%, and this value was taken as the acceptable accuracy for cation F(t) curves (see Appendix E). The instrument settings and relevant theory are outlined in Appendix E, Section E.1.

3.5.2 Anion Analyses

Both Cl^- and SO_4^{2-} were analysed on a Technicon Auto Analyser II. Both methods of automatic analysis required less than 1 ml of solution and depended on specific colormetric reactions and measurement. A detailed description of the methods is outlined in Appendix E, Section E.2.

3.5.3 COD Analyses

The standard COD test was performed on samples of formic, propionic and butyric acids to determine the organic COD equivalent of each of the resins. The COD test is a common method of presenting organic matter concentrations in a sewage effluent [42]. A detailed description and method is outlined in Appendix E, Section E.3.

CHAPTER 4 CONTENTS

presented in detail while, for the 0,50N Na^+/H^+ and both Ca^{2+}/H^+ equilibria, only the final results will be given (the detailed results for these cases being presented in Appendix B). The systems will be compared and discussed in Section 4.2.3.

4.2.1.1 Na^+/H^+ System

(a) 0,125N Concentration:

The method used to determine accurate equilibrium isotherms involved initially obtaining three (or more) rough data points from which a separation factor (α_B^A) could be calculated. Using this α_B^A value, liquid and resin quantities were calculated to produce evenly spaced equilibrium points on the x-y diagram. From these points, an accurate separation factor was calculated from the calculated resin and liquid quantities, and additional points on the curve could be obtained (Equation (4.1)) so as to permit a smooth equilibrium isotherm to be drawn

$$x_A = \frac{\alpha_B^A \cdot y_A}{y_A(\alpha_B^A - 1) + 1} \qquad (4.1)$$

where α_B^A = separation factor;

y_A = ionic fraction A in liquid;

x_A = ionic fraction A in resin.

Table 4.1 presents the initial data points and α_B^A values.

The average $\alpha_{H^+}^{Na^+}$ is 1,31, and this was used to calculate the theoretical resin and liquid quantities (presented in Table 4.2) which will produce evenly spaced, accurate data points.

The detailed liquid and resin results are tabulated in Appendix B, Table B-1. The accurate ion fractions are calculated from these results, together with the data points calculated from an average separation factor of 1,65 (using Equation (4.1)) are tabulated in Table 4.3.

TABLE 4.1

INITIAL EQUILIBRIUM RESULTS FOR
0,125N ZEROLIT 625 Na^+/H^+ SYSTEM

y_A	x_A	$\alpha_{H^+}^{Na^+}$
0,2	0,18	1,24
0,4	0,32	1,42
0,75	0,70	1,29

TABLE 4.2

LIQUID AND RESIN QUANTITIES FOR
0,125N ZEROLIT 625 Na^+/H^+ EQUILIBRIUM

$y_{H_{theor.}}$	ml resin (Na^+ form)	ml 0,125N HCl	ml 0,125 NaCl
0,2	14,65	100	230
0,25	14,65	100	100
0,4	14,65	500	25,6
0,75	14,65	120	29

TABLE 4.3

FINAL EQUILIBRIUM EXPERIMENTAL AND CALCULATED DATA POINTS FOR 0,125N ZEROLIT 625 Na^+/H^+ SYSTEM

x_H	y_H
+0,05	0,08
*0,18	0,27
*0,27	0,39
+0,40	0,54
*0,52	0,68
+0,60	0,72
+0,80	0,88
+0,95	0,97

* Results calculated from experimental data (Table B-1).
+ Results calculated from experimentally determined $\alpha_{H^+}^{Na^+}$ value.

Fig. 4.1 presents the final equilibrium isotherm plotted from the above data points.

(b) 0,50N Concentration:

Detailed results are tabulated in Appendix B, Tables B-2 to B-4.

The final data points, together with those points calculated from the average separation factor ($\alpha_{H^+}^{Na^+}$) of 1,80 (see Table B-4) are presented in Table 4.4.

TABLE 4.4

FINAL EQUILIBRIUM EXPERIMENTAL AND CALCULATED DATA POINTS FOR 0,50N ZEROLIT 625 Na^+/H^+ SYSTEM

x_H	y_H
+0,06	0,11
*0,16	0,23
+0,22	0,36
*0,36	0,50
*0,59	0,75
+0,72	0,84
+0,90	0,95
+0,96	0,98

* Results calculated from experimental data (Table B-4).
\+ Results calculated from experimentally determined $\alpha_{H^+}^{Na^+}$ value.

The equilibrium isotherm represented by this data is plotted in Fig. 4.2.

4.2.1.2 Discussion of Zerolit 625 Na^+/H^+ Equilibria

Figs. 4.1 and 4.2 show the equilibrium isotherms for the Na^+/H^+ system at 0,125N and 0,50N respectively. The separation factors calculated from the experimental data ($\alpha_{H^+}^{Na^+}$ at 0,125N = 1,65 and $\alpha_{H^+}^{Na^+}$ at 0,50N = 1,80) compare well with the value of 1,50 obtained by Giddey [18] at a concentration of 0,05N. (The two figures show both the experimentally determined points and those "fill-in" points calculated from the average separation factor.)

Fig. 4.3 compares the Na^+/H^+ equilibria at the two concentrations. As is shown, the concentration has minimal effect on the equilibrium, and the isotherm is thus satisfactorily represented by an average separation factor

of 1,7. As is discussed and explained in Section 2.4.2.1, systems involving counter-ions of the same valency (as are Na^+ and H^+) do not show any concentration effects. In such a case, any change in Donnan potential with solution concentration would equally affect both counter-ions, and thus no relative change in resin selectivity would be expected.

Concentration effects are, however, very marked in systems involving counter-ions of different valencies (see Sections 4.2.1.4 and 4.2.2.4) [25].

Giddey [18] obtained similar results for the Na^+/H^+ system at concentrations as low as 0,02N.

4.2.1.3 $\underline{Ca^{2+}/H^+}$ System

As for the Na^+/H^+ system, these equilibria were measured at both 0,125N and 0,50N concentrations. The method used to obtain both experimental data points and points calculated from an average separation factor ($\alpha_{H^+}^{Ca^{2+}}$) were similar to that of the previous system.

The detailed results are tabulated in Appendix B, Tables B-5 to B-8. The accurate data points, together with those points calculated from the average separation factors ($\alpha_{H^+}^{Ca^{2+}}$) of 23 and 11,4 (for 0,125N and 0,50N concentrations respectively) (see Tables B-7 and B-8) are presented in Table 4.5.

TABLE 4.5

FINAL EQUILIBRIUM EXPERIMENTAL AND CALCULATED DATA POINTS FOR ZEROLIT 625 Ca^{2+}/H^{+} SYSTEM

0,125N		0,50N	
x_H	y_H	x_H	y_H
*0,01	0,22	*0,04	0,32
+0,10	0,60	*0,22	0,76
*0,21	0,84	*0,43	0,90
+0,40	0,74	+0,64	0,95
+0,75	0,95	+0,80	0,98
+0,90	0,995	+0,90	0,995

* Results calculated from experimental data.
\+ Results calculated from experimentally determined $\alpha_{H^+}^{Ca^{2+}}$.

These data points are plotted as equilibrium isotherms in Figs. 4.4 and 4.5.

4.2.1.4 Discussion of Ca^{2+}/H^{+} Equilibria

Figs. 4.4 and 4.5 show the Ca^{2+}/H^{+} equilibrium isotherms at 0,125N and 0,50N respectively. From these, Fig. 4.6 is drawn, comparing the isotherms at the two different concentrations (graphs 2 and 3). It is immediately evident that the two isotherms differ, due to the concentration difference of the loading solution. As has been commented on in Section 4.2.1.2, the relative resin selectivity for the counter-ions increases with decreasing solution concentration in systems where the counter-ions are of different valencies (as are Ca^{2+} and H^{+}). This effect may be explained by the Donnan Potential [43] (see Section 2.3.3) which states that the forces attracting counter-ions into the resin pore are proportional to the ionic charge of the counter-ion and the

absolute value of the Donnan potential increases with decreasing concentration and increasing resin capacity [25] (see Section 2.4.2.1). This is well demonstrated in Fig. 2.5, where, for the divalent/monovalent Cu^{2+}/Na^{+} system, the equilibrium isotherm moves closer to the diagonal (decreasing selectivity) with increasing solution concentration, until, at a concentration of approximately 2N, it crosses over the diagonal and continues moving away from it in the opposite direction, showing a selectivity change as discussed below.

4.2.1.5 Discussion on the Comparison Between Na^{+}/H^{+} and Ca^{2+}/H^{+} Equilibria

Fig. 4.6 also compares the equilibria of these two systems. It shows that the Na^{+}/H^{+} isotherm is considerably closer to the diagonal than is the Ca^{2+}/H^{+} isotherm. This indicates that the resin has a higher affinity for the Ca^{2+} counter-ion than for the Na^{+} counter-ion. This is evident also from the values of the respective average separation factors - $\alpha_{H^{+}}^{Na^{+}} = 1,7$ and $\alpha_{H^{+}}^{Ca^{2+}} = 20$. This tendency of the resin to be more selective towards the divalent counter-ion stems from the fact that the divalent counter-ion has a higher charge density, due to its relatively small hydrated radius and double charge (see Section 5.2.2.2(b)) and, as stated in Section 4.2.1.4, the greater the ionic charge density on the ion, the stronger the forces attracting them into the resin bead.

The fact that the univalent Na^{+}/H^{+} system shows no concentration effect while the divalent Ca^{2+}/H^{+} system shows a marked concentration effect was explained in Sections 4.2.1.2 and 4.2.1.4.

The reason for the equilibrium isotherms all lying above the diagonal is that the resin is more selective for Na^{+} and Ca^{2+} than for H^{+}. The explanation for this follows on from the discussions above, and is explained in detail in Section 4.2.2.2.

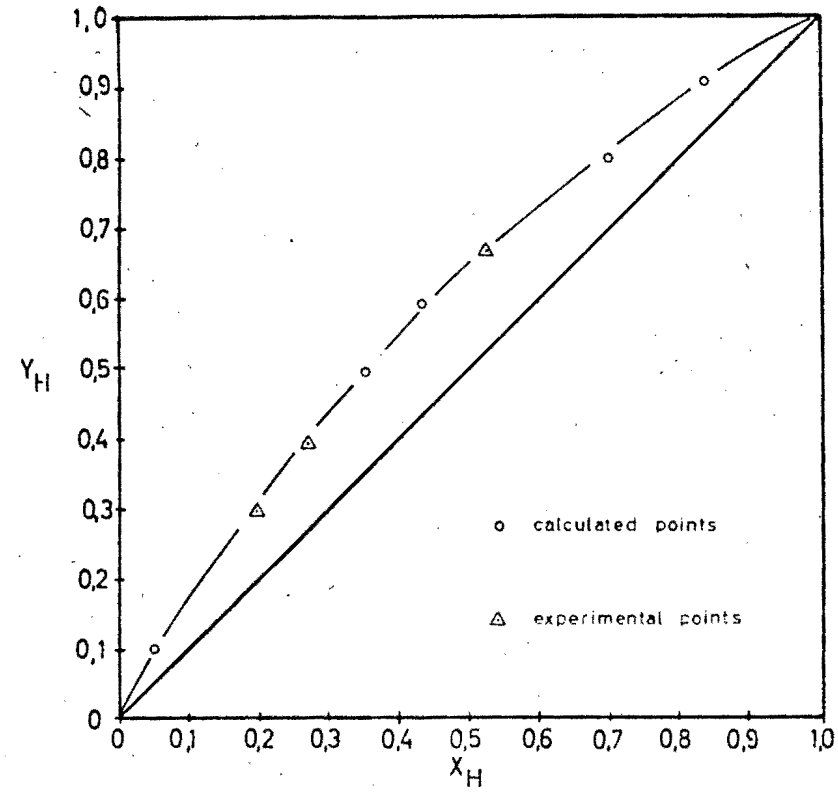

Fig. 4.1: Na^+/H^+ Equilibrium at 0,125N on Zerolit 625

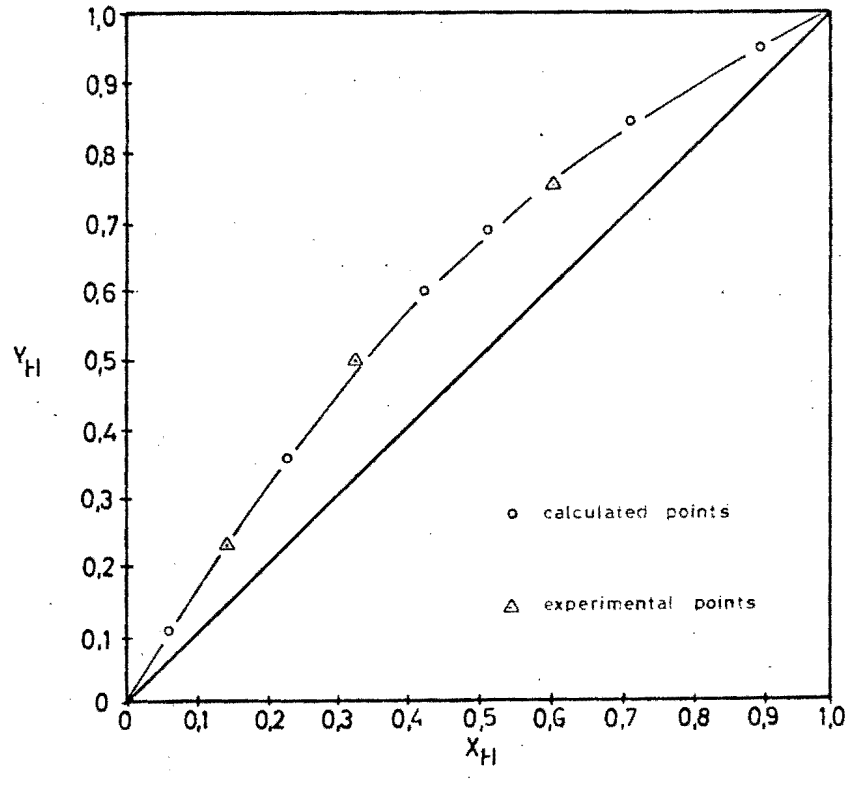

Fig. 4.2: Na^+/H^+ Equilibrium at 0,50N on Zerolit 625

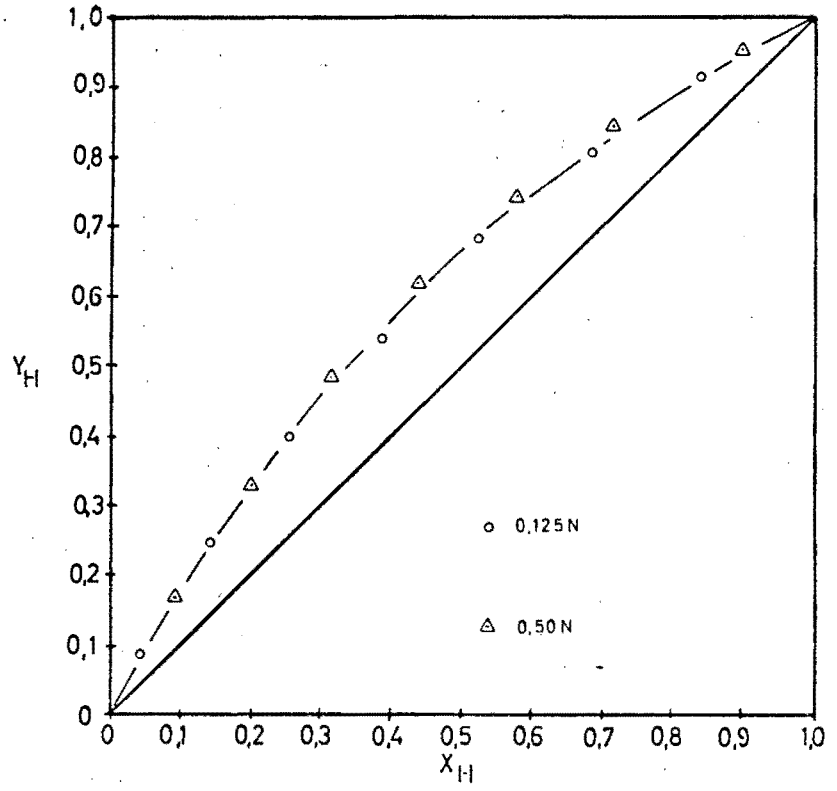

Fig. 4.3: Comparison Between the Na^+/H^+ Equilibria on Zerolit 625 at 0,125N and 0,50N Concentrations

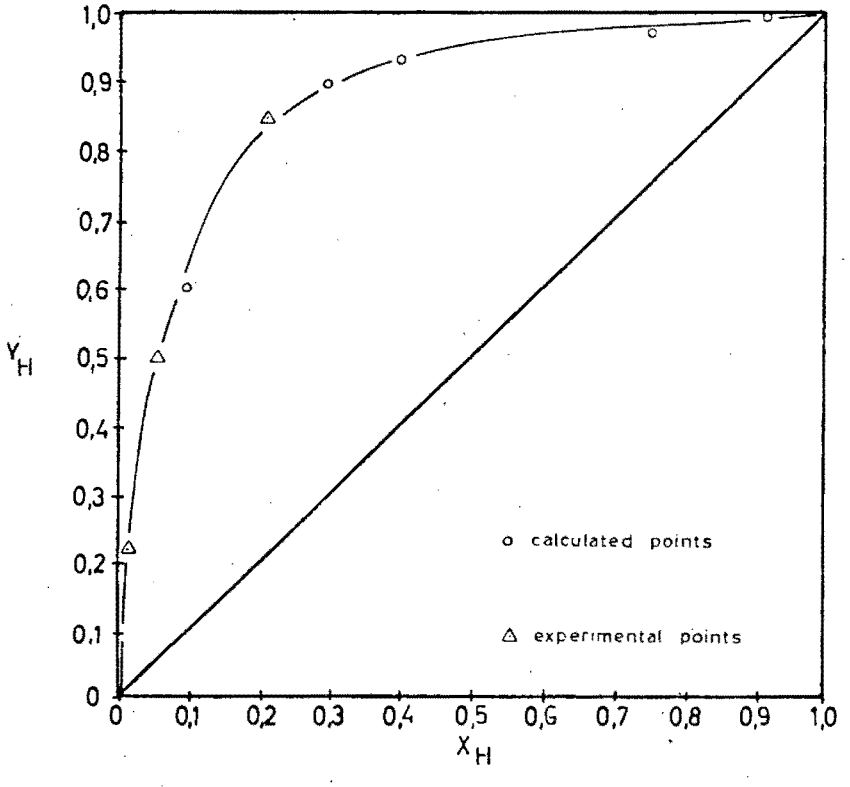

Fig. 4.4: Ca^{2+}/H^+ Equilibrium at 0,125N on Zerolit 625

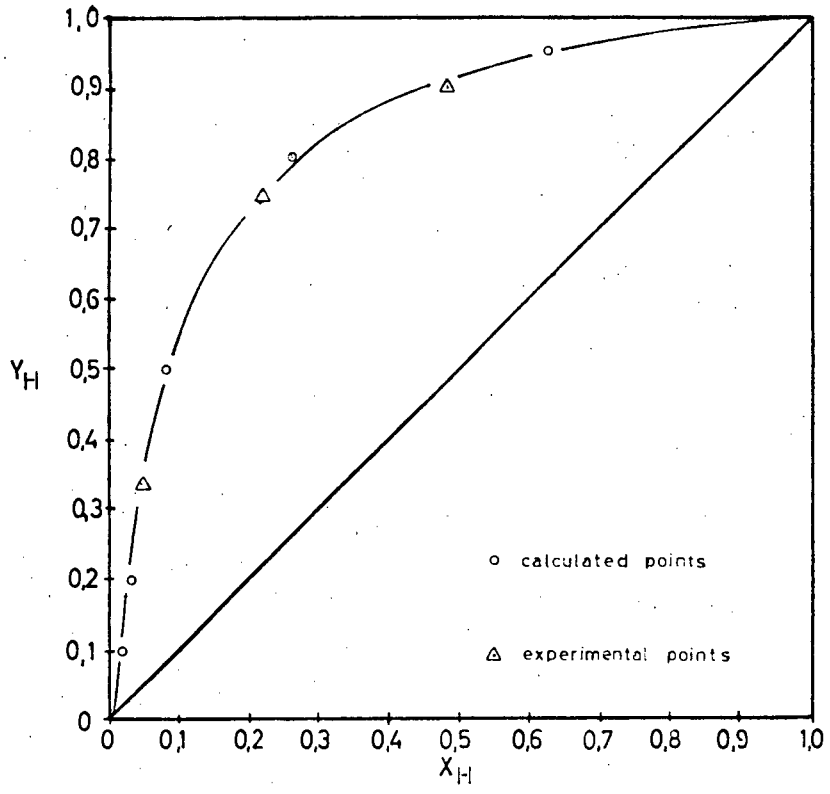

Fig. 4.5: Ca^{2+}/H^+ Equilibrium at 0,50N on Zerolit 625

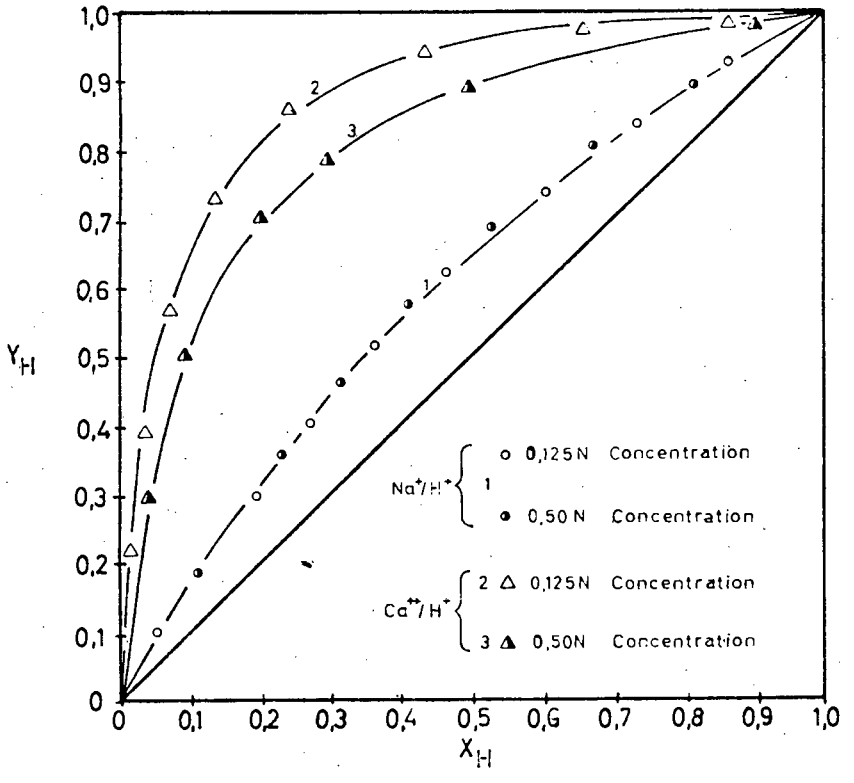

Fig. 4.6: Comparison Between the Ca^{2+}/H^+ Equilibrium at 0,125N and 0,50N Concentrations, and Between Ca^{2+}/H^+ and Na^+/H^+ Equilibria on Zerolit 625

4.2.2 The Gel Resin

As for the macroporous resin, the Na^+/H^+ and Ca^{2+}/H^+ equilibria were investigated at both 0,125N and 0,50N concentrations. A resin of 6,75% DVB content was used throughout these studies.

4.2.2.1 Na^+/H^+ System

The same initial $\alpha_{H^+}^{Na^+}$ values as for Zerolit 625 were taken (i.e. $\alpha_{H^+}^{Na^+}$ at 0,125N = 1,55 and at 0,50N = 1,80), and the calculated resin and liquid quantities for both concentrations are tabulated in Table B-9. The final results are presented in Tables B-10 and B-11, and the data points calculated from these experimental results and calculated using average separation factors ($\alpha_{H^+}^{Na^+}$ at 0,125N = 1,10; $\alpha_{H^+}^{Na^+}$ at 0,50N = 1,20 - see Tables B-10 and B-11) are presented in Table 4.6.

TABLE 4.6

FINAL EQUILIBRIUM EXPERIMENTAL AND CALCULATED DATA POINTS FOR GEL RESIN Na^+/H^+ SYSTEM

0,125N		0,50N	
x_H	y_H	x_H	y_H
*0,17	0,18	*0,21	0,19
*0,31	0,32	*0,38	0,39
*0,53	0,55	*0,56	0,58
*0,74	0,77	*0,76	0,79
+0,89	0,90	*0,93	0,95

* Results calculated from experimental data.

\+ Results calculated from experimentally determined $\alpha_{H^+}^{Na^+}$.

These data points are plotted as equilibrium isotherms in Figs. 4.7 and 4.8.

4.2.2.2 Discussion of Na^+/H^+ Equilibria

Figs. 4.7 and 4.8 show the Na^+/H^+ equilibrium at 0,125N and 0,50N respectively. These two plots are combined in Fig. 4.9, which compares the equilibria at these two concentrations. It is clear from this latter figure that, for the Na^+/H^+ equilibrium of Zerolit 625 resin (Fig. 4.3), the concentration has no effect on the selectivity of the resin and thus a concentration change does not affect the equilibrium isotherms. Since both the counter-ions in the exchange are monovalent (Na^+ and H^+), this result is consistent with theory discussed in Section 4.2.1.2.

The fact that the equilibrium isotherms lie slightly above the diagonal indicates that the resin has marginally greater selectivity for the Na^+ compared with the H^+. This is evident from the fact that the equilibrium curve is deflected to the left of the diagonal, showing that, at equilibrium, the liquid (y) has a larger H^+ ion fraction than the resin. Thus, at the same time, the resin would have a lower ionic fraction of H^+ than the liquid (by material balance), indicating a larger ionic fraction of Na^+. The resin, therefore, has a slightly greater selectivity for Na^+. This is consistent with results found by Dorfner [6], who quotes a selectivity coefficient for H^+ in a sulphonic acid resin as 1,30 and for Na^+ as 1,49.

4.2.2.3 Ca^{2+}/H^+ System

Initial data points were calculated from the separation factors determined for the similar Zerolit MPH system ($\alpha_{H^+}^{Ca^{2+}}$ at 0,125N = 23; $\alpha_{H^+}^{Ca^{2+}}$ at 0,50N = 11,4 - see Tables B-7 and B-8). The resin and liquid quantities are tabulated in Table B-12 and the results from these given in Tables B-13 and B-14. The final experimental and calculated data points are presented in Table 4.7.

The equilibrium isotherms represented by the data points in Table 4.7 are plotted in Figs. 4.10 and 4.11.

TABLE 4.7

FINAL EQUILIBRIUM EXPERIMENTAL AND CALCULATED DATA POINTS FOR GEL RESIN Ca^{2+}/H^{+} SYSTEM

0,125N		0,50N	
x_H	y_H	x_H	y_H
*0,08	0,27	*0,03	0,24
*0,12	0,65	*0,10	0,47
*0,35	0,91	*0,36	0,85
+0,60	0,95	*0,65	0,96
+0,90	0,995	+0,90	0,995

* Results calculated from experimental data points (Tables B-13 and B-14).

\+ Results calculated from experimentally determined $\alpha_{H^+}^{Ca^{2+}}$ values ($\alpha_{H^+}^{Ca^{2+}}$ at 0,125N = 13 and $\alpha_{H^+}^{Ca^{2+}}$ at 0,50N = 11,3).

4.2.2.4 Discussion of Ca^{2+}/H^{+} Equilibria

Figs. 4.10 and 4.11 show the Ca^{2+}/H^{+} equilibrium isotherms of gel resin at 0,125N and 0,50N respectively. Both curves lie well above the diagonal, indicating that the resin is far more selective for Ca^{2+} than it is for H^{+} (see Section 4.2.2.2). This is similar to results found for Zerolit 625 resin (see Section 4.2.1.3) and results found by Giddey [18] and Kunin [1]. Dorfner [6] states that the selectivity of the exchanger for H^{+} ions depends on the strength of the acids formed from the functional group of the exchanger and the H^{+} ion. For strong acid exchangers, the selectivity for the H^{+} ions is usually lower than for the other counter-ion.

Fig. 4.12 compares the Ca^{2+}/H^{+} isotherms at the two different concentrations. It is again evident that concentration has a marked effect on the equilibrium (graphs

2 and 3). This is similar to the results found for the Zerolit 625 resin, and can likewise be explained by the fact that the selectivity for the Ca^{2+} increases with decreasing solution concentration, resulting in the equilibrium isotherm moving away from the diagonal (see Section 4.2.1.4).

4.2.2.5 Discussion on the Comparison Between Na^+/H^+ and Ca^{2+}/H^+ Equilibria

Fig. 4.12 shows, also, the difference in selectivity of the resin for Ca^{2+} as compared with Na^+, as well as the effect of concentration on the two equilibrium systems.

As was found for the macroporous Zerolit 625 (Fig. 4.6), the resin shows a greater selectivity for Ca^{2+} than for Na^+. This is again due to the higher charge density of the Ca^{2+} counter-ion as compared with the Na^+ counter-ion (since the former is divalent compared with the monovalent Na^+, with both having approximately the same hydrated radius). Similar results were obtained by Soldatov and Högfeldt [44] for Na^+/H^+ and Ca^{2+}/H^+ systems. Sections 4.2.1.4 and 4.2.1.5 explain the reasons for this in more detail.

This concentration effect is discussed by both Dorfner [6] and Kunin [1]. Dorfner states that, at low concentrations and at room temperature, all exchangers give preference to polyvalent ions over the monovalent ones in accordance with the typical selectivity sequence of:

$$Na^+ < Ca^{2+} < La^{3+} < Th^{4+} \quad .$$

Kunin quotes values for the selectivity coefficient κ_A^B (see Section 2.4.1.1(b) for definition and use) for a typical sulphonated styrene-divinylbenzene exchange resin of 8% DVB content. The values for H^+/Na^+ and H^+/Ca^{2+} are given as 2,0 and 42 respectively, showing the far greater selectivity of the resin for the Ca^{2+} counter-ion over the Na^+ one.

The effect of the different concentrations on the two systems is also shown in Fig. 4.12. The equilibrium of the

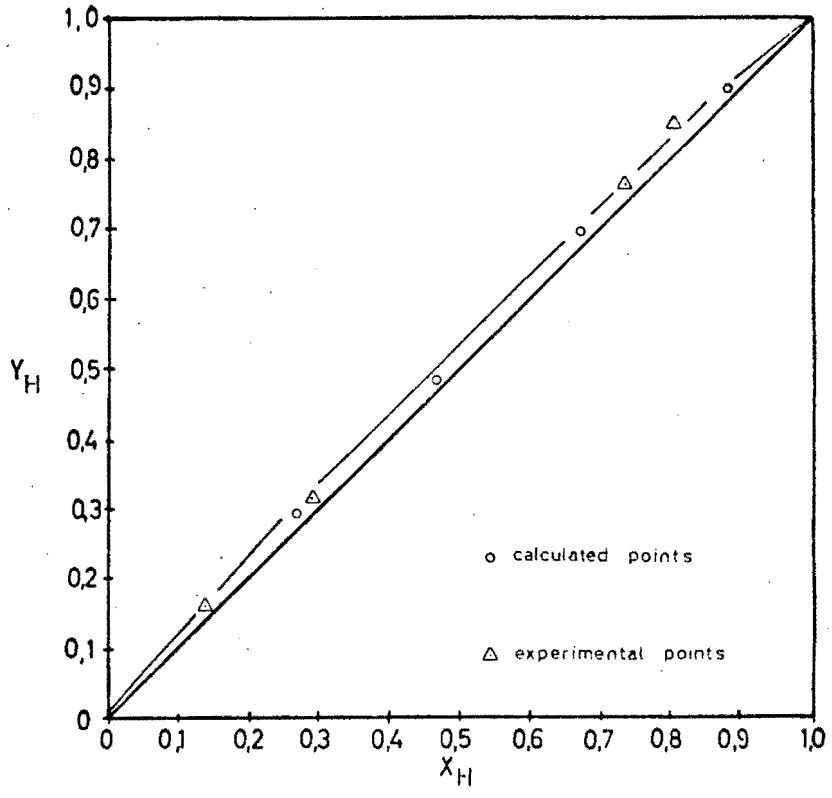

Fig. 4.7: Na^+/H^+ Equilibrium at 0,125N on Cation Fort

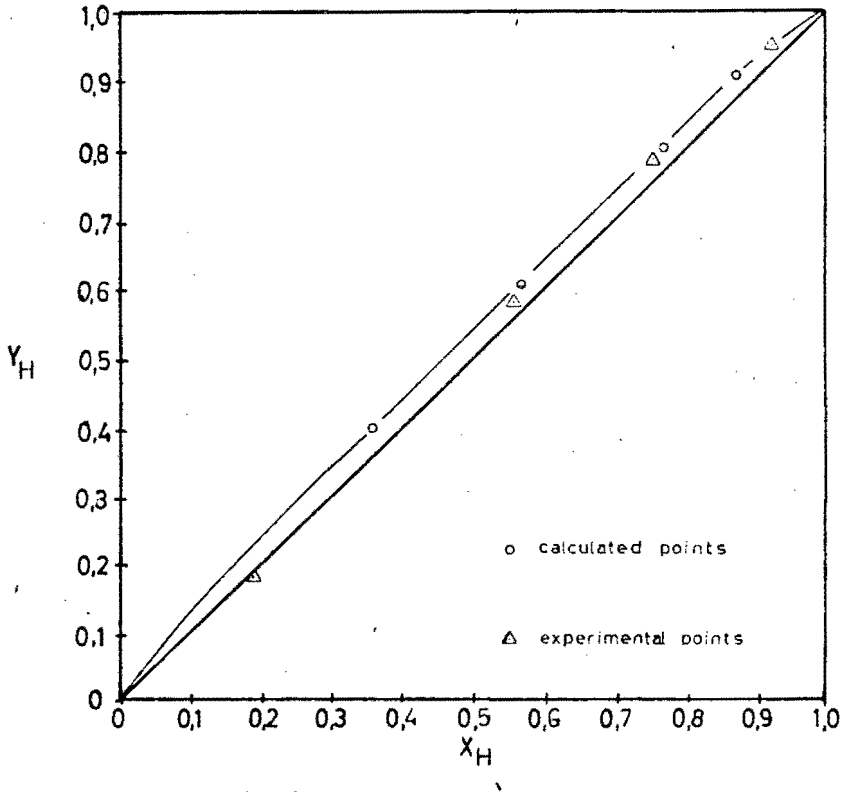

Fig. 4.8: Na^+/H^+ Equilibrium at 0,50N on Cation Fort

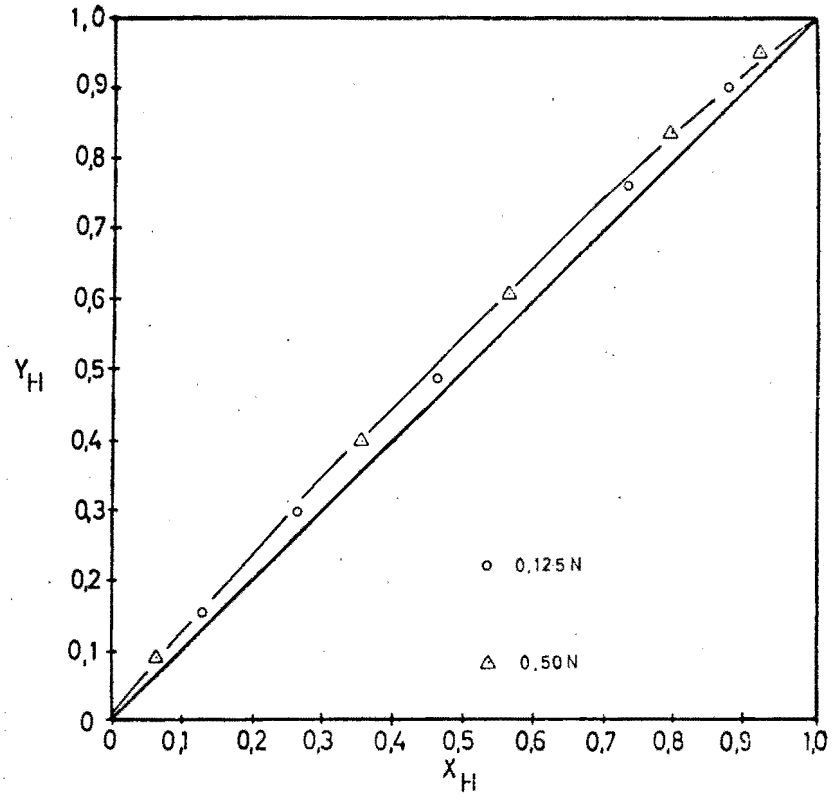

Fig. 4.9: Comparison Between the Na^+/H^+ Equilibria on Cation Fort at 0,125N and 0,50N Concentrations

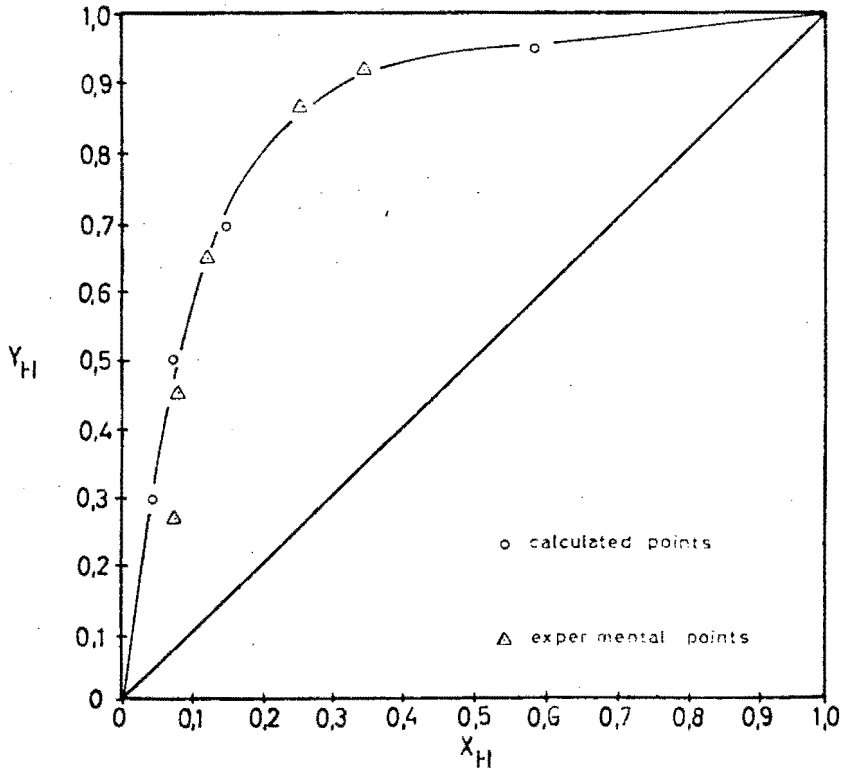

Fig. 4.10: Ca^{2+}/H^+ Equilibrium at 0,125N on Cation Fort

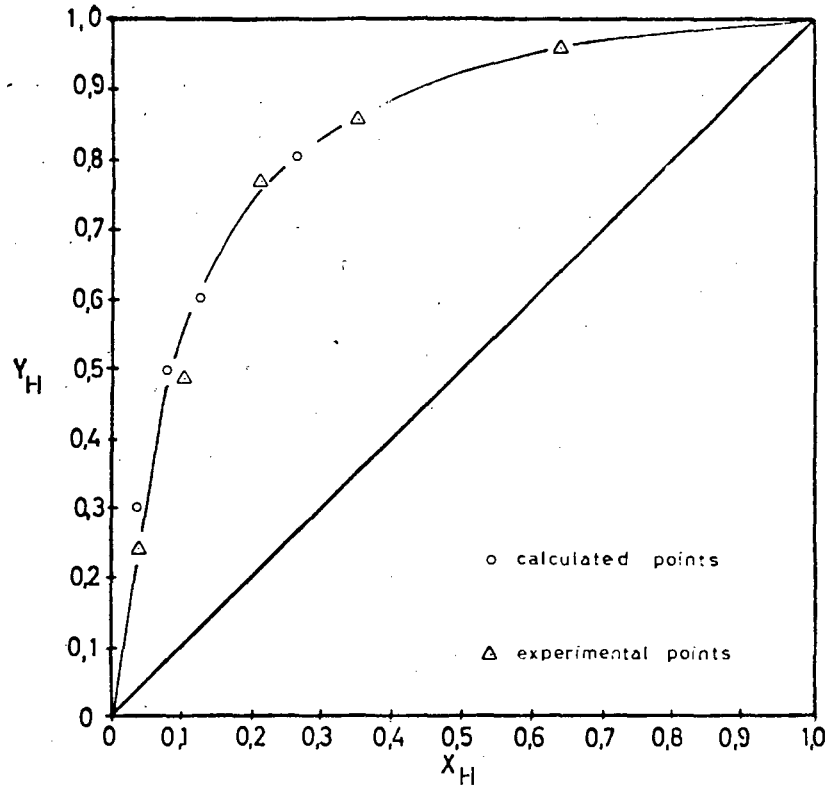

Fig. 4.11: Ca^{2+}/H^+ Equilibrium at 0,50N on Cation Fort

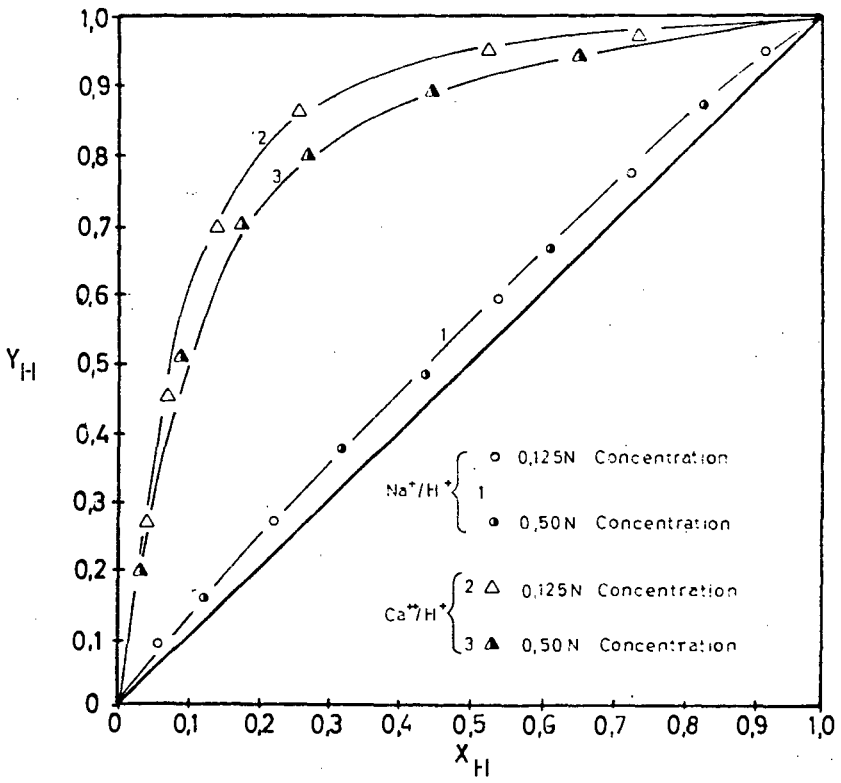

Fig. 4.12: Comparison Between Ca^{2+}/H^+ Equilibria at 0,125N and 0,50N Concentrations and Between Ca^{2+}/H^+ and Na^+/H^+ Equilibria on Cation Fort

mono-monovalent system (Na^+/H^+) is not affected by the concentration change (graph 1), while that of the mono-divalent system (Ca^{2+}/H^+) is (graphs 2 and 3). For this latter system, the equilibrium curve moves closer to the diagonal at increased solution concentration. This effect is again due to the relative selectivity changes of the two counter-ions with changing solution concentration - as the concentration of the bulk solution decreases, the Donnan potential increases. This change affects the counter-ions of different valency individually, and thus for multivalent systems a change in relative selectivity is noticed, while in univalent systems both counter-ions would be affected to an equivalent extent, and no relative change in selectivity would be noticed [18]. Reichenberg [45] sums up this effect for the multivalent Na^+/Ca^{2+} system by stating that "...it may be readily shown that the relative amounts of Ca^{2+} and Na^+ in the exchanger now depend on the total concentration of Ca^{2+} and Na^+ in the solution as well as on their relative concentrations".

4.2.3 Comparison Between the Macroporous Zerolit 625 Resin and the Gel Resin Equilibria

Fig. 4.13 compares the Na^+/H^+ equilibria for the two resin types, while Fig. 4.14 compares the corresponding Ca^{2+}/H^+ equilibrium at both 0,125N and 0,50N concentrations.

4.2.3.1 Na^+/H^+ Equilibrium Comparisons

It is clearly shown from Fig. 4.13 that the macroporous Zerolit 625 exhibits greater selectivity for the Na^+ counter-ion as compared with the gel resin, i.e. the Zerolit 625 isotherm lies further from the diagonal than that of the gel resin. This is further shown by their respective separation factors - $\alpha_{H^+}^{Na^+}$ for the macroporous resin = 1,70, while for the gel resin = 1,15 (see Tables B-1 and B-10). Possible reasons for this phenomenon are given in Section 4.2.3.2.

4.2.3.2 Ca^{2+}/H^{+} Equilibrium Comparisons

It is evident from Fig. 4.14 that, at 0,125N, the gel resin isotherms lie below those of the Zerolit 625 resin. This, however, is not as marked as in the Na^{+}/H^{+} system (see Fig. 4.13). At 0,50N, however, there is minimal difference between the two resins' equilibrium isotherms. Thus it seems that not only is the macroporous resin generally more selective for the loading counter-ion (Na^{+} or Ca^{2+}), but the effect decreases with increasing counter-ion hydrated radius and, where applicable, increasing concentration.

The reasons for these observations cannot all be clearly explained. The selectivity differences could not be attributed to interactions between the counter-ion and the resin matrix, since both resins are polystyrene sulphonated crosslinked polymer structures. Further, both exchanges involve identical solutions and thus co-ion associations in solution could have no effect. Both these factors are common reasons for selectivity differences [25] (see Section 2.4.2).

The difference can most likely be attributed to sieve action effects in the two resin types (see Section 2.4.2.3). The resins generally prefer the counter-ion with the smaller solvated volume [3,25] due to the fact that the absorption of the larger counter-ion results in greater swelling of the matrix and thus greater stress. Since the gel resin has smaller diameter pores than the macroporous resin (see Section 2.2.2), it is logical to assume that this sieve action effect would be more pronounced in the gel resin, tending to further exclude the larger counter-ions from the matrix and resulting in a subsequent decrease in the selectivity for this counter-ion. Fig. 4.15 shows this effect schematically.

Linked to this sieve action is the fact that the gel resin has a lower DVB content than the macroporous Zerolit 625 (6,75% for gel resin and approximately 8,5% for Zerolit 625). It is known [1,25] that a decrease in the DVB content

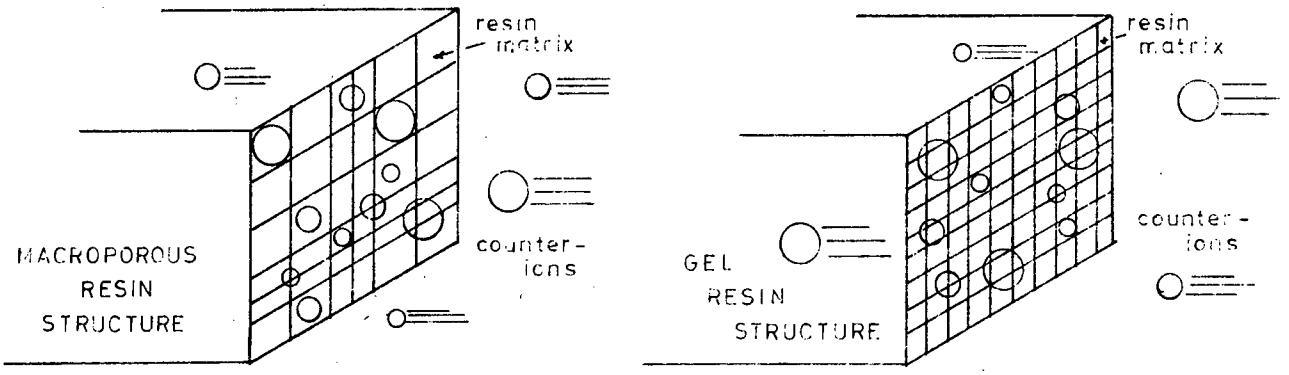

Fig. 4.15: Schematic Representation of Sieve Action in a Macroporous and Gel Resin.

of the resin is accompanied by a decrease in the resin's selectivity for larger counter-ions. This can, similarly, be attributed to sieve action effects of the resin matrix - the higher the degree of crosslinking (% DVB), the more rigid the resin matrix becomes, and thus less able to accommodate the larger counter-ions. The ions involved in the exchange do not themselves significantly affect this change in selectivity. Helfferich [25] quotes equilibrium constants (κ_B^A) for sulphonated polystyrene resins of differing DVB content for the exchange of various counter-ions with Li^+. Typical percent reductions in the κ_B^A values between resins of 4% and 8% DVB content are given in Table 4.8.

Similar data are cited by Kunin [1] for the exchange of various monovalent counter-ions with H^+ on an identical cation resin to that quoted by Helfferich above. Typical percent reductions in κ_B^A between resin of 4% and 8% DVB are given in Table 4.9.

The combinations of this property (viz. the differing DVB contents and the subsequent sieve action effect) could explain the reason for the relatively low selectivity for Ca^{2+} and Na^+ ions of the gel resin.

Since the percent reduction of the κ_B^A value is approximately equal for both the Ca^{2+}/H^+ and Na^+/H^+ systems

TABLE 4.8

K_B^A VALUES AND PERCENT REDUCTIONS FOR VARIOUS EXCHANGES ON SULPHONATED POLYSTYRENE RESIN OF 4% AND 8% DVB CONTENT

Exchanging Counter-Ions	K_B^A		% Reduction
	4% DVB	8% DVB	
Li^+/Na^+	1,58	1,98	20
Li^+/K^+	2,27	2,90	21
Li^+/Rb^+	2,46	3,16	22
Li^+/Ca^{2+}	4,15	5,16	20

TABLE 4.9

K_B^A VALUES AND PERCENT REDUCTIONS FOR VARIOUS MONOVALENT EXCHANGES ON POLYSTYRENE RESIN OF 4% AND 8% DVB CONTENT

Exchanging Counter-Ions	K_B^A		% Reduction
	4% DVB	8% DVB	
H^+/Na^+	1,5	2,0	21
H^+/K^+	2,4	3,0	19
H^+/Ls^+	3,1	3,9	20
H^+/Rb^+	3,3	4,3	23

(± 20%), and the equilibrium isotherms are further from the diagonal for the former system, the difference between the two resin types is not as marked for the Ca^{2+}/H^+ equilibria (see Fig. 4.14). Further, since the size of the Ca^{2+}

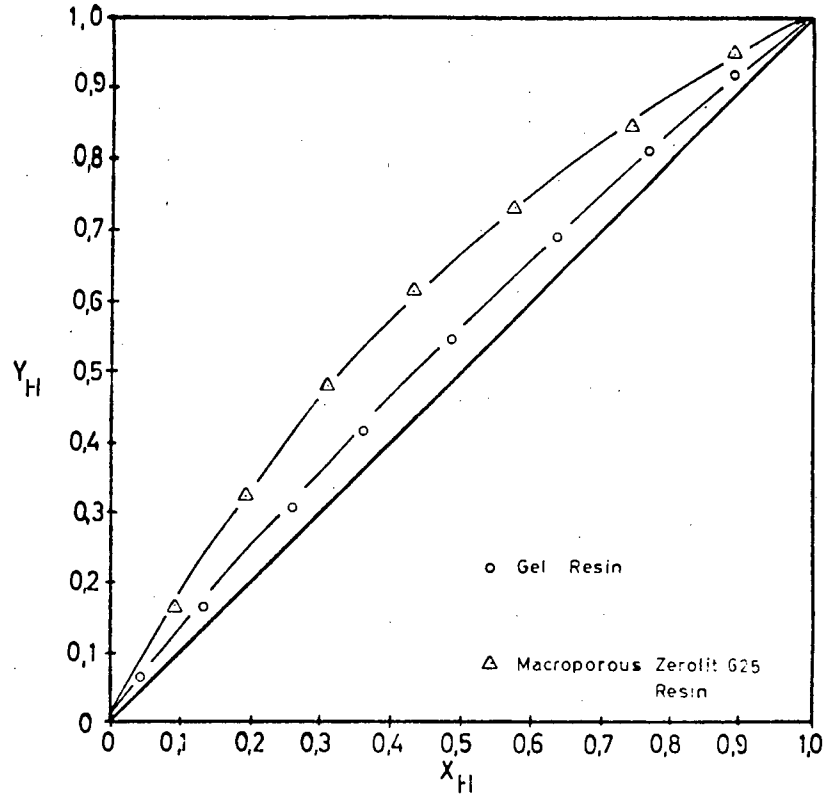

Fig. 4.13: Comparison Between the Na^+/H^+ Equilibria of Macroporous and Gel Resins

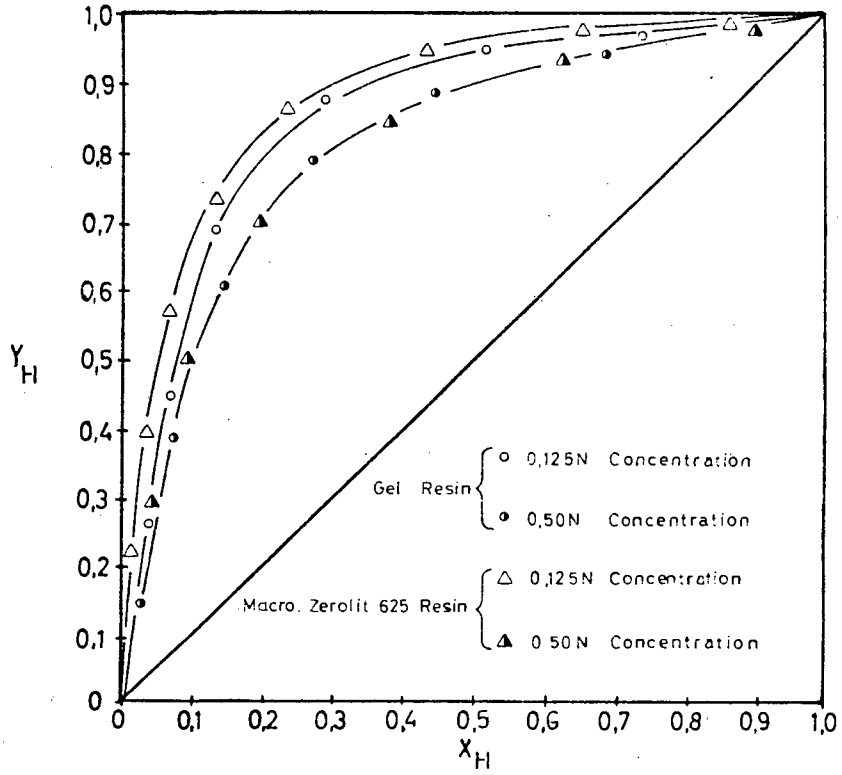

Fig. 4.14: Comparison Between the Ca^{2+}/H^+ Equilibria of Macroporous and Gel Resins

counter-ion does not differ greatly from that of Na^+, the sieve action will not increase between these two counter-ions, resulting in no increase in the "gap" between the resins' isotherms. However, the reason for this "gap" decreasing almost totally at 0,05N concentration is not clear, but could be linked to the tendency of the Ca^{2+}/H^+ selectivity to decrease at higher concentrations.

4.3 ANION RESIN EQUILIBRIUM

4.3.1 OH^-/Cl^- Equilibrium on Zerolit MPH Resin

This equilibrium was measured at 0,05N on Zerolit MPH in the free base (OH^-) form. Similar experimental procedures as for the cation equilibrium determinations were followed.

Assuming a separation factor ($\alpha_{OH^-}^{Cl^-}$) of 1000 (from Giddey [18]), resin and liquid quantities were calculated to give an even data spread. These are tabulated in Appendix B, Table B-15. The final experimental data points, as well as those calculated from an average separation factor of 420 (Table B-16), are presented in Table 4.10.

4.3.2 Discussion of Zerolit MPH OH^-/Cl^- Equilibrium

4.3.2.1 Comment on Equilibrium Isotherm

In order to adopt an equilibrium isotherm diagram similar to that of the cation system discussed previously, an hydroxyl ion (OH^-) was considered to exchange with a Cl^- ion, according to equation (4.2):

$$R - N - OH + HCl \rightleftharpoons R - N - HCl + OH^- \quad . \qquad (4.2)$$

In this way, equivalent ionic fractions of OH^- in each phase can be calculated from the chloride content in that phase, and presented in the form of the standard x-y plot in Fig. 4.16.

TABLE 4.10

FINAL EQUILIBRIUM EXPERIMENTAL AND CALCULATED DATA POINTS FOR ZEROLIT MPH OH^-/Cl^- SYSTEM AT 0,05N

x_{OH^-}	y_{OH^-}
*0,001	0,50
*0,002	0,70
+0,013	0,85
*0,160	0,99
*0,72	0,996

* Results calculated from experimental data (Table B-16).
\+ Results calculated from experimentally determined $\alpha_{OH^-}^{Cl^-}$ value.

Fig. 4.16, together with the high $\alpha_{OH^-}^{Cl^-}$ value, shows that the Zerolit MPH is extremely selective towards Cl^-, since the equilibrium isotherm lies far from the diagonal (see Section 4.2.2.2 for explanation). This results in difficulty in obtaining accurate data points, particularly in the corner area, since, at low x_H values, a very small change in the x_H value results in large changes in the y_H value and, similarly, at high x_H values, a very small change in the y_H value will result in very large changes in the x_H value. This also results in difficulty in obtaining accurate separation factor values, since a small deviation in the ion fraction results in a large deviation in the α value. This is well demonstrated in Table B-16, where $\alpha_{OH^-}^{Cl^-}$ values vary from 64 to 1100.

4.3.2.2 Effect of Selectivity on Anion Kinetics

The separation factor has a marked effect on the kinetics of film-diffusion controlled systems [37]. Since the majority of water desalination systems using ion exchange

incorporate an anion resin system at low (0,01N) concentrations, they involve film-diffusion controlled kinetics (see Section 2.5.3) and thus are susceptible to changing selectivities. Copeland et al. [37] found that, in such systems, where the counter-ion diffusivities were similar, a two-fold increase in the separation factor resulted in a 10-15% increase in the kinetics. Thus it is desirable to choose a system with a high α_B^A value but low D_B/D_A (where D_A refers to the diffusivity of counter-ion A) for the fastest kinetics. This idea is discussed in more detail in Chapter 6, Section 6.2.2.3(a).

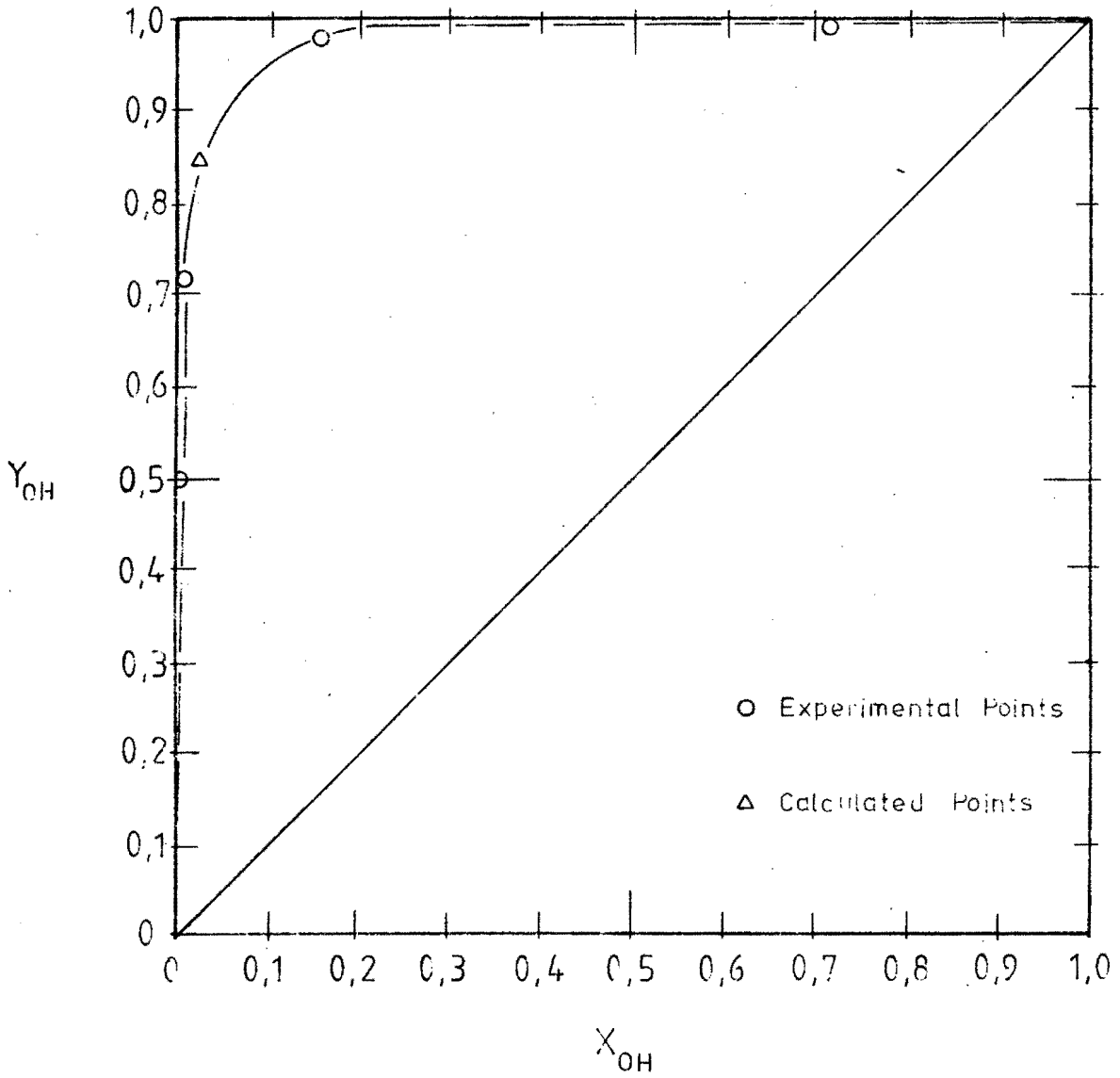

Fig. 4.16: OH^-/Cl^- Equilibrium at 0,05N on Zerolit MPH

CHAPTER 5 CONTENTS

Page

Page

CHAPTER 5

CATION KINETICS : RESULTS AND DISCUSSION

5.1 INTRODUCTION

In this Chapter the results of all the cation kinetic studies are presented and discussed.

The work is divided into two main sections:
(a) the results for Macroporous resin (Zerolit 625), and
(b) the results for the Gel type resin.
Within each of these groups is discussed the Na^+/H^+ and Ca^{2+}/H^+ binary exchange kinetics (binary referring to two counter-ion species involved in the exchange - one initially in the liquid phase and the other initially in the solid (resin) phase); and the $Na^+/Ca^{2+}/H^+$ ternary exchange kinetics (ternary referring to three counter-ion species involved in the exchange - one initially in the liquid phase and the other two initially in the solid (resin) phase; or two in the liquid and one in the resin). A counter-ion is a diffusing ionic species of opposite charge to the charge on the resin.

Regeneration and loading kinetics were studied for the binary system, at both 0,125N and 0,50N concentrations. The ternary kinetics were investigated at only one concentration (0,125N) for 50% Na^+/50% Ca^{2+} and 25% Na^+/75% Ca^{2+} relative initial concentrations for the loading systems, and similar relative degrees of resin preloading for the regeneration cases.

The results are tabulated in detail in Appendix C and presented in the main text in the form of a plot of the fractional approach to equilibrium (F(t)) versus time. The graphs appear after the relevant sections.

At the end of the Chapter, the two resin types are compared.

5.2 PERFORMANCE OF A MACROPOROUS RESIN - ZEROLIT 625

5.2.1 Resin Properties

Zerolit 625 is a strong acid, macroporous cation exchange resin, manufactured and supplied by the Permutit Company. The volume capacity, moisture retention capacity (MRC) and swelling characteristics of the resin were measured according to the method outlined in Section 3.3.3, and the results are given below.

5.2.1.1 Volume Capacity

This is used to determine the "workability" of a resin, and is defined as "the number of ionogenic groups per specified volume of exchanger in the fully water-swollen form" [4,25]. Units used are milliequivalents per millilitre (meq/ml) of free-settled (f.s.) volume of wet resin. In order to obtain the volume capacity from the concentration measurements made, the following relationship is used:

$$\text{Volume Capacity} = \frac{(\text{ppm conc. in 250 ml})(0,25)}{(\text{resin vol. in ml})(\text{ion equiv. weight})} \qquad (5.1)$$

The results for Zerolit 625 are tabulated in Table 5.1.

Different volume capacities were obtained for tapped and free-settled volumes, and tests made on 20 ml tapped volumes of resin gave the results in Table 5.2.

5.2.1.2 Discussion of Volume Capacities

From Table 5.1, the average volume capacity of Zerolit 625 is 1,61 meq/ml of wet resin. This agrees well with the value of approximately 1,60 meq/ml given in the Zerolit manual

The capacity for Ca^{2+} is virtually the same as that for Na^{+} (1,61 meq/ml compared with 1,62 meq/ml), corresponding to

TABLE 5.1

CAPACITIES OF ZEROLIT 625 IN Na^+ AND Ca^{2+} FORMS

ml Resin Used	Form	Elutant	ppm in 250 ml	Capacity (meq/ml)
14,65	Ca^{2+}	HCl	1850	1,58
14,65	Ca^{2+}	$MgCl_2$	1920	1,64
				average Ca^{2+} : 1,61
14,65	Na^+	HCl	2175	1,61
14,65	Na^+	$MgCl_2$	2175	1,61
20,0	Na^+	HCl	2968	1,61
20,0	Na^+	$MgCl_2$	3010	1,64
				average Na^+ : 1,62

TABLE 5.2

COMPARISON BETWEEN CAPACITIES OF TAPPED AND FREE-SETTLED VOLUMES OF RESIN

ml Resin	Form	ppm in 250 ml	Volume Capacity (meq/ml)
20,0 (f.s.)	Na^+	2970	1,61
20,0 (tapped)	Na^+	3110	1,69

their similar ionic radii (0,99 Å for Ca^{2+} compared with 0,97 Å for Na [3]).

From Table 5.2, it can be shown that the tapped volume contains approximately 5% more resin than does the f.s. volume. Since the f.s. form has been used throughout this investigation, it is clear that care had to be taken in order to eliminate any possible error in resin volume measurement.

value becomes lower due to the increased volume taken up by the larger ion. The variation is approximately in the ratio of the ions' atomic radii - Ca^{2+} is 2% larger than Na^{+} and the corresponding MRC value for Na^{+} is thus 2% greater than that of Ca^{2+}. Similarly, there is a larger difference between the MRC of the H^{+} form and that of the Na^{+} form, due to the relatively large difference in ionic radius.

5.2.1.5 Swelling Diameters

These were obtained for Zerolit 625 in 0,5N solutions of HCl, NaCl and $CaCl_2$.

Resin diameters were measured using a graticule on a microscope with four times magnification; first dry, and then after the resin bead had been standing for twelve hours in the respective solution. The dry resin beads were obtained by placing the respective resin samples in an oven at 105-110°C for twelve hours.

TABLE 5.4

DIAMETERS OF DRY AND WET ZEROLIT 625 RESIN BEADS

Solution	Dry Diameter (mm)	Wet Diameter (mm)	Swelling (mm)	% Swelling
NaCl	0,72	0,77	0,05	6,5
$CaCl_2$	0,63	0,67	0,04	6,0
HCl	0,82	1,00	0,18	18,0

5.2.1.6 Discussion of Swelling Diameters

Table 5.4 shows that the overall swelling is relatively small, compared with those of gel resins cited by Kunin in "Ion Exchange Resins" [3], in which swelling data for

Amberlite IR-120 and IR-105 in both the Na^+ and H^+ forms are given. Kunin gives typical results of 43% and 73% for IR-120 in the H^+ and Na^+ forms respectively, and 107% and 99% for IR-105 in H^+ and Na^+ forms respectively. These figures are much larger than those quoted in Table 5.4, and the difference results from the fact that the macroporous Zerolit 625 resin is far more rigid in structure that the gel resins quoted above.

The fact that the H^+ form of the resin exhibits such an increase in swelling is not obvious. It would seem from Kunin's results that the loading of the larger ion should result in greater swelling. However, Kunin quotes data showing that IR-105 portrays similar traits to those of Zerolit 625, while most other Amberlite resins do not.

The tests also served as a check on the efficiency of screening. Section 3.3.1 describes how the resin was screened between 0,60 mm and 0,85 mm. The microscopic examination made in determining swelling diameters indicated that approximately 98% of the screened resin samples examined fell within this range.

5.2.2 Binary Kinetic Systems

As indicated in Section 5.1, the two binary kinetic systems studied were the Na^+/H^+ and Ca^{2+}/H^+ ones. Each of these was investigated at both 0,125N and 0,50N total concentration, at a stoichiometric ratio (or resin to liquid fraction) of 0,5, for both regeneration and loading.

The experimental procedure used in all the kinetic runs is described in Section 3.3.5.1. Equation (5.3) was used to calculate the fractional approach to equilibrium (F(t)) values:

$$F(t) = \frac{C_A(t) - C_{A_0}}{C_{A_\infty}} \qquad (5.3)$$

where:

$C_A(t)$ = concentration of ion A in liquid at time t;

C_{A_o} = initial concentration of ion A in liquid;

C_{A_∞} = equilibrium concentration of ion A in liquid;

$F(t)$ = fractional approach to equilibrium.

5.2.2.1 Regeneration Kinetics

These were performed as described in Section 3.3.5.1. The quantities used in the four systems studied are given in Table 5.5:

TABLE 5.5

RESIN AND LIQUID QUANTITIES USED IN MACROPOROUS BINARY REGENERATION KINETICS

Initial Conc. (N)	Counter-ion Studied	R/L	Resin Volume (ml)	Liquid Volume (ml)
0,125	Na^+	0,5	31,1	800
	Ca^{2+}	0,5	31,1	800
0,50	Na^+	0,5	124	800
	Ca^{2+}	0,5	124	800

The resulting kinetic data are tabulated in Appendix C (Tables C-1 and C-2), and plotted, as fraction to equilibrium vs time (calculated from Equation (5.3)), in Figs. 5.1 to 5.4.

5.2.2.2 Discussion of Regeneration Kinetics

(a) General Exchange Theory:

It is normally accepted [3,4] that exchange takes place in five distinct steps:

i) the diffusion of ions through the solution to the surface of the resin bead;

ii) diffusion of those ions through the resin pore;

iii) the exchange of the ions with those already on the resin;

iv) diffusion of those displaced ions back out of the pores;

v) diffusion of these latter ions through the bulk solution (see Section 2.5.3 for detailed description).

The overall kinetics are governed, therefore, by diffusion rates and not by the actual exchange.

As regards which diffusion mechanism controls, Helfferich [25] predicts that liquid film controls at concentrations of less than 0,05N. Thus in these experiments, where the concentration is always greater than or equal to 0,1N, it would be expected that pore diffusion controls.

(b) The Effect of the Counter-Ion:

Figs. 5.1 to 5.4 give the basic plots for the binary systems listed above. From these four graphs Fig. 5.5 is drawn, showing that for both 0,125N and 0,50N regeneration the Na^+ kinetics are faster than the Ca^{2+} kinetics.

As has been indicated previously, at the concentrations used in these experiments it can be assumed that the kinetics are significantly pore diffusion controlled [5,25]. The diffusion within the resin pore will be proportional to the diffusing ion's hydrated radius - the larger the hydrated radius, the slower the diffusion. Since Na^+ and Ca^{2+} have similar ionic radii (0,97 Å and 0,99 Å respectively), but Ca^{2+} has double the charge, the hydrated radius of the Ca^{2+} ion will be greater than that of the Na^+, resulting in slower inter-pore diffusion rates. This is supported by Tombalakian [46], who studied the exchange of univalent, divalent and trivalent counter-ions with H^+ across an ion exchange membrane. He states that "...the rate of cation

interchange decreases with increasing valence and ionic size in hydrated form of the counter-ion...".

(c) The Effect of Concentration:

Fig. 5.5 shows that both Na^+ and Ca^{2+} kinetics are significantly faster at higher concentrations. This is indicative of film diffusion control, since the diffusion inside a pore is independent of solution concentration, whereas the diffusion in the Nernst film surrounding the resin bead is affected by the concentration of the bulk solution (the driving force - see Section 2.5.4 and Figs. 2.10 and 2.11).

Thus, although Kunin [3] and Helfferich [25] indicate that at concentrations exceeding approximately 0,05N, the kinetics become predominantly particle diffusion controlled, the present experimental data at 0,125N indicates at least some film diffusion control effects. Helfferich states that the concentration is not the only factor that affects the rate-controlling step, but that factors such as the concentration of the fixed ionic groups on the resin, the interdiffusion coefficient of the exchanger and the film, the film thickness and the separation factor, play an equally important role. Since these early workers had only gel resins available to them, it is possible that the different structure of the macroporous resin used in these experiments could affect one of those factors, such that the film-control characteristics become predominant at much higher concentrations.

As discussed in Section 2.2.2.2, macroporous resins consist of a gel type structure polymerised to form microspheres (< 20 Å diameter), which in turn are cemented or joined together at points of contact to form pores which are not part of the actual chemical structure [20,29,30]. Thus macroporous exchange resins consist of a gel as well as a macroreticular pore structure, and both of these affect the exchange kinetics.

Fig. 5.6 shows electron micrographs of a macroporous

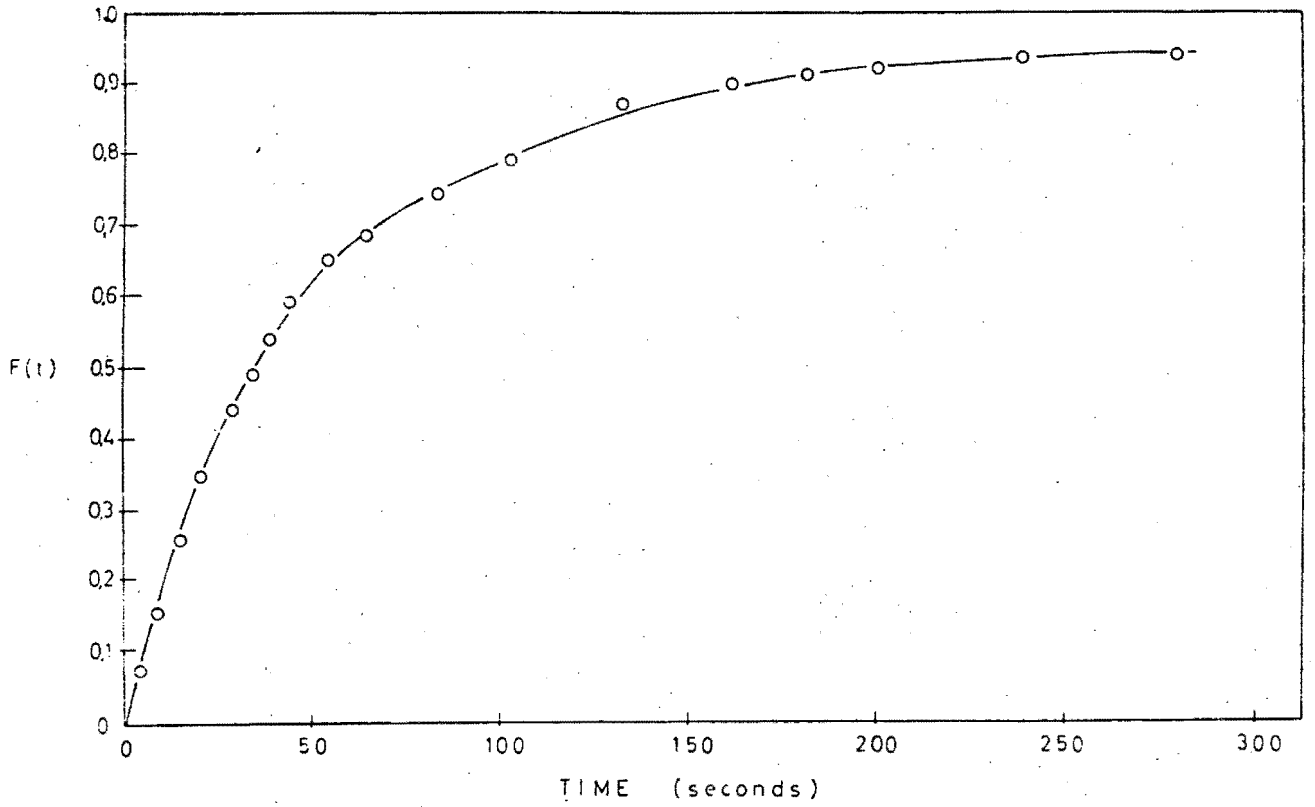

Fig. 5.1: Regeneration of Na^+ Form Zerolit 625 Resin at 0,125N Concentration

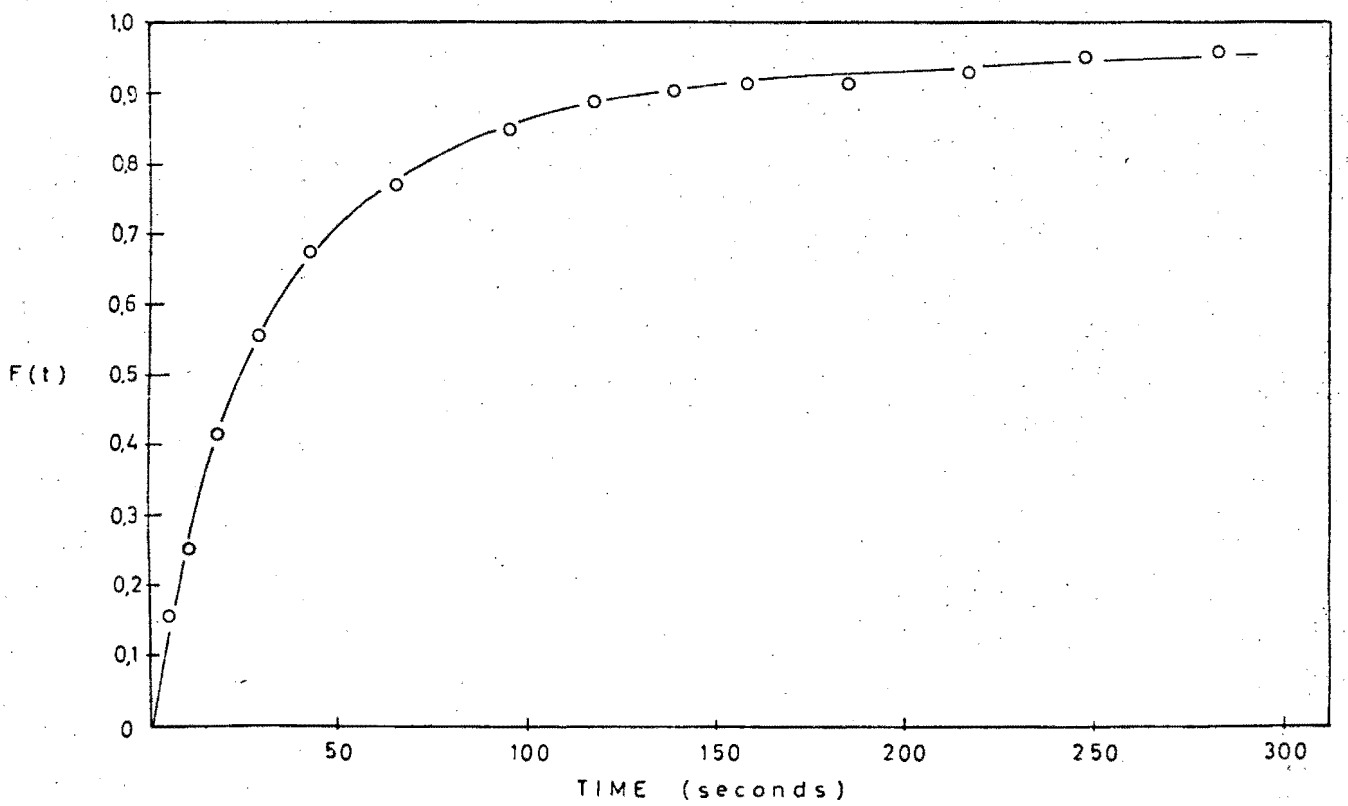

Fig. 5.2: Regeneration of Na^+ Form Zerolit 625 Resin at 0,50N Concentration

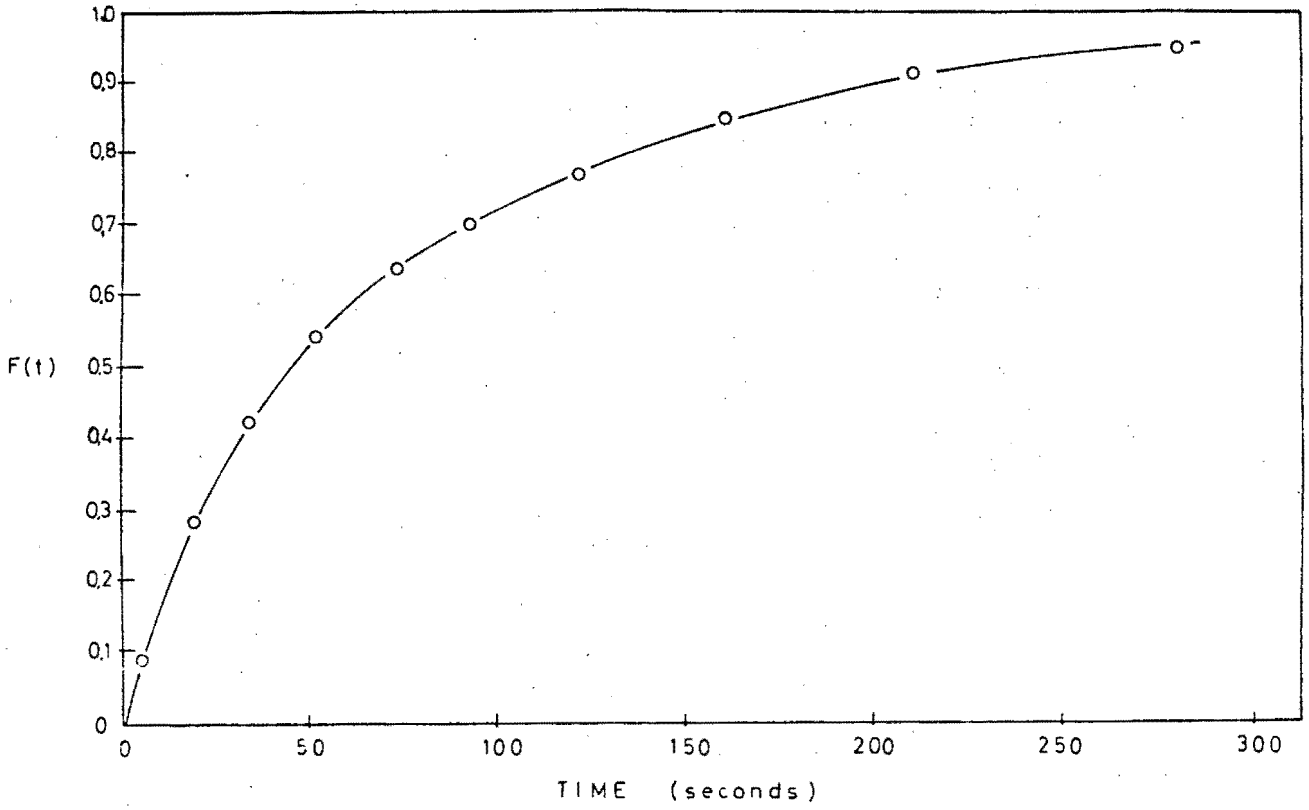

Fig. 5.3: Regeneration of Ca^{2+} Form Zerolit 625 Resin at 0,125N Concentration

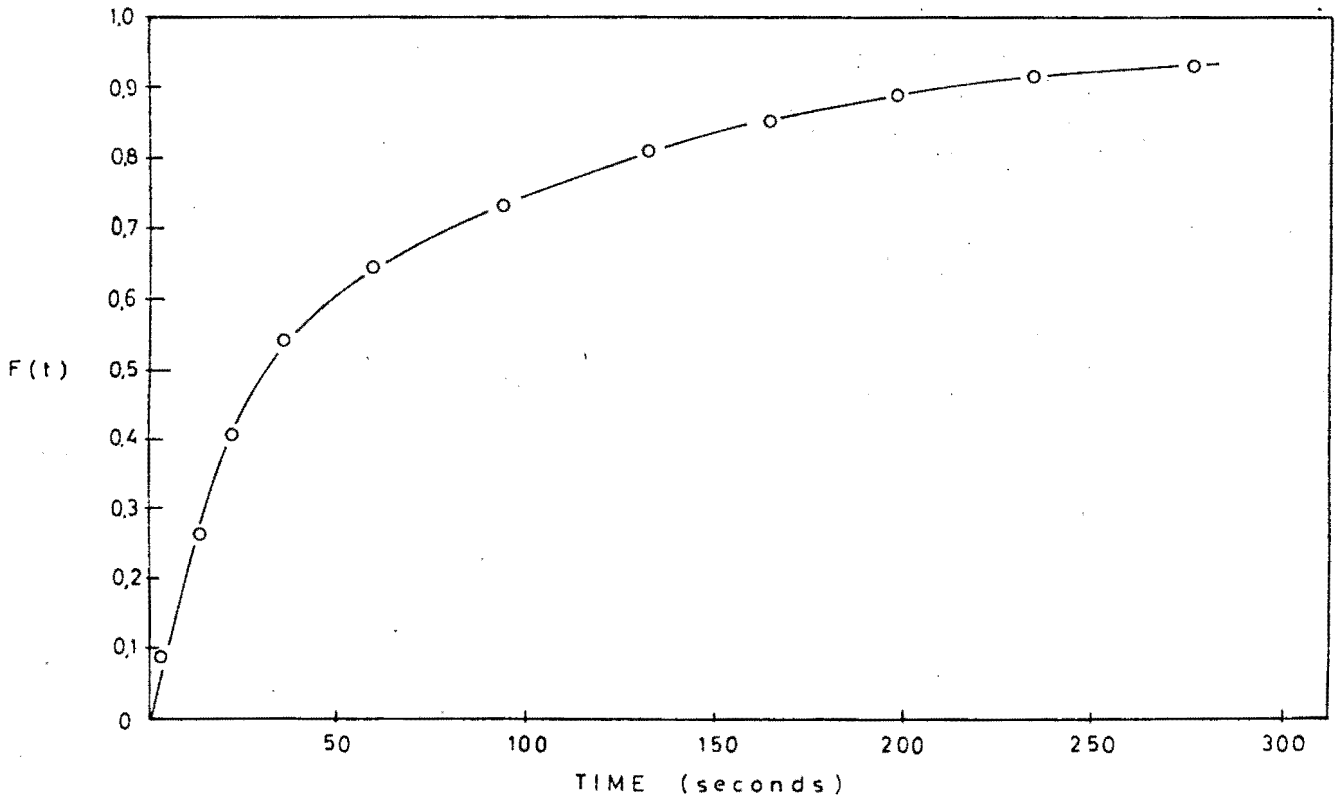

Fig. 5.4: Regeneration of Ca^{2+} Form Zerolit 625 Resin at 0,50N Concentration

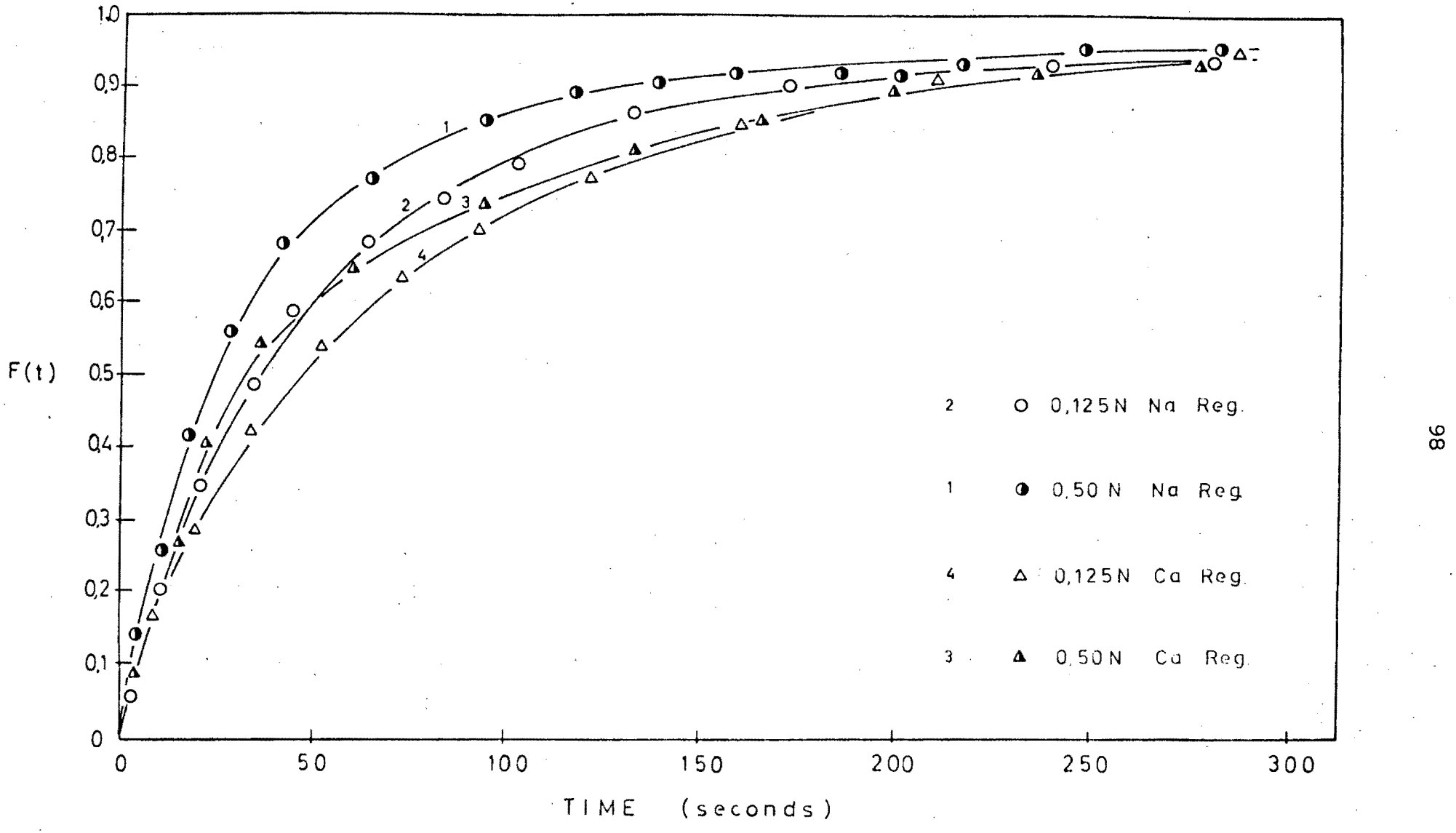

Fig. 5.5: Comparison Between Regeneration Kinetics of Na^{+} and Ca^{2+} Form Zerolit 625 Resin at 0,125N and 0,50N Concentrations

resin at two different magnifications [20,30].

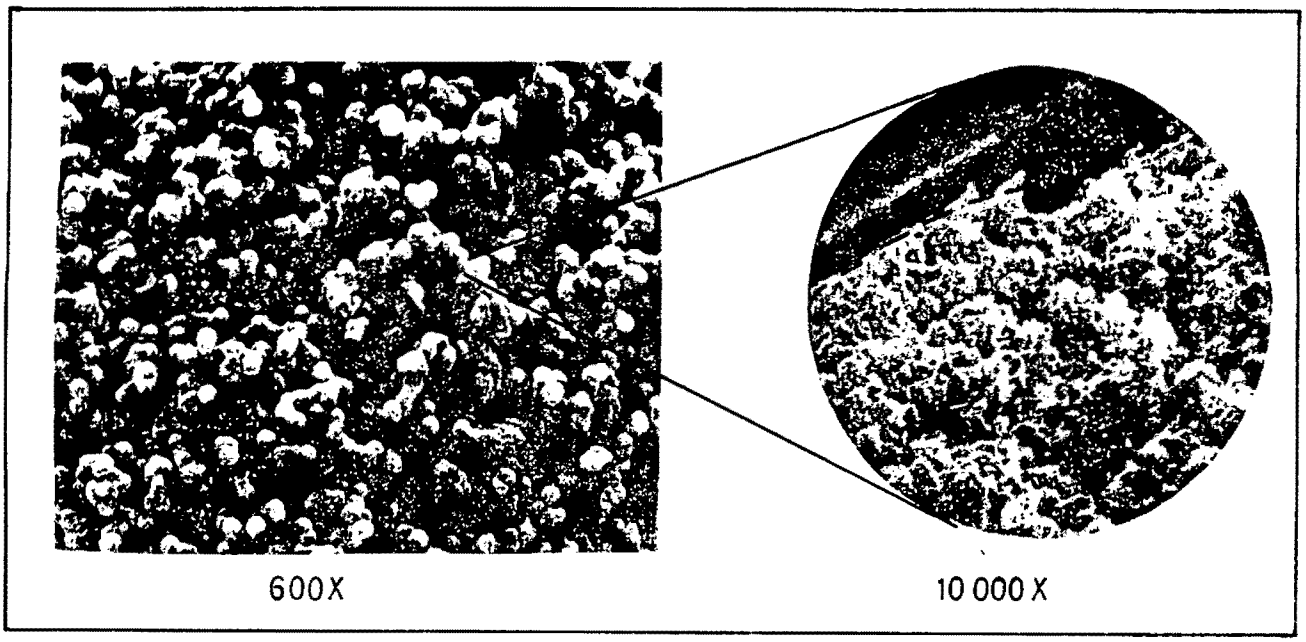

Fig. 5.6: Electron Micrographs of Macroporous Resin Bead [20].

Further, this macroporous structure of Zerolit 625 might encourage film-diffusion control by the fact that a significant amount of the pore space is large enough for the diffusivity of the counter-ion within the pore to increase, thus allowing the diffusion within the liquid film to have a greater effect on the kinetics.

Further indication of partial film-diffusion control of Zerolit 625 is discussed in Section 5.2.2.4.

5.2.2.3 Loading Kinetics

These were performed as described in Section 3.3.5.1 at only 0,125N concentration. The systems and respective quantities are given in Table 5.6. The resulting kinetic data are tabulated in Appendix C (Tables C-3 and C-4) and plotted in Figs. 5.7 and 5.8.

5.2.2.4 Discussion of Loading Kinetics

Figs. 5.7 and 5.8 show the F(t) versus time plots for Na^+ and Ca^{2+} loading onto regenerated Zerolit 625 resin at

TABLE 5.6

RESIN AND LIQUID QUANTITIES FOR BINARY LOADING KINETICS

Initial Conc. (N)	Counter-ion Studied	R/L	Resin Volume (ml)	Liquid Volume (ml)
0,125	Na^+	0,5	31,1	800
0,125	Ca^{2+}	0,5	31,1	800

0,125N. From these, Fig. 5.9 is drawn, giving a comparison between the loading and regeneration kinetics of the Na^+ and Ca^{2+} systems.

Another indication of the fact that, even at these relatively high concentrations, the kinetics are not entirely pore-diffusion controlled in a macroporous resin comes from a consideration of the forward and reverse (loading and regeneration) kinetic data. It can be seen from Fig. 5.9 that, for both the Na^+ and Ca^{2+} kinetics, the loading and regeneration rates are almost identical. Helfferich [25] states that, for pore-diffusion controlled systems, the exchange is faster when the more mobile counter-ion is initially in the resin. In the systems investigated, the H^+ counter-ion is the most mobile, since it has the smallest hydrated radius and thus the highest diffusivity. Thus, if the Na^+/H^+ and Ca^{2+}/H^+ systems were entirely pore-diffusion controlled one would expect the loading kinetics to be faster than the regeneration kinetics. However, this is not the case: the two kinetic rates, as shown in Fig. 5.9, are similar for a particular system. (It will be shown later that the gel resins are pore-diffusion controlled, and that the regeneration kinetics are slower than the loading kinetics.)

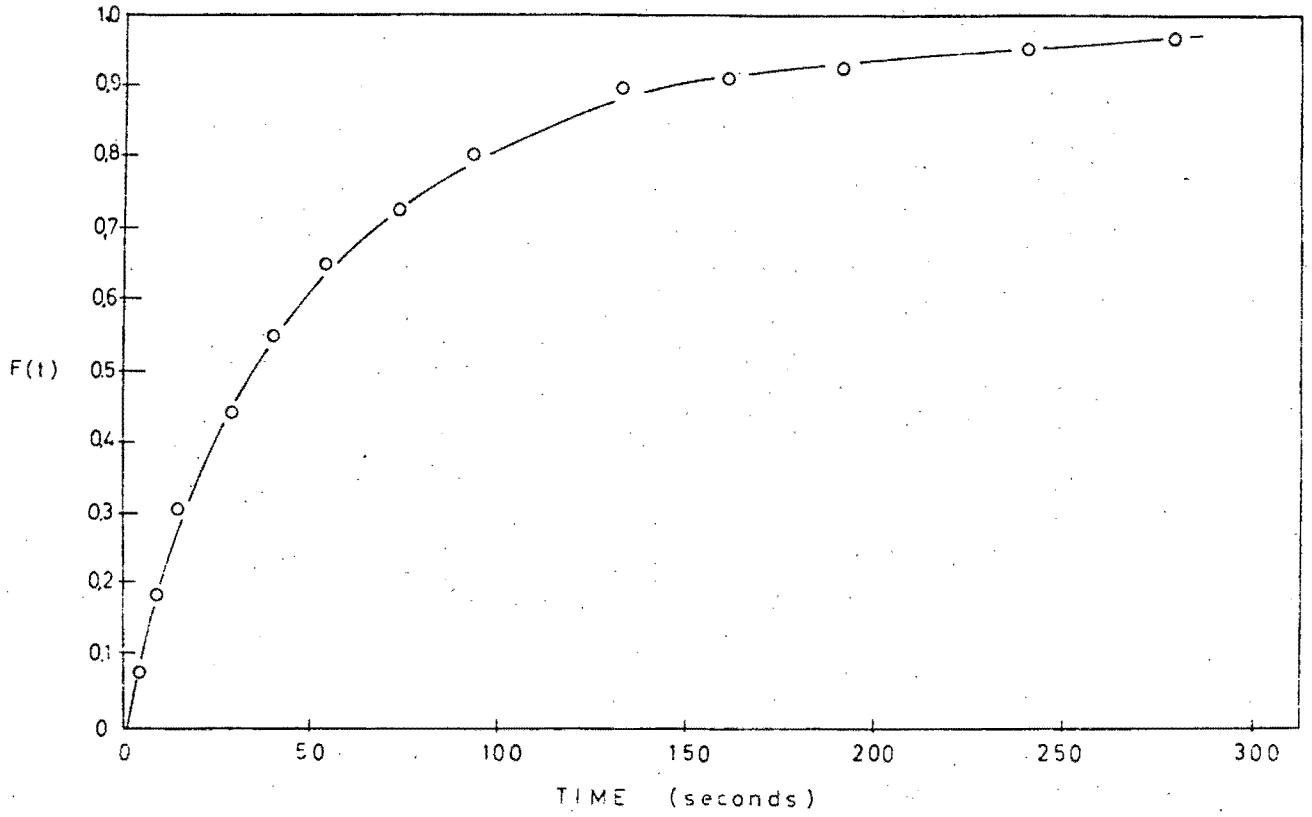

Fig. 5.7: Na^{+} Loading onto Zerolit 625 Resin at 0,125N Concentration

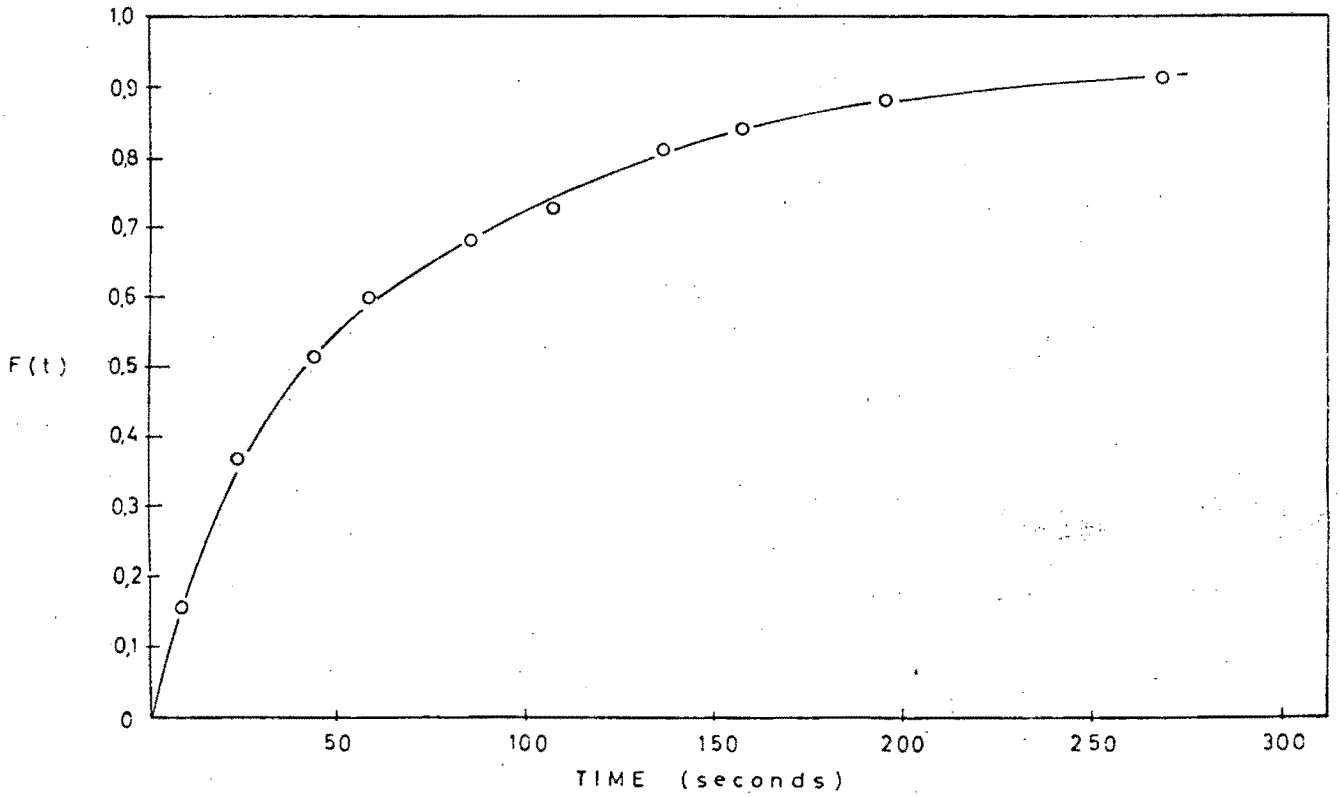

Fig. 5.8: Ca^{2+} Loading onto Zerolit 625 Resin at 0,125N Concentration

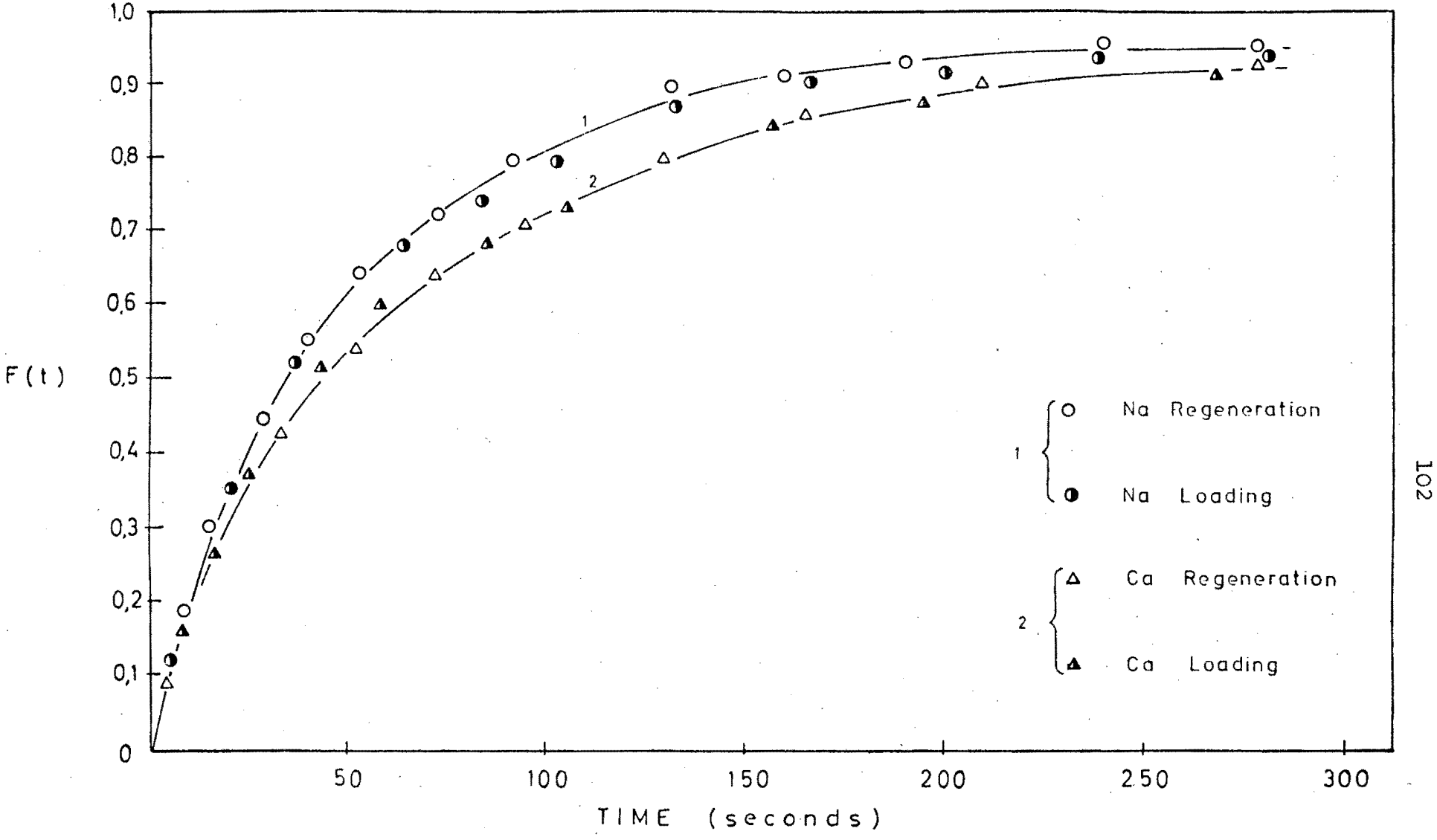

Fig. 5.9: Comparison Between Na^+ and Ca^{2+} Regeneration and Loading Kinetics on Zerolit 625 Resin at 0,125N Concentration

5.2.3 Ternary Kinetic Systems

These systems, involving the loading or regeneration of two competing species (Na^+ and Ca^{2+}), were investigated at 0,125N initial total concentration and an R/L ratio of 0,5.

For loading, two separate conditions were investigated: that where the loading liquid consisted of approximately 50% Na^+ and 50% Ca^{2+}, and that where the loading liquid consisted of approximately 25% Na^+ and 75% Ca^{2+} (the resin being in the H^+ form).

For regeneration, similarly, two conditions were investigated: that where the resin was preloaded with approximately 50% Na^+ and 50% Ca^{2+}, and that where the resin was preloaded with approximately 25% Na^+ and 75% Ca^{2+}. The detailed experimental procedure is described in Section 3.3.2.

Only H^+ kinetic curves are shown on the F(t) plots, since the total co-ion (Cl^-) concentration differs according to whether Na^+ or Ca^{2+} is being exchanged, and thus direct F(t) curve comparison of Na^+ and Ca^{2+} kinetics is not valid.

Two sets of curves are given for each set of results, these being the F(t) curve (described in Section 5.2.2 and either the F'(t) curve in the case of loading, or the F''(t) curve in the case of regeneration. As described earlier, in the latter two methods of presentation (described by Dranoff and Lapidus [47]), F'(t) represents the ion fraction on the resin, while F''(t) represents the ion fraction in the liquid. The respective equations are given in Table 5.7.

5.2.3.1 Regeneration Kinetics

(a) Preloaded Resin Compositions:

The resin was preloaded in mixtures of NaCl and $CaCl_2$, calculated to give (i) 50% Na^+ and 50% Ca^{2+}, and (ii) 25% Na^+ and 75% Ca^{2+} relative concentrations. In order to check

TABLE 5.7

EQUATIONS USED FOR TERNARY SYSTEM KINETIC GRAPHS

Loading		Regeneration	
F(t)	F'(t)	F(t)	F''(t)
$F_{Na} = \frac{C_{Na_o} - C_{Na}(t)}{C_{Na_o} - C_{Na_\infty}}$	$F'_{Na} = \frac{C_{Na_o} - C_{Na}(t)}{C_{H_\infty}}$	$F_{Na} = \frac{C_{Na}(t)}{C_{Na_\infty}}$	$F''_{Na} = \frac{C_{Na}(t)}{125^*}$
F_{Ca} = similar to F_{Na}	F'_{Ca} = similar to F'_{Na}	$F_{Ca} = \frac{C_{Ca}(t)}{C_{Ca_\infty}}$	$F''_{Ca} = \frac{C_{Ca}(t)}{125^*}$
$F_H = \frac{C_H(t)}{C_{H_\infty}}$	$F'_H = \frac{C_{H_\infty} - C_H(t)}{C_{H_\infty}}$	$F_H = \frac{125 - C_H(t)}{125^* - C_{H_\infty}}$	$F''_H = \frac{C_H(t)}{125^*}$

* 125 corresponds to the total concentration of the system in meq/ml.

the resultant preloaded compositions, the resin samples were eluted with 5N HCl solution and the actual relative compositions of Na^+ and Ca^{2+} calculated from analytical results. The results are tabulated in Table 5.8:

TABLE 5.8

ACTUAL PRELOADED ZEROLIT 625 RESIN COMPOSITIONS FROM ELUTIONS

Theoretical Composition	meq Na^+	meq Ca^{2+}	Actual Composition
50% Na^+/50% Ca^{2+}	38,7	35,0	53% Na^+/47% Ca^{2+}
25% Na^+/75% Ca^{2+}	20,1	54,0	27% Na^+/73% Ca^{2+}

(b) Resin and Liquid Quantities:

For both the 50% Na^+/50% Ca^{2+} and 25% Na^+/75% Ca^{2+} systems, 31,1 ml of suitably preloaded resin was reacted with 800 ml 0,125N HCl, in order to achieve an R/L ratio of 0,5.

The results are tabulated in Appendix C, Tables C-4 and C-5, and plotted in Figs. 5.10 to 5.13.

5.2.3.2 Discussion of Regeneration Kinetics

(a) Individual Systems:

Figs. 5.10 to 5.13 give the results for the regeneration kinetics of 50% Na^+/50% Ca^{2+} and 25% Na^+/75% Ca^{2+} preloaded Zerolit 625 resin with 0,125N HCl at an R/L ratio of 0,5.

Figs. 5.11 and 5.13 show that the Ca^{2+} regeneration is appreciably slower than the Na^+ regeneration. The reasons for this are similar to those of the binary kinetic systems - primarily the effect of the larger hydrated radius and higher change density of the Ca^{2+} counter-ion, as discussed in Section 5.2.2.2(b).

The most important fact evident from these figures is that there is no Na^+ "overshoot" of the equilibrium value, as is found in the ternary loading systems (see Section 5.2.3.3). Although Helferich [25] states that such an overshoot can occur in a regeneration system for reasons similar to those described in Section 5.2.3.4, other experimental data for ternary regeneration follows the same pattern as those given here, and there is then no supporting experimental evidence for a regeneration "overshoot".

If one studies the steps involved in a ternary system regeneration, it will be seen why an "overshoot" would not be expected. The steps involved in a regeneration are depicted in Fig. 5.14. Initially, H^+ ions diffuse into the pore and exchange with both the Na^+ and Ca^{2+} ions on the resin exchange sites, although the Na^+ will be released to a greater extent due to its lower resin affinity. This is demonstrated in

The H^+ kinetics are computed using a cation mass balance over the system. Since the total concentration of the loading liquid is always constant at 0,125 eq/l (one counter-ion in the liquid exchanging for one counter-ion on the resin site), the milliequivalents of H^+ can be computed from the milliequivalents of Na^+ and Ca^{2+} which are known from measurement (only three cations are present in the system). The H^+ plots thus represent the general, overall kinetics - a combination of the individual Na^+ and Ca^{2+} kinetics.

(b) Comparison Between 50% Na^+/50% Ca^{2+} and 25% Na^+/75% Ca^{2+} Systems:

Figs. 5.15 and 5.16 show a comparison between these two systems. They are plotted on F''(t) and F(t) axes respectively.

From Fig. 5.15, the system whose resin initially contained the greater fraction of Ca^{2+} equilibrates at a higher ion fraction of Ca^{2+} in the liquid (F''(t) value) than that of Na^+, and similarly, the system whose resin initially contained the greater fraction of Na^+ equilibrates at a higher F''(t) Na^+ value. This is explained by the fact that, initially, a larger amount of the respective counter-ion was available for stripping, and this is reflected in the ion fractions of the bulk solution.

In the 25% Na^+/75% Ca^{2+} system, the relative increase in the Ca^{2+} kinetics is somewhat less than would be expected from the rather marked corresponding decrease in the Na^+ kinetics. The reason for this is, once again, that the Ca^{2+}, due to its higher resin affinity, is more difficult to strip than is the Na^+.

The overall (H^+) rate of exchange as depicted in Fig. 5.16 is approximately equal between the two systems. Again, the overall kinetics are governed by the diffusion of the Ca^{2+} counter-ion, which remains constant and independent of the initial degree of preloading.

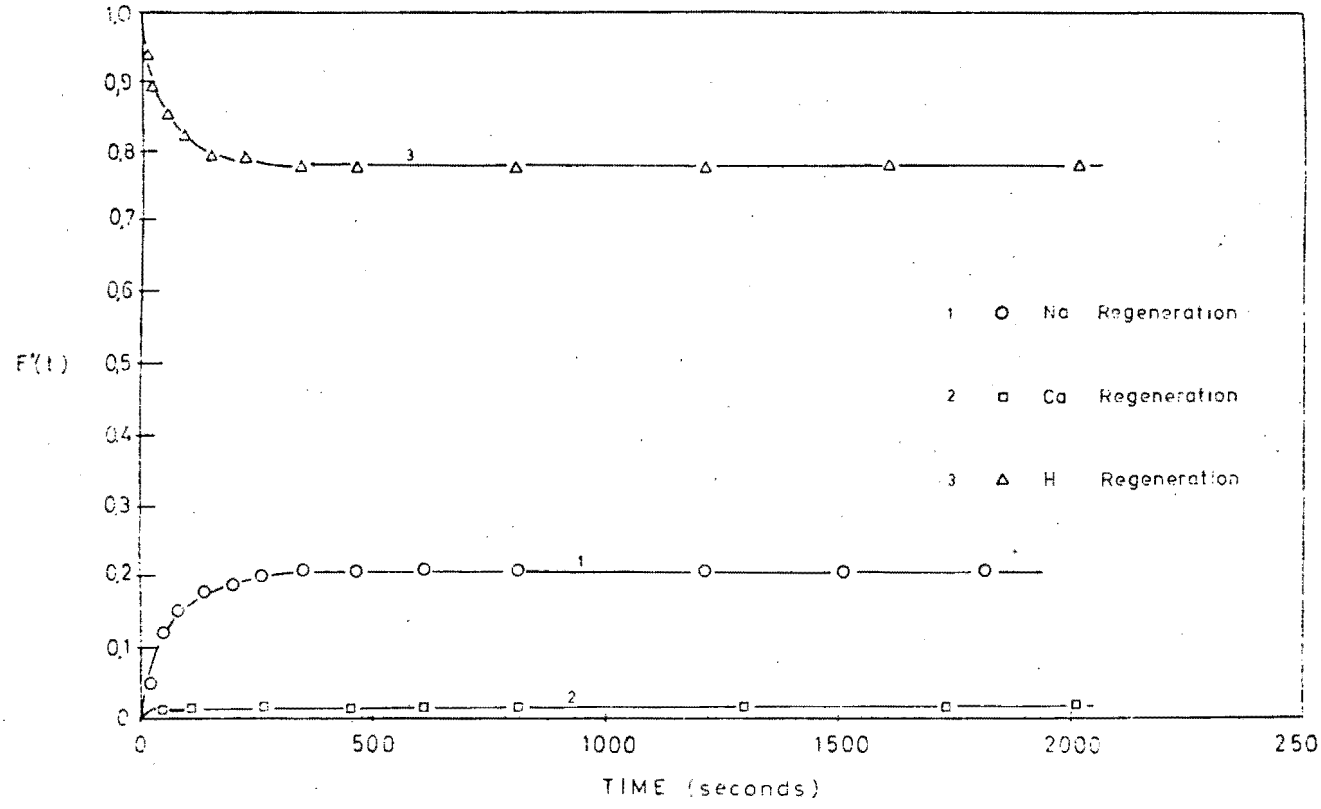

Fig. 5.10: F" (t) Plot of Regenerating a 50%/50% Preloaded Zerolit 625 Resin at 0,125N Concentration

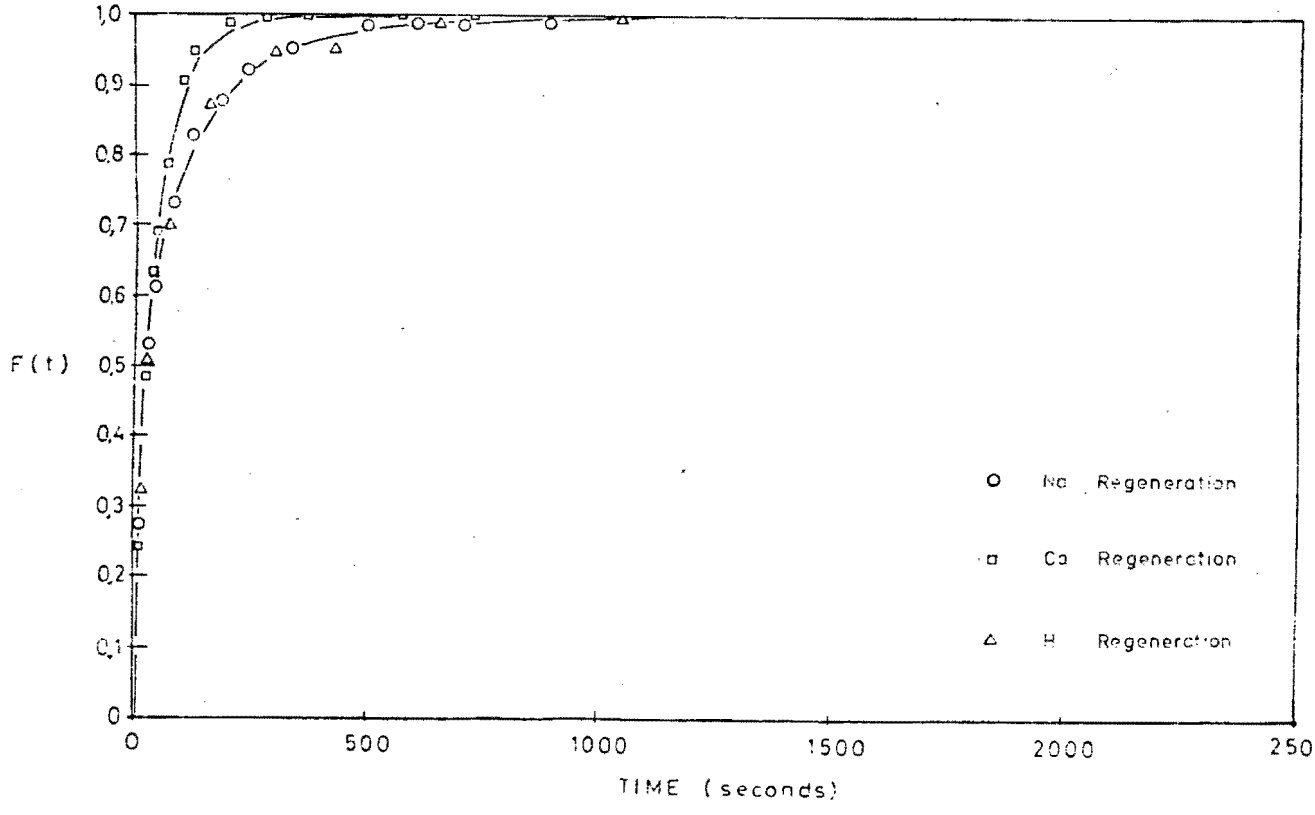

Fig. 5.11: F(t) Plot of Regenerating a 50%/50% Preloaded Zerolit 625 Resin at 0,125N Concentration

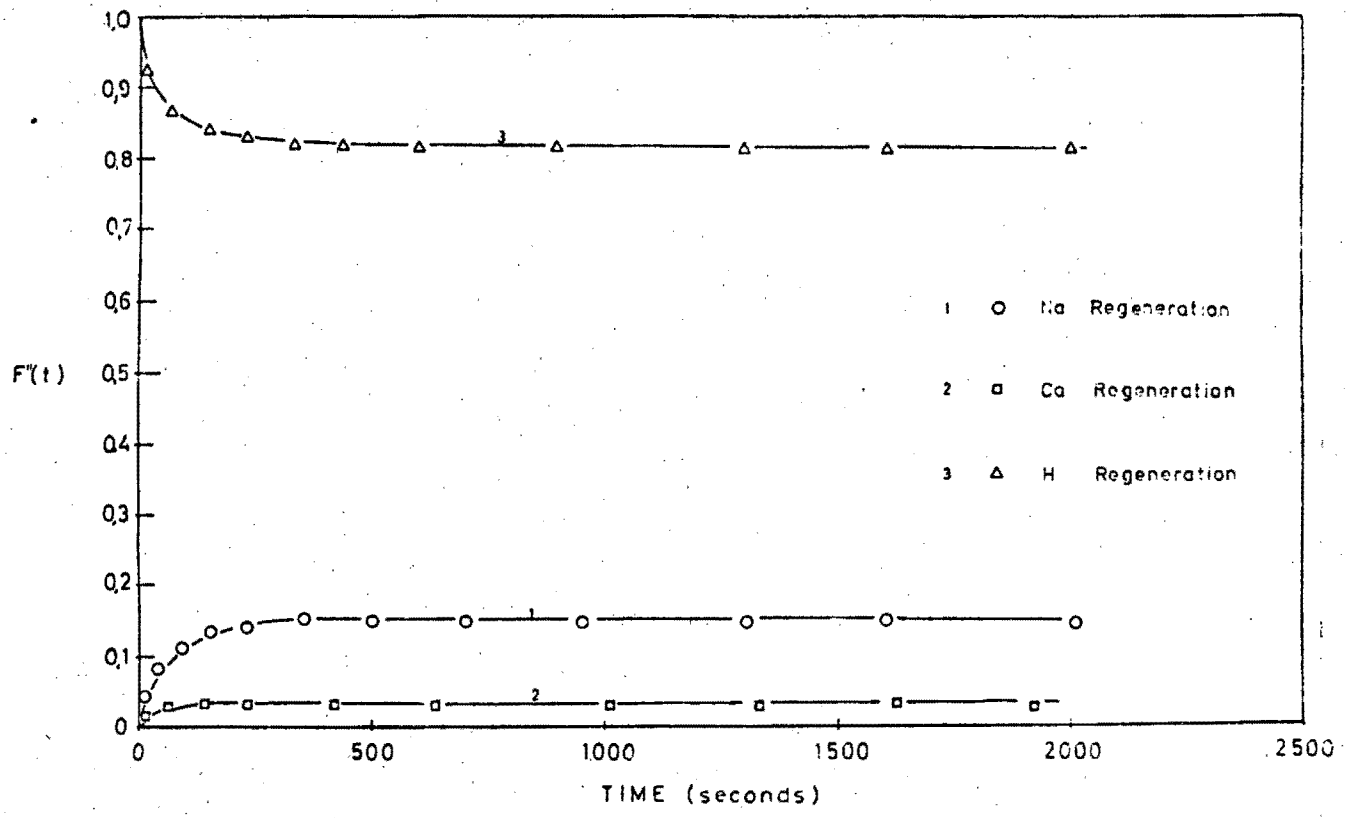

Fig. 5.12: F" (t) Plot of Regenerating a 25%/75% Preloaded Zerolit 625 Resin at 0,125N Concentration

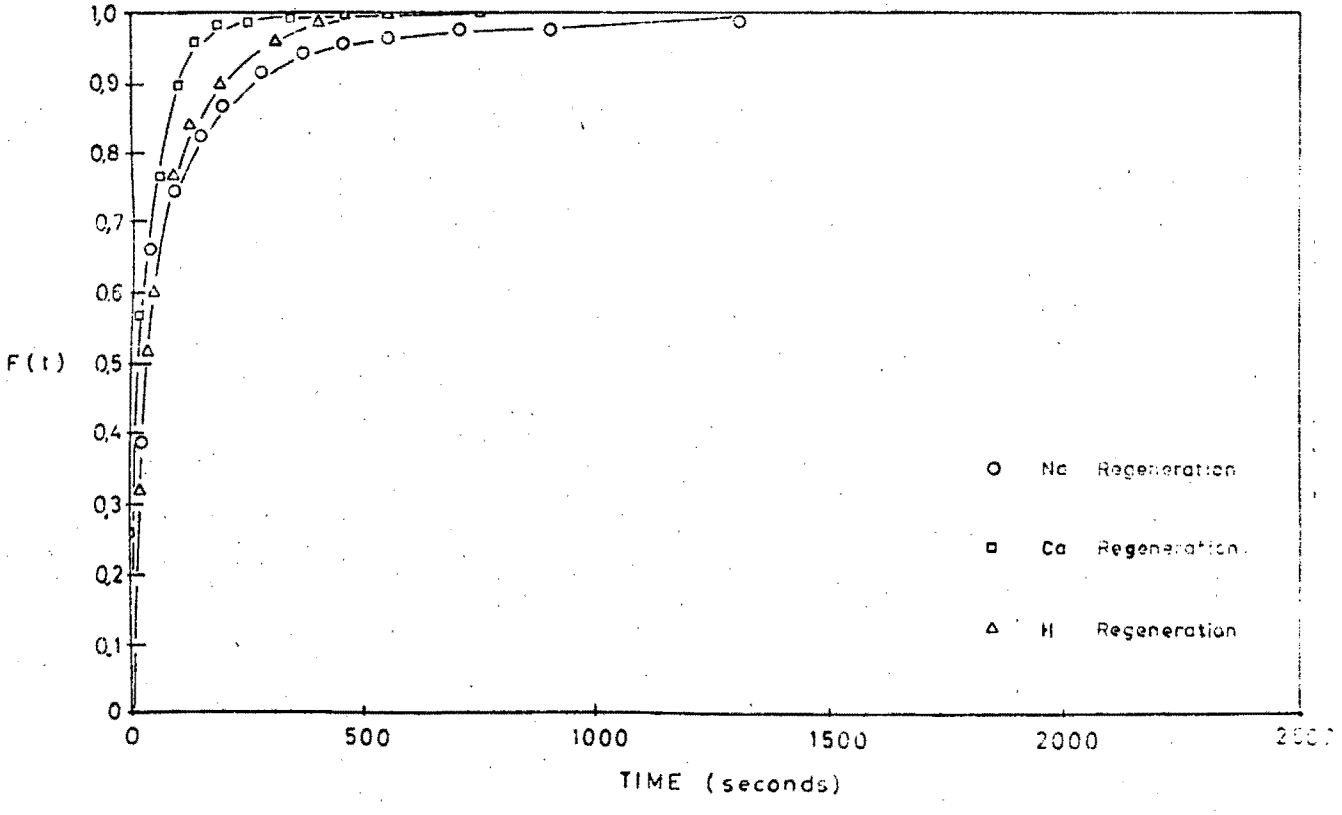

Fig. 5.13: F(t) Plot of Regenerating a 25%/75% Preloaded Zerolit 625 Resin at 0,125N Concentration

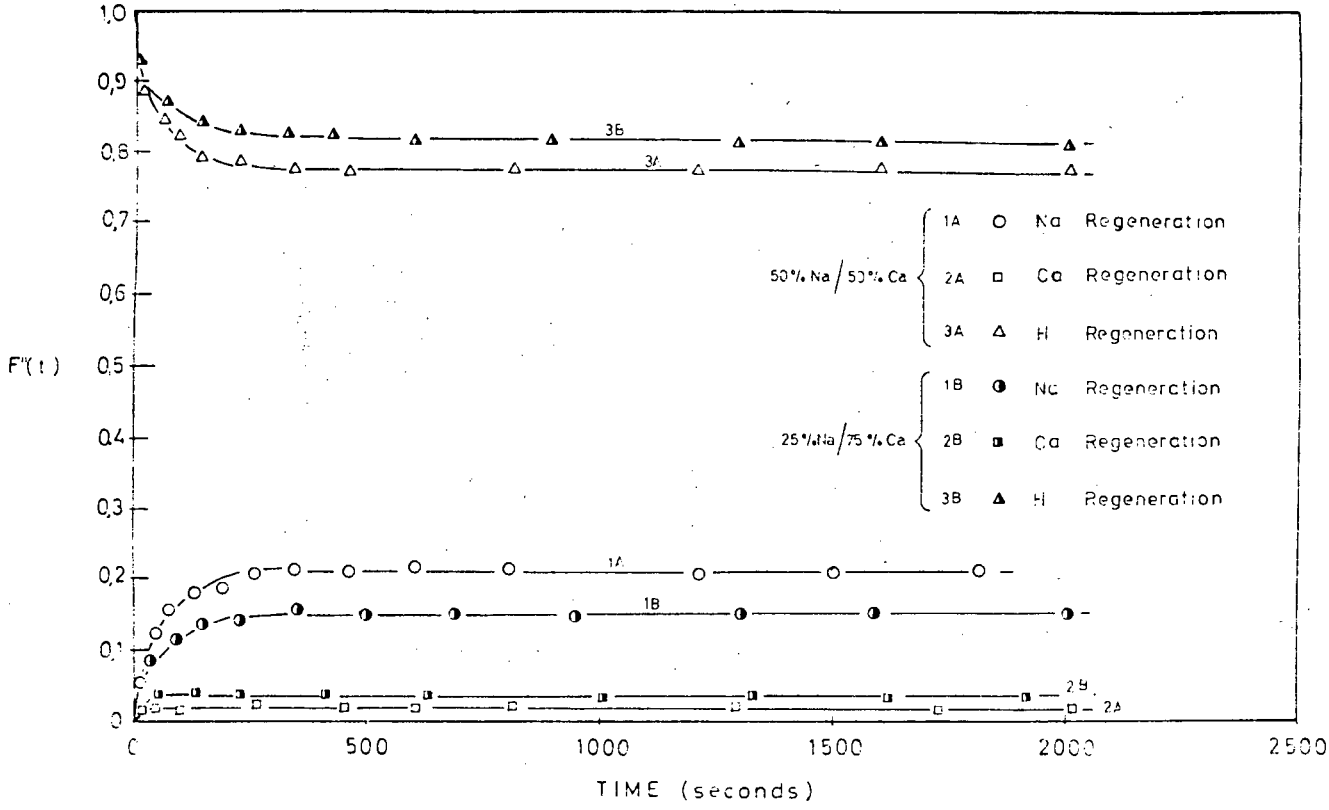

Fig. 5.15: F'' (t) Comparative Plot of Regeneration at 0,125N of Zerolit 625 Preloaded to 50%/50% and 25%/75%

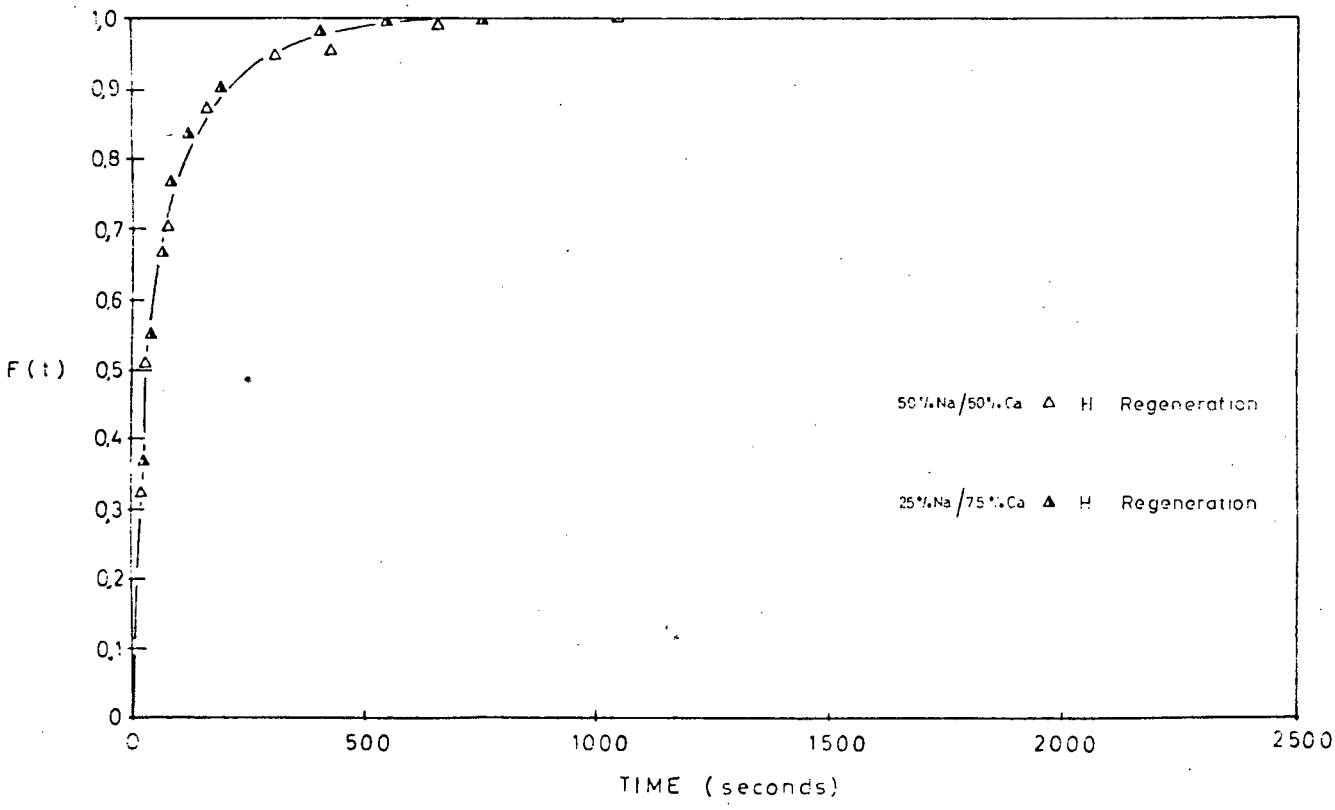

Fig. 5.16: F(t) Comparative Plot of Regeneration at 0,125N of 50%/50% and 25%/75% Preloaded Zerolit 625 Resin

5.2.3.3 Loading Kinetics

Resin and Liquid Quantities:

For the 50% Na^+/50% Ca^{2+} system, 400 ml of each 0,125N NaCl and 0,125N $CaCl_2$ were used to load 31,1 ml of Zerolit 625 in the H^+ form.

For the 25% Na^+/75% Ca^{2+} system, 200 ml of 0,125N NaCl and 600 ml of 0,125N $CaCl_2$ were used to load the same quantity of H^+ form Zerolit 625 resin. The experimental procedure in each case is described earlier. The results are tabulated in Tables C-6 and C-7 and plotted in Figs. 5.17 to 5.20.

5.2.3.4 Discussion of Loading Kinetics

(a) Individual System:

Figs. 5.17 to 5.20 give the results, both in F'(t) and F(t) form, of a 50% Na^+/50% Ca^{2+} and 25% Na^+/75% Ca^{2+} mixture loaded onto Zerolit 625 which was initially in the H^+ form. It is clearly shown for both systems that the Na^+ "overshoots" its equilibrium value, i.e. the resin becomes "supersaturated" with Na^+ before returning to its normal equilibrium concentration.

The reason for this phenomenon, which is depicted in Fig. 5.17, is due to the relative mobilities of the two loading counter-ions (Na^+ and Ca^{2+}). Na^+ is the more mobile (see Section 5.2.1) due to its smaller hydrated radius, and thus will diffuse into the resin at a faster rate. Since the exchange is (partially) pore-diffusion controlled, the majority of the Na^+ ions will reach the exchange sites before any significant number of Ca^{2+} ions do. These Na^+ ions, therefore, exchange for the H^+ on the sites - see Fig. 5.21 graphs 1 and 2. However, the resin has a higher affinity for the Ca^{2+} (being a divalent ion), and thus, as the Ca^{2+} counter-ions reach the exchange sites a finite time later, they will exchange in turn with some of the Na^+ already loaded. The displaced Na^+ ions will diffuse back out of the pore into the bulk solution. The Na^+ concentration in the loading solution

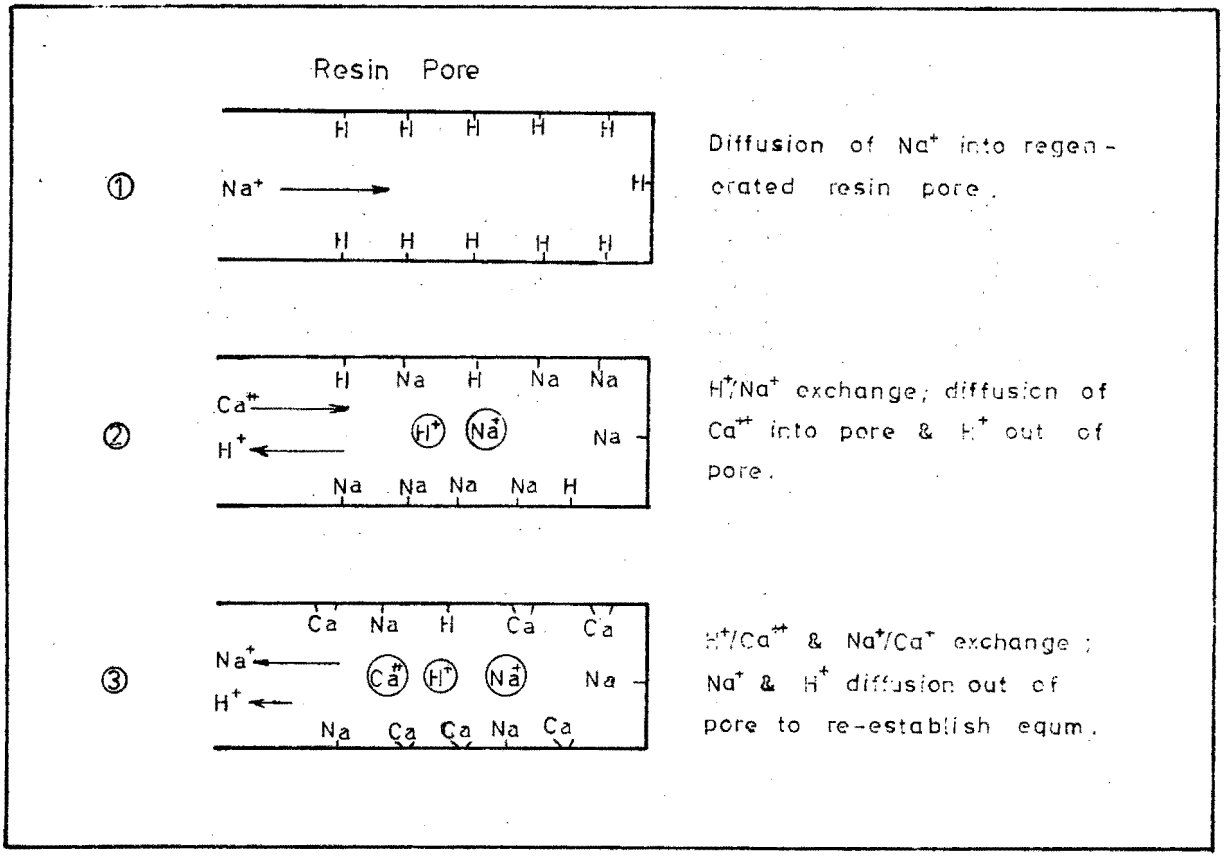

Fig. 5.21: Schematic Steps of Ternary Loading Systems.

thus goes through a maximum, as depicted in Figs. 5.17 to 5.20.

Corresponding results have been quoted by a number of researchers in the field. Helfferich [25], referring to a similar loading system, states that "...if B is more mobile than A, B will rapidly replace A in the resin, and the uptake of C will lag far behind. Later, C will follow, partly replacing the B ions... . Thus B goes through a maximum.".

Dranoff and Lapidus [47] performed an equivalent set of experiments using the systems $H^+ - Ag^+ - Na^+$ and $H^+ - Ag^+ - Cu^{2+}$. Comparable results were obtained, with the degree of "overshoot" far greater in the second system than the first, since the larger the difference in selectivity between the two loading counter-ions, the larger the quantity of initially loaded ions that will be displaced by the second counter-ion, and thus the larger the concentration difference in the bulk solution.

As an additional point of interest, the total time for the $Ag^+ - Cu^{2+}$ and $Ag^+ - Na^+$ systems to reach equilibrium was considerably shorter than for the $H^+ - Na^+ - Ca^{2+}$ system discussed earlier ($H^+ - Na^+ - Ca^{2+}$ system reached equilibrium in approximately 600 secs - see Figs. 5.17 and 5.19; while the $H^+ - Ag^+ - Na^+$ and $H^+ - Ag^+ - Cu^{2+}$ systems reached equilibrium in approximately 100 secs). The reason is related to the difference in resin sizes used in the two sets of experiments. Dranoff and Lapidus used resin in the size range 50-100 mesh (0,25 mm to 0,51 mm), while in all resins in this project the resin was screened between 0,60 mm and 0,85 mm. It has been proved [13] that the smaller the resin particle, the faster the kinetics.

It should be noted that, at equilibrium, almost all the H^+ initially on the resin is replaced by Na^+ and Ca^{2+}. Further, the rate of loading of the Ca^{2+} is much slower than the rate of loading of Na^+. This is consistent with the above discussion.

Fig. 5.22 compares the H^+ kinetics of the 25% Na^+/75% Ca^{2+} loading system on Zerolit 625, with binary Na^+ and Ca^{2+} kinetics. It further shows that the ternary system kinetics are very similar to the binary Ca^{2+} kinetics, indicating that it is indeed the Ca^{2+} diffusion which is the controlling mechanism in these ternary systems.

(b) Comparison Between 50% Na^+/50% Ca^{2+} and 25% Na^+/75% Ca^{2+} Systems:

Figs. 5.23 and 5.24 give a comparison, on F'(t) and F(t) coordinates respectively, between the kinetics of the two systems above.

It can be seen from Fig. 5.23 that the difference in relative counter-ion loading concentration affects both the individual Na^+ and Ca^{2+} kinetics, but not the overall H^+ kinetics. The diffusion of Ca^{2+} (whether in the liquid film surrounding the resin bead, or in the pores, or both) controls the rate of loading, and hence the overall kinetics should not

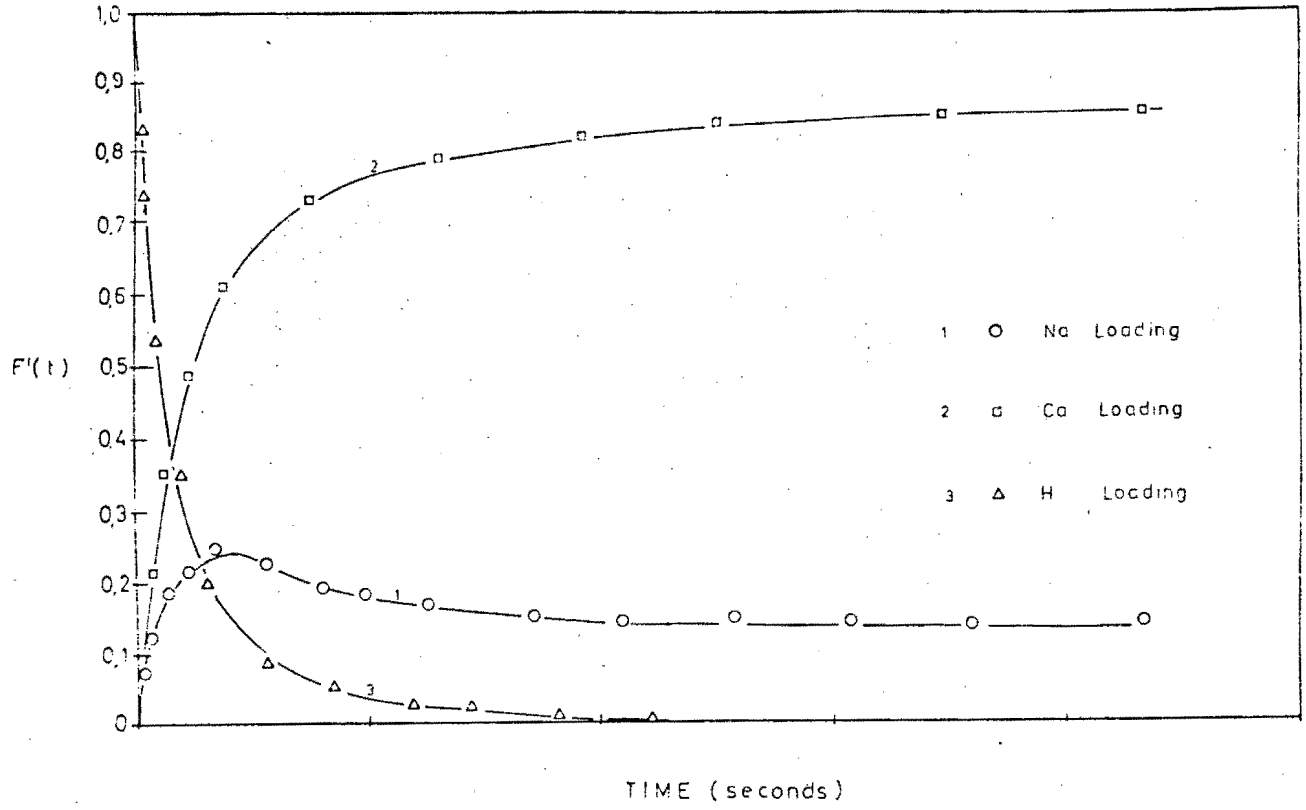

Fig. 5.17: F'(t) Plot of Loading 50%/50% Mixture onto Zerolit 625 at 0,125N

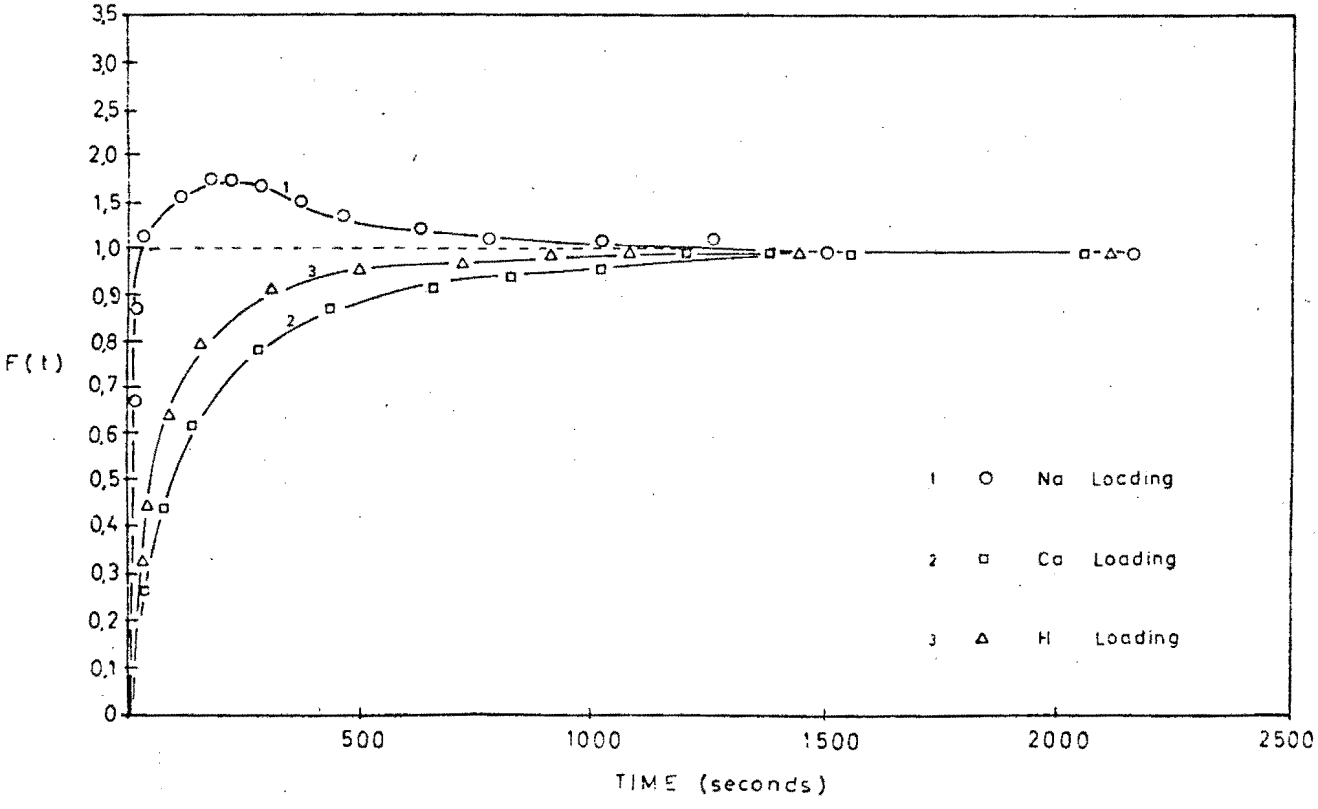

Fig. 5.18: F(t) Plot of Loading 50%/50% Mixture onto Zerolit 625 at 0,125N

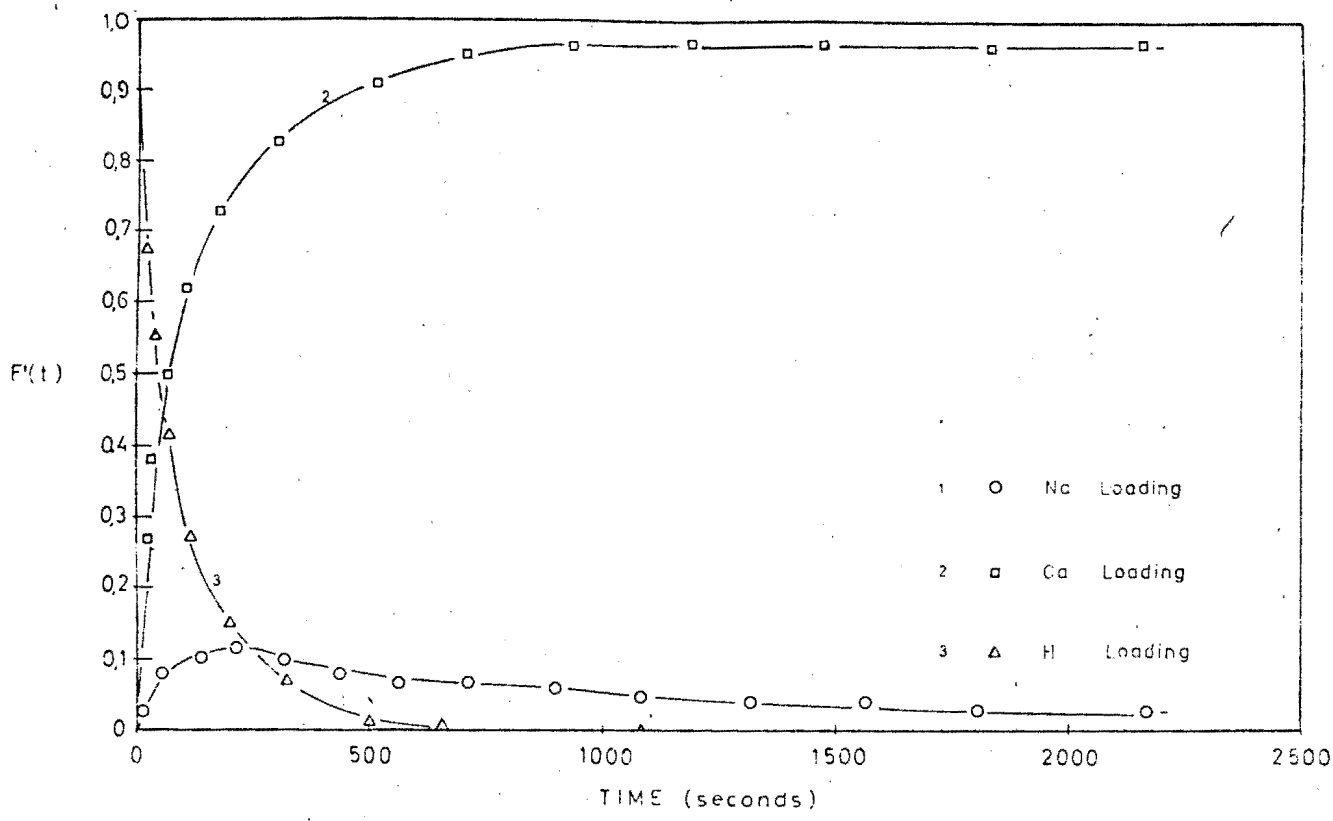

Fig. 5.19: F'(t) Plot of Loading 25%/75% Mixture onto Zerolit 625 at 0,125N

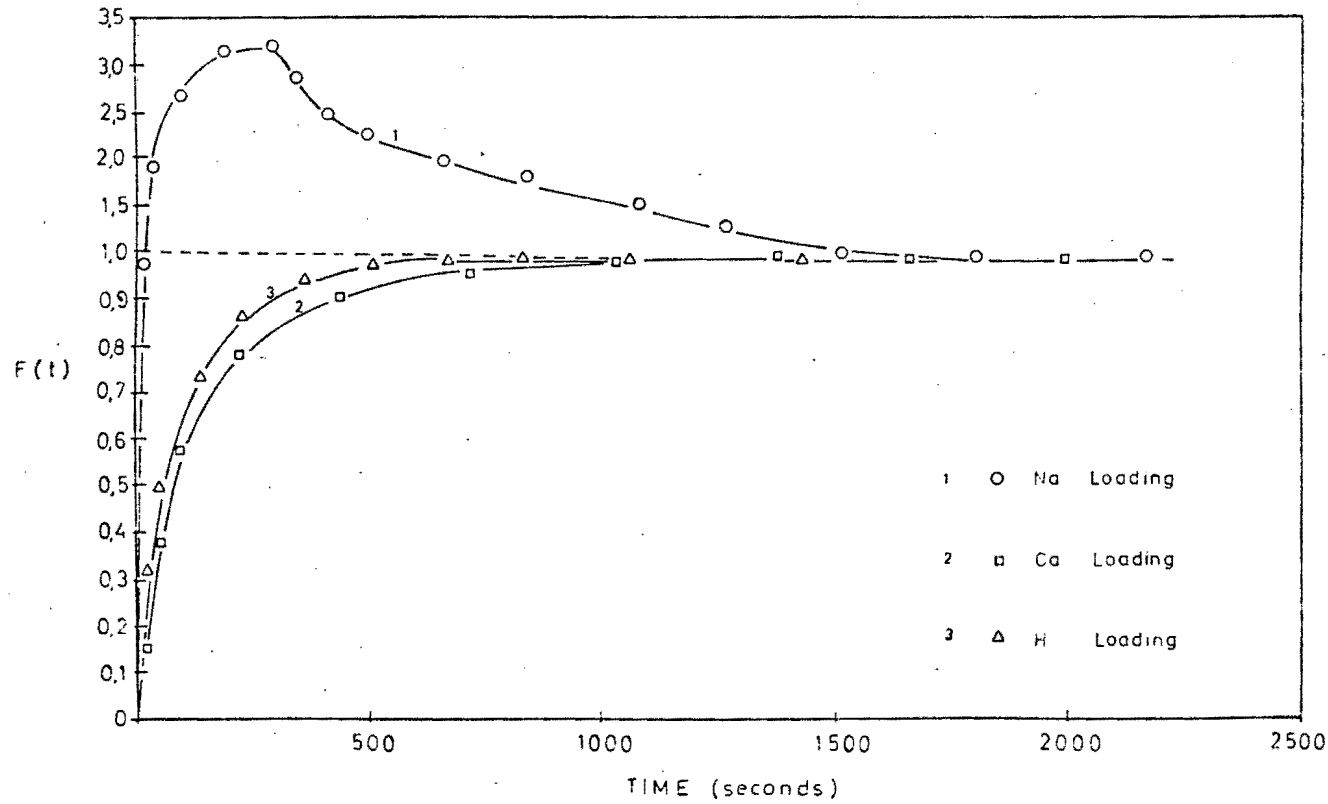

Fig. 5.20: F(t) Plot of Loading 25%/75% Mixture onto Zerolit 625 at 0,125N

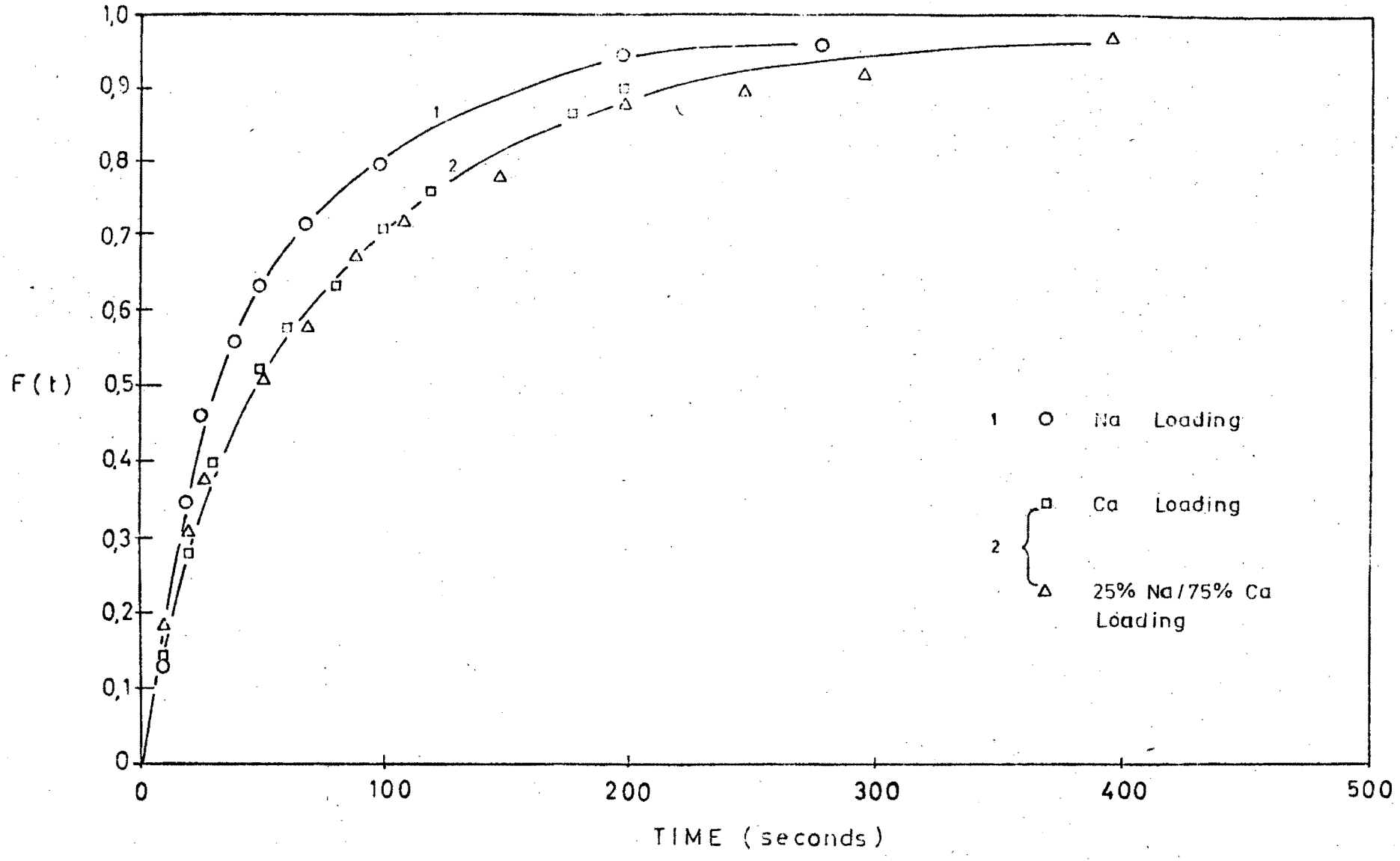

Fig. 5.22: F(t) Comparative Plot of 25%/75% Loading and Binary Na^{+} and Ca^{2+} Loading onto Zerolit 625 at 0,125N

be affected by the relative counter-ion concentrations (see Section 5.2.3.2(b) for regeneration equivalent). Proof of this is shown in Fig. 5.23, graph 3 and Fig. 5.24, where the H^+ kinetic curves for both systems on both F'(t) and F(t) coordinates remain similar. The total number of milliequivalents of Na^+ and H^+ on the resin remains constant, even though the individual milliequivalents change.

The increase in Ca^{2+} concentration, however, causes faster kinetics (see Fig. 5.23). This reinforces the theory that some film controlling characteristics exist, since liquid concentration should not affect the kinetics in a pure film diffusion controlled system.

From Fig. 5.23 it can also be seen that τ_{max}, the time to reach maximum Na^+ "overshoot", is approximately equal to 250 seconds for both systems. This results from the fact that Ca^{2+} diffusion is the rate controlling step, and independent, therefore, of initial relative concentration. Thus, while there are Ca^{2+} ions present in the loading solution, they will require a definite, constant time to reach the exchange site irrespective of initial relative concentration. The preloaded relative concentration will affect only the extent of loading before re-exchange takes place, but not the time at which it does so. This is dependent only on the counter-ions themselves and the resin type (pore structure). (Thus Dranoff and Lapidus [47] who used two different systems, obtained τ_{max} values of 18 seconds for the $H^+ - Ag^+ - Na^+$ system, and 11 seconds for the $H^+ - Ag^+ - Cu^{2+}$ system.)

5.3 PERFORMANCE OF A GEL RESIN - CATION FORT

The gel resin results are discussed in the same sequence as those of Zerolit 625 in the previous section.

5.3.1 Resin Properties

Cation Fort is a strong acid, gel type cation exchange resin, manufactured by Dia-Prosim, France, and supplied by Sentrachem Ltd., South Africa. The resin was supplied screened between approximately 0,60 mm and 0,85 mm, and having five different degrees of crosslinking - 4,5; 5,5; 6,75; 7,6 and 8,5 percent divinylbenzene (% DVB) respectively.

Before commencing the kinetic studies, the volume capacity and moisture retention capacity of each of the above five resins were measured. Section 5.2.1 gives the relevant definitions and Section 3.3.3 describes the methods used.

5.3.1.1 Volume Capacity:

This was measured only on resins in the Na^+ form, since it was shown in Section 5.2.1.1 that the nature of the loaded ion had minimal effect on the capacity. 14,65 ml aliquots of resin were used in all capacity determinations, and equation (5.1) was used to calculate the relevant results. The resulting data are tabulated in Table 5.9 and plotted in Fig. 5.25.

5.3.1.2 Discussion of Resin Volume Capacities

The capacity increases fairly uniformly with increasing crosslinking or divinylbenzene content within the degree of crosslinking investigated here (see Fig. 5.25). It must be anticipated, however, that the volume capacity will level off at some higher level of crosslinking [18,25].

This increase in capacity can be explained by the fact that a weakly crosslinked resin will swell to a greater extent than one which is more firmly crosslinked. Since the number of fixed ionic sites remains constant, the resin with the larger volume will have a lower volume capacity. (As defined per unit volume.) This explanation is supported by Helfferich [25], who states that "A weakly crosslinked resin

TABLE 5.9

VOLUME CAPACITIES OF GEL RESINS OF DIFFERING CROSSLINKING

% DVB	ml of resin	ppm Na^+ 1st elution in 250 ml	ppm Na^+ 2nd elution in 250 ml	Capacity meq/ml
4,5	14,65	1520	72	1,18
5,5	14,65	1860	-	1,43
6,75	14,65	2022	-	1,56
7,6	14,65	2289	-	1,76
8,5	14,65	2360	80	1,82

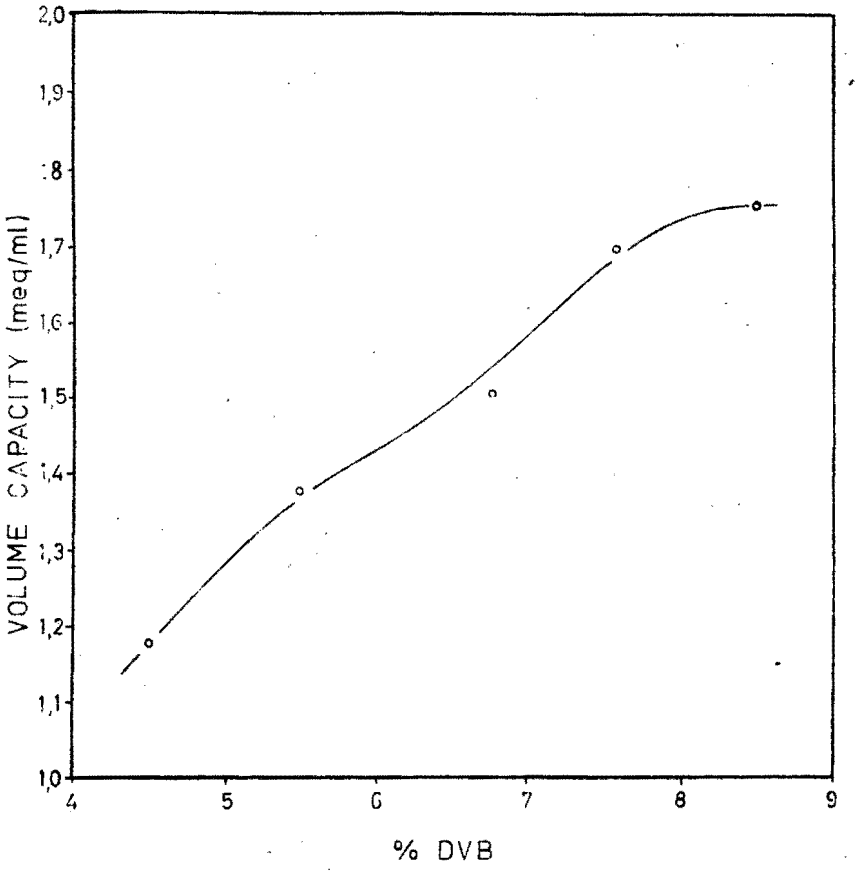

Fig. 5.25: % DVB Versus Volume Capacity Plot.

swells more strongly and thus has a lower capacity per unit volume".

As is shown in Table 5.9, the 4,5% DVB and 8,5% DVB resins were subjected to a second elution in order to determine the efficiency of the first elution. It was found that an average of 3,8% more Na^+ was stripped off on the second elution, and thus the remaining results were corrected using this value.

5.3.1.3 Moisture Retention Capacity

These were similarly performed for each of the five different crosslinked gel resins. The MRC furnishes a measure of the resin's water-holding capacity or swelling. Table 5.10 tabulates the results.

5.3.1.4 Discussion of MRC Results

As was found for Zerolit 625 resin (Section 5.2.1.4), the MRC value decreases with increasing loading ion ionic radius (see Table 5.10).

Further, as the degree of crosslinking increases, the lower the MRC value becomes. The reason is that the resin becomes more rigid with increasing DVB content, allowing less expansion in solution. Fig. 5.26 shows this general trend for each of the three resin forms - H^+, Na^+ and Ca^{2+}. It should be noted that, for all three resin forms, the reduction in MRC is most significant at low DVB levels, and becomes much less so at DVB levels above about 8%. The Dowex Ion Exchange Book [23] gives MRC data for Dowex 50 in the H^+ form, which corresponds closely with these H^+ form results.

5.3.2 Binary Kinetic Systems

As for the Zerolit 625 case, the Na^+/H^+ and Ca^{2+}/H^+ systems, which were the two binary kinetic systems studied, are discussed in this section. Both of these kinetic

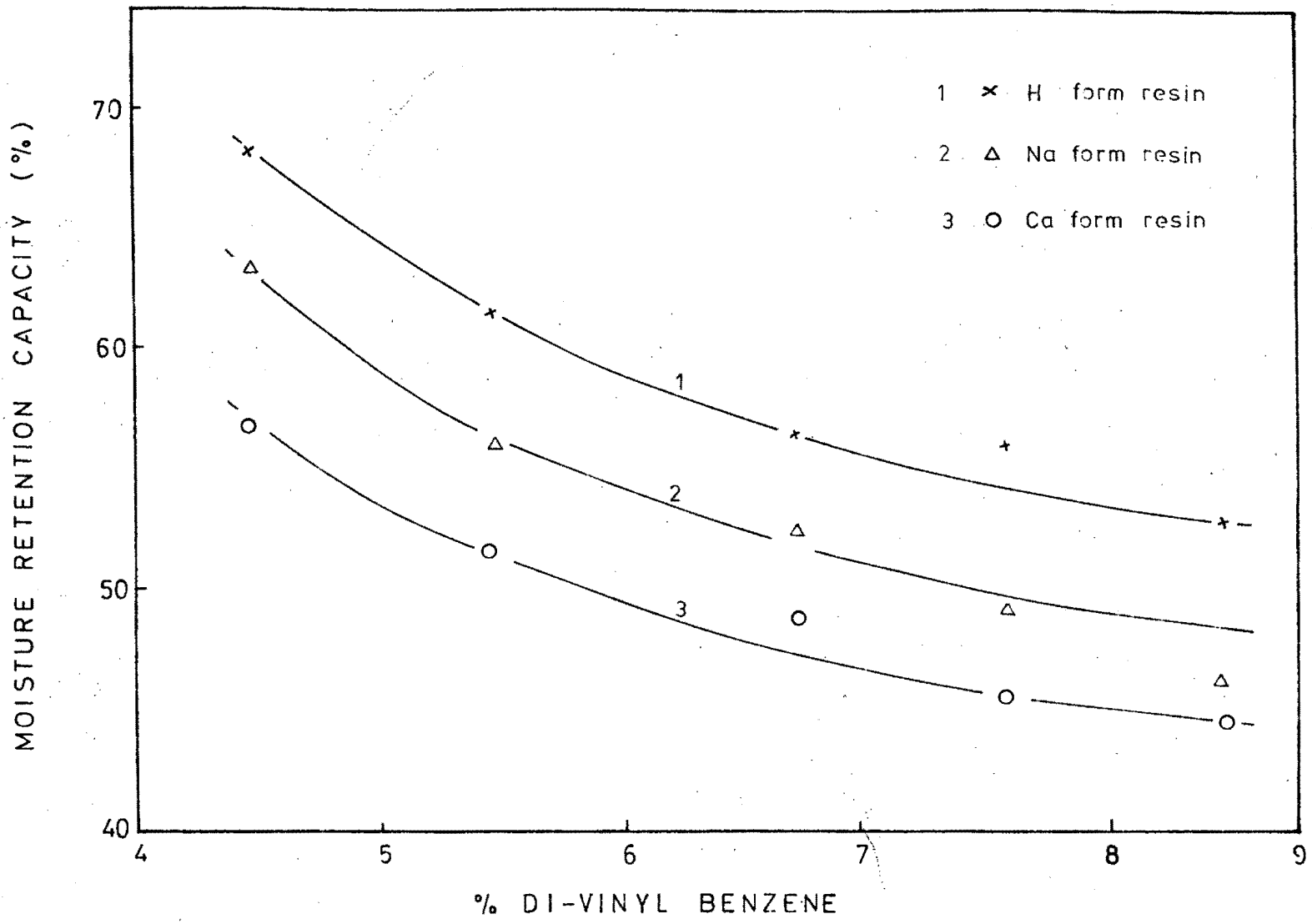

Fig. 5.26: Moisture Retention Capacity Variation with DVB Content.

TABLE 5.10

MOISTURE RETENTION CAPACITIES OF GEL RESINS OF DIFFERING CROSSLINKING

% DVB	Form	Wet Resin	Water	MRC	Average
4,5	H^+	4,1061	2,8001	68,19	68,48
4,5	H^+	3,2254	2,2181	68,77	
4,5	Na^+	3,6686	2,3328	63,59	63,78
4,5	Na^+	3,0725	1,9569	63,69	
4,5	Ca^{2+}	4,7974	2,7445	57,21	57,17
4,5	Ca^{2+}	3,4894	2,9933	57,13	
5,5	H^+	4,0957	2,5388	61,99	61,89
5,5	H^+	3,5885	2,2167	61,78	
5,5	Na^+	5,0942	2,8636	56,21	56,22
5,5	Na^+	3,1629	1,7783	56,22	
5,5	Ca^{2+}	4,1578	2,1522	51,76	51,91
5,5	Ca^{2+}	3,9501	2,0563	52,05	
6,75	H^+	4,9774	2,8297	56,85	56,85
6,75	H^+	4,5202	2,5701	56,86	
6,75	Na^+	3,6308	1,9175	52,81	52,77
6,75	Na^+	4,0430	2,1319	52,73	
6,75	Ca^{2+}	3,2462	1,5900	48,98	48,95
6,75	Ca^{2+}	3,9988	1,9559	48,91	
7,6	H^+	4,7946	2,6764	55,82	55,91
7,6	H^+	2,4016	1,3451	56,00	
7,6	Na^+	3,7497	1,8551	49,47	49,42
7,6	Na^+	2,6519	1,3090	49,36	
7,6	Ca^{2+}	5,3496	2,4550	45,89	45,89
7,6	Ca^{2+}	3,4095	1,2473	36,58	
8,5	H^+	5,5295	2,9294	52,98	52,96
8,5	H^+	3,3348	1,7651	52,93	
8,5	Na^+	6,1678	2,8452	46,13	46,15
8,5	Na^+	3,9746	1,8348	46,16	
8,5	Ca^{2+}	4,5567	2,0264	44,47	44,44
8,5	Ca^{2+}	2,5596	1,1367	44,41	

systems were performed at 0,125N and 0,50N concentrations, at a stoichiometric ratio of 0,5. Resin of 6,75% DVB content was used in the majority of the standard runs, as a mid-range representative resin of the resin set studied.

Equation (5.2) was used to calculate F(t) values from liquid concentrations. The experimental procedure is described in Section 3.3.5.1.

5.3.2.1 Regeneration Kinetics

These were performed as described in Section 3.3.5.1. The quantities used in the four systems studied are given in Table 5.11:

TABLE 5.11

RESIN AND LIQUID QUANTITIES USED IN GEL RESIN BINARY REGENERATION KINETICS

Initial Conc. (N)	Counter-ion Studied	R/L	Resin Vol. (ml)	Liquid Vol. (ml)
0,125	Na^+	0,5	33,4	800
	Ca^{2+}	0,5	33,4	800
0,50	Na^+	0,5	84	500
	Ca^{2+}	0,5	84	500

The resulting kinetic data are tabulated in Tables C-8 and C-9 and plotted in Figs. 5.27 to 5.30.

5.3.2.2 Discussion of Regeneration Kinetics

(a) Effect of the Counter-Ion:

Figs. 5.27 to 5.30 show the F(t) plots of the Na^+ and Ca^{2+} regeneration kinetics at 0,125N and 0,50N. From these

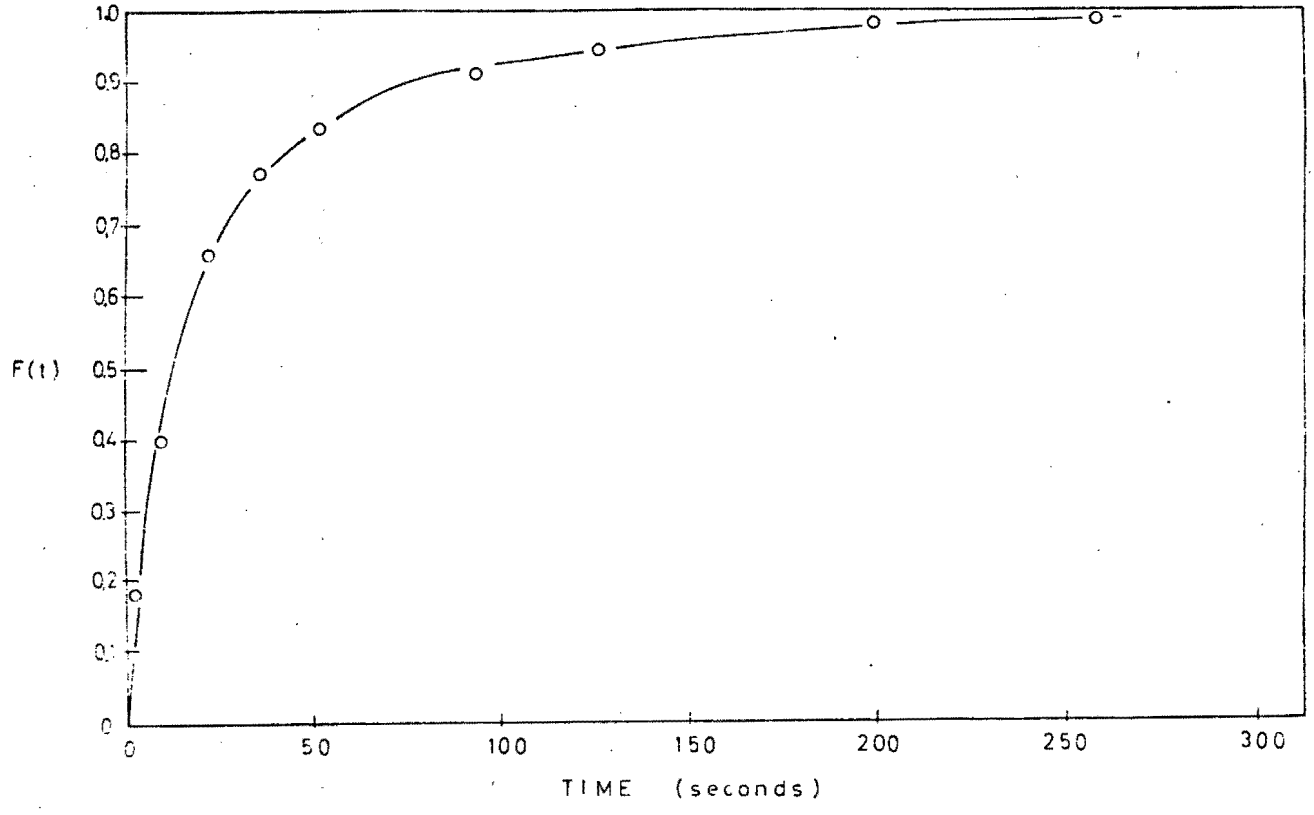

Fig. 5.27: Regeneration of Na^+ Form Cation Fort at 0,125N Concentration

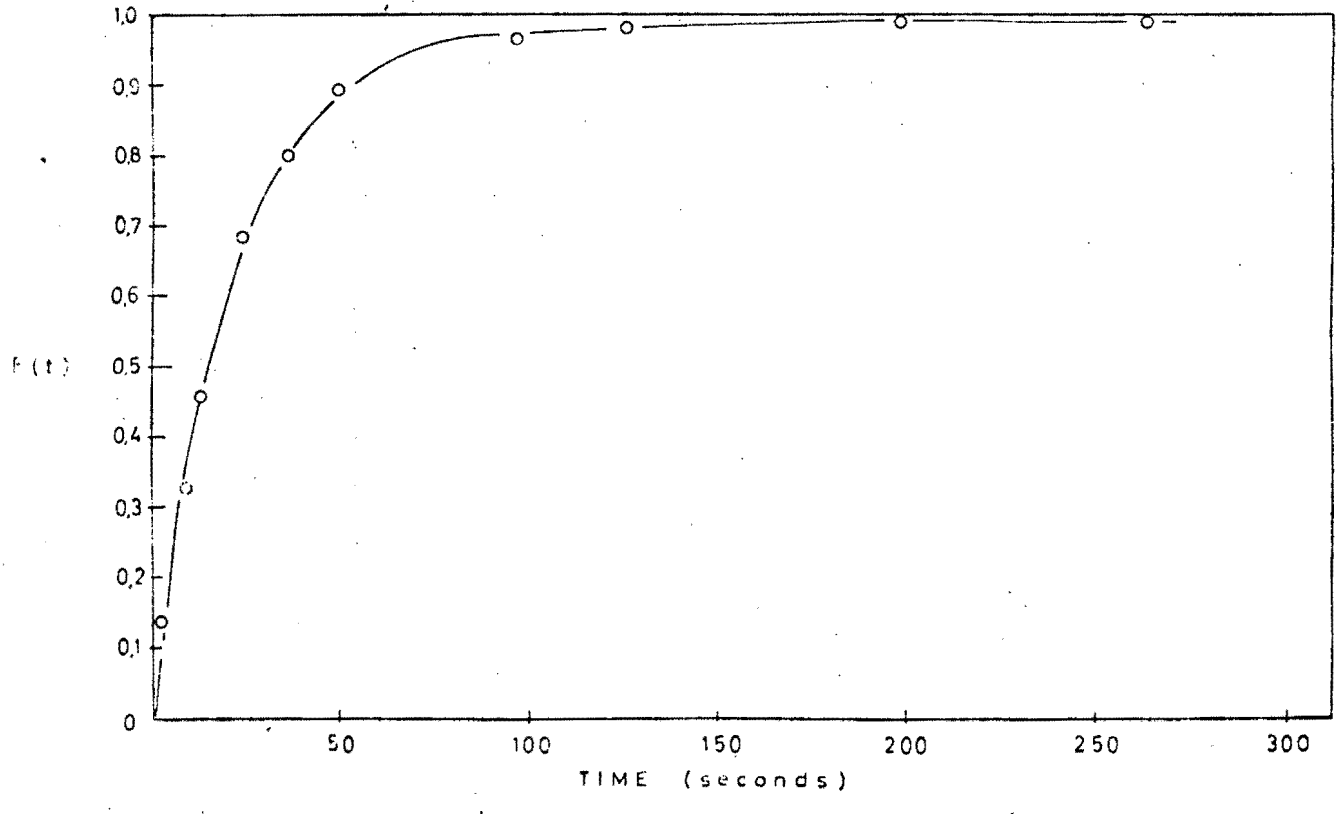

Fig. 5.28: Regeneration of Na^+ Form Cation Fort at 0,50N Concentration

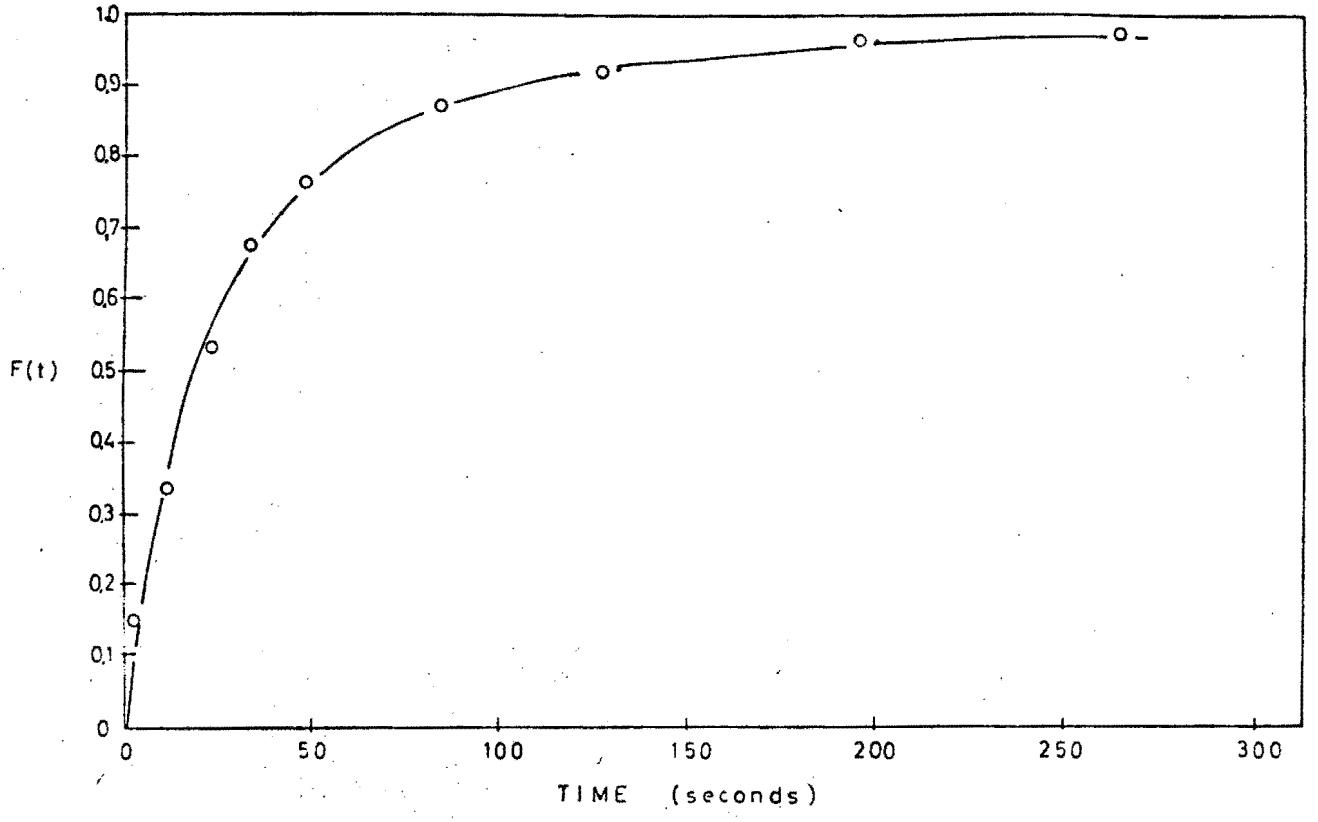

Fig. 5.29: Regeneration of Ca^{2+} Form Cation Fort at 0,125N Concentration

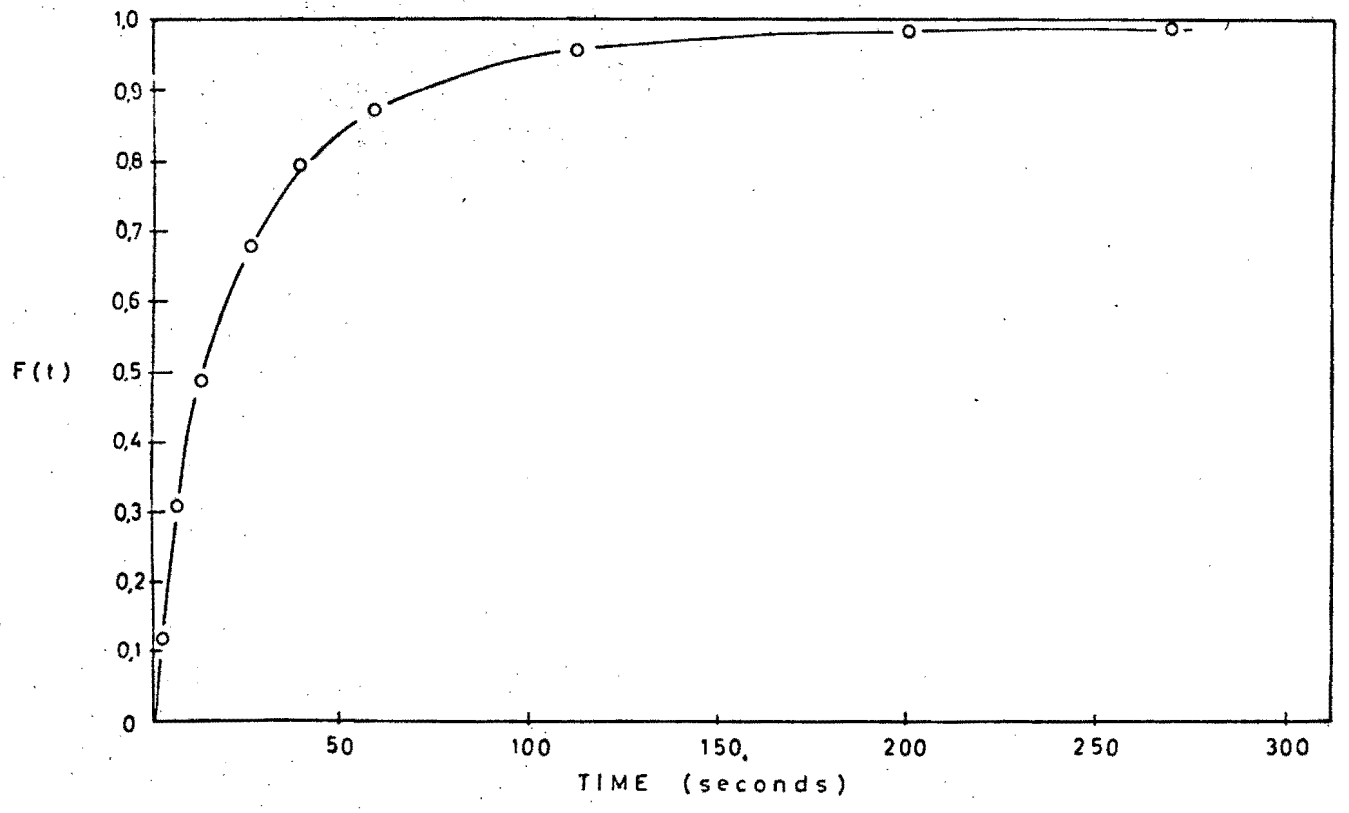

Fig. 5.30: Regeneration of Ca^{2+} Form Cation Fort at 0,50N Concentration

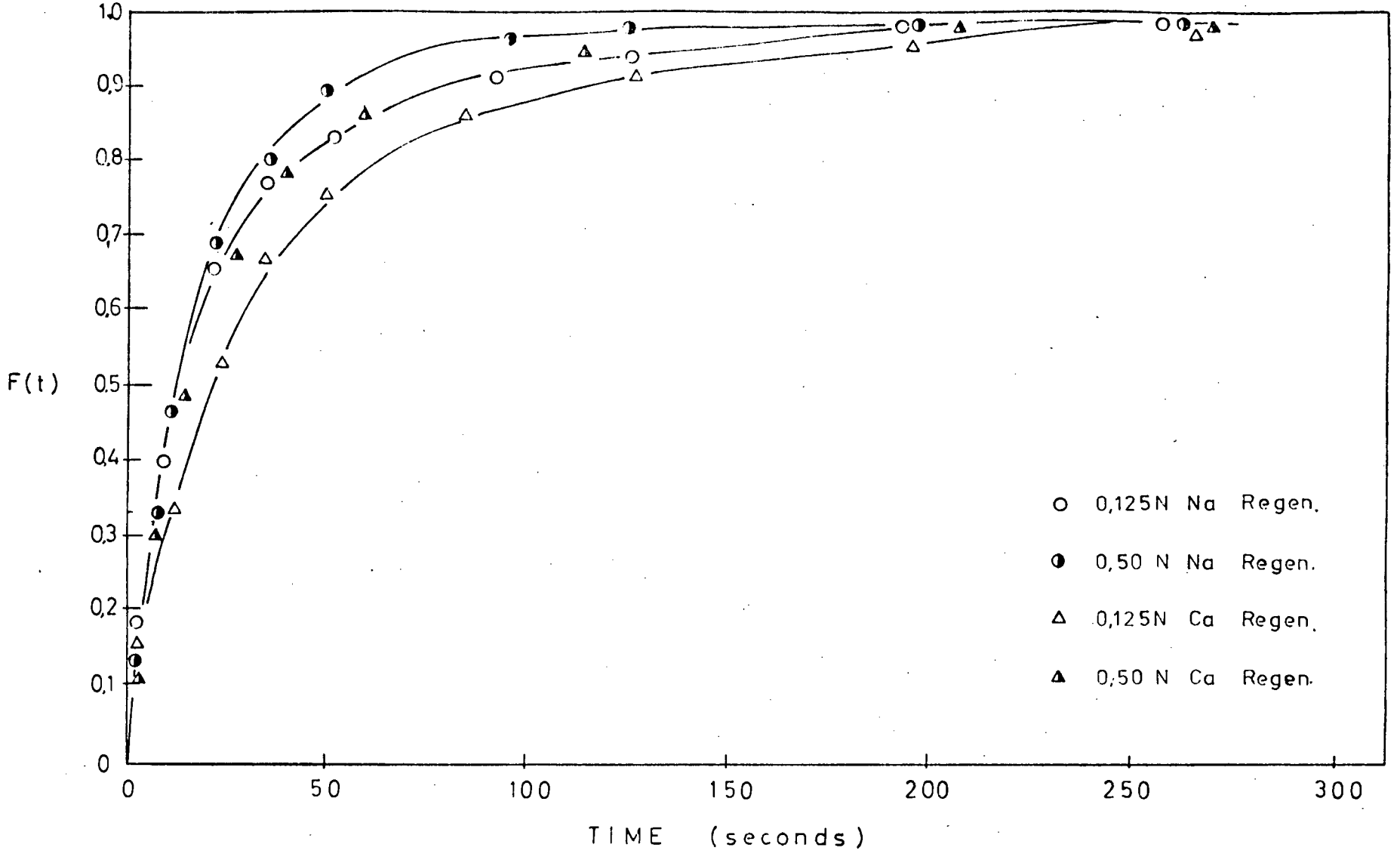

Fig. 5.31: Comparison Between Cation Fort Na^+ and Ca^{2+} Regeneration at 0,125N and 0,50N Concentrations

graphs, Fig. 5.31 was drawn, showing a comparison between the two systems. For both the 0,125N and 0,50N concentrations the Na^+ kinetics are faster than the Ca^{2+} kinetics. This result is similar to that found for the Zerolit 625 system, and the explanation is the same as that given in Section 5.2.2.2.

(b) Effect of Concentration:

Fig. 5.31 shows that the higher concentration results in faster kinetics.

5.3.2.3 Loading Kinetics

This run was performed at 0,125N concentration only. 33,4 ml of resin in the H^+ form was reacted with 800 ml of NaCl, in order to attain an R/L ratio of 0,5. The results are tabulated in Table C-10 and plotted in Fig. 5.32.

5.3.2.4 Discussion of Forward and Reverse Kinetics

Fig. 5.32 shows the results of the Na^+ regeneration and loading, at 0,125N and at an R/L of 0,5, on gel resin of 7,5% DVB content.

It can be seen that there is an appreciable difference between the loading and regeneration kinetics - the loading kinetics being faster. This coincides with Helfferich's [25] description of a pore-diffusion controlled system (Section 5.2.2.4) in which it is stated that the kinetics are faster when the more mobile counter-ion is initially in the resin. This corresponds to the loading kinetics in the systems being studied. It is evident, therefore, that the gel resin portrays greater pore-diffusion control characteristics than does the macroporous 625 resin.

It was shown in Fig. 5.31 (see Section 5.3.2.2(b)) that solution concentration affects the kinetics, although to a lesser extent than in the case of Zerolit 625. In the gel resin, a four-fold increase in the concentration results in an

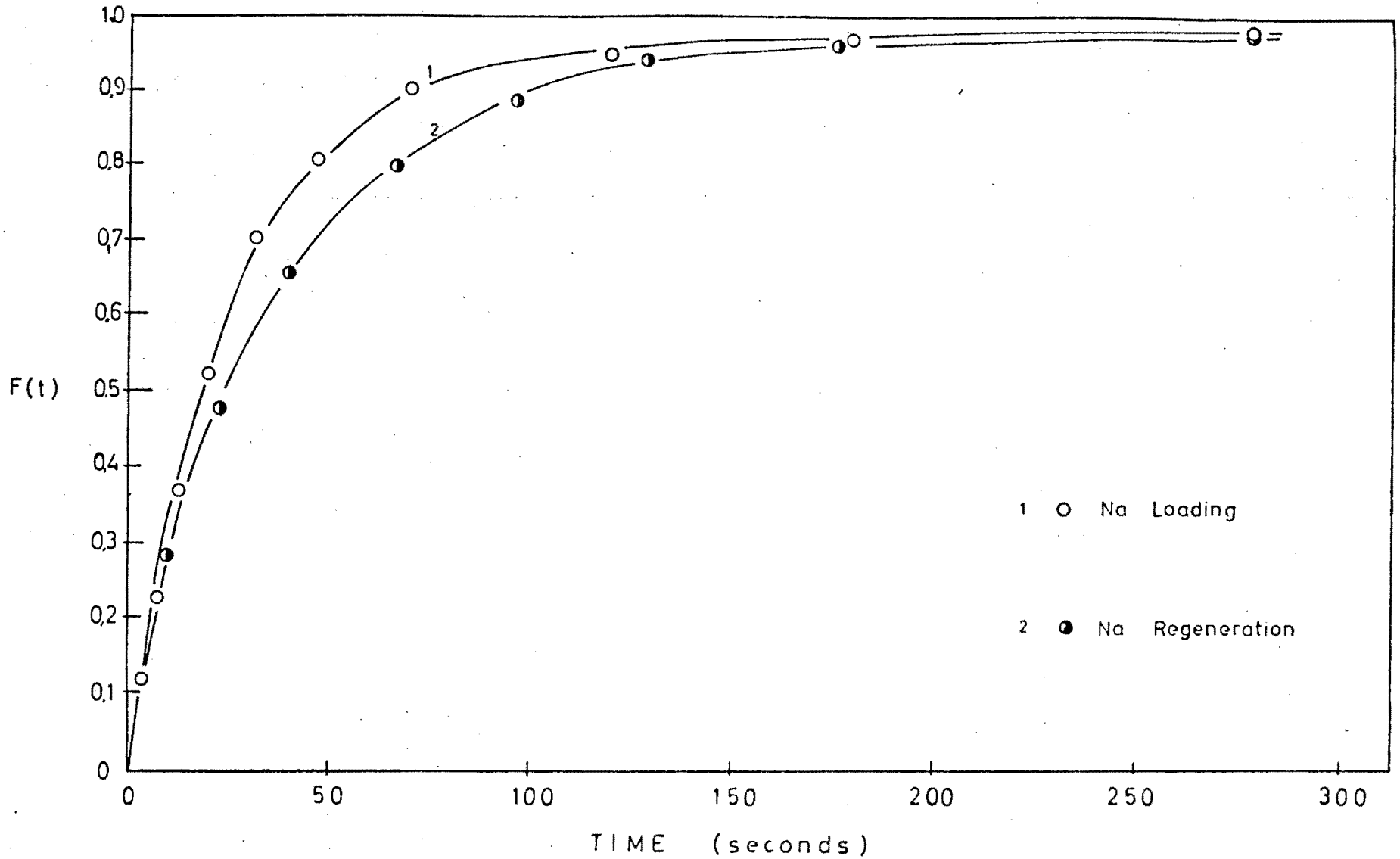

Fig. 5.32: Comparison Between Cation Fort Na^+ Loading and Regeneration at 0,125N Concentration

8-10% increase in the kinetics compared with a 15-20% increase in the case of Zerolit 625. This provides further confirmation of the greater degree of pore-diffusion control in the case of the gel resin as compared with the macroporous resin (under similar operating conditions).

5.3.2.5 Na^+ Regeneration on Gel Resins of Different DVB Content

In addition to the gel resin of 6,75% DVB content on which the majority of the previous kinetic tests were performed, Na^+ regeneration kinetics were measured at 0,125N and at an R/L of 0,5 on gel resins of three further DVB contents - 5,5; 7,6 and 8,5 (%) (see Section 5.3.1 for physical characteristics of these respective resins).

800 ml of 0,125N HCl was used for all the runs, and the respective quantities of resin used are tabulated in Table 5.12, calculated to give an R/L ratio of 0,5.

TABLE 5.12

RESIN QUANTITIES FOR Na^+ REGENERATION ON DIFFERING % DVB GEL RESINS

% DVB	ml Wet Resin Used
5,5	36,2
7,6	29,4
8,5	28,6

The results are tabulated in Tables C-11 to C-13 and plotted in Fig. 5.33.

5.3.2.6 Discussion of Na^+ Regeneration on Gel Resins of Different DVB Content

The results of the Na^+ regeneration on gel resins of different DVB content are shown in Fig. 5.33.

Helfferich [25] states that, for pore-diffusion controlled exchange systems, the rate of exchange decreases with increasing crosslinking. This result is fairly obvious, since the retardation by the resin matrix of diffusion of the counter-ions increases with reduced fractional pore volume, which is affected primarily by the degree of crosslinking (see Section 5.2.1 for the effect of crosslinking on the moisture retention capacities). Helfferich indicates a reduction of the self-diffusion coefficient with increasing DVB content (crosslinking), initially rapid and flattening out after approximately 15% DVB, as illustrated in Fig. 5.34.

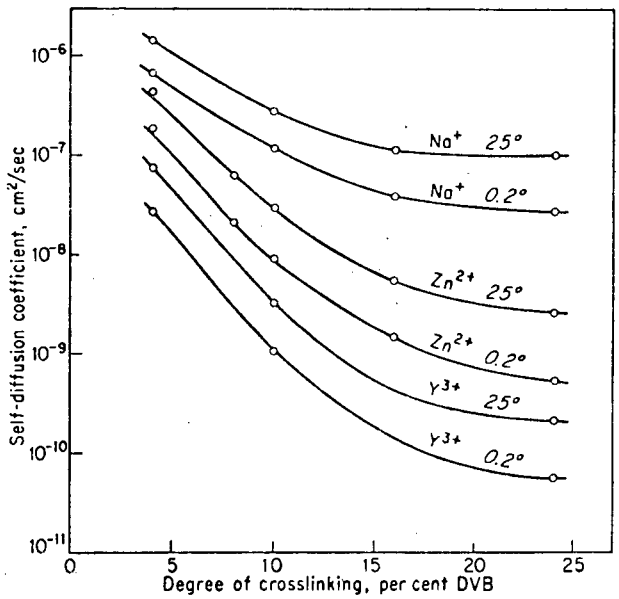

Fig. 5.34: Dependence of Self-Diffusion Coefficient on Degree of Crosslinking.

Fig. 5.33 shows that the 5,5%, 7,6% and 8,5% DVB resins' kinetics decrease with increasing percent crosslinking, as predicted above. Further, between 5,5% and 7,6% DVB the kinetic rate is retarded to a greater extent than between 7,6% and 8,5% DVB, since the difference in DVB content is

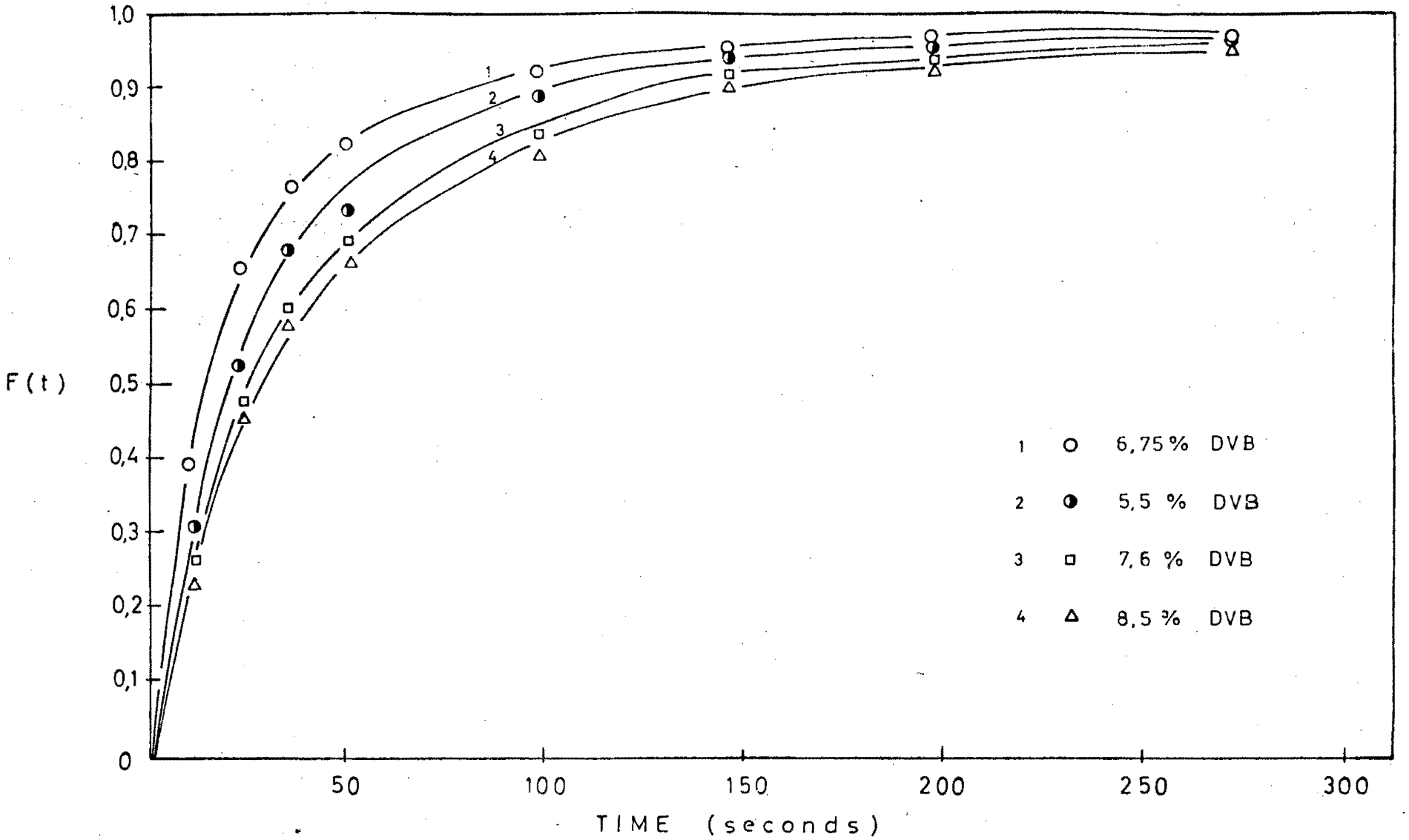

Fig. 5.33: Comparison of Cation Fort Na^+ Regeneration of Resin of Different Crosslinking

proportionately larger.

It would be expected that the 6,75% DVB gel resin kinetics would fall between the 5,5% and 7,6% DVB resin kinetic curves. However, as is shown in Fig. 5.33, this is not the case. The kinetics for the 7,65% DVB resin are faster than those for the 5,5% DVB resin. This is probably due to some factor in the resin manufacture (such as a different batch of basic polymer base or different manufacturing reaction conditions) leading to an increase in the kinetic properties of this particular resin. This behaviour of the 6,75% DVB gel resin is apparent throughout these studies.

5.3.3 Ternary Kinetic Systems

The kinetics for the regeneration and loading of Na^+ and Ca^{2+} as competing species on a gel resin were performed at 0,125N and at a stoichiometric ratio of 0,5, following a similar procedure to that for the macroporous 625 resin, i.e. in the regeneration case, two differently preloaded resins were tested, while for loading, two different liquid compositions were used. Corresponding kinetic tests are described in the following sections.

As for Zerolit 625, results are presented in both F(t) and F'(t) or F"(t) form. The relevant equations are given in Table 5.7.

5.3.3.1 Regeneration Kinetics

(a) Preloaded Resin Compositions:

Resin samples (preloaded resin mentioned in Section 5.3.3) were eluted with 5N HCl solution and the actual concentrations measured. The results are given in Table 5.13.

(b) Resin and Liquid Quantities:

For both comparative systems, 34 ml of suitably preloaded resin was reacted with 800 ml of 0,125N HCl, in

TABLE 5.13

ACTUAL GEL RESIN RELATIVE PRELOADED CONCENTRATIONS FROM ELUTIONS

Theoretical Composition	meq Na^+	meq Ca^{2+}	Actual Composition
50% Na^+/50% Ca^{2+}	32,6	29,8	52% Na^+/48% Ca^{2+}
25% Na^+/75% Ca^{2+}	17,8	46,1	28% Na^+/72% Ca^{2+}

order to obtain a stoichiometric ratio of 0,5.

The results are tabulated in Tables C-14 and C-15, and plotted in Figs. 5.35 to 5.38.

5.3.3.2 Discussion of Regeneration Kinetics

(a) Individual Systems:

Figs. 5.35 to 5.38 give the results for the regeneration of 50% Na^+/50% Ca^{2+} and 25% Na^+/75% Ca^{2+} gel resin with 0,125N HCl at an R/L ratio of 0,5. As before (see Section 5.2.3.2(a)), there is no Na^+ "overshoot" evident in these results.

From Fig. 5.36 it will be seen that the Na^+ and Ca^{2+} regeneration kinetics are virtually identical. The kinetics are extremely fast, so that, although a small dip in the kinetics of the two cases probably does exist, it is not detectable with this system.

In Fig. 5.37 a small difference at high F(t) value is noticeable, since the kinetics are slightly slower in this case.

Figs. 5.35 and 5.37 (the two F"(t) curves, representing the liquid ion fractions) show that, in both comparative systems, only a small proportion of Ca^{2+} is stripped off the

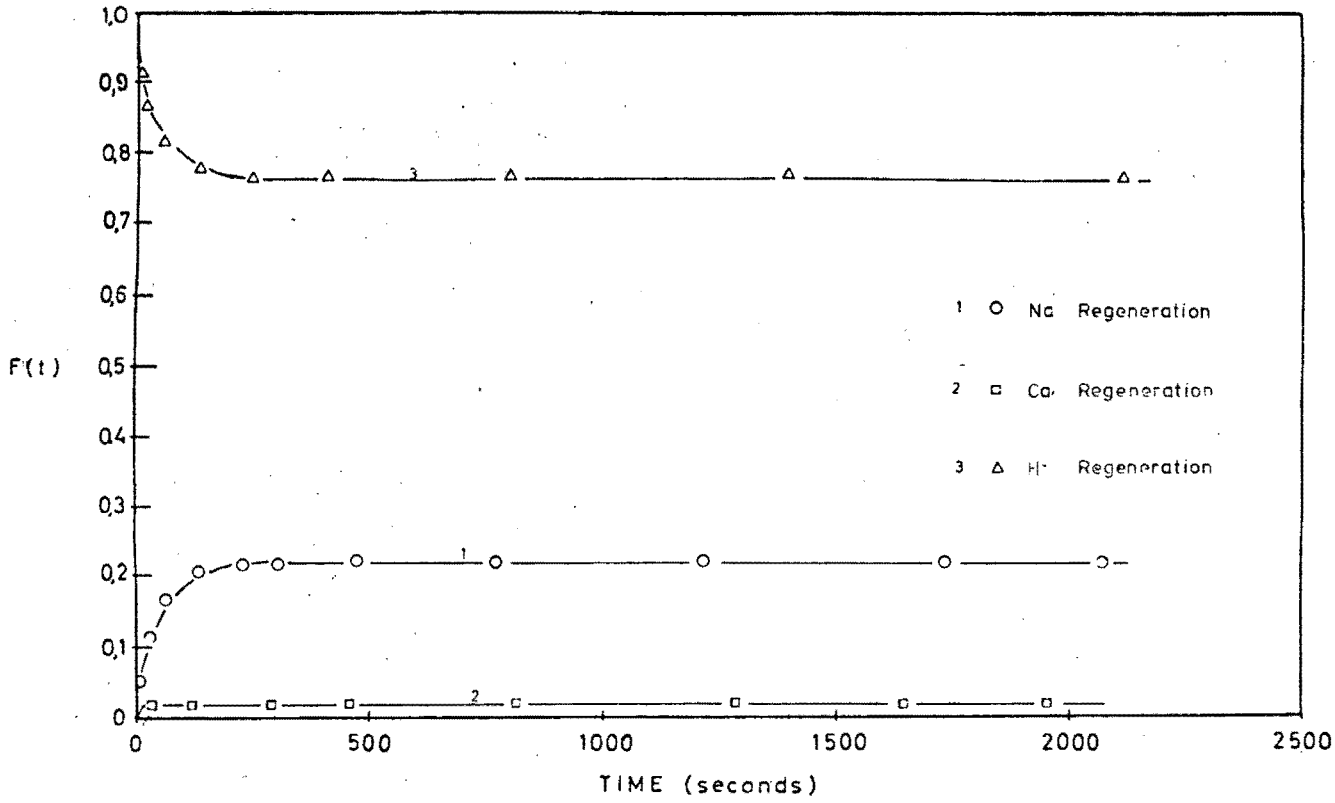

Fig. 5.35: F'' (t) Plot of Regenerating a 50%/50% Preloaded Cation Fort Resin at 0,125N Concentration

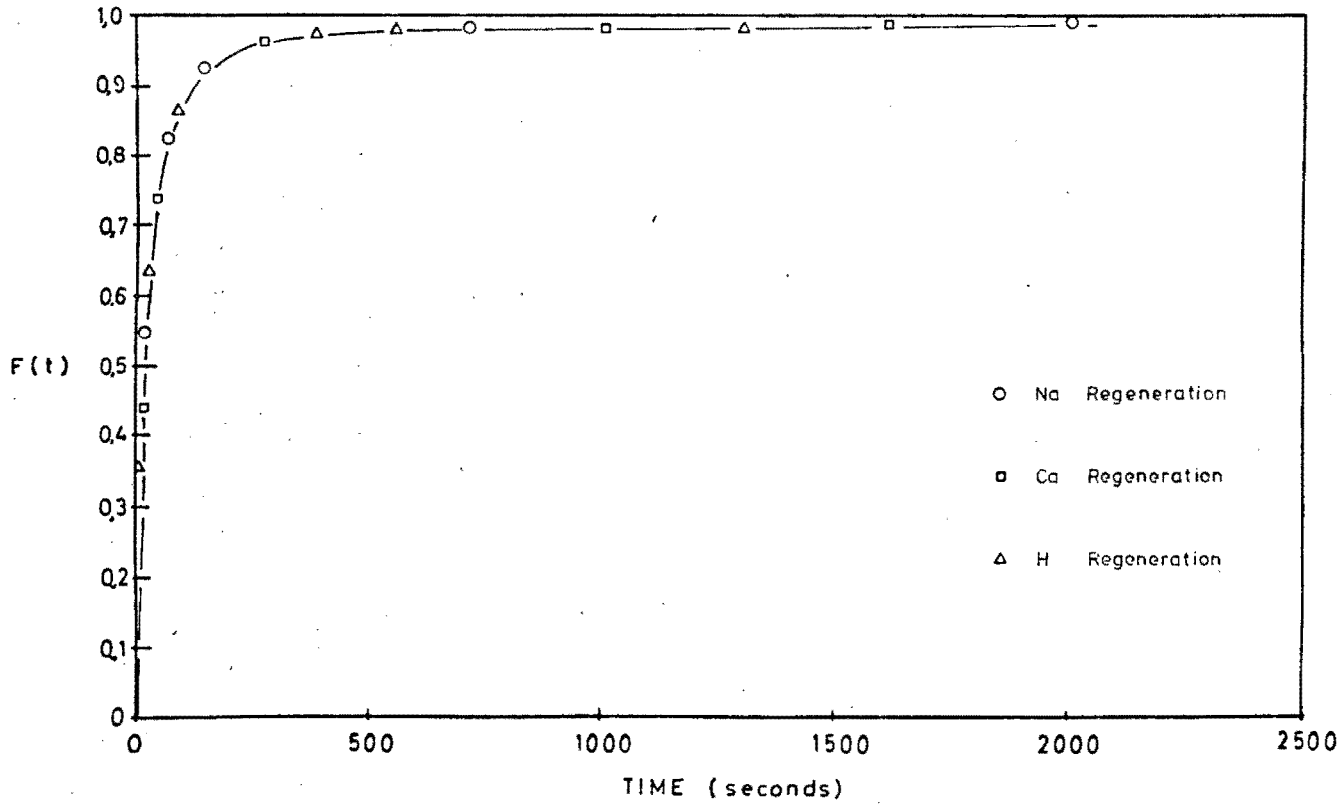

Fig. 5.36: F(t) Plot of Regenerating a 50%/50% Preloaded Cation Fort Resin at 0,125N Concentration

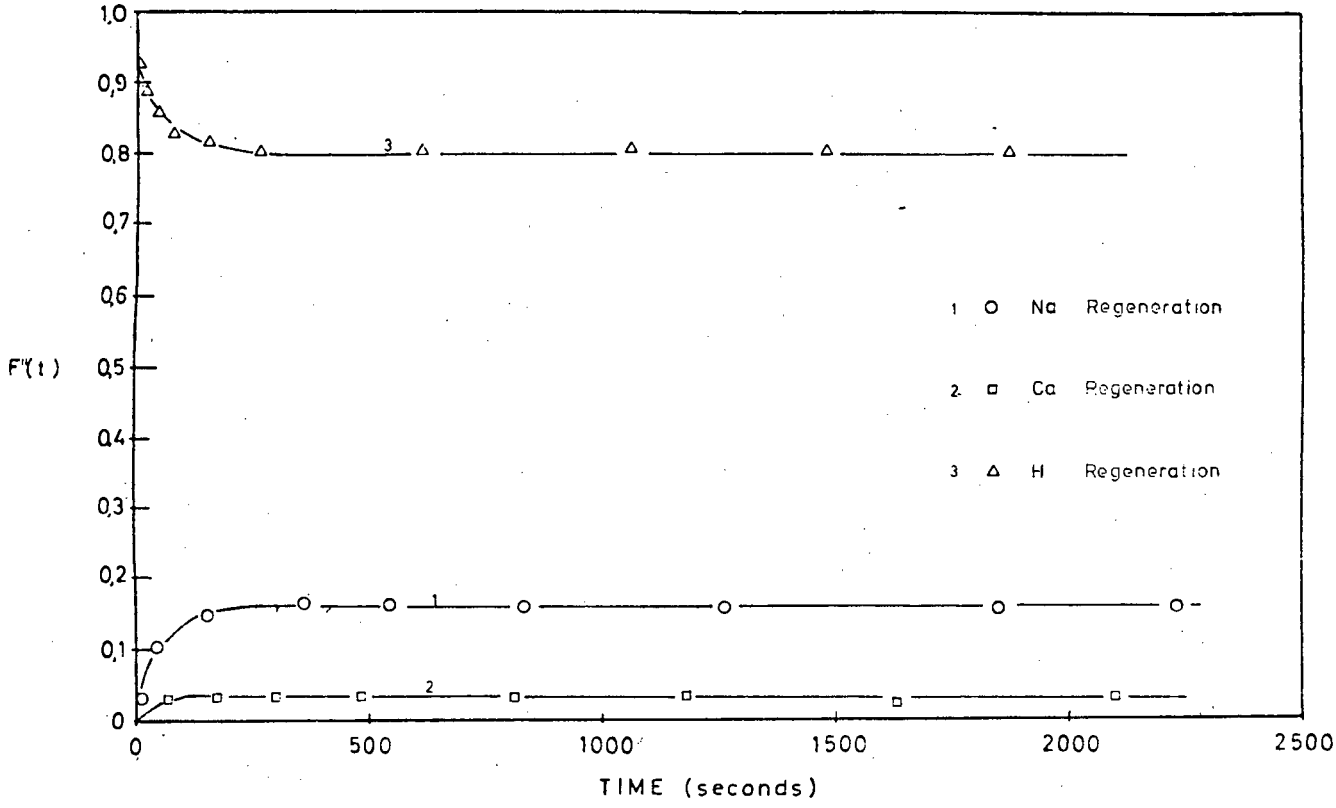

Fig. 5.37: F''(t) Plot of Regenerating 25%/75% Preloaded Cation Fort Resin at 0,125N Concentration

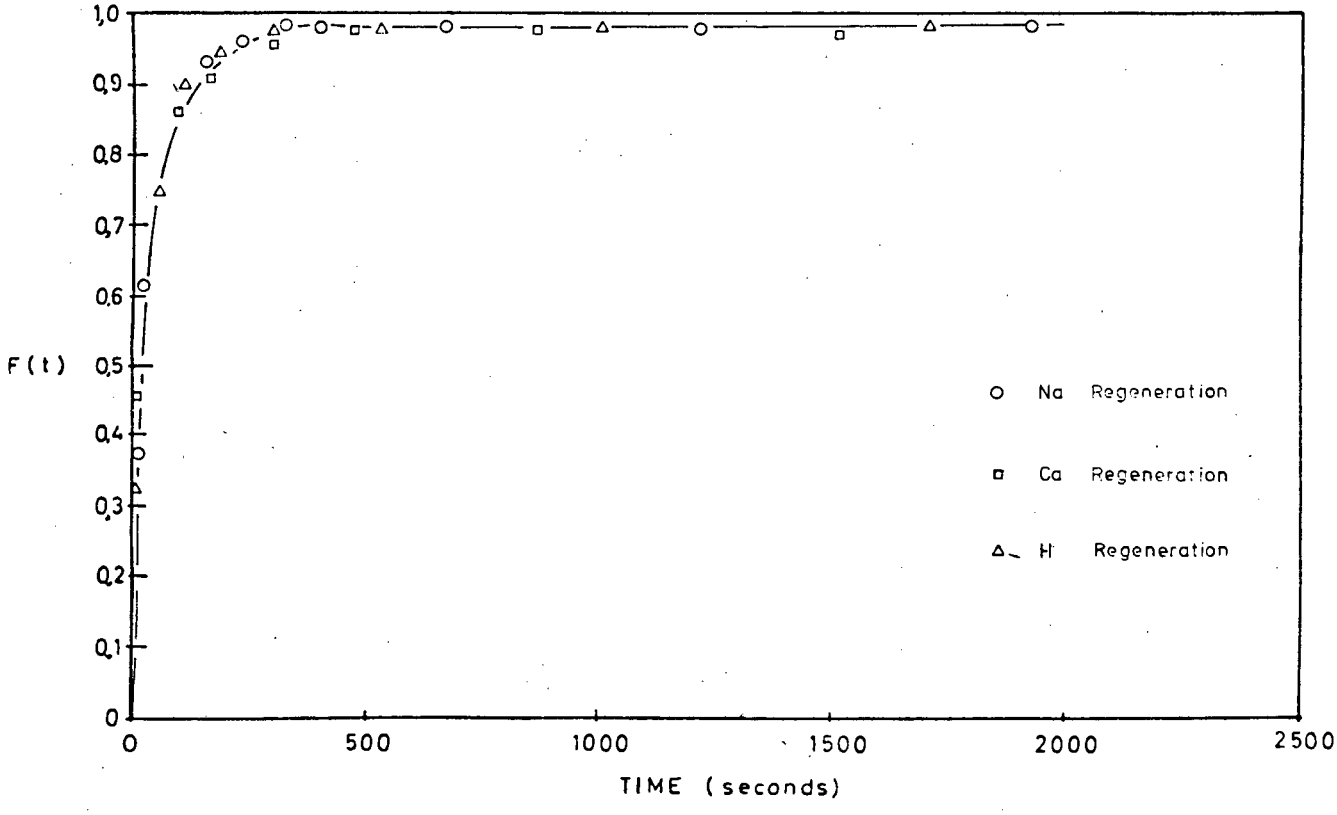

Fig. 5.38: F(t) Plot of Regenerating 25%/75% Preloaded Cation Fort Resin at 0,125N Concentration

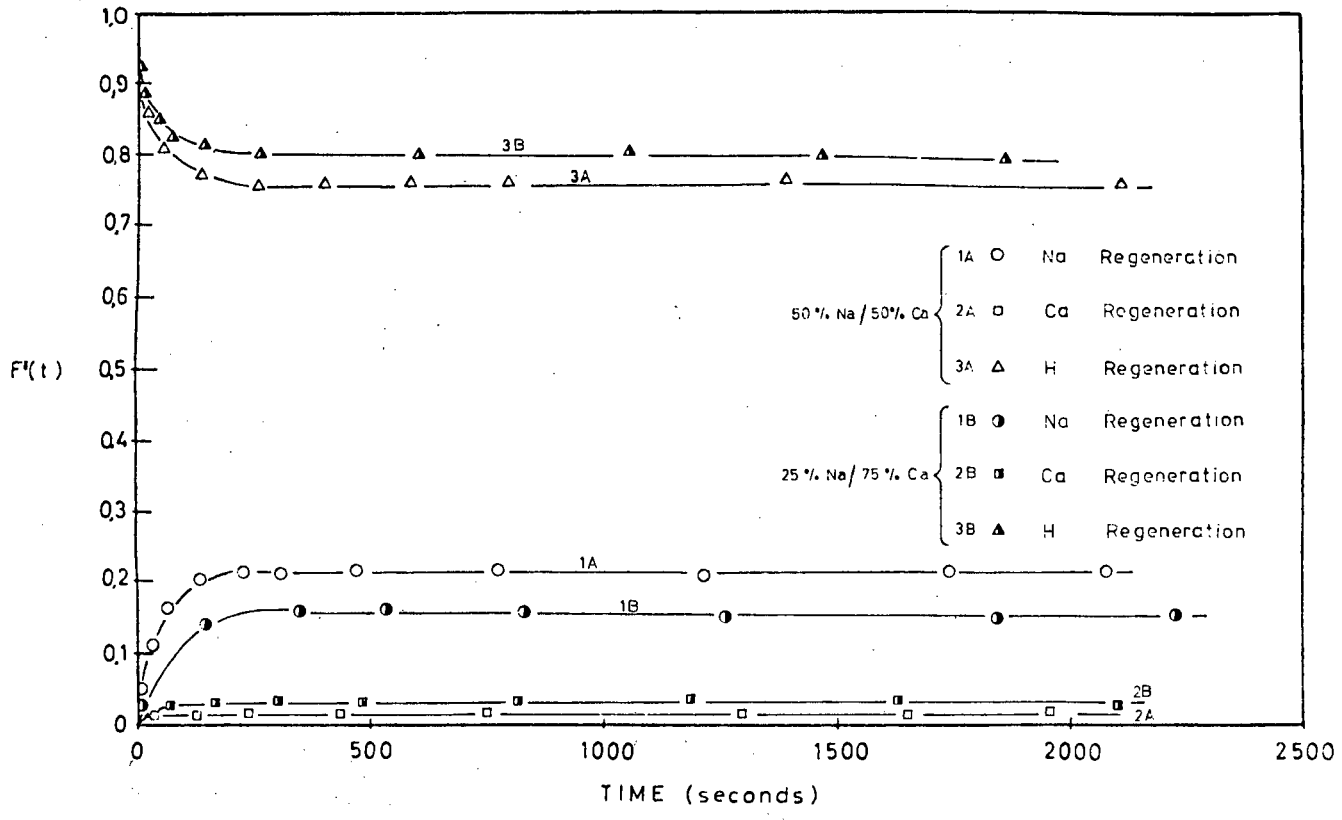

Fig. 5.39: F'' (t) Comparative Plot of Regeneration of 50%/50% and 25%/75% Preloaded Cation Fort Resin at 0,125N

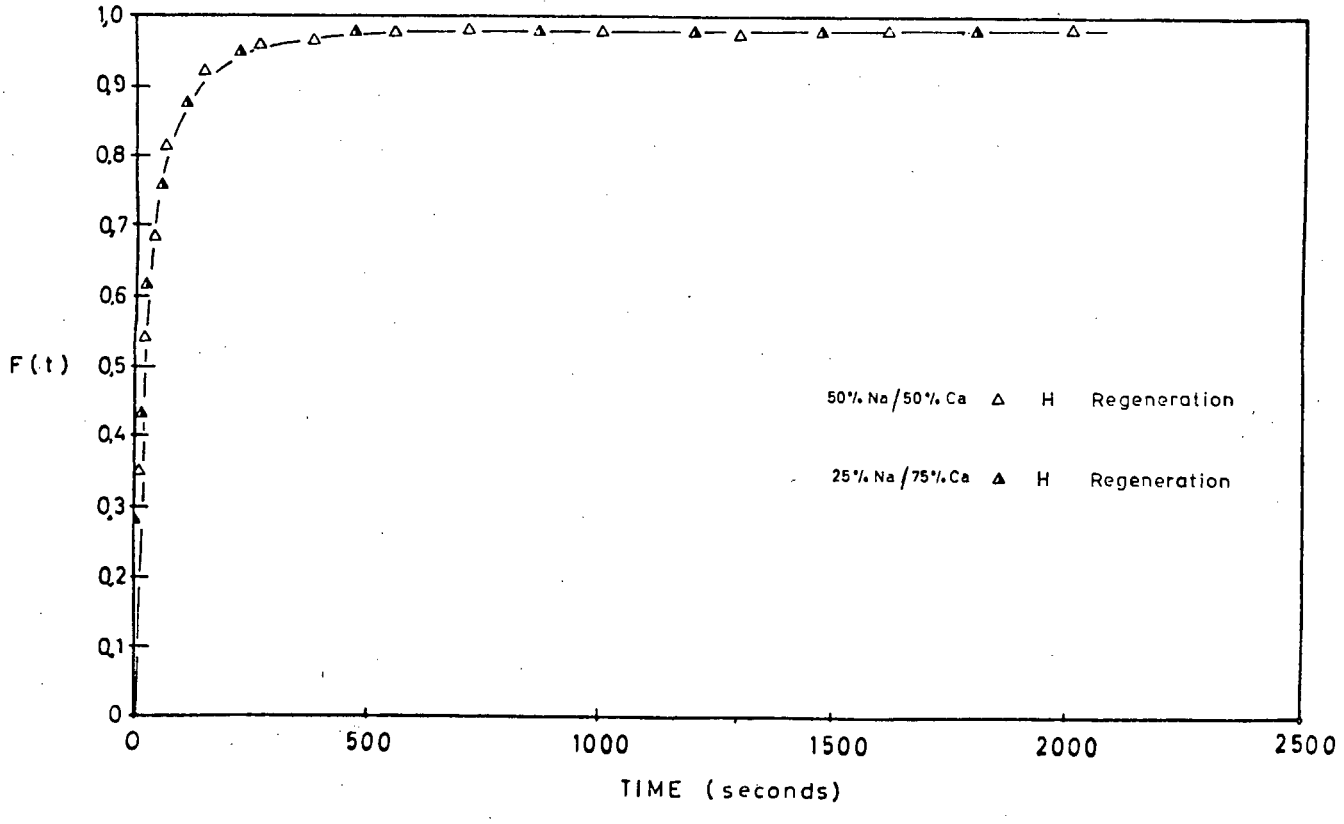

Fig. 5.40: F(t) Comparative Plot of Regeneration of 50%/50% and 25%/75% Preloaded Cation Fort Resin at 0,125N

resin in comparison with the Na^+. Since the resin has a much higher affinity for Ca^{2+}, Na^+ would tend to come off in preference to the Ca^{2+} as is evident in these results.

(b) Comparison Between 50% Na^+/50% Ca^{2+} and 25% Na^+/75% Ca^{2+} Systems:

Figs. 5.39 and 5.40 give a comparison, on F"(t) and F(t) coordinates respectively, between the 50% Na^+/50% Ca^{2+} and 25% Na^+/75% Ca^{2+} preloaded gel resin regeneration kinetics.

In Fig. 5.39 it is shown that the system, for which the resin has the higher Ca^{2+} preloading , has a final F"(t) equilibrium value (liquid ion fraction) for Ca^{2+} higher than that for the second system (see Fig. 5.39, graphs 2A and 2B). A similar trend is shown for the Na^+ case. However, the change between the two different preloaded systems is greater for Na^+ than for Ca^{2+}, since the former is far more easily stripped off the resin. This affects the F"(t) H^+ kinetic values (Fig. 5.39, graphs 3A and 3B), since the total number of milliequivalents exchanged are different (compared with the loading case where total milliequivalents loaded is independent of initial concentrations - see Section 5.3.3.4(b)). However. when plotted on the normalised F(t) system (Fig. 5.40), the two kinetic curves are almost identical. This shows that the overall rate of regeneration exchange is independent of initial degree of preloading , but the total exchanged milliequivalents is not.

5.3.3.3 Loading Kinetics

For both comparative systems, 34 ml of suitably regenerated gel resin was loaded with 400 ml of (i) 50% NaCl and 50% $CaCl_2$ solution, and (ii) 25% NaCl and 75% $CaCl_2$ solution, in order to obtain a stoichiometric ratio of 0,5.

The results are tabulated in Tables C-16 and C-17, and plotted in Figs. 5.41 to 5.44.

5.3.3.4 Discussion of Loading Kinetics

(a) Individual Systems:

Figs. 5.41 to 5.44 give the results of loading the 50% Na^+/50% Ca^{2+} and 25% Na^+/75% Ca^{2+} solutions onto gel resin at 0,125N and an R/L ratio of 0,5. It is again evident that the Na^+ "overshoots" its equilibrium value in both systems. The reasons for this are similar to those for the macroporous Zerolit 625 (see Section 5.2.3.4(a)).

In both systems, the Ca^{2+} kinetics are again slower than the Na^+ because of the former counter-ion's decreased mobility. The overall H^+ kinetics are somewhat slower than Na^+ kinetics.

In the same way as for the Zerolit 625 results in Fig. 5.22, an F(t) plot in Fig. 5.45 shows a comparison between the H^+ kinetics of the 25% Na^+/75% Ca^{2+} loading system with the straight binary Na^+ and Ca^{2+} loading onto gel resin. Although the two kinetic graphs are similar, the ternary system tends to follow the Ca^{2+} kinetics, again indicating that the Ca^{2+} diffusivity controls the ternary kinetics, as was discussed in Section 5.2.3.4(a).

(b) Comparison Between 50% Na^+/50% Ca^{2+} and 25% Na^+/75% Ca^{2+} Systems:

Figs. 5.46 and 5.47 give a comparison on both F'(t) and F(t) coordinates, between the 50% Na^+/50% Ca^{2+} and 25% Na^+/75% Ca^{2+} systems on gel resin.

Fig. 5.45 indicates that the individual Na^+ and Ca^{2+} kinetics vary with composition, but the H^+ (overall) kinetics do not, i.e. kinetic rates are not affected by the initial amount of Ca^{2+} in the loading liquid (see Section 5.2.3.4(a)). This is shown, on a normalised F(t) plot, in Fig. 5.47. Similar results were found for the Zerolit 625 kinetics (Section 5.2.3.4(b)) and indicate, once again, that the rate controlling mechanism is the Ca^{2+} diffusion. This explains why the overall kinetics are independent of relative concentration - while Ca^{2+} is present, it will control the

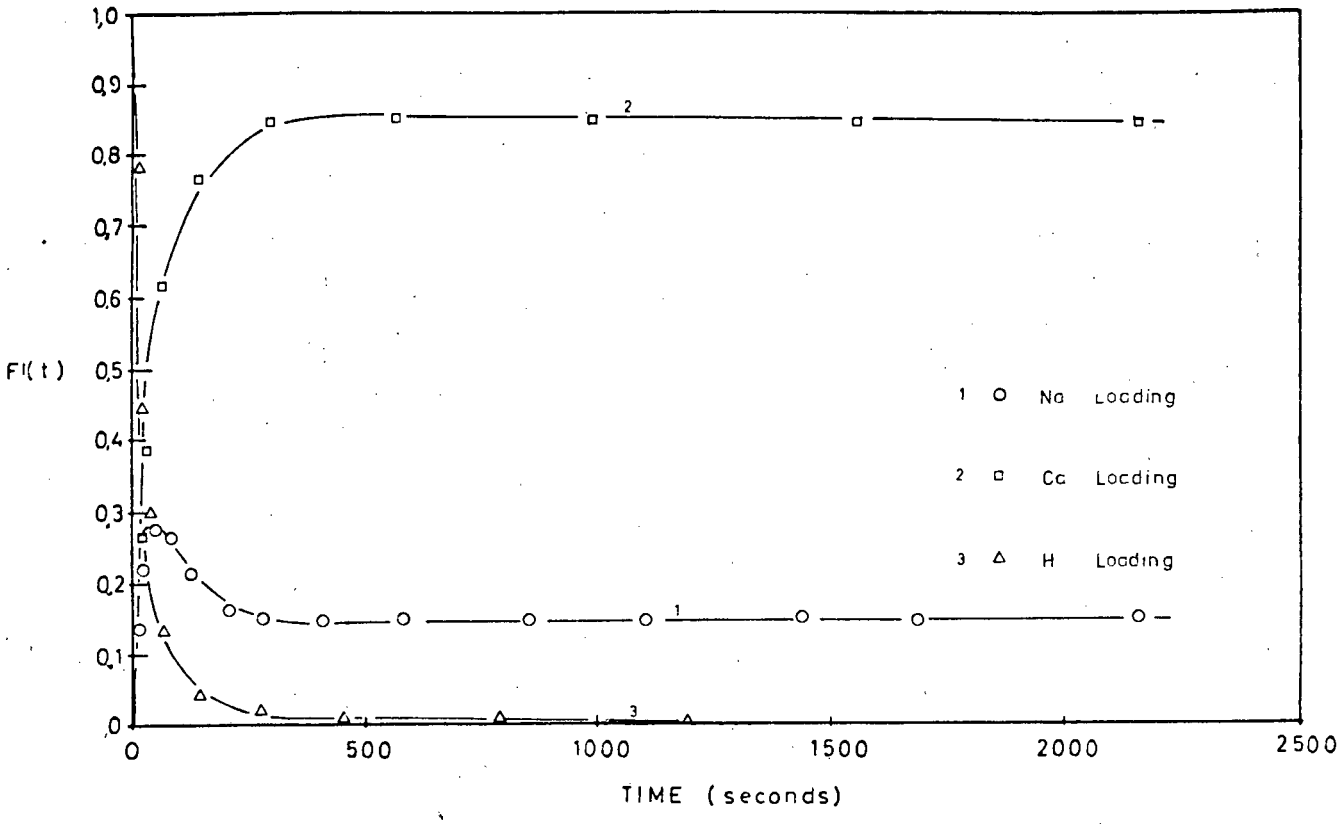

Fig. 5.41: F'(t) Plot of Loading 50%/50% Mixture onto Cation Fort at 0,125N

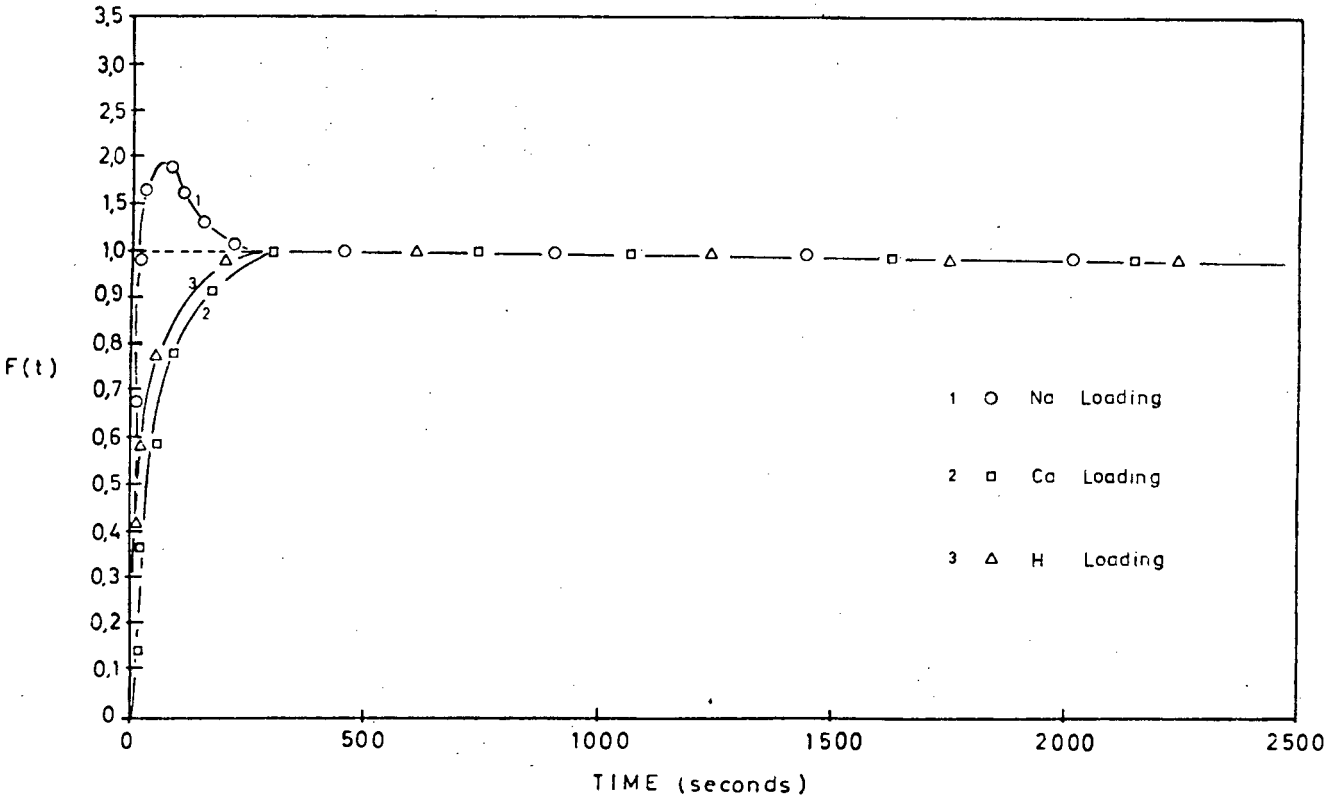

Fig. 5.42: F(t) Plot of Loading 50%/50% Mixture onto Cation Fort at 0,125N

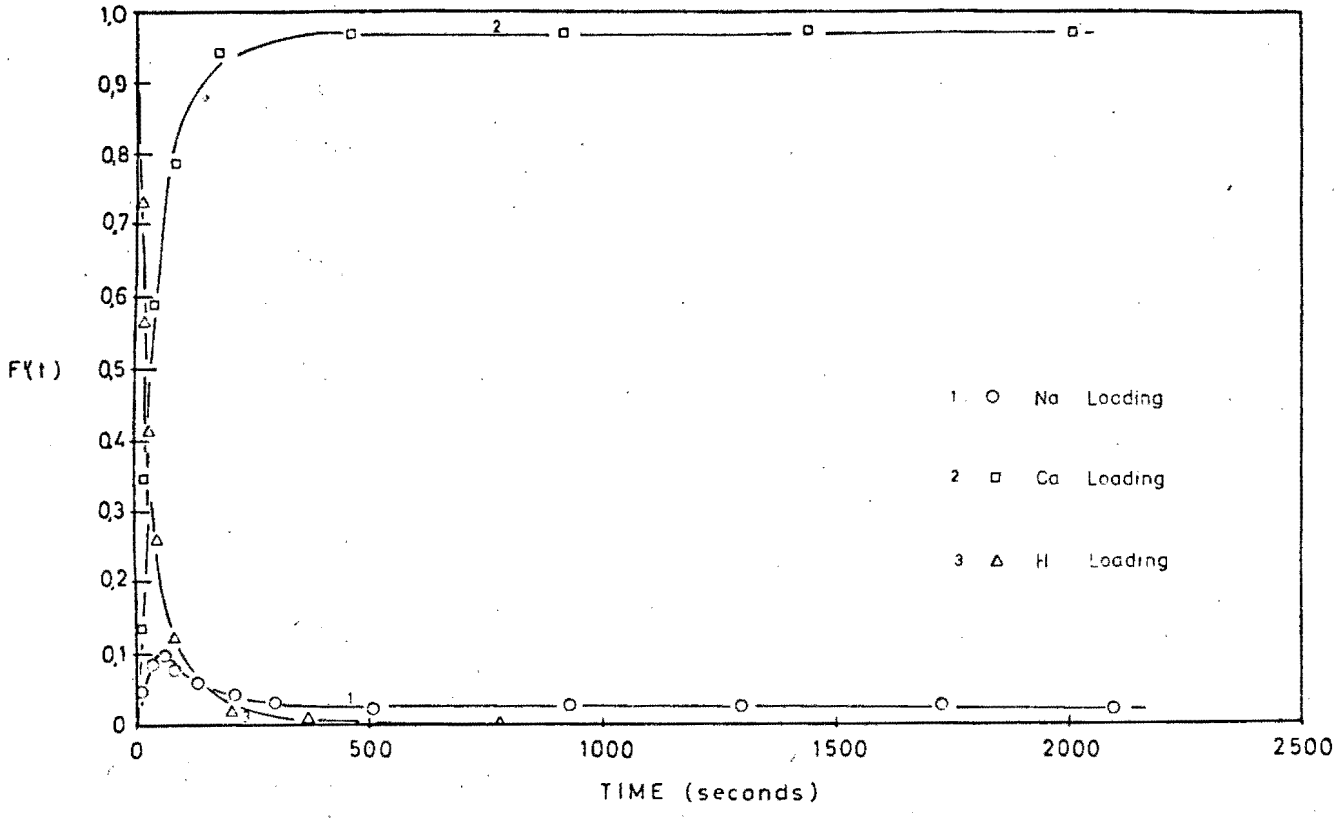

Fig. 5.43: F'(t) Plot of Loading 25%/75% Mixture onto Cation Fort at 0,125N

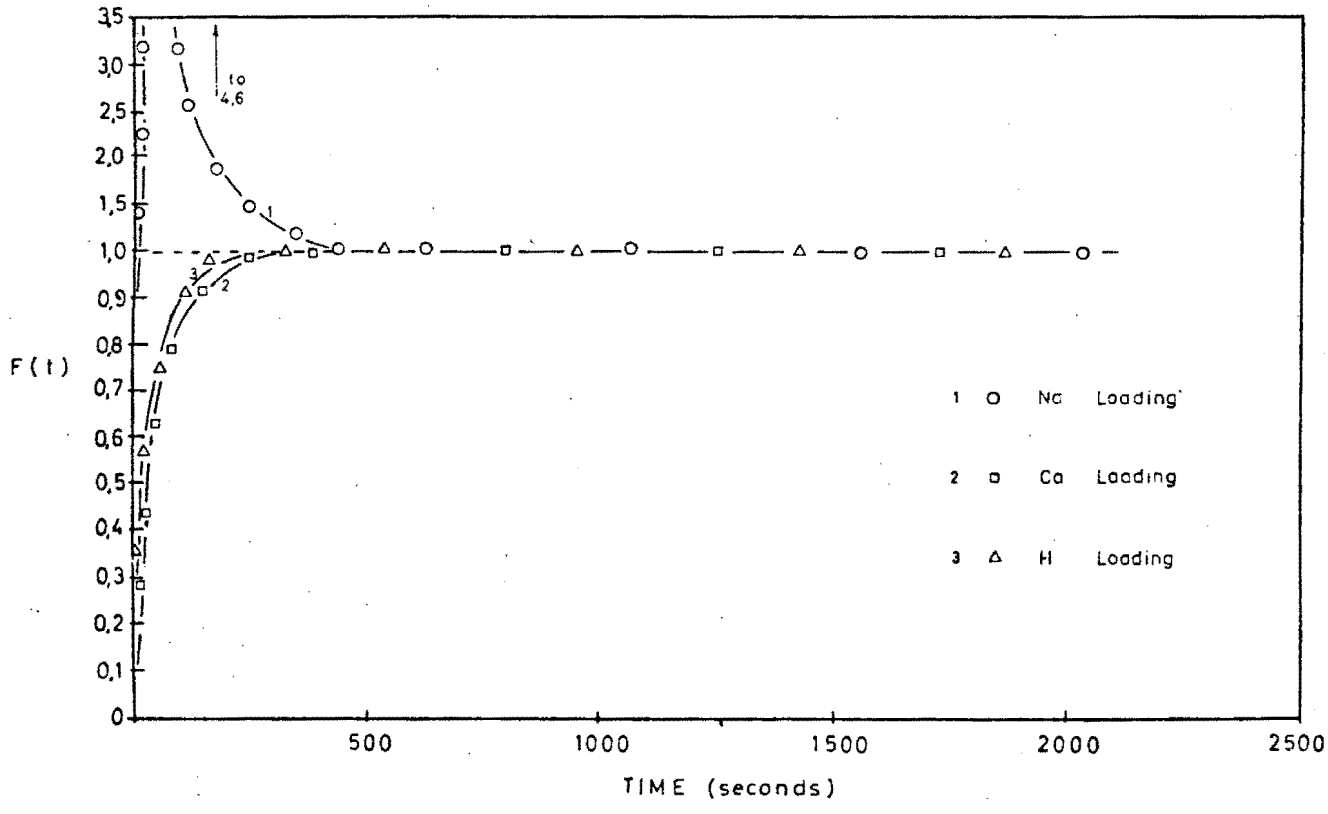

Fig. 5.44: F(t) Plot of Loading 25%/75% Mixture onto Cation Fort at 0,125N

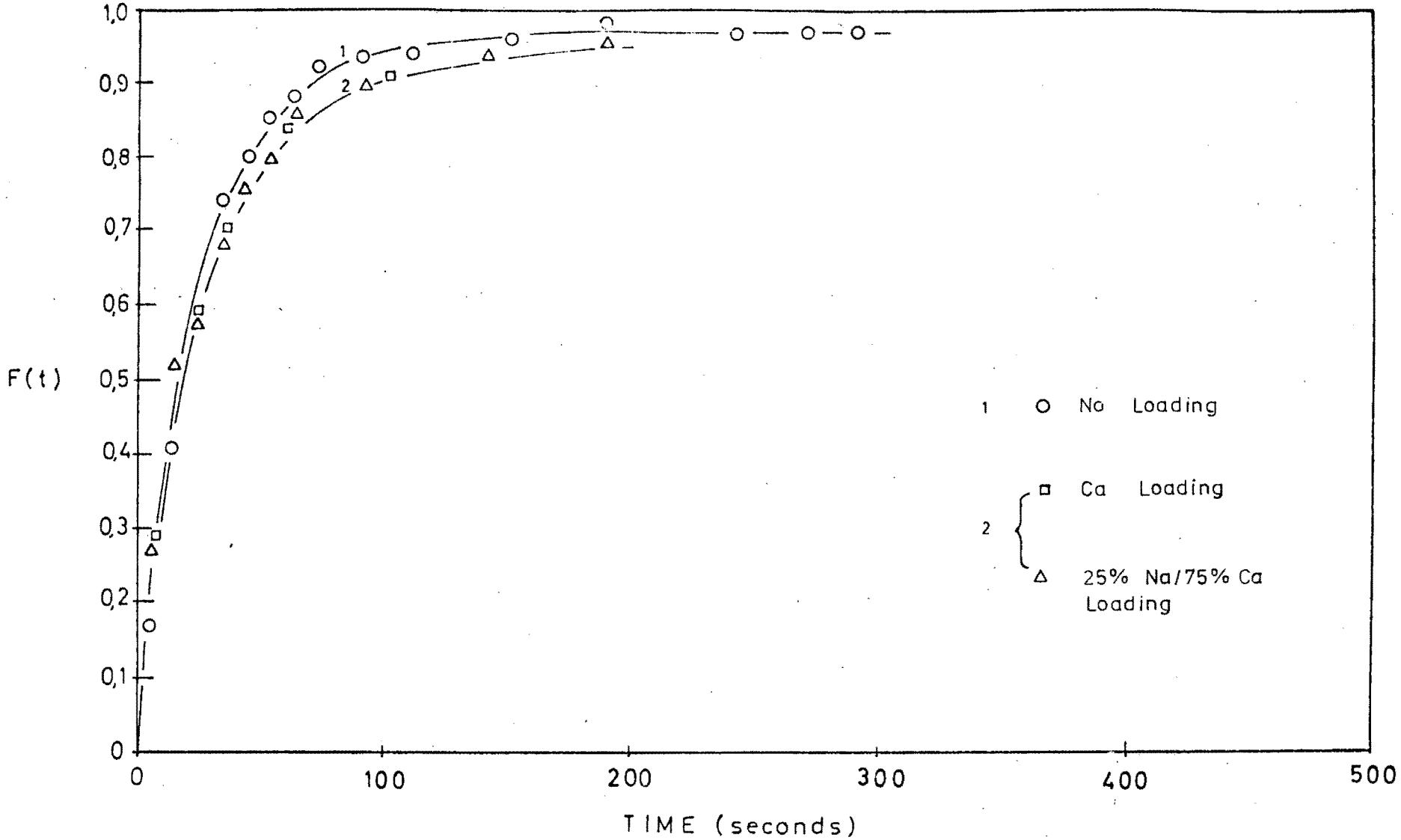

Fig. 5.45: F(t) Comparative Plot of 25%/75% Loading and Binary Na^+ and Ca^{2+} Loading onto Cation Fort at 0,125N

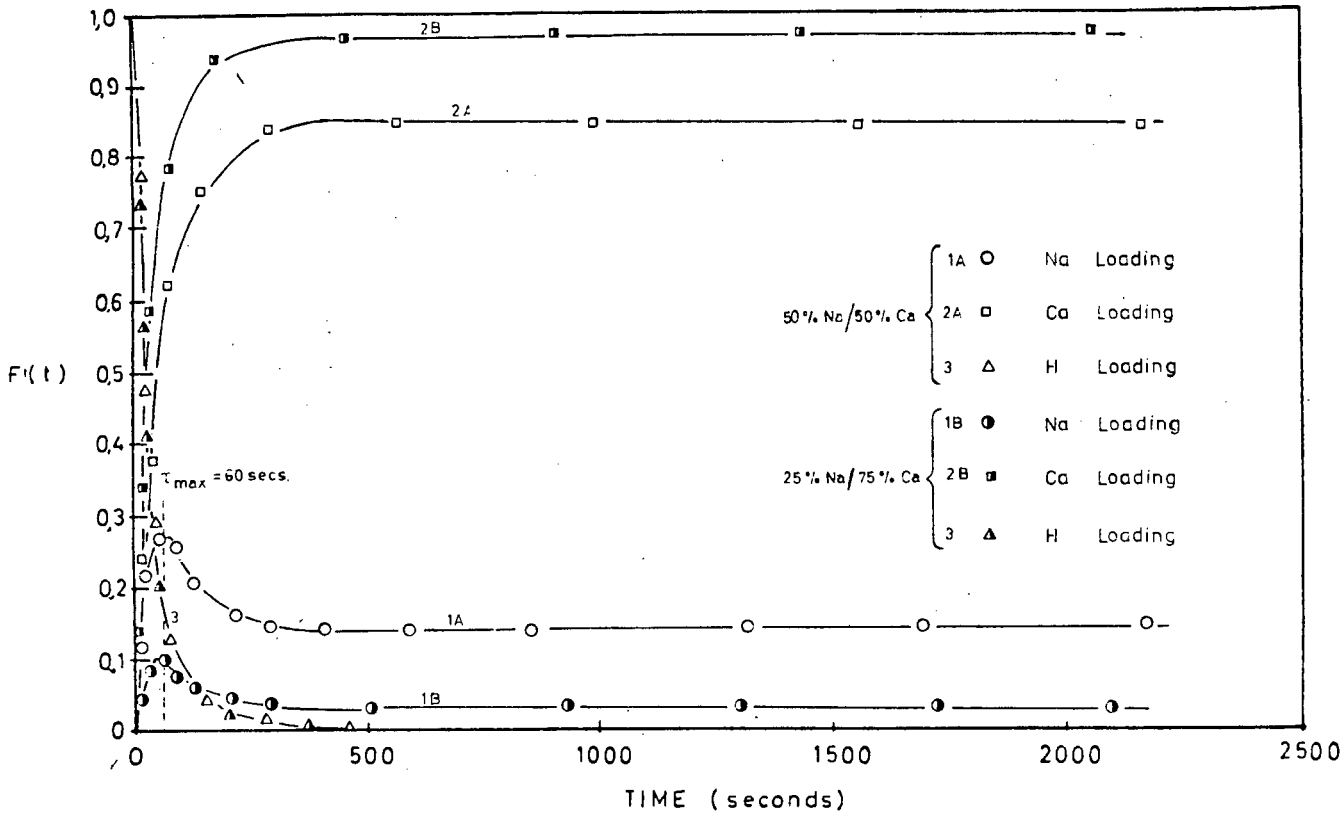

Fig. 5.46: F'(t) Comparative Plot of Loading 50%/50% and 25%/75% Mixtures onto Cation Fort at 0,125N

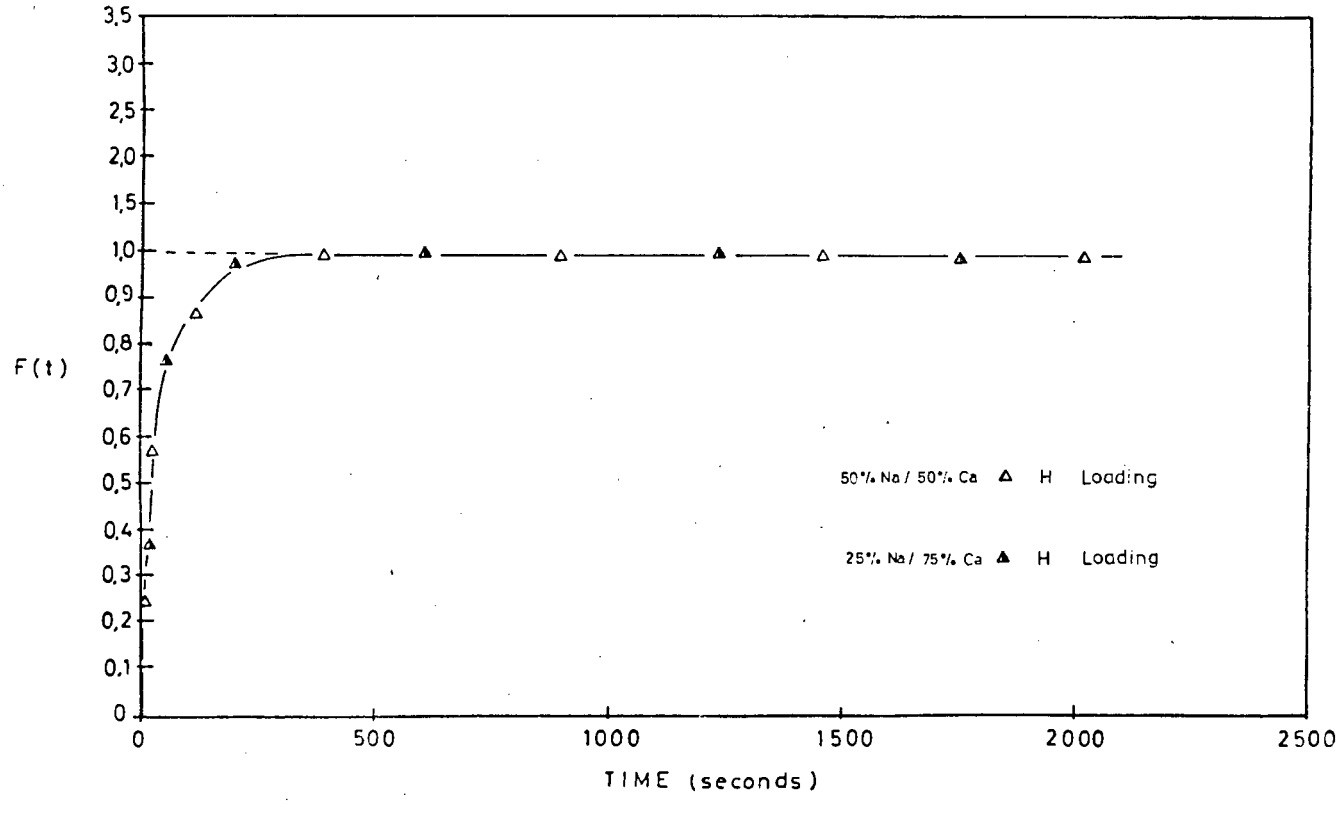

Fig. 5.47: F(t) Comparative Plot of Loading 50%/50% and 25%/75% Mixtures onto Cation Fort at 0,125N

kinetic rate.

Again, the initial, relative concentration of Na^+ and Ca^{2+} do not affect the time of maximum Na^+ "overshoot" (τ_{max}). For both systems, τ_{max} occurs at 60 seconds. Section 5.2.3.4(b) discusses the reasons for this phenomenon.

The time taken to reach equilibrium for the individual counter-ions is not affected by the initial relative liquid concentrations. In Fig. 5.46 the Na^+ reaches equilibrium in approximately 400 seconds for both systems, and the Ca^{2+} in approximately 450 seconds. However, as was evident in the regeneration systems (see Section 5.3.3.2(b)), the individual counter-ion equilibria are dependent on relative ionic concentration. This is shown in Fig. 5.46, where the individual counter-ion's final equilibrium F'(t) values differ between the two systems. It was shown in Chapter 4 that these equilibria are independent of total concentration, but are dependent on the concentration of ions present if the system involves more than one counter-ion. Thus the above results would be expected.

Fig. 5.47 shows that the kinetic results for the two systems, normalised on an F(t) plot, are identical.

5.4 COMPARISON BETWEEN THE KINETICS OF ZEROLIT 625 AND GEL RESINS

5.4.1 Introduction

The predominant feature, when comparing the kinetic rates of these two resins, is the fact that, throughout all the comparisons, the gel resin exhibits faster kinetics compared with the macroporous Zerolit 625 resin. This is contrary to expectations since the larger, more uniform pore size of the macroporous resin would be expected to enhance the kinetic properties compared with the gel resin, which possesses smaller, less uniform and well defined pores.

It has been shown (Section 5.2.2.2(c)) that the Zerolit 625 resin portrays more pronounced film-diffusion control characteristics as compared with the more pore-diffusion controlled gel resin. Helfferich [25], referring to gel resins, states that the kinetic properties governed by film-diffusion control are slower than those governed by pore-diffusion control. It is possible, therefore, that this applies when considering macroporous resins, and that the pronounced degree of film-diffusion control shown to exist (Section 5.2.2.2) in the macroporous case is the reason for the slower kinetics found in the gel case.

5.4.2 Resin Properties - Moisture Retention Capacities

From Tables 5.6 and 5.10 it is shown that the macroporous Zerolit 625 resin has a larger moisture retention capacity (MRC), i.e. a larger internal total pore volume, than the gel resin of equivalent crosslinking and resin form. (Of the range of DVB-content gel resins available, the comparison of MRC values is made on the basis of the 8,5% DVB which is the approximate crosslinking of the macroporous Zerolit 625.) Typically, for Na^+ form resin, Zerolit 625 has an MRC value of 49,3% compared with 46,1% for the gel resin of 8,5% DVB content. Since macroporous resins have a more open pore structure than gel resins (Section 2.2.2.1), the above results would be expected.

5.4.3 Binary Kinetic Comparisons

Figs. 5.48 to 5.50 give the plots for the relevant comparisons.

Fig. 5.48 compares the Na^+ regeneration of the two resins for both 0,125N and 0,50N concentrations. As discussed earlier, the gel resin kinetics are faster than those of Zerolit 625. It is evident from these results, however, that the Zerolit 625 kinetics differ far more with concentration than do those of the gel resin. It has been established (Section 5.2.2.2(c)) that for pure pore-diffusion

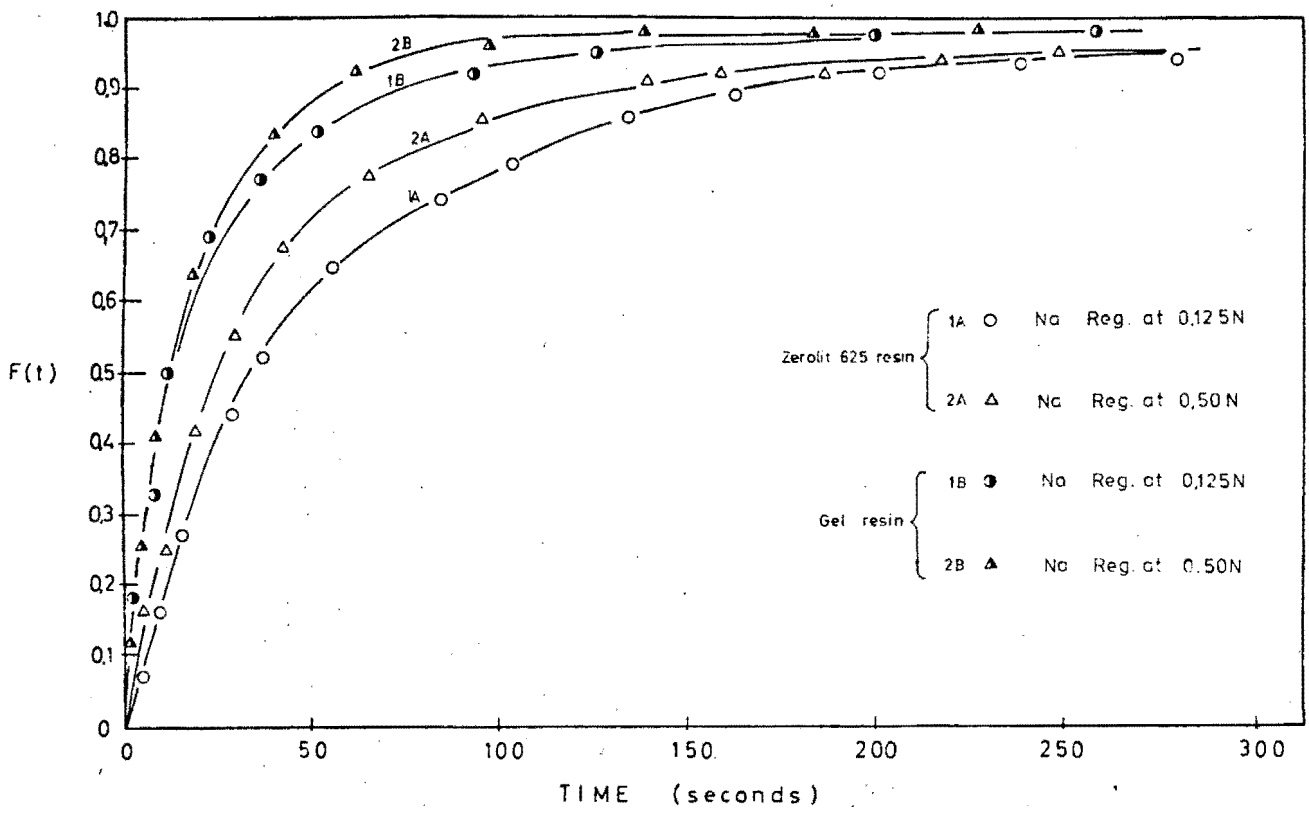

Fig. 5.48: Comparison Between Na^+ Regeneration of Zerolit 625 and Cation Fort Resins at 0,125N and 0,50N Concentrations

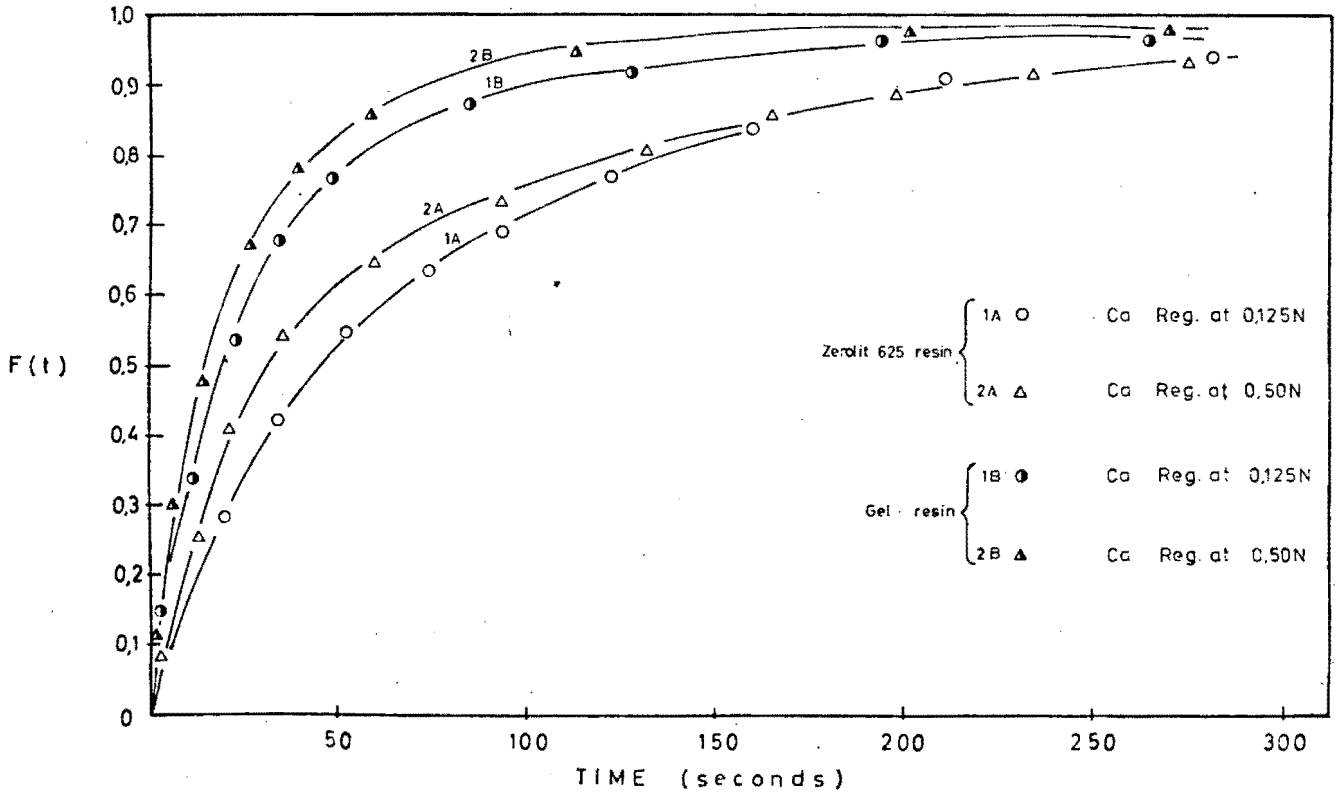

Fig. 5.49: Comparison Between Ca^{2+} Regeneration of Zerolit 625 and Cation Fort Resins at 0,125N and 0,50N Concentrations

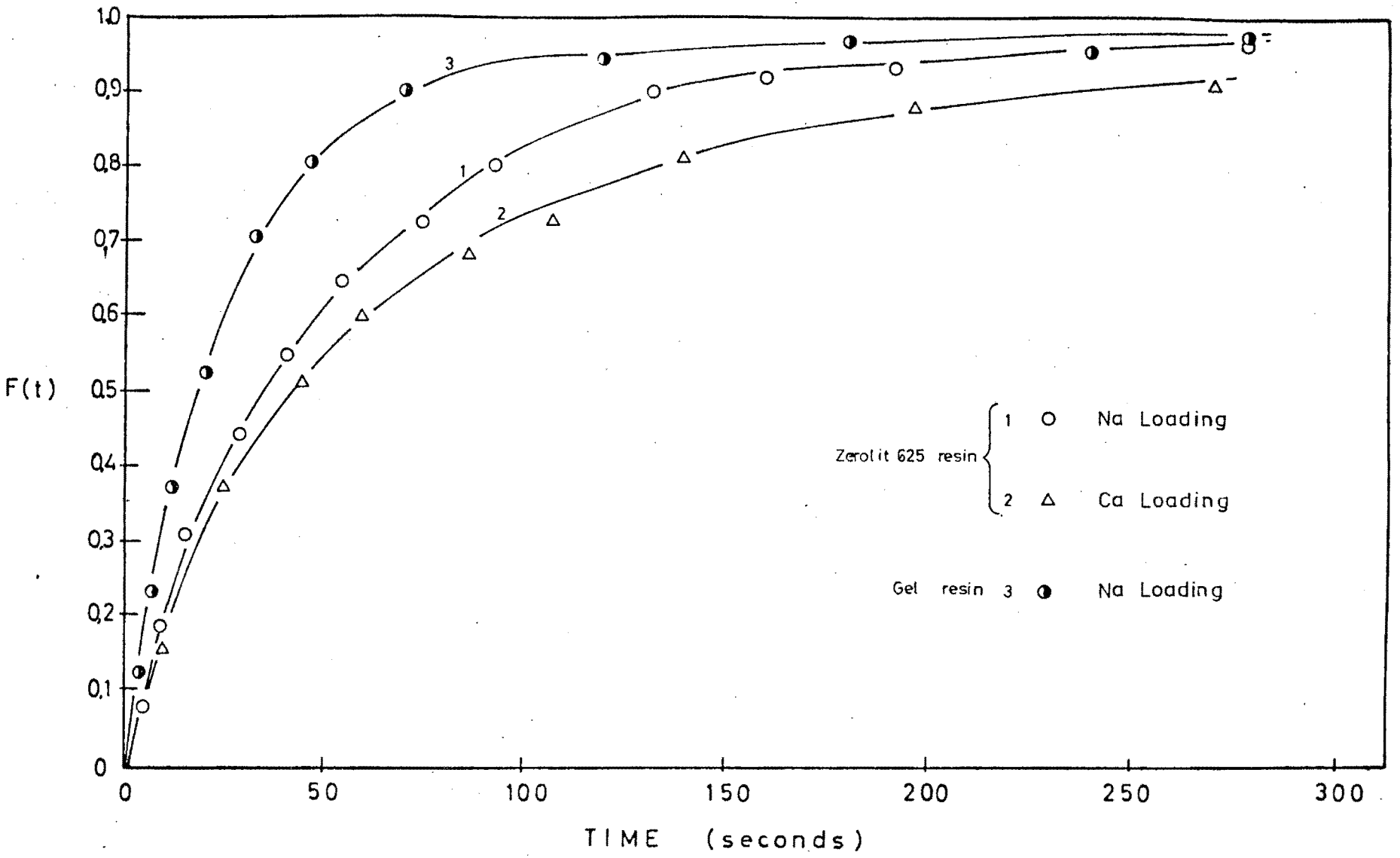

Fig. 5.50: Comparison Between Na^{+} and Ca^{2+} Loading of Zerolit 625 and Cation Fort Resins at 0,125N Concentration

control, the concentration of the external bulk solution has no effect on the exchange kinetics. This is another indication that the Zerolit 625 resin exchange kinetics are film-diffusion controlled to a greater extent than those of the gel resin [13,25].

Fig. 5.49 compares the Ca^{2+} regeneration for the two resins at both 0,125N and 0,50N concentrations. Again, the gel resin displays faster kinetics than Zerolit 625. A larger difference in the kinetics of the two resins in the Ca^{2+} form is evident, compared with the Na^{+} form kinetics plotted in Fig. 5.48. This retardation is due to the lower diffusivity of the larger Ca^{2+} counter-ion.

Fig. 5.50 compares the Na^{+} and Ca^{2+} loading at 0,125N. The loading kinetics follow the same pattern as discussed above for regeneration; that is, the fastest loading is for the Na^{+} counter-ion in a gel resin, while the slowest is for Ca^{2+} on a macroporous resin.

5.4.4 Ternary Kinetic Comparisons

5.4.4.1 Regeneration Systems

Figs. 5.51 and 5.52 compare the results for the regeneration kinetics of the two resins for the 50% Na^{+}/50% Ca^{2+} and 25% Na^{+}/75% Ca^{2+} preloaded resin systems respectively. It is evident from these figures that the resin type (i.e. whether gel or macroporous) does not affect the final F"(t) value, but does affect, to a minimal extent, the time taken to reach this value. Since both resins are strong acid cation exchangers, with comparable capacities (approximately 1,6 meq/ml wet resin), this result would be expected. Thus the equilibrium values are not affected by pore structure (the basic difference between the gel and macroporous resins), but by the relative concentrations of the counter-ions in solution (see Fig. 5.39).

Fig. 5.53 shows, for both resins, that the overall

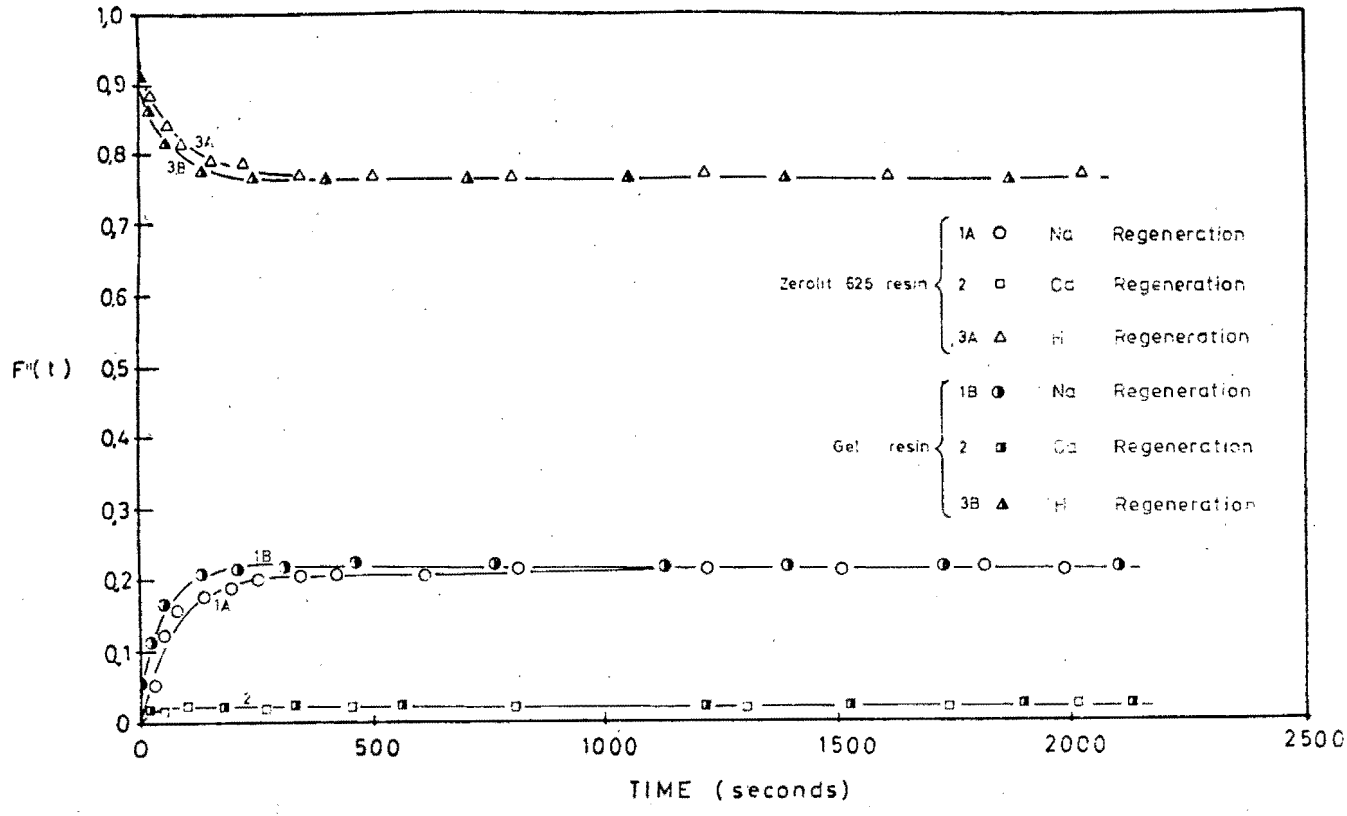

Fig. 5.51: F" (t) Comparative Plot of Regenerating 50%/50% Preloaded Zerolit 625 and Cation Fort Resins at 0,125N

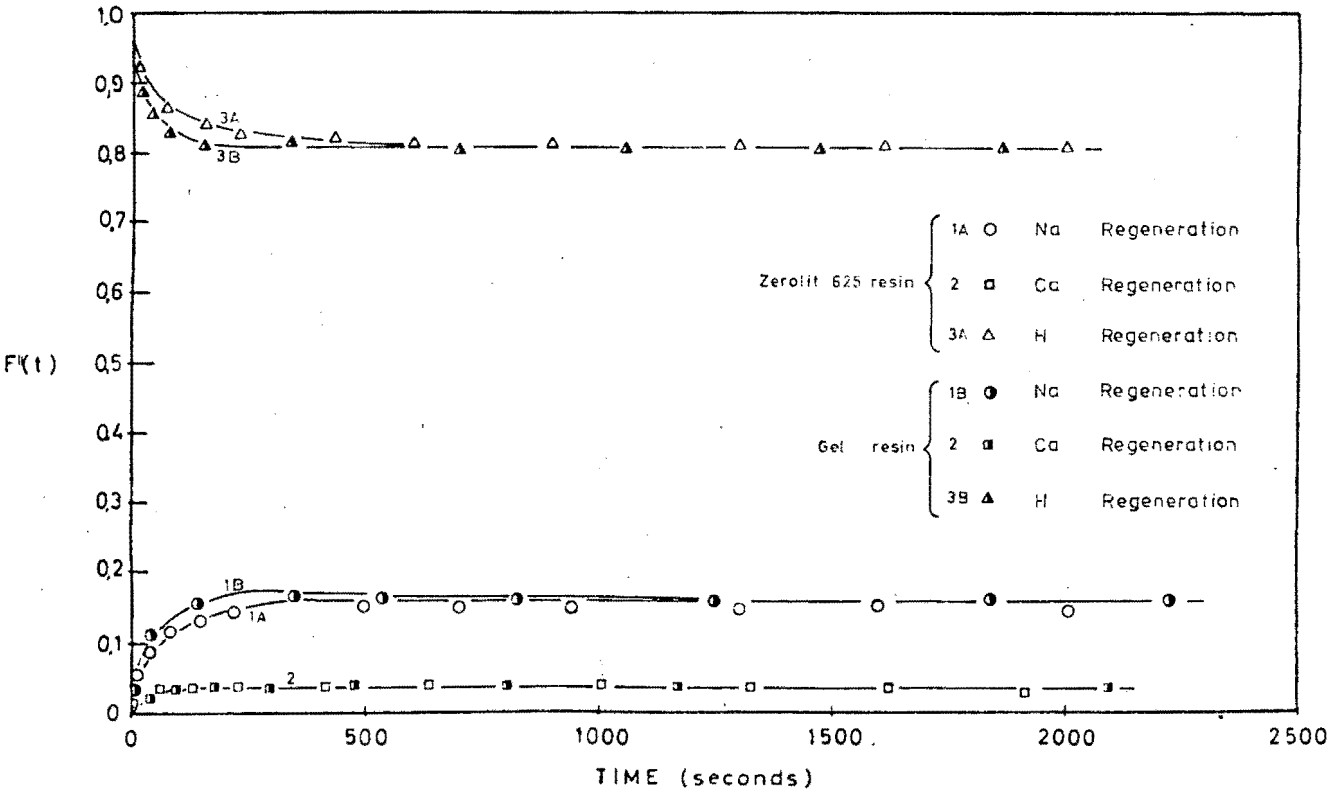

Fig. 5.52: F" (t) Comparative Plot of Regenerating 25%/75% Preloaded Zerolit 625 and Cation Fort Resins at 0,125N

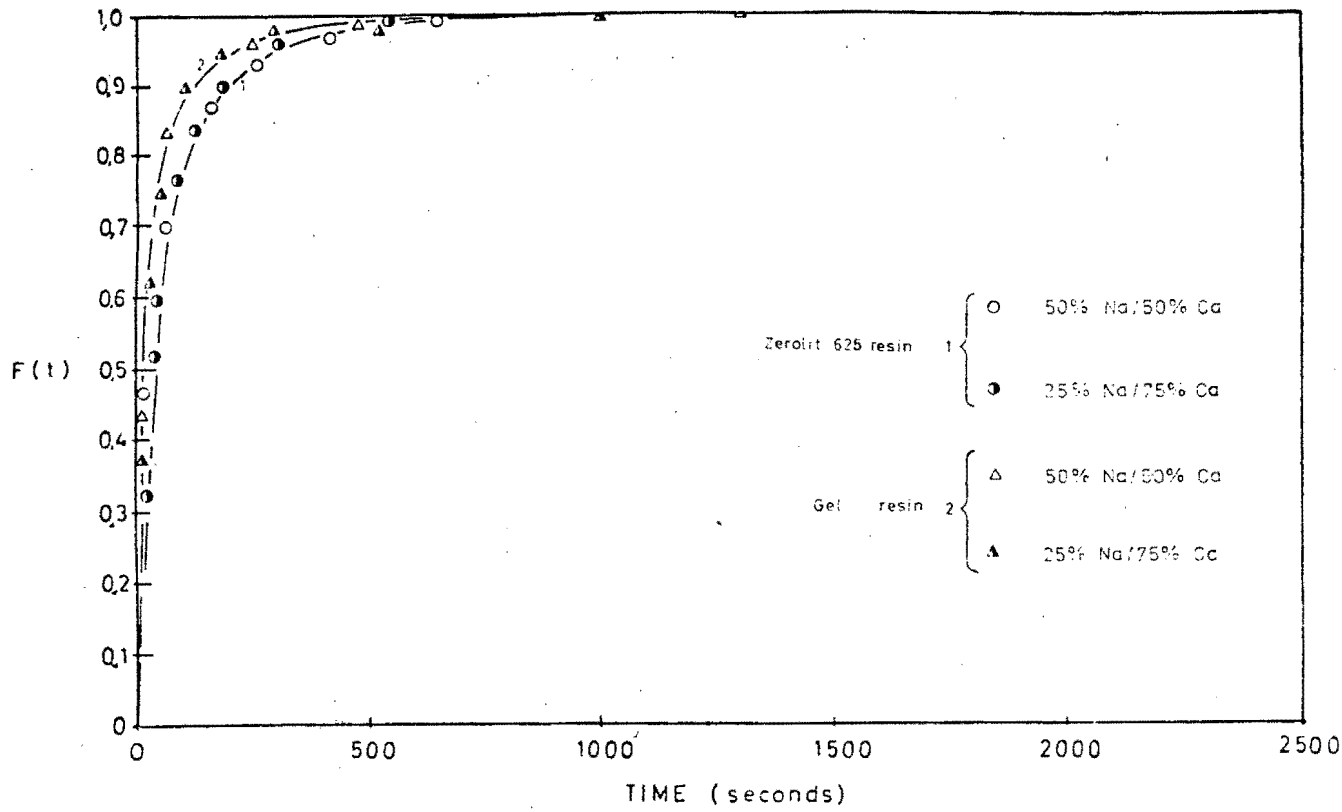

Fig. 5.53: F(t) Comparative Plot of Regenerating 50%/50% and 25%/75% Preloaded Zerolit 625 and Cation Fort Resins at 0,125N

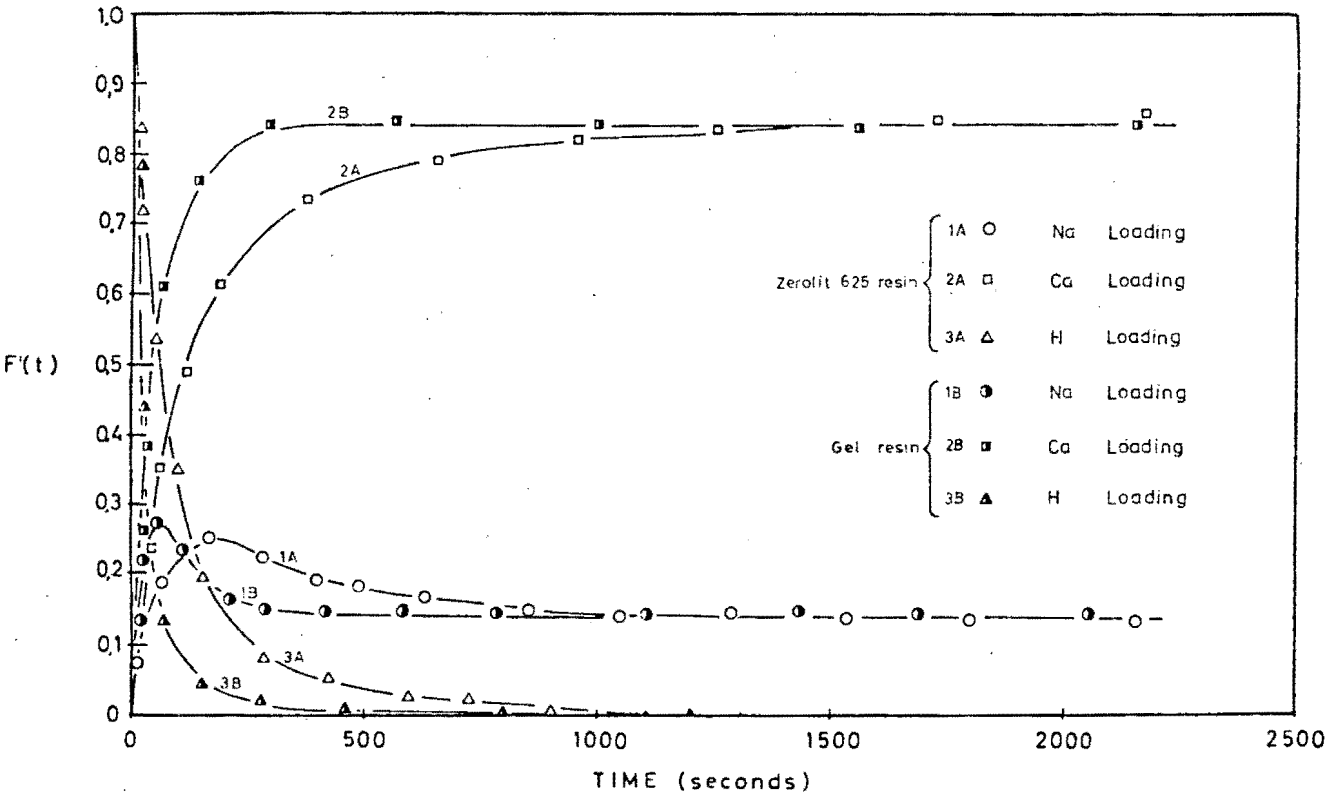

Fig. 5.54: F'(t) Comparative Plot of Loading 50%/50% Mixture onto Zerolit 625 and Cation Fort Resins at 0,125N

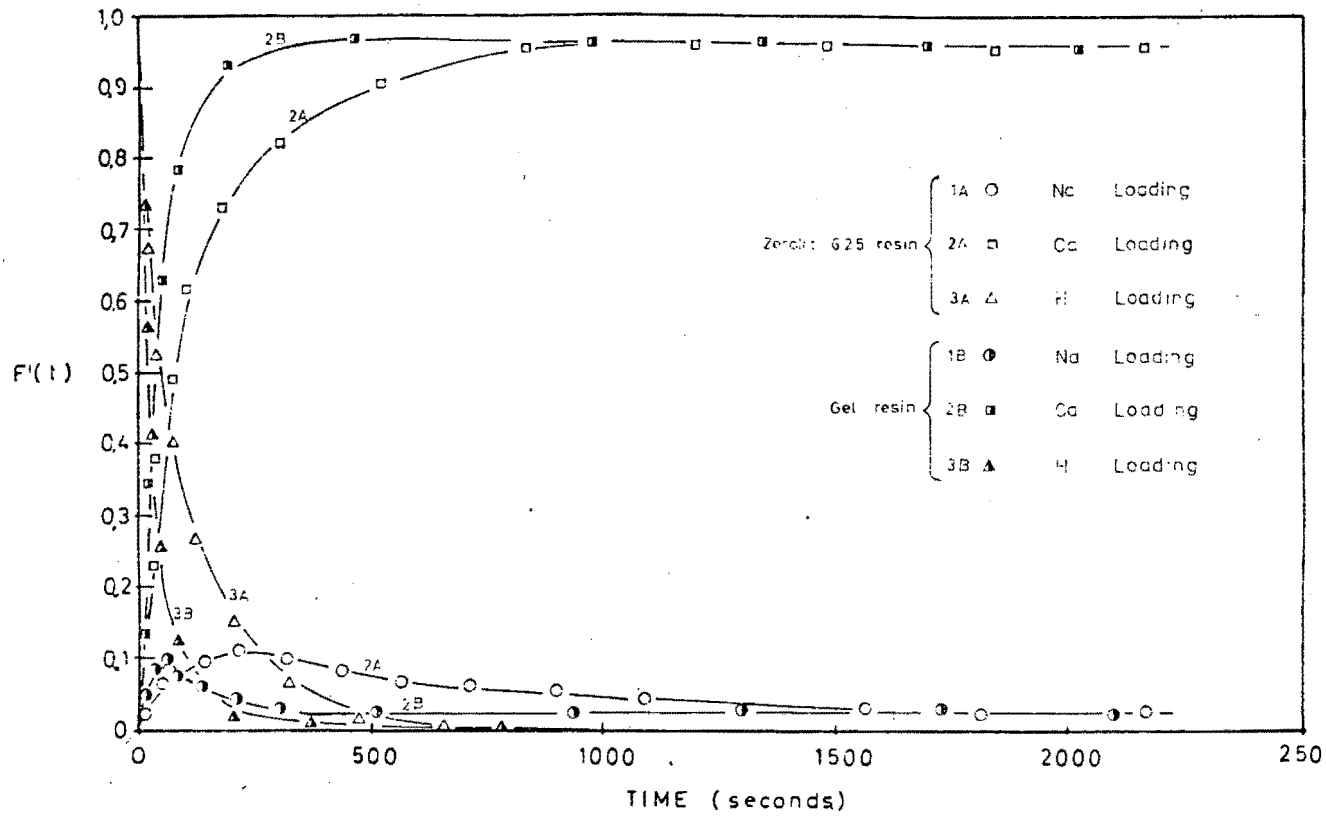

Fig. 5.55: F'(t) Comparative Plot of Loading 25%/75% Mixture onto Zerolit 625 and Cation Fort Resins at 0,125N

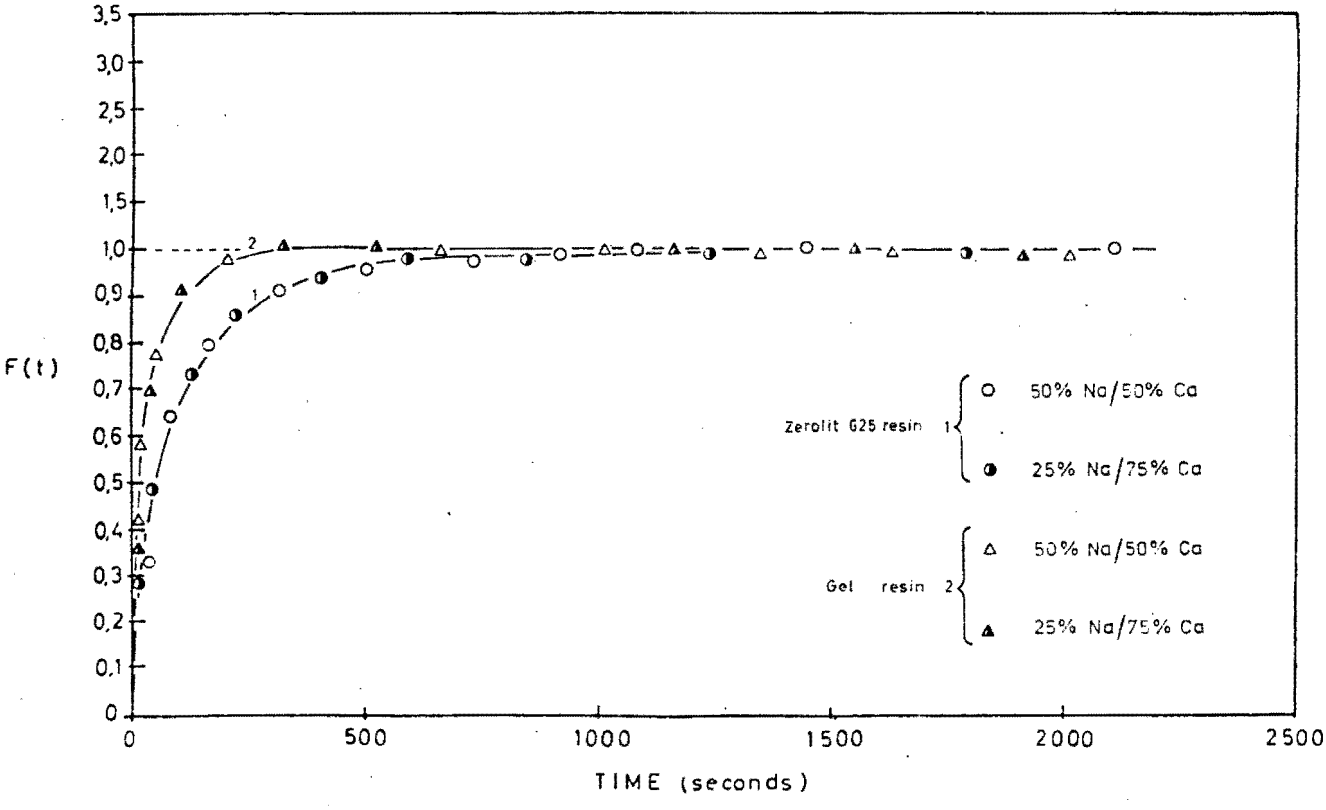

Fig. 5.56: F(t) Comparative Plot of Loading 50%/50% and 25%/75% Mixtures onto Zerolit 625 and Cation Fort Resins at 0,125N

CHAPTER 6 CONTENTS

Page

Page

CHAPTER 6

ANION KINETICS : RESULTS AND DISCUSSION

6.1 INTRODUCTION

In this Chapter, the kinetic performances of a normal density macroporous weak base resin and a high density isoporous weak base resin are presented and discussed.

Similarly to the cation kinetic results in Chapter 5, these results are divided into two main sections:

(i) the results for Zerolit MPH, the normal density anion resin; and

(ii) the results for Senbrix, the high density anion resin.

The binary loading and regeneration of Cl^-, SO_4^{2-} and artificial COD material onto the free base (OH^-) form of both resins (at 0,05N and 0,01N concentrations), as well as the regeneration of Senbrix resin (at 0,05N concentration only) loaded with artificial COD material, were investigated. In addition, the loading of Cl^- at 0,05N concentration onto Senbrix resin preloaded with 25, 50 and 60 percent Cl^-, as well as the loading of Cl^- onto Senbrix resin of different crosslinking, were studied. The final section compares similar kinetics of the two resins.

The results are tabulated in detail in Appendix D, and presented in the main text in the form of the plot of fractional approach to equilibrium (F(t)) versus time. These graphs appear after the relevant sections.

6.2 THE PERFORMANCE OF A NORMAL DENSITY MACROPOROUS ANION EXCHANGE RESIN - ZEROLIT MPH

6.2.1 Resin Properties

Zerolit MPH is a weak base, macroporous, crosslinked

polystyrene anion exchange resin manufactured and supplied by the Permutit Company. The volume capacity and moisture retention capacity (MRC) of the resin were measured according to the method outlined in Section 3.3.3. The results are presented in Sections 6.2.1.1 and 6.2.1.3. All resin samples were screened between 0,60 and 0,85 mm.

6.2.1.1 Volume Capacity

The relevant definitions are given in Section 5.2.1.1. Free-settled (f.s.) volumes were used throughout these studies and the results are quoted in milliequivalents per millilitre of wet resin (meq/ml) and tabulated in Table 6.1.

TABLE 6.1

VOLUME CAPACITIES OF ZEROLIT MPH RESIN

ml resin	Form	Eluting Solution	Capacity (meq/ml)
14,65	Cl^-	H_2SO_4	1,38
14,65	Cl^-	H_2SO_4	1,37
14,65	SO_4^{2-}	HCl	1,38
14,65	SO_4^{2-}	HCl	1,36

6.2.1.2 Discussion of Volume Capacities

The average volume capacity of 1,38 meq/ml for both the Cl^- and SO_4^{2-} forms of the resin compares well with the value of 1,45 meq/ml given in the Zerolit manual [48]. It would be expected, however, that the capacity value of the resin in the free-base (OH^-) form would be greater than the value quoted for the resin in the Cl^- and SO_4^{2-} forms, since the resin volume is significantly less in the OH^- form than in the Cl^- or SO_4^{2-} forms [48], and since capacity is defined as

meq (which remains constant) per unit volume, this value will increase with decreasing volume.

6.2.1.3 Moisture Retention Capacities

The definition and relevant equation (5.2) are given in Section 5.2.1.3, while the experimental procedures used to determine MRC values are described in Section 3.3.3.2.

The MRC values of Zerolit MPH resin were measured in the free-base and Cl^- forms (in duplicate), and are presented in Table 6.2.

TABLE 6.2

MOISTURE RETENTION CAPACITIES OF ZEROLIT MPH RESIN

Form	Wet Resin wt (gms)	Water (gms)	% Moisture	Average MRC
Cl^-	4,0742	2,2631	44,5	44,5
Cl^-	3,4991	1,9249	44,4	
OH^-	3,3302	1,6600	50,2	50,2
OH^-	4,4374	1,7151	50,1	

6.2.1.4 Discussion of MRC Results

Although the free-base form of some resins is known to decompose at high temperatures [49] , this does not occur to any significant extent on Zerolit MPH resin since it is shown that the Cl^- form of the resin has a lower MRC value than the corresponding free-base form. This is consistent with data of Sharma and Subramanian [49], who obtained similar results for Dowex AG 1 anion resin, drying the free-base resin samples carefully at below 50°C and 1 mm Hg vacuum.

The HCl molecule has a larger hydrated radius than the molecule normally on the resin in the free-base form (see Chapter 2), and thus the total internal bead volume (MRC value) is smaller when the resin is in the Cl^- form.

6.2.2 Binary Cl^- and SO_4^{2-} Kinetics

As indicated in Section 6.1, the binary loading kinetics of Cl^- and SO_4^{2-} onto free-base form of Zerolit MPH resin were studied at 0,01N and 0,05N initial concentrations, at a stoichiometric ratio of 0,5.

The experimental procedure used in all the kinetic runs is described in Section 3.3.5. Equation (6.1) was used to calculate the fractional approach to equilibrium (F(t)) values:

$$F(t) = \frac{C_{A_o} - C_A(t)}{C_{A_o} - C_{A_\infty}} \qquad (6.1)$$

where $F(t)$ = fractional approach to equilibrium;
C_{A_o} = initial concentration of ion A in liquid;
C_{A_∞} = equilibrium concentration of ion A in liquid;
$C_A(t)$ = concentration of ion A in liquid at time t.

Results are plotted on a standard F(t) versus time graph.

6.2.2.1 Mechanism of Anion Exchange

The mechanism of weak base anion exchange differs from that of cation exchange. Thus in a cation resin the counter-ion is exchanged directly for one on the resin, for example:

$$R^- - Na^+ + K^+ \rightleftharpoons R^- - K^+ + Na^+ \qquad (6.2)$$

There is thus no change in the total counter-ion concentration of the solution during the reaction.

However, the weak base anion resins acquire their properties from primary, secondary or tertiary amine groups within the resin matrix (see Section 2.2.1.4), and a typical

reaction occurs in two steps as depicted in Equations (6.3) and (6.4):

$$R - NH_2 + H^+ \rightleftharpoons R - NH_3^+ \qquad (6.3)$$

$$R - NH_3^+ + Cl^- \rightleftharpoons R - NH_3^+ - Cl^- \qquad (6.4)$$

Thus, as can be seen, an exchange as such does not take place, but rather the absorption of an entire molecule onto the resin site - an HCl molecule in the above example. As a result of this, the reaction does not occur at a constant concentration, but rather the counter-ion concentration decreases during the course of the exchange. If high R/L ratios are used (i.e. unity and above), the solution counter-ion concentration towards the end of the run would become very low and would influence the exchange kinetics (particularly by switching the controlling mechanism from pore-diffusion to film-diffusion control). To overcome this effect, all runs were performed at an R/L ratio of 0,5 which ensured that the maximum concentration drop was half of the initial value.

Offset against the above consideration is the fact that accurate analyses become more difficult as the R/L ratio becomes smaller. The R/L ratio determines the difference between the initial and final solution concentrations - the lower this ratio, the smaller the total concentration difference becomes. If one takes, as is typically the case in the anion runs, between 30 and 40 samples during the course of a run, the concentration difference between successive samples may become too small for the analytical machines to determine accurately, and the kinetic curves thus become inaccurate. The total concentration difference should therefore be large enough to render this problem insignificant, and an R/L ratio of 0,5 successfully accomplishes this.

6.2.2.2 Loading Kinetics

The quantities of resin and liquid used in these studies are given in Table 6.3.

TABLE 6.3

RESIN AND LIQUID QUANTITIES USED IN ZEROLIT MPH BINARY KINETIC STUDIES

Initial Concentration (N)	Counter-ion Studied	R/L	Resin (ml)	Liquid (ml)
0,01	Cl^-	0,5	2,86	800
0,01	SO_4^{2-}	0,5	2,86	800
0,05	Cl^-	0,5	14,3	800
0,05	SO_4^{2-}	0,5	14,3	800

The detailed kinetic data are tabulated in Appendix D, Tables D-1 to D-4, and plotted in Figs. 6.1 to 6.4.

6.2.2.3 Discussion of Loading Kinetics

(a) The Effect of the Counter-Ion:

Figs. 6.1 to 6.4 show the basic plots for the binary kinetics of the two counter-ions being studied. From these plots is constructed Fig. 6.5, which compares the kinetics of both systems with respect to concentration and counter-ion.

It is evident from Fig. 6.5 that, for both 0,01N and 0,05N initial concentrations, the SO_4^{2-} loading is faster than the Cl^- loading. This is particularly evident at the lower concentration.

Film-diffusion control differs from pore-diffusion control in the fact that the kinetics are not solely dependent on the diffusivities of the exchanging counter-ions

(whether in the pore or in the Nernst film), but also on the concentration of the solution (see Section 2.5.4.2) and on the selectivity coefficient of the resin for the counter-ions involved [25,50]. The reason for this latter effect is given by Helfferich [25] who states that, even at the start of a run (where the bulk solution remains free of one of the counter-ions), both counter-ions will be present at the exchanger/film interface. Since it is the concentration gradient over the film that controls the rate of exchange (kinetics), the selectivity coefficient is of importance by virtue of the fact that it dictates the concentration of counter-ions at this interface. Copeland et al. [50] relate the effect of the diffusivity ratio (D_A/D_B) and the selectivity coefficient (α_B^A) to the kinetics for monovalent film-controlled systems. They show that, for a typical binary ion exchange system, the kinetics become slower as the diffusivity of the loading counter-ion decreases, and faster as the selectivity coefficient increases. This is shown in Fig. 6.6.

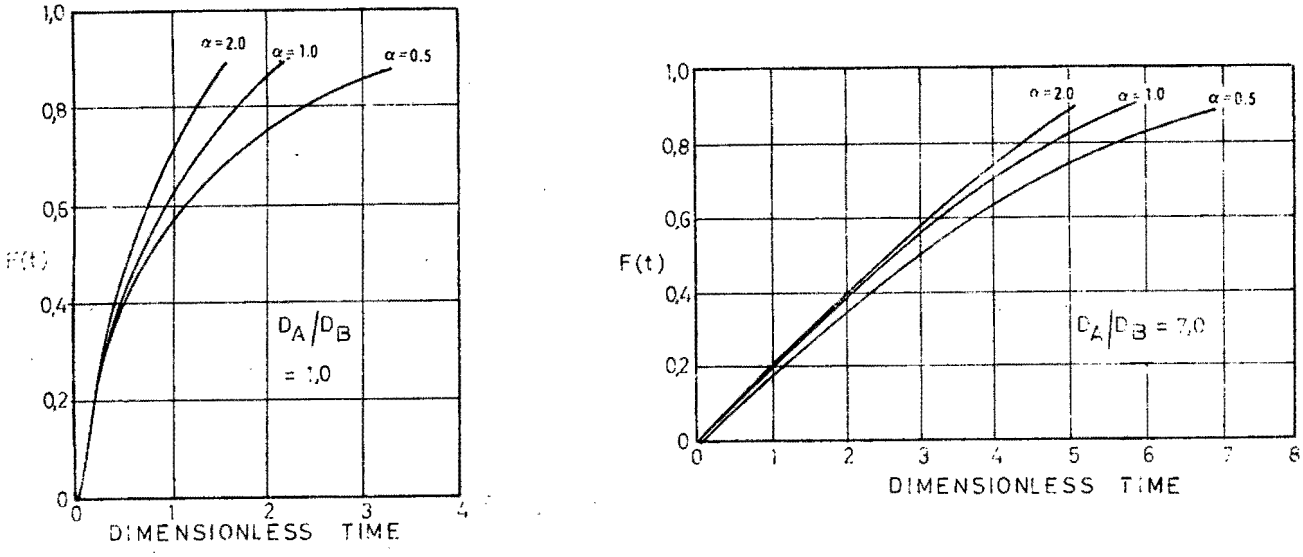

Fig. 6.6: Effect of Diffusivity Ratio and Selectivity Coefficient on the Kinetics of Monovalent Film-Diffusion Controlled Systems [50].

For the two systems studied in the present work the HCl has a higher diffusivity than H_2SO_4 - at 25°C the diffusivity coefficient (D_L) of HCl = $3,1 \times 10^{-5}$ cm^2/sec, while for H_2SO_4, under the same conditions, $D_L = 1,97 \times 10^{-5}$ cm^2/sec [51]. Thus the Cl^- loading kinetics would be expected to be an order of magnitude faster than the SO_4^{2-} loading kinetics. However, as is shown in Fig. 6.5, this is not always the case, and this apparent discrepancy can be attributed to the selectivity effects.

Fig. 6.6 shows how the diffusivity and selectivity coefficients affect the kinetics of a mono-monovalent system. From these graphs it is evident that a change in the D_A/D_B value by a factor of 7 significantly alters the kinetics ($t_{½}$ for α = 0,5 and a D_A/D_B value of 1,0 = 0,85, while $t_{½}$ for α = 0,5 and a D_A/D_B value of 7,0 = 3), while a change in the α value by a factor of 4 does not have as great an effect ($t_{½}$ at a D_A/D_B value of 1,0 and an α value of 0,5 = 0,85, while for the same system at an α value of 2,0, $t_{½}$ = 0,50). In the Zerolit MPH Cl^- and SO_4^{2-} binary loading kinetic comparisons, two factors should be borne in mind. These are, firstly, that the difference in diffusivity ratios (D_{H^+}/D_{Cl^-} and $D_{H^+}/D_{SO_4^{2-}}$) is approximately a factor of 1,6, which is much smaller than those given in Fig. 6.6; and, secondly, that Fig. 6.6 refers to a mono-monovalent system, while the present work investigates a mono-divalent system. The selectivity of the resin for SO_4^{2-} is significantly higher than for Cl^- since the former is a divalent ion and the resin has a higher affinity for multivalent ions compared with monovalent ones (see Section 2.4.2.1). Thus the selectivity effect will be more marked than is evident from Fig. 6.6, and results in the reversal of the trend set up by the diffusivity differences to make the SO_4^{2-} kinetics faster than the Cl^- kinetics.

(b) The Effect of Concentration:

Fig. 6.5 shows, also, that both the Cl^- and SO_4^{2-} kinetics are considerably slower at the lower concentrations. This

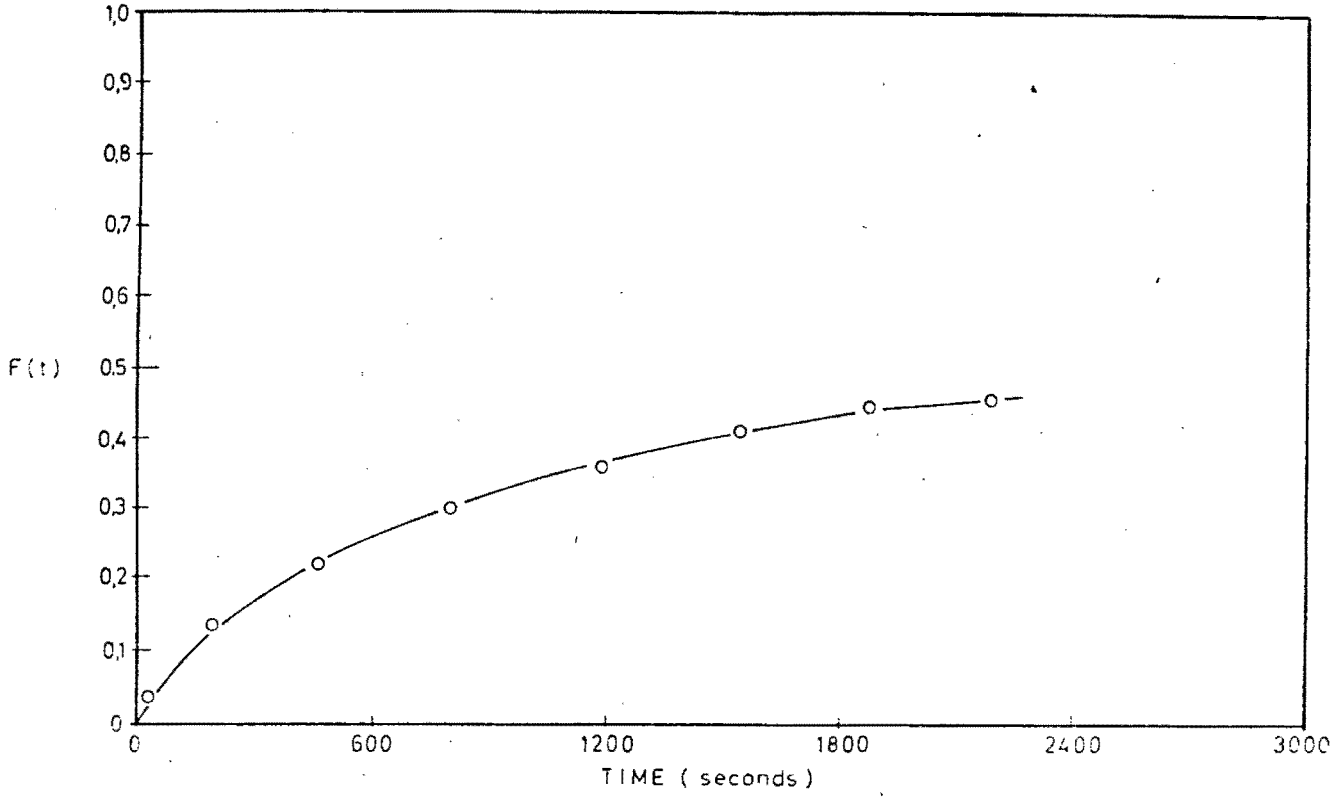

Fig. 6.1: Cl^- Loading at 0,01N Initial Concentration on Free-base Zerolit MPH Resin

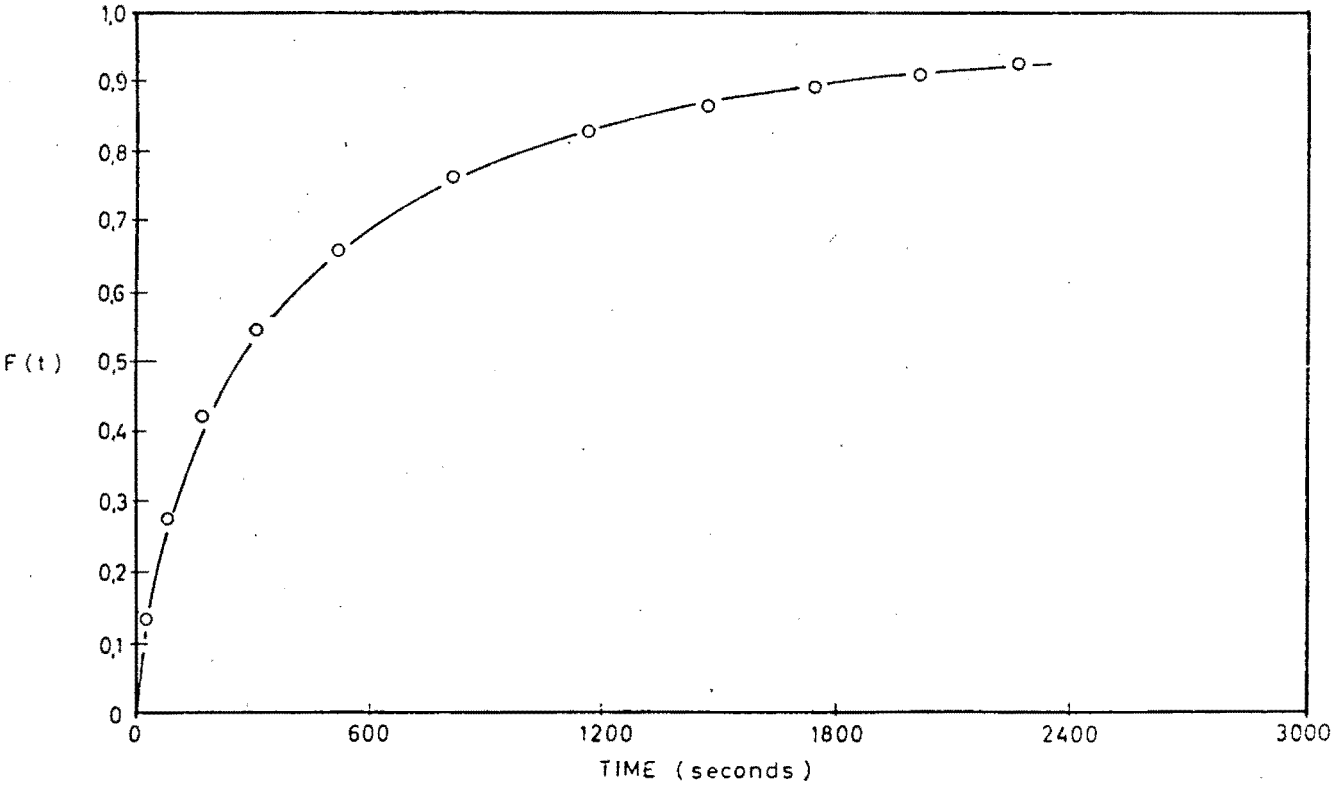

Fig. 6.2: Cl^- Loading at 0,05N Initial Concentration on Free-base Zerolit MPH Resin

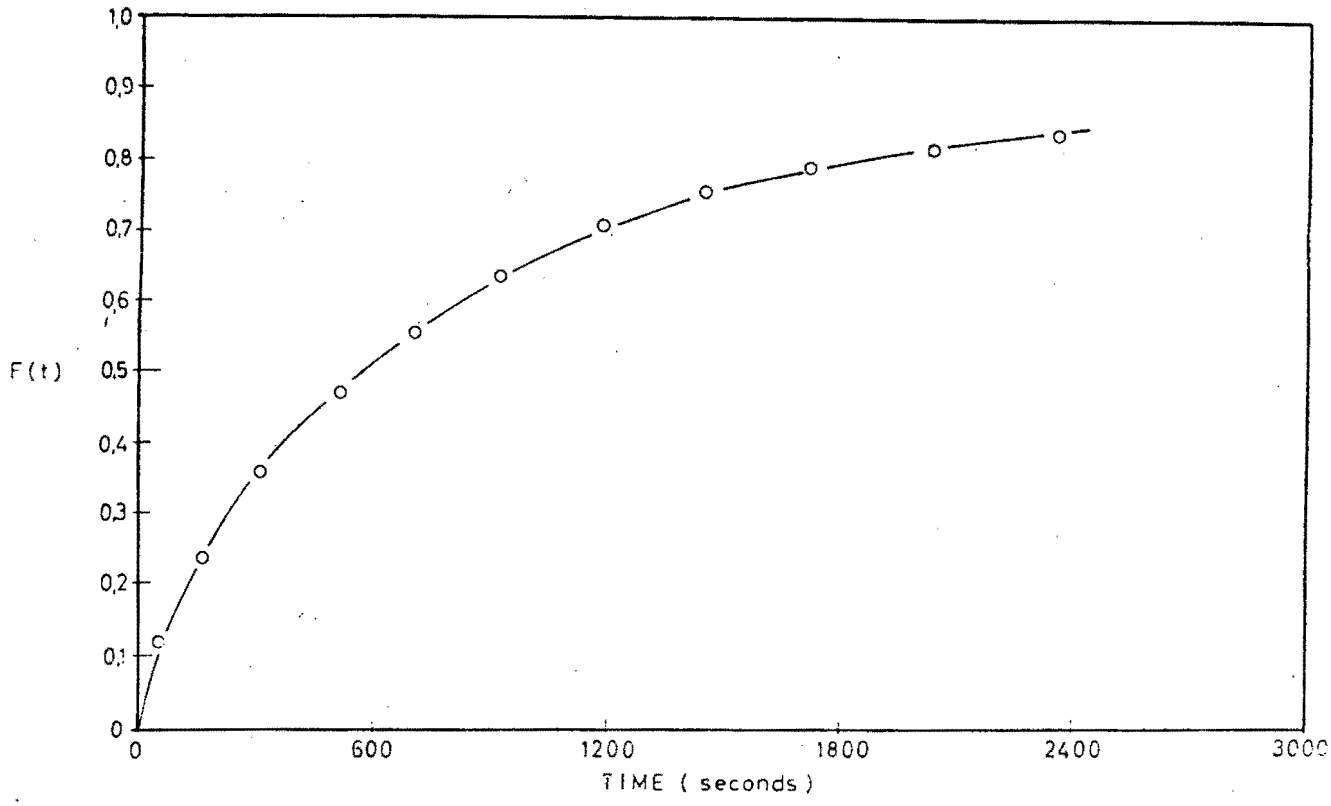

Fig. 6.3: SO_4^{2-} Loading at 0,01N Initial Concentration on Free-base Zerolit MPH Resin

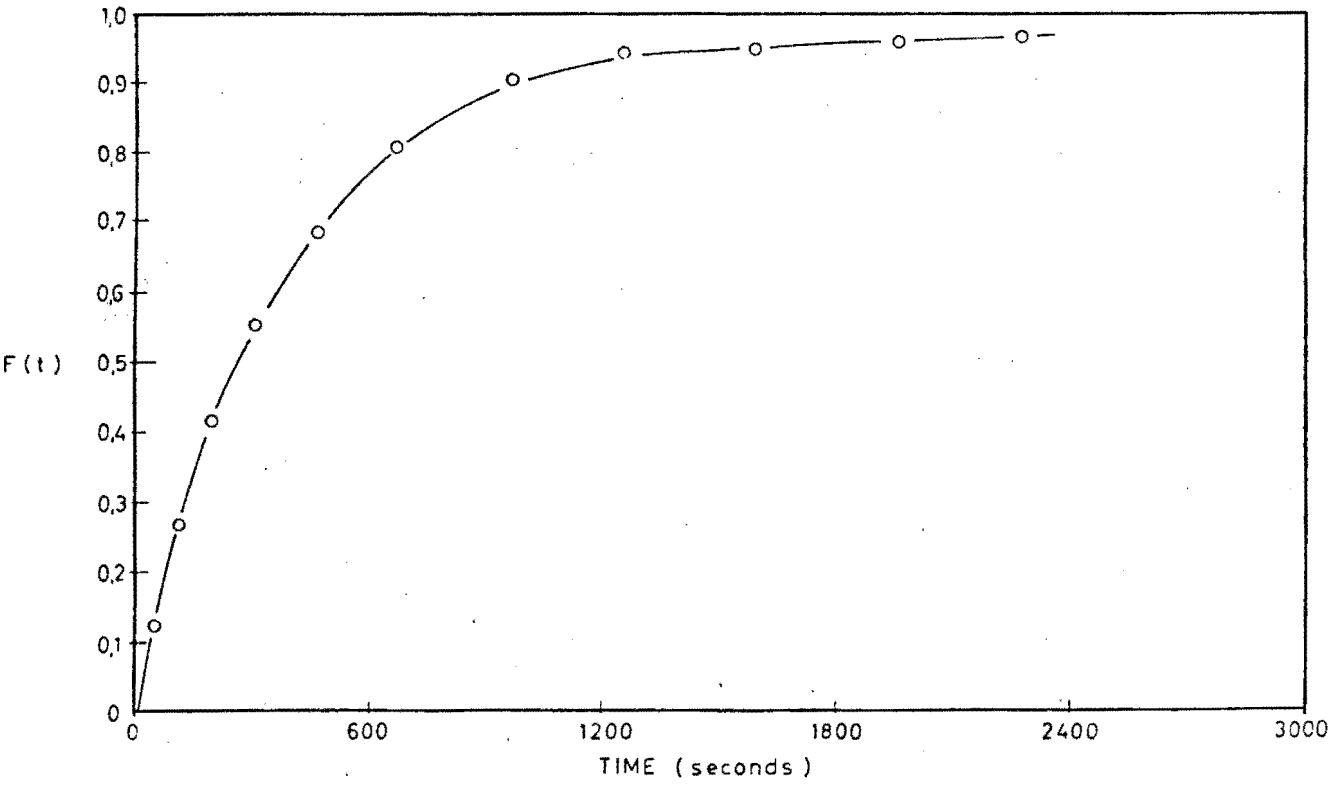

Fig. 6.4: SO_4^{2-} Loading at 0,05N Initial Concentration on Free-base Zerolit MPH Resin

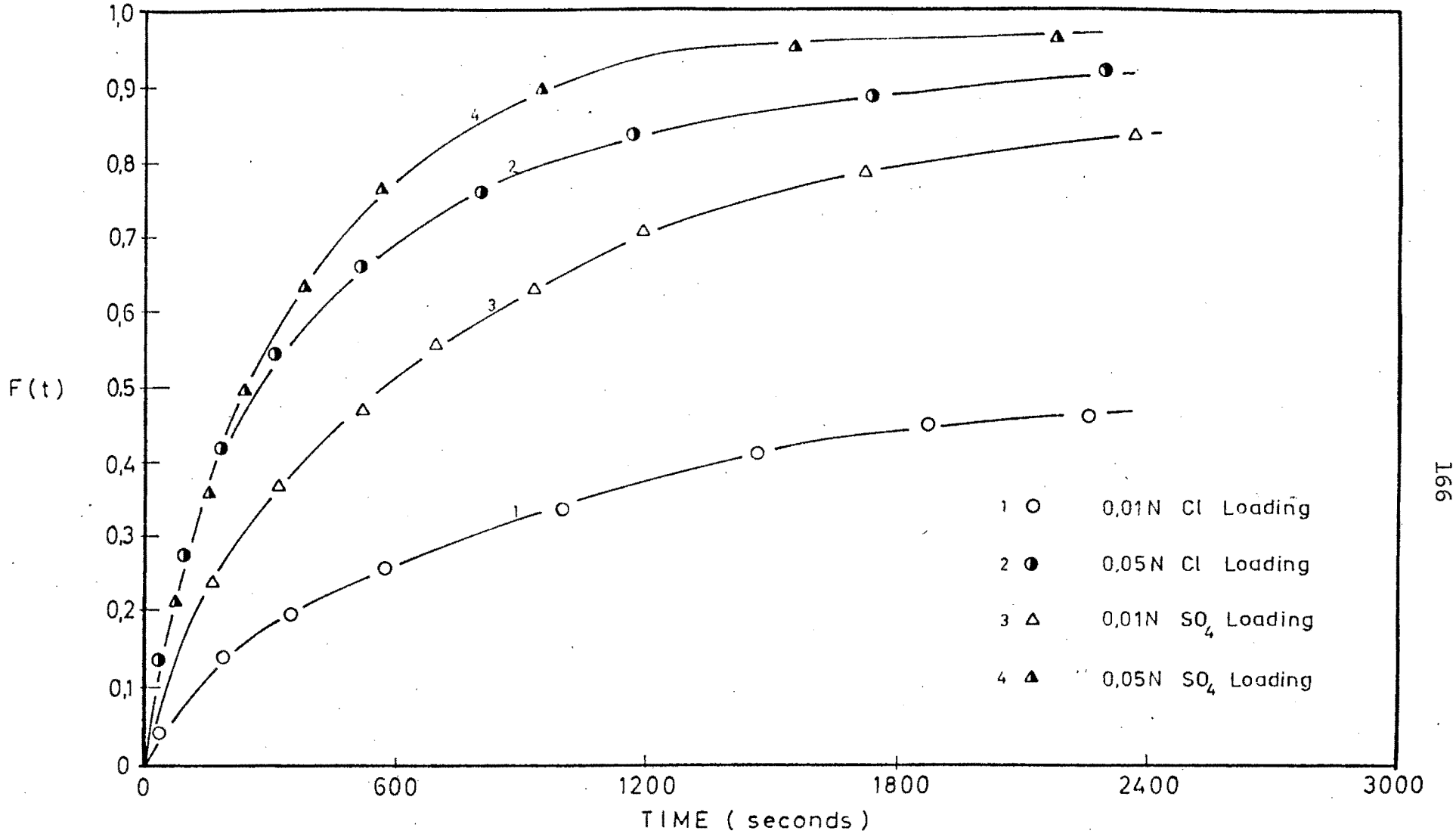

Fig. 6.5: Comparison Between Cl^- and SO_4^{2-} Loading at 0,01N and 0,05N Initial Concentrations on Free-base Zerolit MPH Resin

is consistent with film-diffusion theory (see Section 2.5.4.2(a)), since, at higher solution concentrations, the concentration gradient over the Nernst film will be greater and therefore the kinetics will be faster due to the larger driving force.

Further, the "selectivity effect" reversal of the Cl^- and SO_4^{2-} kinetics discussed in (a) above becomes more pronounced at lower concentrations (i.e. the SO_4^{2-} kinetics become faster relative to the equivalent Cl^- kinetics). This can be explained in terms of the relationships between the diffusivity coefficient (D_L) and the selectivity coefficient (α). The diffusivity coefficient is not very sensitive to concentration, varying only slightly over a reasonably large concentration difference (at 0,1N, D_L for HCl = $3,1 \times 10^{-5}$ cm^2/sec, while at 1,0N, D_L = $3,4 \times 10^{-5}$ cm^2/sec [52]). The selectivity coefficient, however, is very sensitive to concentration, increasing significantly at greater dilution (see Section 2.4.2.1). Thus, the increased "selectivity effect" at the lower concentration would tend to increase the SO_4^{2-} kinetics relative to the Cl^- kinetics (Fig. 6.5, graphs 3 and 1).

Matějka and Eliášek [53], who performed HCl kinetic loading experiments on a polystyrene macroporous weak base resin (Amberlite IRA 93), quote similar varying half-time values ($t_{½}$) with changing concentration - $t_{½}$ at 0,1N = 31 seconds, at 0,01N = 240 seconds, and at 0,005N = 600 seconds. Considering these results, and the results shown in Fig. 6.5, it can be safely assumed that these simple binary kinetics are pure film-diffusion controlled.

6.2.3 COD Kinetics

6.2.3.1 General

(a) Introduction:

The majority of anion resins have the ability of reversibly absorbing organic matter [25,48]. This property

becomes especially important in ion exchange water treatment plants, where it is desirable to remove the largest possible fraction of the organic matter present. Reclaimed sewage water, in particular, can have a high organic content [7,54] - relatively "clean" humus tank effluent has an average COD content of approximately 80 mg/ℓ [55]. However, the mechanism and kinetics of organic absorption are not well understood. In addition, anion resins are susceptible to fouling (defined as the irreversible absorption of organic matter onto the resin) in water of high organic content [27, 32,56], and thus the rate of loading of some organic compounds would be of interest in the design of large size water reclamation plants.

There are more than a thousand organic (and biological) compounds present in water, particularly sewage effluent, which, before discharge, has undergone chlorination [14,57,58,59]. Many of these have been identified [14,42] as complex molecules, of which polychlorinated biphenyls, biocides and steroids are examples. These are extremely difficult to simulate in the laboratory. However, Rebhun and Manka [42] have identified simpler compounds such as humic and fulvic acids (which are also formed, together with volatile halogenated hydrocarbons, during chlorination [60,61]) in typical secondary effluents. They state that, in a typical secondary effluent of 185 mg/ℓ COD (as O_2 after centrifugation), approximately 40% are organic acids, 20% are proteins, 11% are carbohydrates and the remainder consist of ethers, detergents and tannins [42,61].

(b) Initial Studies:

The initial decision was to choose a suitably absorbable organic material that was both freely available and easily analysed. The chemical oxygen demand (COD) was chosen as the method of determining the organic concentration. This method, which expresses the organic content in mg/ml, depends on oxidation by a powerful chemical oxidising agent, and can be performed in about 2½ hours (see Appendix E,

Section E.3 for detailed description of the method)[58,62].

Two possible artificial COD materials were available and seemed suitable. These were:

(i) The substance usually used as COD standard - potassium-hydrogen phthalate ($C_8H_5KO_4$, MW = 204); and

(ii) Mono-carboxylic acids.

The potassium-hydrogen phthalate was found to be unacceptable, since it was not absorbed readily enough onto the resin, and analysis with small samples was found difficult because of its low buffering capacity, resulting in dissolved CO_2 from the air giving inconsistent results.

Organic acids (such as butyric acid) were found to be far more suitable. These lower molecular weight compounds were soluble in water, readily available, and easily analysed by means of the standard COD test. Further, the reaction could be followed conductiometrically, producing a concentration versus time plot on a pen recorder (see Section 3.3.5.2 for experimental apparatus and method). Thus it was decided to use as artificial COD material, three mono-carboxylic acids of different molecular weight, namely formic acid (CH_2O_2, MW = 46), propionic acid ($C_3H_6O_2$, MW = 73) and butyric acid ($C_4H_8O_2$, MW = 88).

COD tests were performed on known concentration samples of each of the acids in order to determine their COD equivalent. 50 meq/ℓ standards of each acid were made up (acid quantities are given in Table 6.4) and diluted 20 ml samples were analysed for COD. The results are presented in Table 6.4.

It would be expected that, under the severe oxidising conditions of the COD test, the acids would be totally oxidised to carbon dioxide and water. It is shown in Table 6.5 that, on comparison of COD results, total oxidation can be assumed to occur.

TABLE 6.4

CARBOXYLIC ACID COD CORRELATION RESULTS

Acid	gms Acid for 50 meq/ℓ Standard	Dilution Factor	ml FAS	mg/ℓ COD of 50 meq/ℓ Acid Standard
Formic	2,30	1	3,4	837
		2	13,3	835
Propionic	3,65	10	8,3	6290
Butyric	4,40	10	2,5	8760
Normality of FAS = 0,106			ml FAS for Blank = 23,15	

TABLE 6.5

ACID OXIDATION EQUATIONS AND COD EQUIVALENTS

Acid	Total Oxidation Equation	mg COD Equivalent of 1 mg Acid	Calculated COD	Experimental COD
Formic	$CH_2O_2 + O \rightarrow CO_2 + H_2O$	0,348	801	836
Propionic	$C_3H_6O_2 + 7\ O \rightarrow 3CO_2 + 3H_2O$	1,534	5600	6290
Butyric	$C_4H_8O_2 + 10\ O \rightarrow 4CO_2 + 4H_2O$	1,818	8000	8760

Considering the errors involved in the dilution of the propionic and butyric acid samples, the correlation between the calculated and experimental COD values was assumed close enough to prove total oxidation. Thus, although the majority of the COD results are presented as mg/ℓ acid, these results are easily converted to COD equivalents using the above factors.

(c) Compatibility of Fractional Sampling and Conductiometric Methods:

In order to check whether the two methods of kinetic curve determination (viz. fractional sampling and conductiometric) were compatible, a similar test run was performed on both sets of apparatus, and the kinetic curves compared.

The loading of Cl^- onto free-base form of Senbrix resin at 0,05N concentration was chosen as the most suitable system, and the comparative kinetic curves are presented in Fig. 6.7 (the detailed results are tabulated in Appendix D, Table D-5). It is clearly shown that there is negligible difference between the two curves, and thus data obtained by the different methods can be directly compared.

(d) Systems Investigated:

Binary kinetic runs were performed on the loading of each of the three acids onto Zerolit MPH resin (in the free-base form) at 0,05N concentration and an initial R/L ratio of 0,5. In addition, runs were performed at two further concentrations (0,025N and 0,0125N) on the same system, in order to compare the effect of solution concentration.

6.2.3.2 Loading Kinetics of Different Monocarboxylic COD Substances

The quantities of resin and liquid used in these kinetic runs are given in Table 6.6.

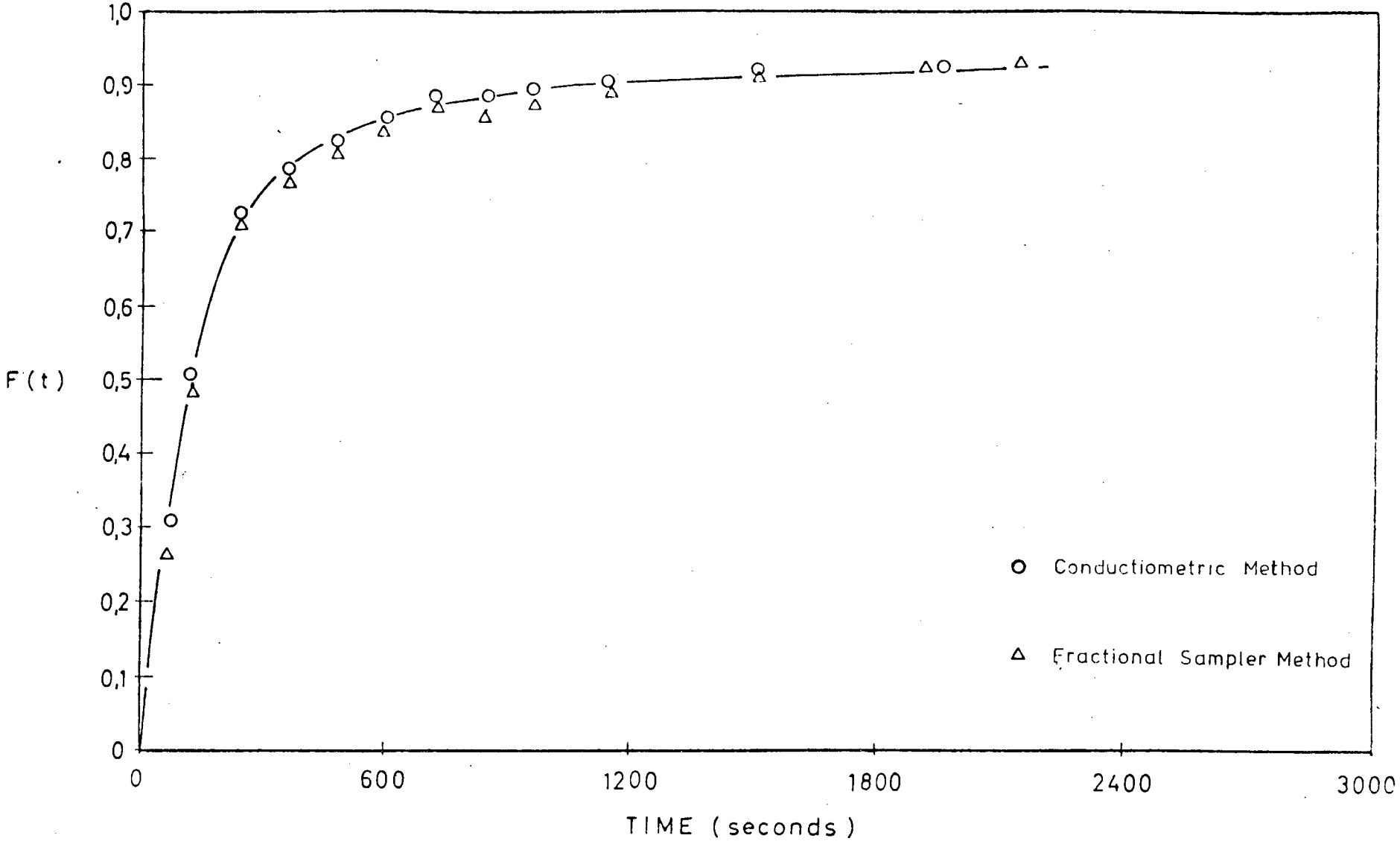

Fig. 6.7: Comparison Between Cl^- Loading at 0,05N Initial Concentration on Free-base Senbrix Resin Using Fractional Sampling and Conductiometric Analytical Techniques

TABLE 6.6

RESIN AND LIQUID QUANTITIES USED FOR ZEROLIT MPH COD KINETIC STUDIES AT 0,05N

Loading Acid Type	R/L*	ml Resin	ml Acid
Formic	0,5	17,86	800
Propionic	0,5	17,86	800
Butyric	0,5	17,86	800

* It is assumed that each acid molecule occupies one resin site.

The detailed kinetic data are tabulated in Appendix D, Tables D-6 to D-8, and plotted in Fig. 6.8.

6.2.3.3 Discussion of Loading Kinetics of Different Artificial COD Materials at 0,05N

(a) Direct Comparisons:

Fig. 6.8 compares the kinetics of loading formic, propionic and butyric acids onto Zerolit MPH resin at 0,05N concentration

If the COD loading kinetics are compared with those of the Cl^- and SO_4^{2-} loading (see Fig. 6.9) at similar conditions (see Figs. 6.2 and 6.4 respectively), it is clear that, in general, the organic molecules exchange slower. This is even the case for the smallest COD molecule investigated, formic acid - $t_{\frac{1}{2}}$ (the time taken to reach an F(t) value of 0,5) = approximately 200 seconds for the OH^-/Cl^- exchange at 0,05N (see Fig. 6.2), while $t_{\frac{1}{2}}$ for the OH^-/CH_3O_2 exchange at the same conditions = 300 seconds.

The major difference between the different loading materials is their respective molecular weights. Thus,

since these systems are assumed to be diffusion controlled [32] (see Section 6.2.2.3), the effect of changing kinetic rates (between loading systems involving species of differing molecular weights) must be directly related to their diffusivities. It is clear that a molecule of low molecular weight will have a significantly higher diffusivity than one of high molecular weight, and the lower the diffusivity (and thus the mobility) of the counter-ion in the liquid film, the slower the kinetics will become [25,27]. This trend is shown in Fig. 6.8. The higher the molecular weight of the acid counter-ion, the slower the kinetics. Even when compared with the Cl^- exchange above, the formic acid has a higher molecular weight (44 compared with 35,5 of Cl^-) and thus has slightly slower kinetics.

Therefore, each different loading species possesses kinetics which are greatly affected by their respective molecular weights (see Figs. 6.8 to 6.10) - the greater the molecular size, the slower the kinetics. However, this is not the only factor which affects the kinetic distribution of different systems. Such apparent inconsistencies (as shown in Fig. 6.8, where the propionic and butyric acid kinetics are significantly slower than the formic acid kinetics) cannot be attributed to mobility differences alone (which are, however, the cause of the much smaller difference between the propionic and butyric acid kinetics). This can be explained by the nature of the macroporous Zerolit MPH pore distribution. As described in Section 2.2.2.2, this structure consists of pores with a large size distribution, i.e. there is a larger pore diameter variation (between 60 Å and 400 Å [20]). Fig. 2.2 shows a schematic diagram of a macroporous resin bead, where the pore diameters are either fairly small or relatively large, but relatively few of medium size. It is therefore probable that Zerolit MPH possesses such a pore structure, and that the formic acid molecule is small enough to penetrate the majority of the pores, but that the propionic acid molecule is not. The larger propionic and butyric acid molecules therefore diffuse as rapidly as the formic acid molecules through the liquid film and into the

large pores, but are severely retarded by the smaller ones. The diffusion thus becomes partly pore controlled, as the molecular size becomes larger than the "small pore fraction" of the resin. Bieber et al. [64] show that, for some systems at low concentration, it is possible for the internal diffusion resistance to be of the same order of magnitude as the liquid phase mass transfer coefficient.

This reduction in the kinetics of the two larger acid molecules can be attributed to both the lower mobility of the larger counter-ion, and the slightly increased pore-diffusion control exerted by the "small pore fraction". It would be anticipated that a similar large "drop" in the kinetics would occur with very much larger molecules being affected by the larger "pore fraction" of the resin. As the counter-ion size increased, sieve action would become increasingly important, preventing the molecule from loading.

Matějka and Eliášek [53] performed a similar set of experiments on a polystyrene macroporous resin (Amberlite IRA 93) using sulfosalicylic and caproic acids as artificial COD materials. They discovered that the longer caproic acid ($CH_3(CH_2)_4CO_2H$) loaded slower than the sulfosalicylic acid ($C_7H_6O_6S$) at 0,02N - $t_{\frac{1}{2}}$ for caproic acid = 1530 seconds while $t_{\frac{1}{2}}$ for sulfosalicylic acid = 640 seconds, and this they attributed to both electrostatic and sterric interferences in the resin matrix.

Section 6.4.4.1 compares the Zerolit MPH and Senbrix results.

(b) Comparisons with Binary Kinetics:

Fig. 6.9 compares the formic acid loading kinetics with the Cl^- and SO_4^{2-} loading kinetics at the same conditions.

In systems involving similar solution concentrations and resins, the counter-ion mobility is not the only factor affecting the kinetics. The selectivity of the resin over the differing ionic species plays an important role [25] - the

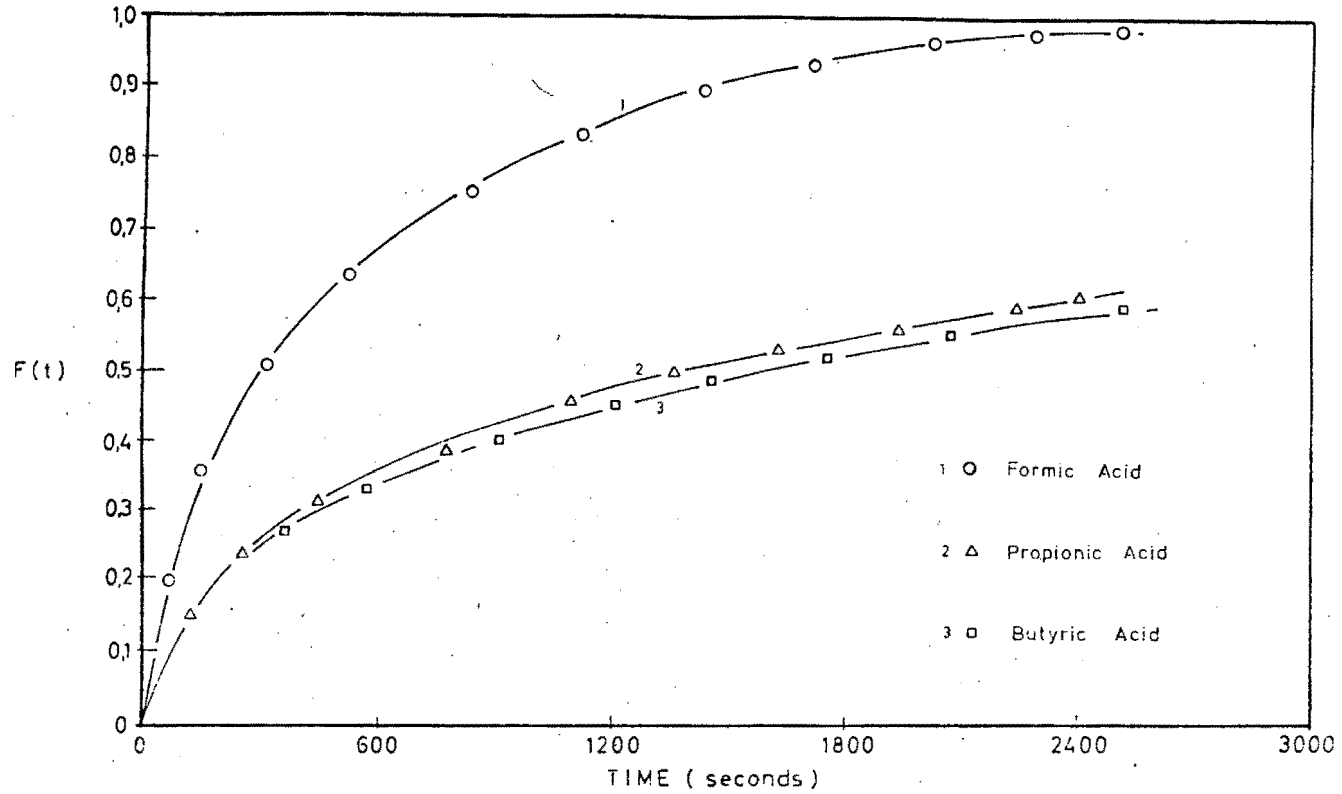

Fig. 6.8: Comparison of Three Different COD Materials Loading at 0,05N Initial Concentration on Free-base Zerolit MPH Resin

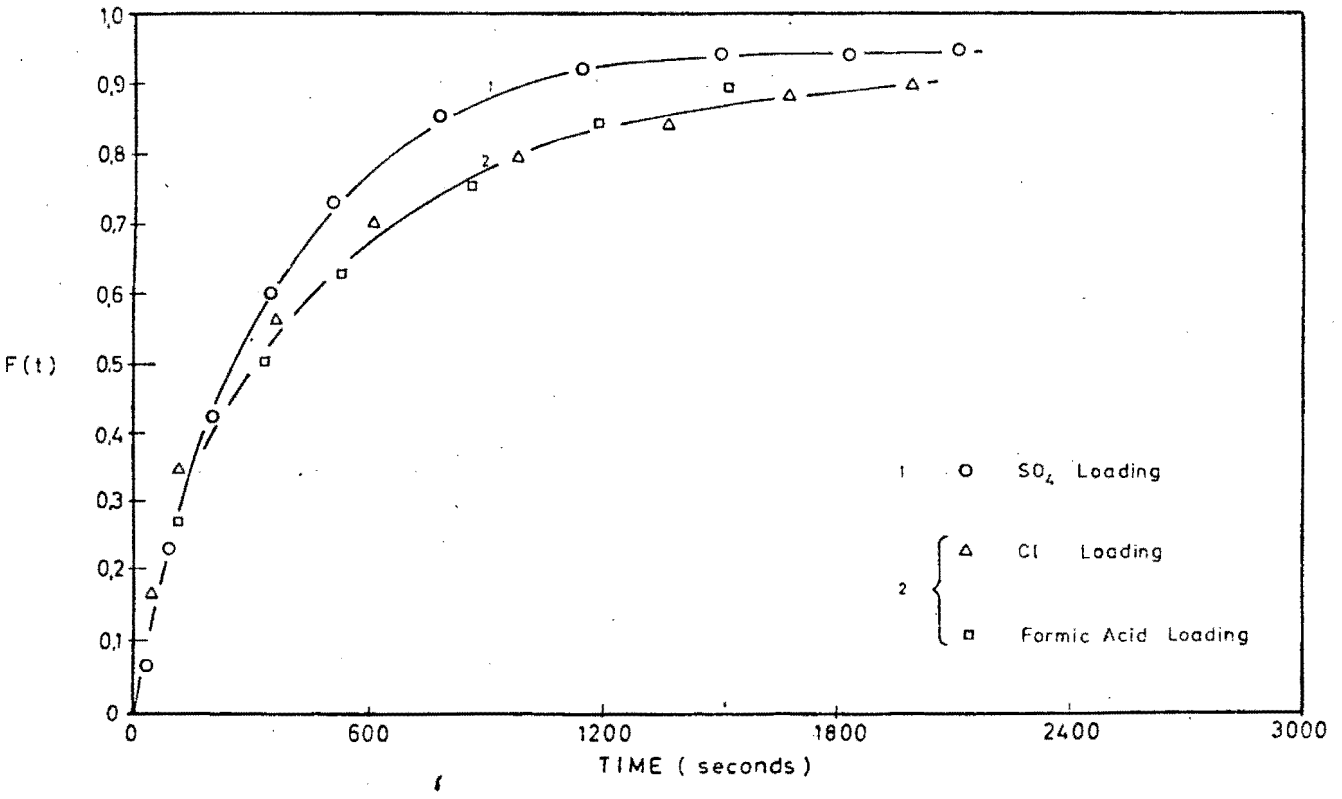

Fig. 6.9: Comparison of the Loading at 0,05N Initial Concentration, of Cl^-, SO_4^{2-} and Formic Acid on Zerolit MPH Resin

counter-ion is taken up at a higher rate (see Section 6.2.2.3). Thus, when comparing the SO_4^{2-} and COD kinetics, the OH^-/SO_4^{2-} exchange is faster (see Fig. 6.4) than the OH^-/CH_3O_2 exchange (see Fig. 6.8), even though the formic acid has a lower molecular weight than the SO_4^{2-}. The selectivity effect counteracts the mobility effect (see Section 6.2.2.3).

From Fig. 6.9 it is also shown that the Cl^- counter-ion has similar loading kinetics to the formic acid kinetics. Although the acid molecule is larger, the resin pore size is large enough to accommodate each differing species equally.

6.2.3.4 Butyric Acid Loading at Different Concentrations

The resin and liquid quantities used in these kinetic runs are given in Table 6.7.

TABLE 6.7

RESIN AND LIQUID QUANTITIES USED FOR BUTYRIC ACID LOADING AT DIFFERENT CONCENTRATIONS ON FREE-BASE ZEROLIT MPH AT 0,05N

Initial Concentration (N)	R/L	ml Resin	ml Butyric Acid
0,025	0,5	8,93	800 ml
0,0125	0,5	4,46	800 ml

The detailed kinetic data of these two runs are tabulated in Appendix D, Tables D-9 and D-10 and plotted, together with the 0,05N kinetic results (presented in Section 6.2.3.2) in Fig. 6.10.

6.2.3.5 Discussion of the Butyric Acid Loading Kinetics at Different Concentrations

Fig. 6.10 compares the kinetic curves for butyric acid

loaded onto free base form of Zerolit MPH at three different initial solution concentrations - 0,05N, 0,025N and 0,0125N.

It is shown that there is a reduction in the rate of exchange as the concentration decreases, such that the difference between the 0,05N and 0,025N systems is small compared with the difference between the 0,025N and 0,0125N systems; i.e. there is a sharp decrease in the kinetics from 0,025N to 0,0125N initial concentration.

This effect can be explained by the fact that, in normal exchange systems, the cross-over between pore- and film-diffusion control occurs at approximately 0,5N [25], while in systems using macroporous resins and counter-ions of large molecular weight, this concentration limit may be lowered (see Section 6.2.3.3), since the larger molecules are restricted by the small pores of the resin imparting partial pore-diffusion control characteristics to the system.

This is well demonstrated in Fig. 6.10. From a concentration of 0,05N to 0,0125N, the kinetic rate drops a small amount due to the weaker driving force across the film (the larger pores still contribute partial film-diffusion control characteristics to the system), while, from a concentration of 0,025N to 0,0125N, the kinetic rate drops significantly since the solution concentration is low enough to ensure that both "pore size fractions" of the resin are film-diffusion controlled. Thus the lower solution concentration again leads to a weaker driving force across the film (which now controls the entire kinetics) and results in slower kinetics.

In the following section, the kinetics of the more isoporous Senbrix resin is discussed, and in the final section, the two resins' kinetics are compared with respect to their structure.

loaded onto free base form of Zerolit MPH at three different initial solution concentrations - 0,05N, 0,025N and 0,0125N.

It is shown that there is a reduction in the rate of exchange as the concentration decreases, such that the difference between the 0,05N and 0,025N systems is small compared with the difference between the 0,025N and 0,0125N systems; i.e. there is a sharp decrease in the kinetics from 0,025N to 0,0125N initial concentration.

This effect can be explained by the fact that, in normal exchange systems, the cross-over between pore- and film-diffusion control occurs at approximately 0,5N [25], while in systems using macroporous resins and counter-ions of large molecular weight, this concentration limit may be lowered (see Section 6.2.3.3), since the larger molecules are restricted by the small pores of the resin imparting partial pore-diffusion control characteristics to the system.

This is well demonstrated in Fig. 6.10. From a concentration of 0,05N to 0,0125N, the kinetic rate drops a small amount due to the weaker driving force across the film (the larger pores still contribute partial film-diffusion control characteristics to the system), while, from a concentration of 0,025N to 0,0125N, the kinetic rate drops significantly since the solution concentration is low enough to ensure that both "pore size fractions" of the resin are film-diffusion controlled. Thus the lower solution concentration again leads to a weaker driving force across the film (which now controls the entire kinetics) and results in slower kinetics.

In the following section, the kinetics of the more isoporous Senbrix resin is discussed, and in the final section, the two resins' kinetics are compared with respect to their structure.

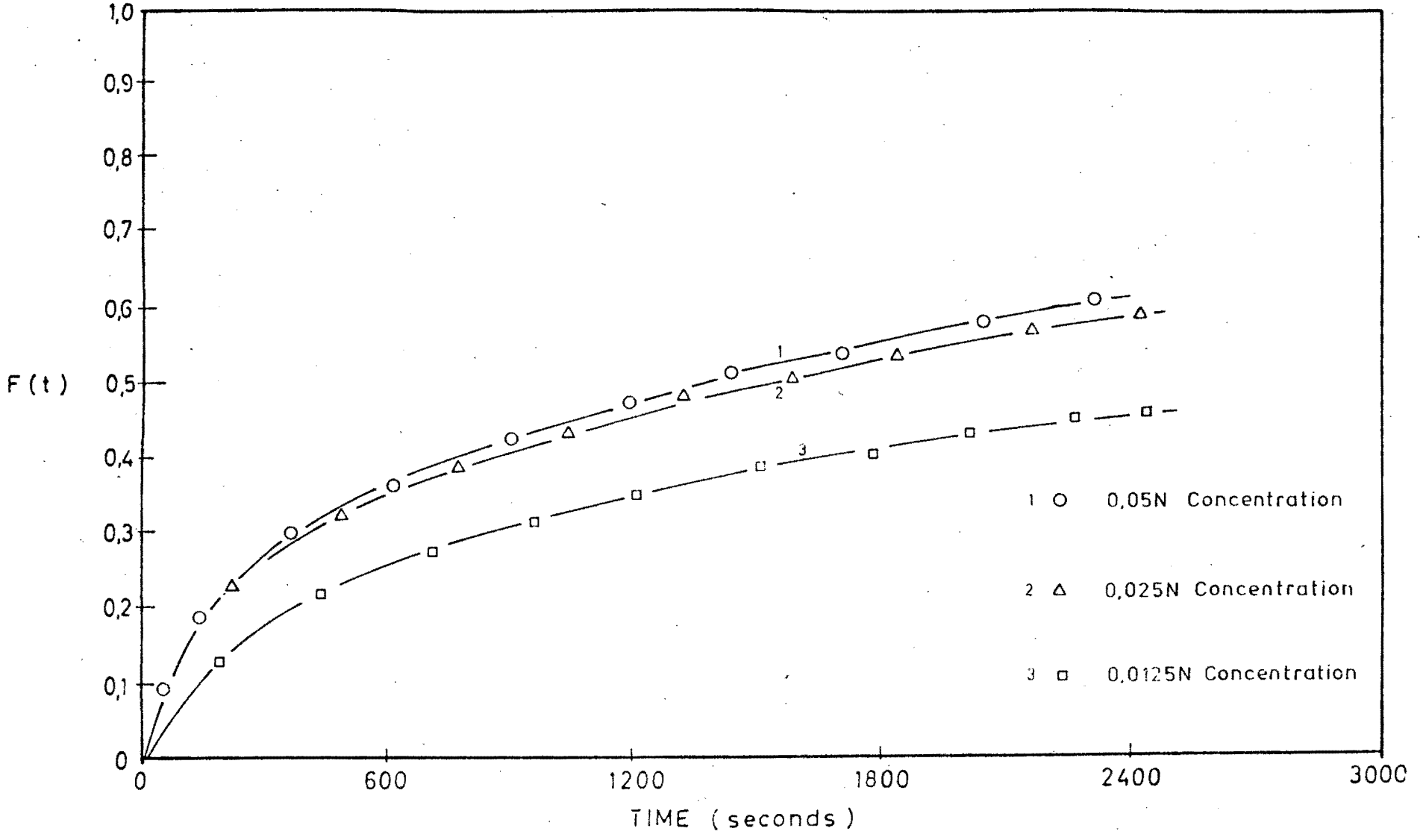

Fig. 6.10: Comparison of Butyric Acid Loading at Three Different Concentrations on Free-base Zerolit MPH Resin

6.3 PERFORMANCE OF A HIGH DENSITY ISOPOROUS ANION EXCHANGE RESIN - SENBRIX

The results in this section follow a similar order to those of Section 6.2.

6.3.1 Resin Properties

Senbrix is a weak base, isoporous, crosslinked polystyrene high density anion exchange resin manufactured by Dia-Prosim, France, and supplied by Sentrachem Ltd. Samples were supplied screened between 0,60 mm and 0,85 mm and having three different degrees of crosslinking - 6,5 , 8 and 12% DVB content respectively. The additional resin of unspecified DVB content, and having between 6,5 and 8,0% strong base character, was used for all studies where crosslinking was not a parameter being investigated.

Before commencing the kinetic studies, the volume capacity and MRC's of each of the above resins were measured. Section 5.2.1 describes the relevant definitions.

6.3.1.1 Volume Capacity

The capacities of all the resin types were measured in the Cl^- form, this being the most accepted and accurate form to measure.

Back titration methods were again used in all the capacity determinations, the method of which is described in Section 3.3.3.1(b). The results are presented in Table 6.8.

6.3.1.2 Discussion of Resin Volume Capacities

From Table 6.8 it is shown that, for the resins with known crosslinking, the volume capacities are not significantly affected by an increase in the DVB content. However, the general resin (of unspecified DVB content) has a significantly greater capacity (similar to that of Zerolit MPH - see Section 6.2.1.1)'.

TABLE 6.8

VOLUME CAPACITIES OF SENBRIX RESINS

ml resin	% DVB	Form	Capacity (meq/ml)
14,65	6,5	Cl^-	1,18
14,65	8	Cl^-	1,19
14,65	12	Cl^-	1,15
14,65	unspecified	Cl^-	1,38*

* see Discussion (6.3.1.2) for reason for inconsistent value.

The inconsistency of the capacity to DVB content seems to indicate that the resin swelling (in this DVB range) is not greatly affected by the degree of crosslinking, since the resin volume change of the cation resin resulted in their volume capacities increasing significantly with increasing DVB content (see Section 5.3.1.1).

The higher capacity of the general Senbrix resin is probably due to the fact that, since it was manufactured in a separate batch, it possesses some characteristic (most likely methylene bridging - see Section 2.2.1.3) which alters the degree of crosslinking (and thus the capacity) independent of the DVB content.

6.3.1.3 Moisture Retention Capacities

These were measured for each of the resins described in Section 6.3.1. Table 6.9 tabulates the results.

6.3.1.4 Discussion of MRC Results

As the degree of crosslinking increases, the MRC value decreases. This result is similar to those found for the Cation Fort resins (see Section 5.3.1.3), and is due to the fact that a resin with a higher DVB content cannot expand to

TABLE 6.9

MOISTURE RETENTION CAPACITIES OF SENBRIX RESINS

% DVB	Form	Wet Resin wt. (gm)	Water (gm)	% MRC
6,5	Cl^-	3,8420	2,1299	55,44
*6,5	Cl^-	2,5251	1,3802	54,66
6,5	OH^-	2,7681	1,3562	48,99
*6,5	OH^-	3,3191	1,6040	48,33
8	Cl^-	4,0297	1,7963	44,58
*8	Cl^-	2,8661	1,2720	44,38
8	OH^-	4,3334	1,4891	34,36
*8	OH^-	4,0134	1,3326	33,20
12	Cl^-	4,3338	1,6669	38,46
+12	Cl^-	2,7842	1,0746	38,60
12	OH^-	3,8836	1,2275	31,61
+12	OH^-	2,6613	0,8355	31,39
unspecified	Cl^-	3,4398	1,9174	44,30
*unspecified	Cl^-	3,5197	1,9636	44,29
unspecified	OH^-	3,2555	1,5608	52,10
*unspecified	OH^-	3,2851	1,5775	52,04

* repeat run with sample from separately loaded resin batch.
+ repeat run with sample from the same resin batch.

the same extent as one with a lower DVB content (since the former is less firmly internally "bound"). This results in a lower final internal total pore volume. Similar results were found by Sharma and Subramanian [49] for Dowex AG 1. Fig. 6.11 shows this general trend for Senbrix resin in the free-base and Cl^- forms. As was found for the cation resins, the decrease in MRC value is most significant between resins of lower DVB content.

The general Senbrix resin exhibits MRC values which

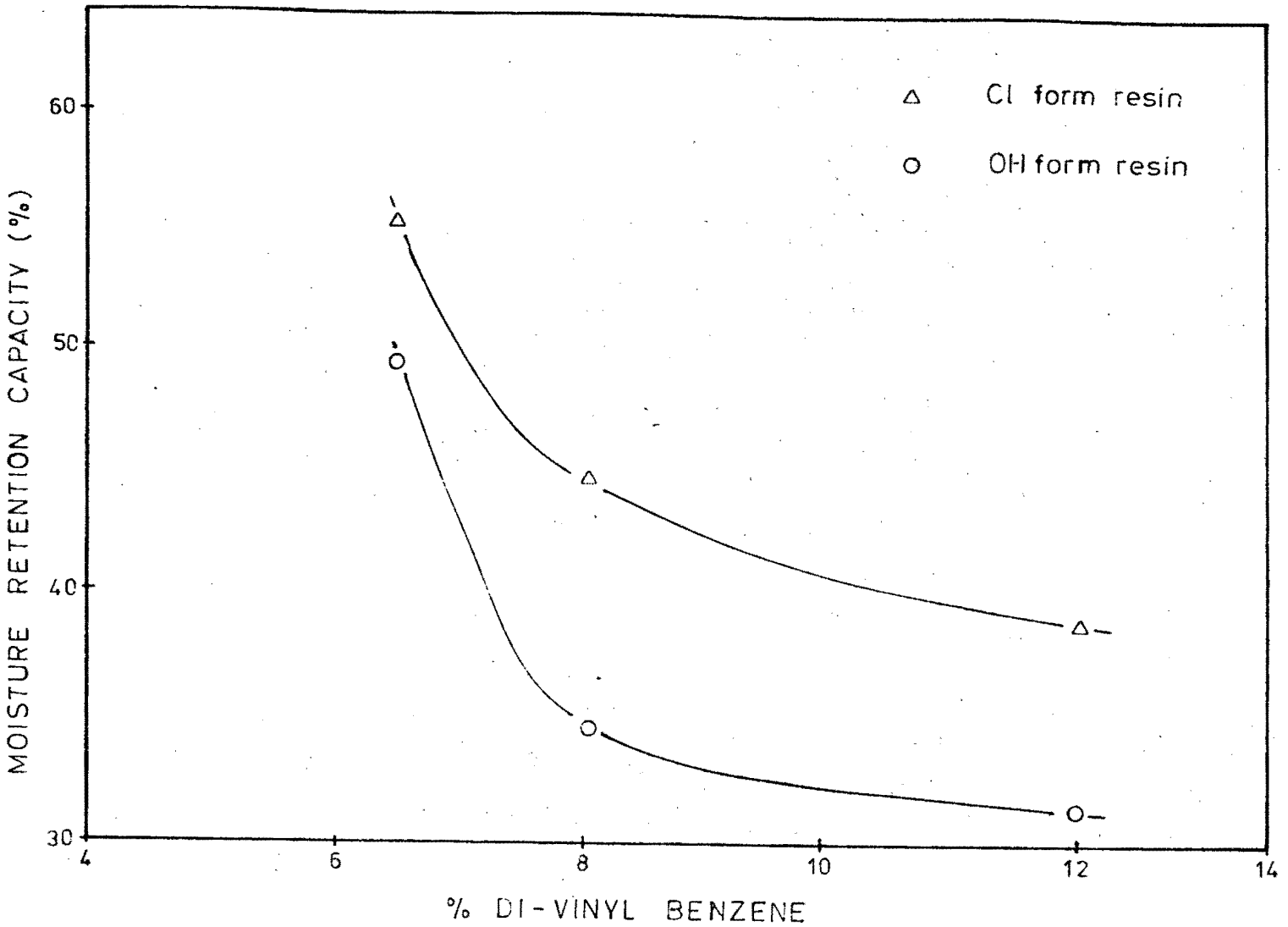

Fig. 6.11: Variation of MRC Value With % DVB for Senbrix Resin in OH^- and Cl^- Form

follow the same trend as those of Zerolit MPH (see Section 6.2.1.3), i.e. the Cl^- form of the resin has the lower value due to its relatively large ionic radius. However, the other resins of known crosslinking show the opposite trend, i.e. the Cl^- form of the resins have a higher MRC value than those in the free-base form. This can only be attributed to excessive decomposition of the free-base resin when dried at 105°C [25]. Sharma and Subramanian, working with the free-base form, obtained results consistent with those of Cl^- (drying carefully at 45°C and under 1 mmHg vacuum) which further suggests thermal decomposition of the resins in Table 6.9.

Table 6.9 shows that the results repeat well; those repeated within a resin batch (marked +) are consistent to within 1% (as was found for all other MRC determinations), while those repeated from an entirely separately loaded resin batch repeat to within 3%. Thus this method is accurate for determining the total internal pore volume.

6.3.2 Binary Cl^- and SO_4^{2-} Kinetics

As discussed in Section 6.1, the binary loading kinetics of Cl^- and SO_4^{2-} on free-base form of Senbrix resin were studied at 0,01N and 0,05N concentrations, at an initial R/L ratio of 0,5.

Equation (6.1) was used to calculate the F(t) values, and the results are plotted on F(t) versus time graphs which follow each respective section. The simplifying assumptions used are discussed in Section 6.2.2.1.

6.3.2.1 Loading Kinetics

The quantities of resin and liquid used in these studies are tabulated in Table 6.10.

The detailed results are tabulated in Appendix D, Tables D-11 to D-14, and plotted in Figs. 6.12 to 6.15.

TABLE 6.10

RESIN AND LIQUID QUANTITIES USED FOR SENBRIX BINARY KINETIC STUDIES

Initial Concentration (N)	Counter-ion Studied	R/L	Resin (ml)	Liquid (ml)
0,01	Cl^-	0,5	2,86	800
0,01	SO_4^{2-}	0,5	2,86	800
0,05	Cl^-	0,5	14,3	800
0,05	SO_4^{2-}	0,5	14,3	800

6.3.2.2 Discussion of Loading Kinetics

(a) The Effect of the Counter-Ion:

Figs. 6.12 to 6.15 show the basic F(t) plots for the two counter-ions studied at both 0,01N and 0,05N concentrations. From these plots Fig. 6.15, which compares the kinetics of both systems with respect to concentration and counter-ion, is drawn.

It is clearly shown (as for the Zerolit MPH binary kinetics - see Section 6.2.2.3 and Fig. 6.5) that these binary kinetics are significantly affected by the properties of the loading counter-ion, since, for both the 0,01N and 0,05N systems, the Cl^- loading kinetics differ from those of SO_4^{2-}. However, the effect is not consistent with results obtained with Zerolit MPH resin, since, at 0,01N concentration, the SO_4^{2-} loading is faster than the Cl^- loading, while at 0,05N the opposite is the case - the SO_4^{2-} loading is slower than the Cl^- loading.

This apparent inconsistency can be explained in terms of mobility and resin selectivity. As is discussed in Section 6.2.2.3, film-diffusion controlled kinetics are affected by both the counter-ion's mobility in the liquid film surrounding

the resin bead, and the resin's selectivity towards that particular ion. In general, the diffusivity (and thus mobility) of a counter-ion increases with decreasing hydrated radius, and the selectivity of the resin towards that counter-ion increases with increasing ionic valence and decreasing solution concentration (see Section 2.4.2.1). Further, the resin selectivity is a function, amongst others, of the pore structure - the cause of sieve action (see Section 2.4.2.3). If the resin has a very uniform, large pore structure (as is the case for the isoporous Senbrix), selectivity effects are reduced, compared with a resin with a large pore size distribution (such as a macroporous resin).

These facts can help explain the characteristics of the Cl^- and SO_4^{2-} kinetics plotted in Fig. 6.16. The Cl^- counter-ion has a higher mobility than that of the SO_4^{2-}, since it has a smaller hydrated radius. Thus, if selectivity effects were negligible, the Cl^- loading kinetics would be faster than those of the SO_4^{2-}, at both 0,01N and 0,05N concentrations. However, this is an idealised case, and selectivity does have a marked effect, particularly on systems involving both monovalent and divalent counter-ions. The selectivity of the resin for SO_4^{2-} is considerably greater than for Cl^- (since SO_4^{2-} is a divalent ion compared with the monovalent Cl^- ion), and this effect decreases with increasing solution concentration. Thus, at 0,01N the selectivity effect is stronger than the mobility effect, and the SO_4^{2-} loading kinetics are faster than the Cl^- loading kinetics (see Fig. 6.16 - graphs 1 and 3). However, at the higher concentration, the reverse is true - the selectivity effect is reduced because of the increased concentration, and the mobility effect becomes predominant, resulting in the Cl^- kinetics becoming faster than the SO_4^{2-} kinetics (see Fig. 6.16 - graphs 2 and 4). The resin type (especially pore structure) and the counter-ion involved in the exchange have a marked effect on the kinetics.

The results obtained for the macroporous Zerolit MPH differ slightly from those of Senbrix, and the respective

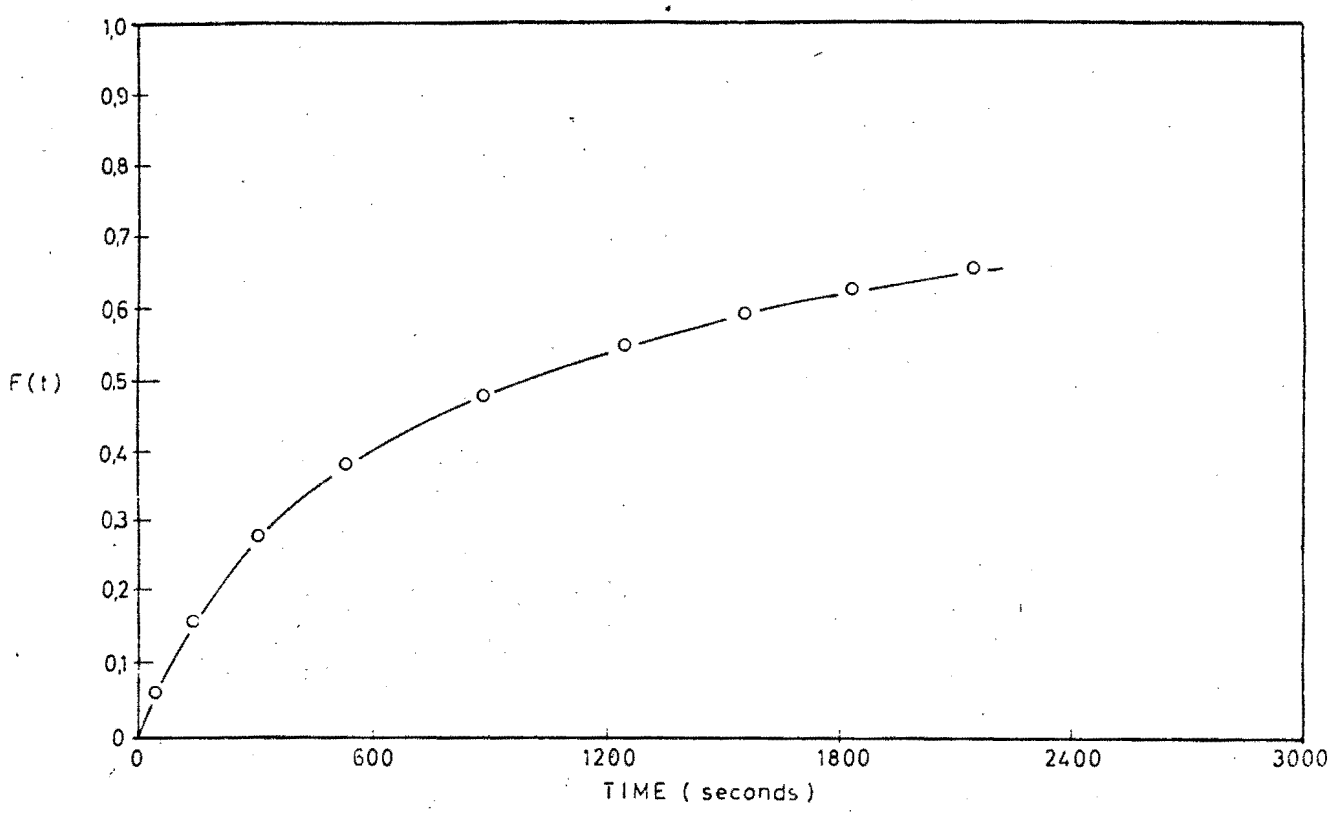

Fig. 6.12: Cl^- Loading at 0,01N Initial Concentration on Free-base Senbrix Resin

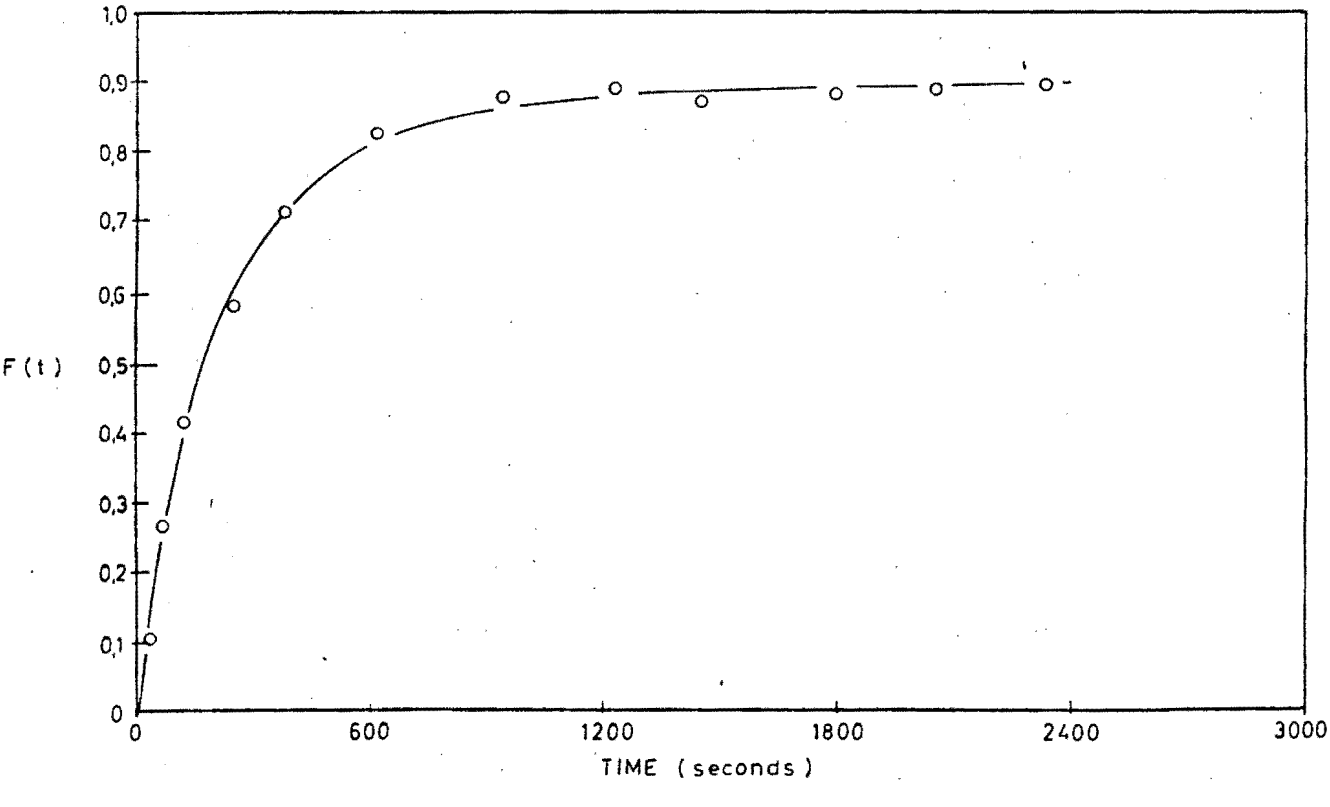

Fig. 6.13: Cl^- Loading at 0,05N Initial Concentration on Free-base Senbrix Resin

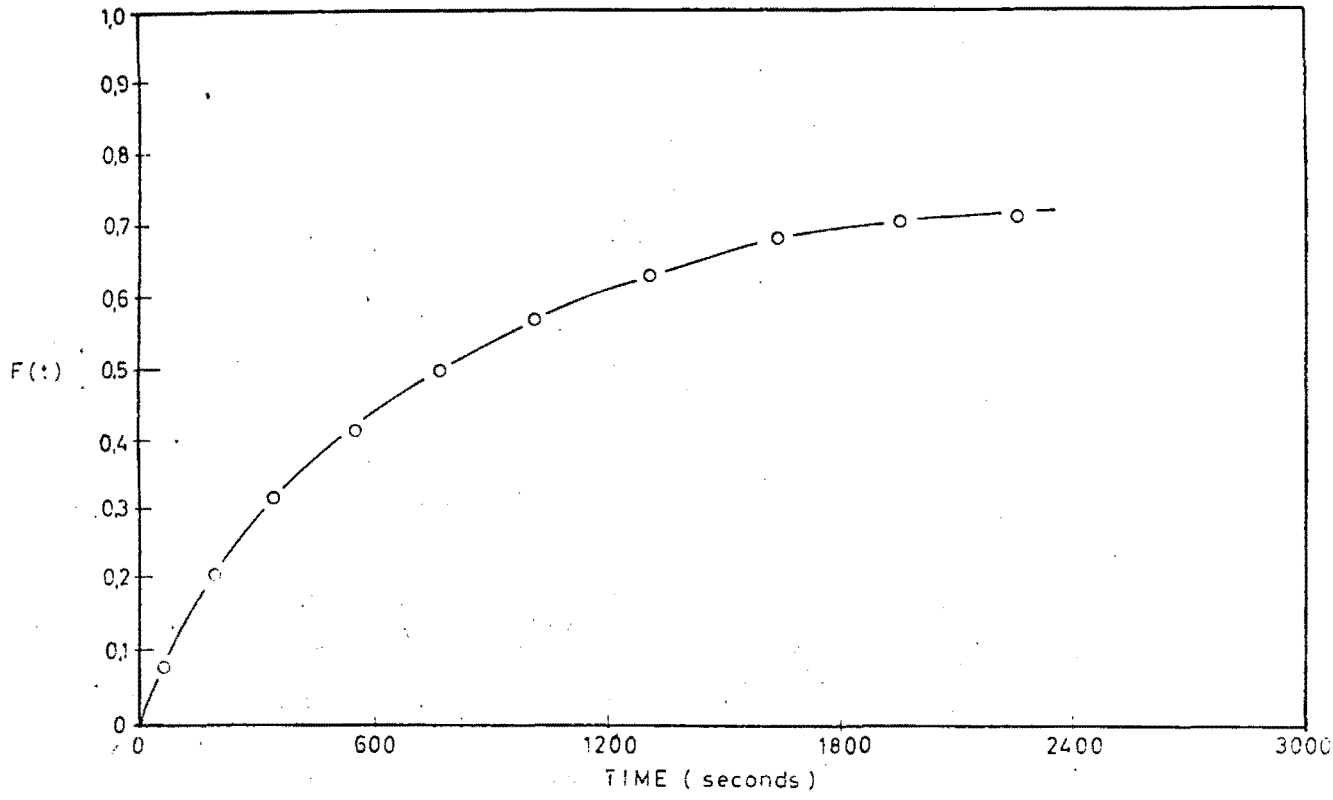

Fig. 6.14: SO_4^{2-} Loading at 0,01N Initial Concentration on Free-base Senbrix Resin

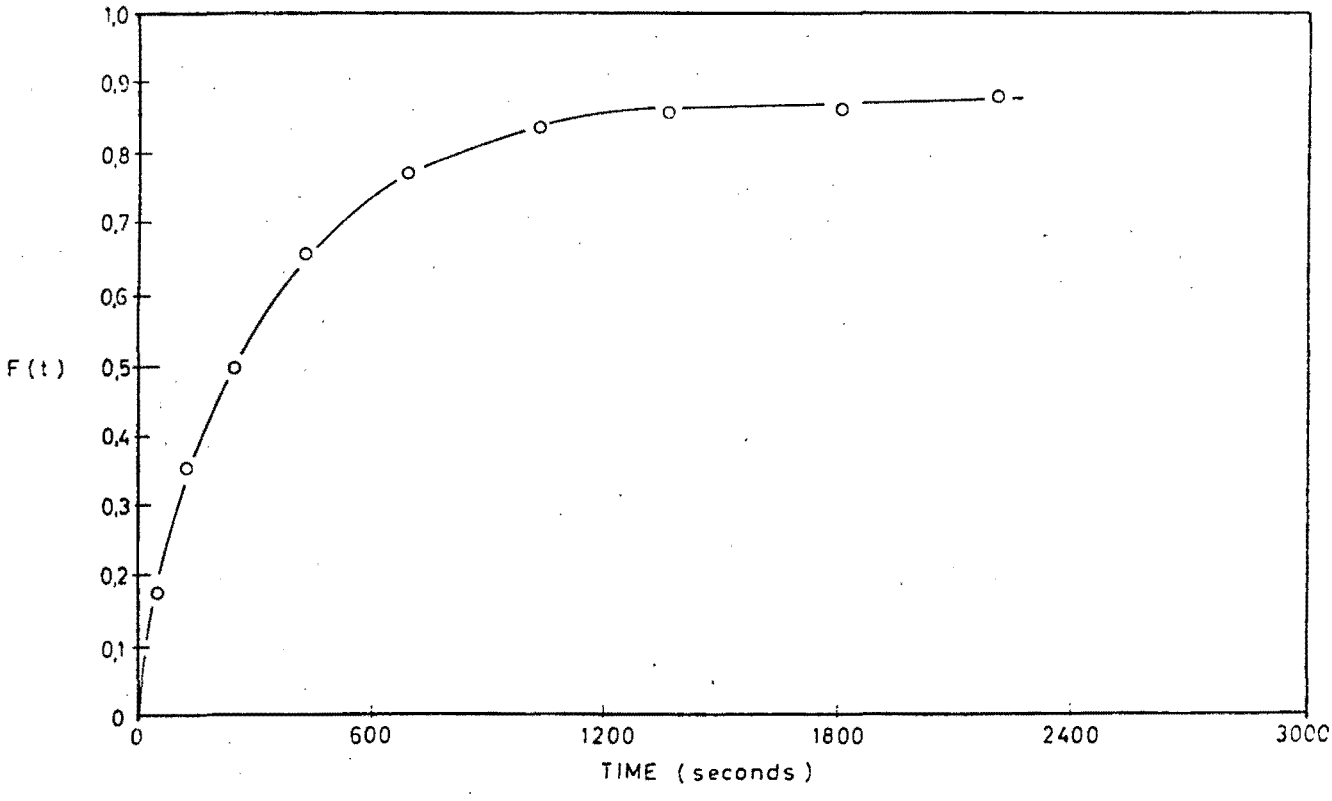

Fig. 6.15: SO_4^{2-} Loading at 0,05N Initial Concentration on Free-base Senbrix Resin

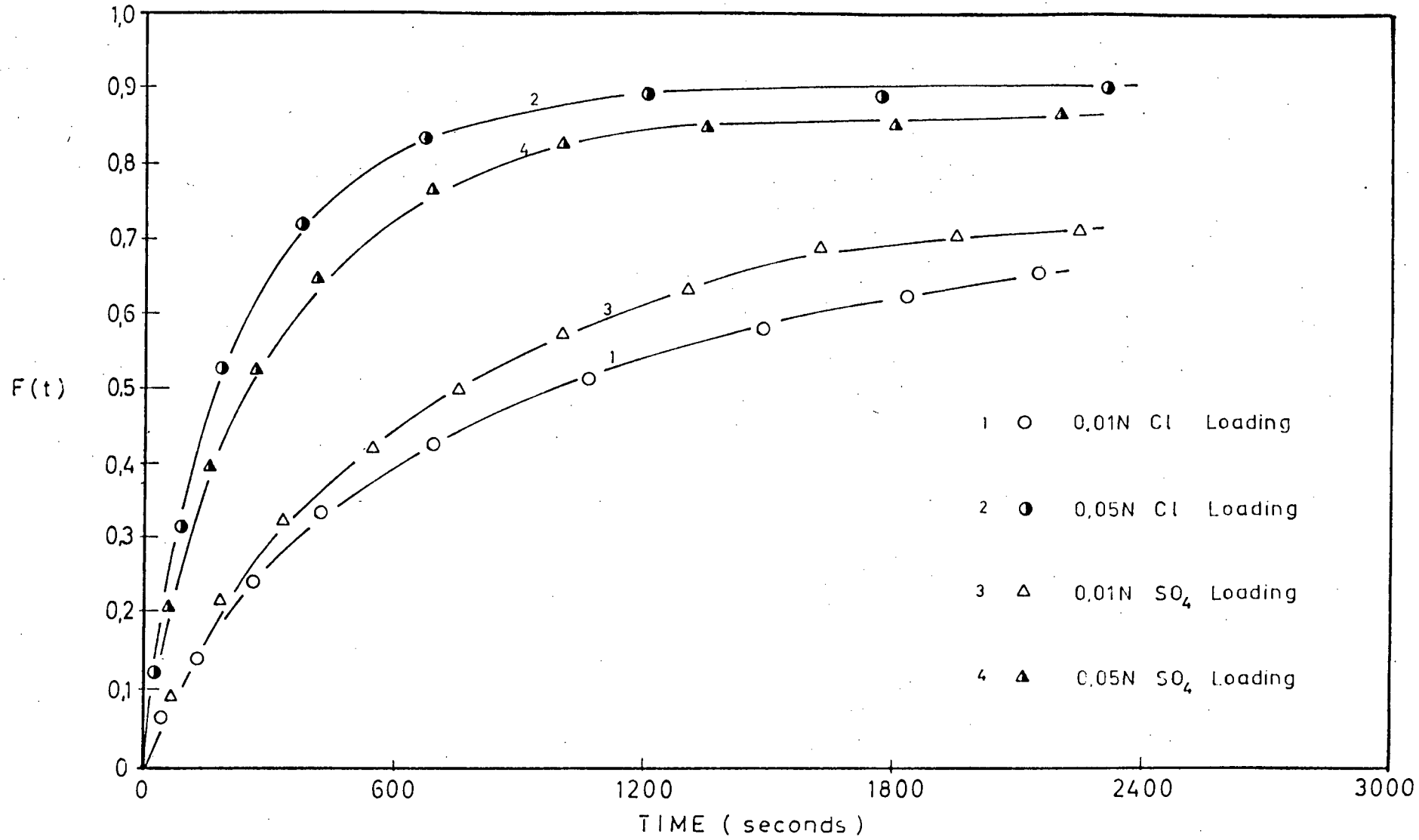

Fig. 6.16: Comparison Between Cl^- and SO_4^{2-} Loading at 0,01N and 0,05N Initial Concentrations on Free-base Senbrix Resin

resins' binary kinetics are compared and discussed in Section 6.4.3.

(b) The Effect of Concentration:

Fig. 6.16 shows, also, that the binary kinetics are sensitive to concentration. For both Cl^- and SO_4^{2-} loading, the 0,05N kinetics are faster than those at 0,01N.

These observations and trends are consistent with film diffusion kinetic theory (see Section 2.5.4.2(a)). The driving force is equivalent to the concentration gradient between the bulk solution and the solution/resin interface, and this will increase with increasing solution concentration, resulting in an increase in the kinetic exchange rate [25].

It is shown from Fig. 6.16 that the concentration effect for the Cl^- loading is greater than that for the SO_4^{2-} loading. The reasons for this are related to the combined counter-ion mobility/selectivity effect discussed in Section 6.3.2.2(a).

6.3.2.3 The Kinetics of Cl^- Loading on Resin of Different DVB Content

The Cl^- loading kinetics at 0,05N initial concentration on high density resin of 6,5%, 8% and 12% DVB contents were studied. 800 ml of liquid and 21,8 ml of free-base form resin were used in all the runs in order to obtain an initial R/L ratio of 0,5.

The detailed results are tabulated in Appendix D, Tables D-15 to D-17, and plotted in Fig. 6.17.

6.3.2.4 Discussion of Cl^- Loading Kinetics on Resin of Different DVB Content

Fig. 6.17 compares the kinetic F(t) plots of the 6,5%, 8% and 12% DVB Senbrix resins with Cl^- loading at 0,05N. It is clearly shown that the 8% and 12% DVB resins exhibit similar kinetics (the 8% resin's kinetics being slightly

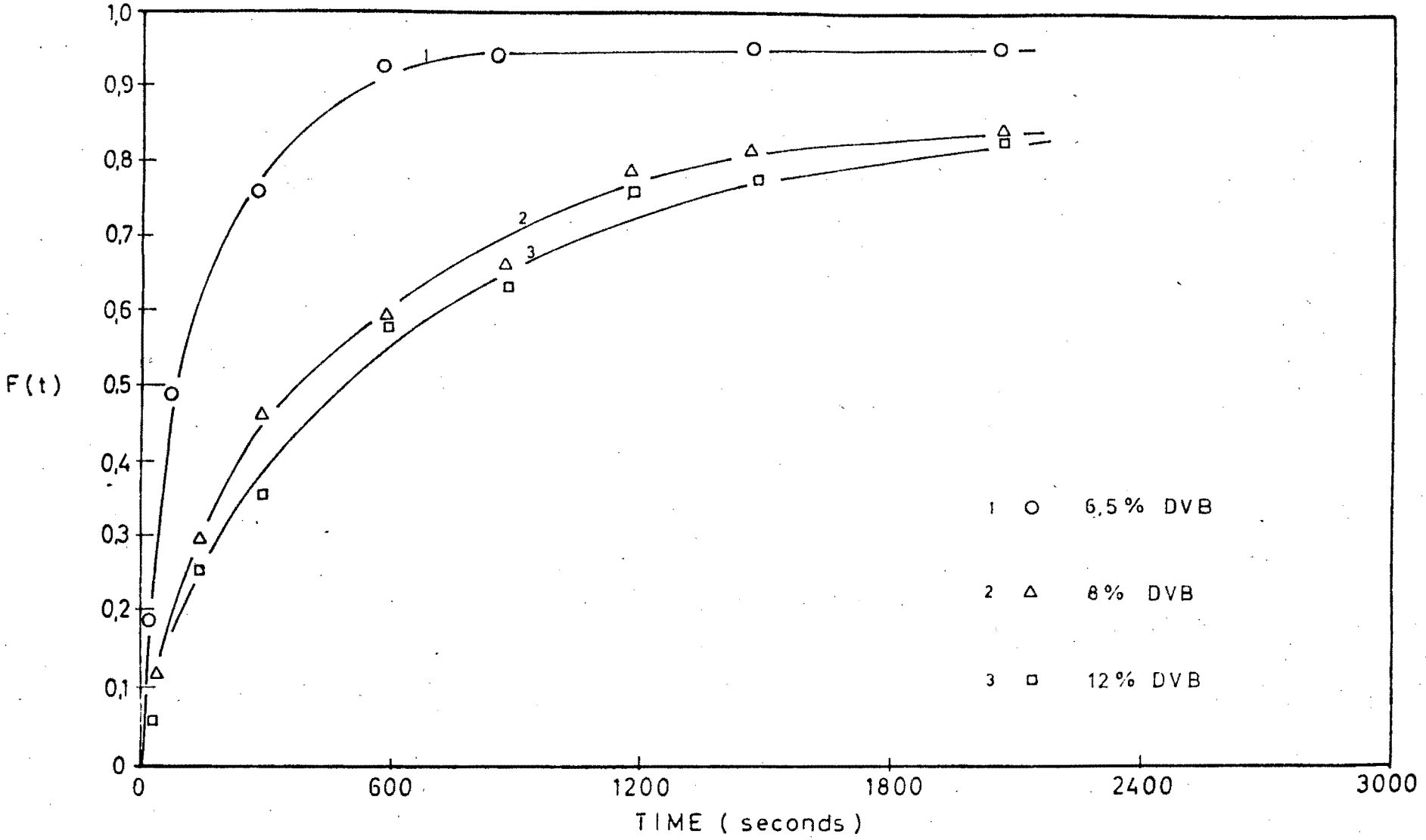

Fig. 6.17: Comparison Between Cl^- Loading at 0,05N Initial Concentration on Senbrix Resin of Different Crosslinking

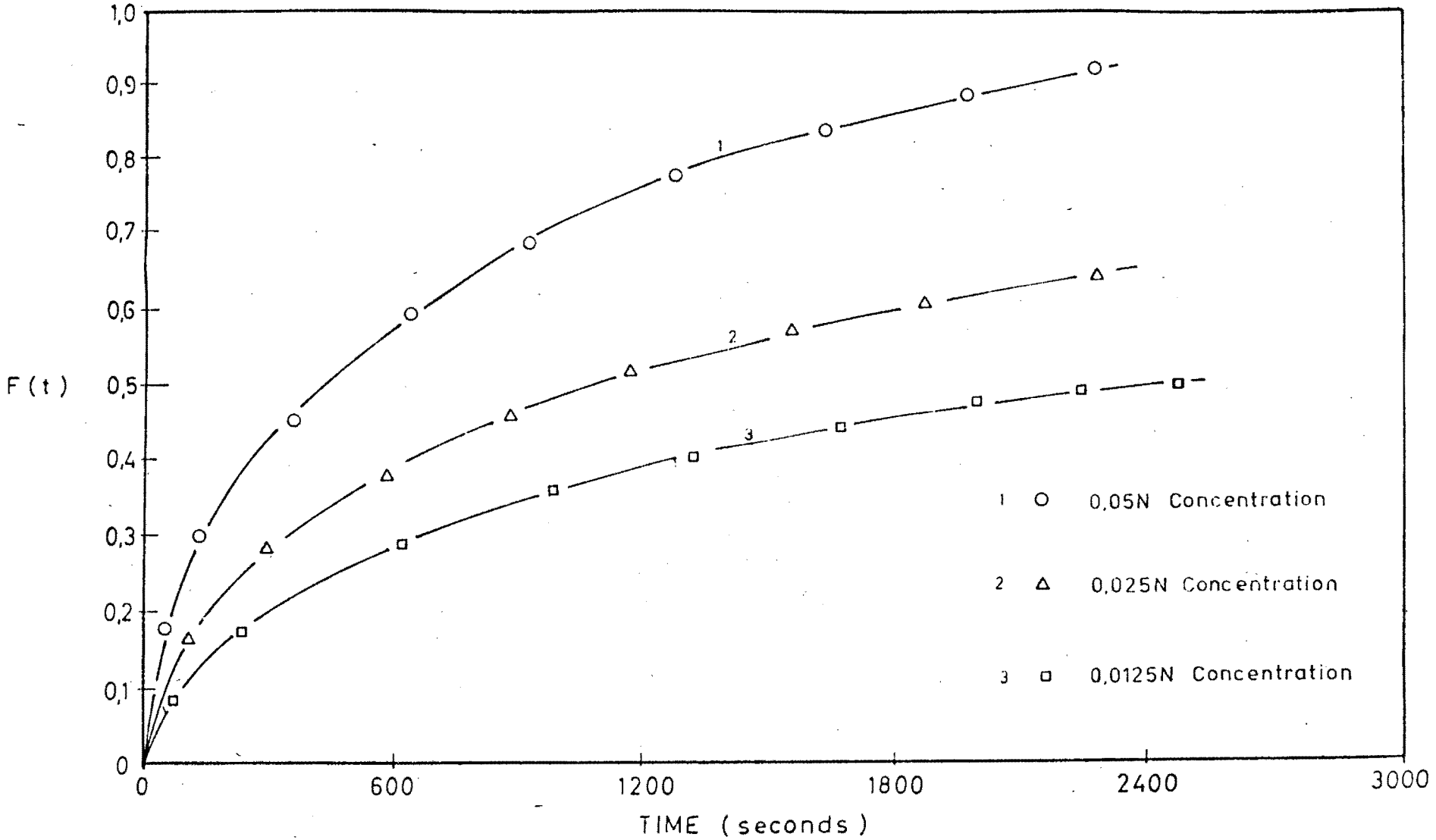

Fig. 6.21: Comparison of Butyric Acid Loading at Three Different Concentrations on Free-base Senbrix Resin

TABLE 6.13

RESIN AND LIQUID QUANTITIES USED FOR THE LOADING OF BUTYRIC ACID AT DIFFERENT CONCENTRATIONS ON FREE-BASE SENBRIX RESIN

Initial Concentration (N)	R/L	ml Resin	ml Butyric Acid
0,025	0,5	9,20	800 ml
0,0125	0,5	4,60	800 ml

It is evident that the kinetic rate decreases with increasing concentration of the bulk solution. Furthermore, the decrease from one successive F(t) curve to another is fairly constant. These results indicate that the system is film-diffusion controlled, as would be expected from such an isoporous resin at a concentration below 0,1N.

The comparison between the Zerolit MPH and Senbrix results are discussed in Section 6.4.

6.3.3.5 Regeneration of Butyric Acid Loaded Resin

To complete the COD studies, a run was performed in order to obtain kinetic data on the regeneration of Senbrix resin loaded with butyric acid, using 0,05N NaOH solution at an R/L of 0,5.

14,3 ml of resin and 800 ml of 0,05N NaOH were reacted together and the results are tabulated in Appendix D, Table D-26.

6.3.3.6 Comparison Between Butyric Acid Loading and Regeneration

Fig. 6.22 compares the kinetics of the loading and regeneration of butyric acid of Senbrix resin at 0,05N.

The regeneration kinetics are seen to be appreciably faster than the loading kinetics at the same initial concentration ($t_{\frac{1}{2}}$ for regeneration = 120 seconds, while $t_{\frac{1}{2}}$ for loading = 250 seconds).

The reason for the significantly more favourable regeneration kinetics is due to the acid dissociation constant variation at changing pH. At high pH (alkali), organic acids will dissociate to a larger extent than at low (acid) pH (i.e. the dissociation constant is higher at high pH). The loading of weak base anion resins involves the entire molecule (see Section 6.2.2.1) as compared with the counter-ion only being involved in strong base anion and all cation systems. Thus, for the loading of a weak base resin, an associated molecule is required in the pore before the weakly basic resin will dissociate it prior to loading the two ion pairs (see Section 6.2.2.1, equations (6.3) and (6.4)). The resin site therefore must be protonated before exchange can take place, and therefore the entire molecule is required at the exchange site before dissociation, and subsequent loading, can occur. The higher the degree of association (and thus the lower the pH) in the solution, the more favourable the loading kinetics become.

A similar situation is relevant for regeneration. The higher the degree of dissociation which is achieved inside the pore (i.e. the higher the solution pH), the more easily the resin will be regenerated and the faster the kinetics become.

When comparing the regeneration and loading kinetics, the relative degrees of dissociation are important. The weak organic acid, coupled to the weakly basic resin, does not result in as favourable a loading dissociation profile as the strong alkali used during regeneration. The latter results in complete, almost immediate, dissociation of the organic acid, required for total regeneration, resulting in faster kinetics shown in Fig. 6.22.

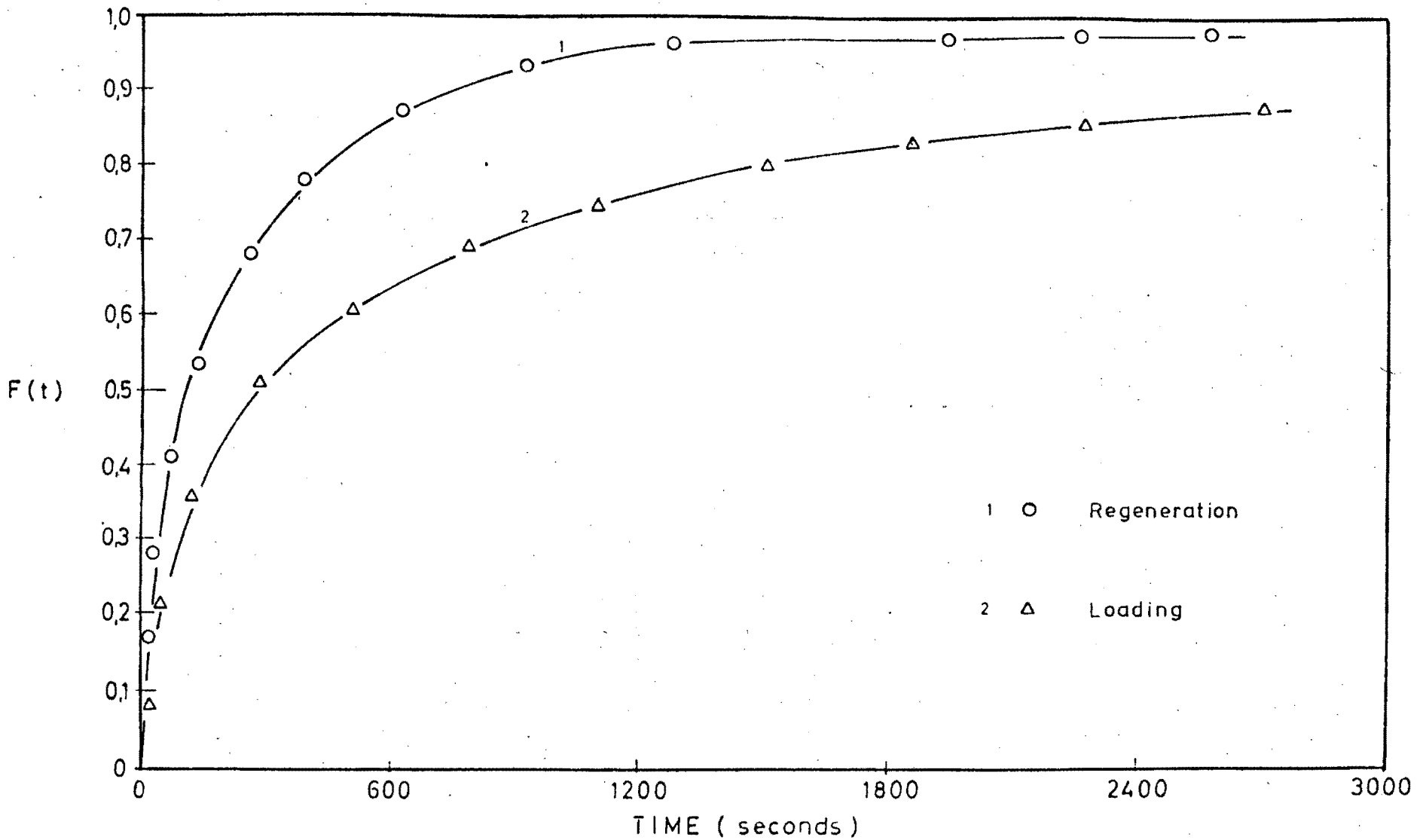

Fig. 6.22: Comparison Between Butyric Acid Loading and Regeneration at 0,05N Initial Concentration of Senbrix Resin

6.4 COMPARISON BETWEEN THE KINETICS OF ZEROLIT MPH AND SENBRIX RESINS

6.4.1 Introduction

The kinetic results that were similarly performed for the two resin types are compared in this section.

The important difference between the physical structure of these two resins is their respective pore size distribution. The macroporous Zerolit MPH resin, like most older macroporous resins, comprises both a "small pore fraction", consisting of pores of diameter approximately equivalent to the hydrated radius of the larger counter-ions (e.g. low molecular weight acids), as well as a "large pore fraction", comprising significantly larger diameter pores (approximately 10^3 Å). There are relatively few pores of medium size, and therefore the two "pore fractions" each exert their own effects, almost independently, on the kinetics. The Senbrix resin, by comparison, has a more isoporous resin matrix containing more uniform size distribution. There are few smaller pores, and the large majority, therefore, are slightly smaller than the average diameter of the macroporous "large pore fraction". This difference in the resins' structure is due to the different methods of synthesis. (Senbrix is the more modern resin, and the technology of resin manufacture has improved the final resin structure in the above way.) The structure and properties of the resins are discussed in Section 2.2.2 and Section 6.2.3.3.

In addition, the Senbrix is a high density resin, compared with the normal density Zerolit MPH resin. The method of obtaining higher density in a weak base resin (which tends to have very low swollen densities) is to introduce a Br^- ion into the resin matrix during synthesis. This Br^- ion is inert, and does not affect the kinetics directly. However, the improved density of the resin would result in higher flow rates being used (and thus higher throughput) in continuous counter-current fluidised stage ion

exchange systems. This improved flow-rate results in decreased contact time within a stage, and thus a corresponding improvement in the kinetics is also desirable. This section determines if this additional property is present.

6.4.2 Resin Properties - Moisture Retention Capacity

Tables 6.2 and 6.9 present the MRC values of the two resin types. The Zerolit MPH resin has an MRC value (in the Cl^- form) of 44,5%, while the 8% Senbrix resin has an MRC value of 44,4%. (Zerolit MPH is a mid-range DVB content resin, and thus it is compared with its closest counterpart, the 8% Senbrix resin.) Since both resins would be expected to have similar total internal pore volumes (the macroporous resin has both large and small pores while the more isoporous resin has more uniform pores of a size slightly smaller than the "large pore fraction" of the macroporous resin - see Section 6.2.1), the approximately similar MRC values are consistent with what would be expected, since the two resin pore types should average out at a similar volume.

6.4.3 Cl^- and SO_4^{2-} Binary Kinetics

Fig. 6.23 compares the Cl^- loading kinetics of the two resins at both 0,01N and 0,05N, and Fig. 6.24 similarly compares the SO_4^{2-} kinetics of the two resins.

Both graphs show that, although one resin may have faster kinetics compared with the other, the differences in both the Cl^- and SO_4^{2-} systems between the 0,01N curves and the 0,05N curves are consistent for both resins. (In Fig. 6.23, for example, the difference between graphs 1A and 2A is approximately equal to the difference between graphs 1B and 2B.) The counter-ions (Cl^- and SO_4^{2-}) are not large enough to be affected by the difference in resin pore structure (see Section 6.4.1), and thus the above results are consistent with expected results.

Comparing Figs. 6.23 and 6.24, it will be noted that the

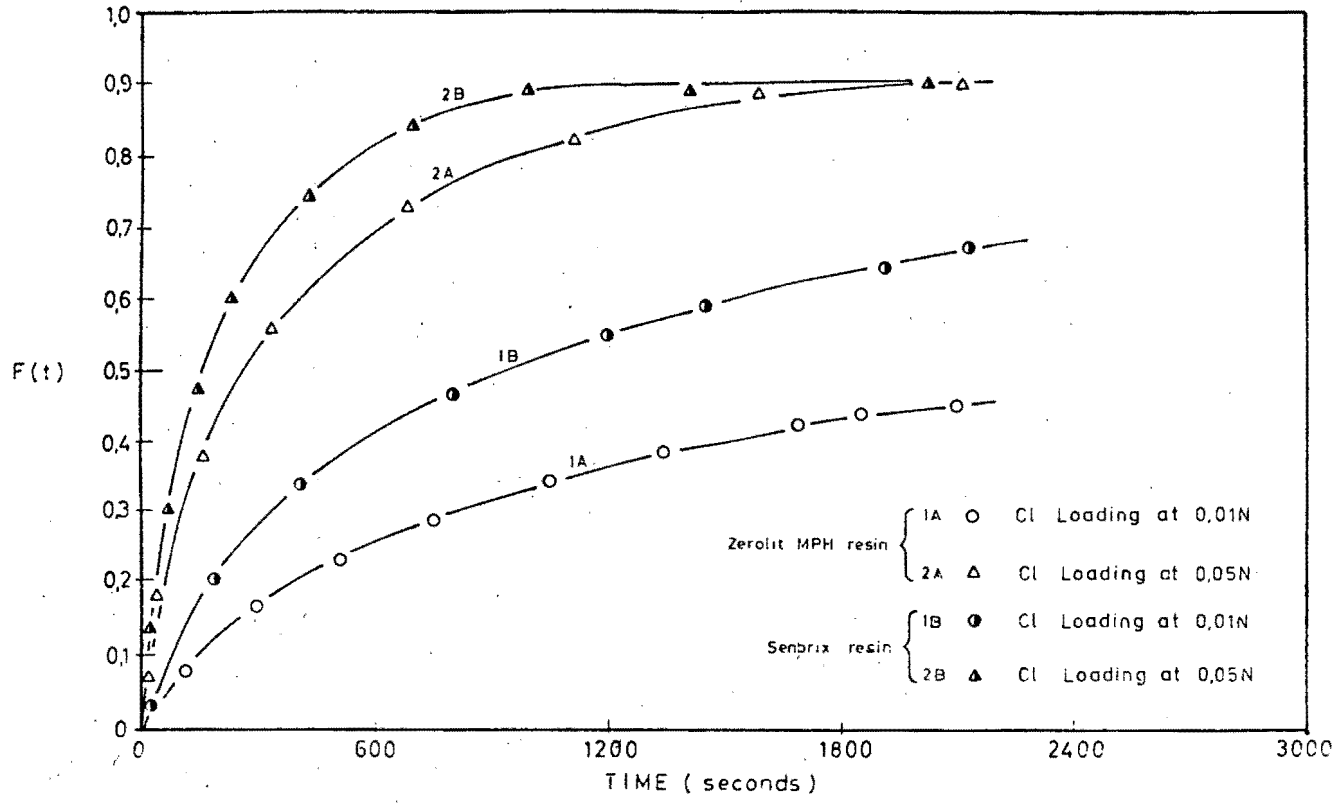

Fig. 6.23: Comparison Between Loading of Cl^- at 0,01N and 0,05N Initial Concentrations on Free-base Zerolit MPH and Senbrix Resins

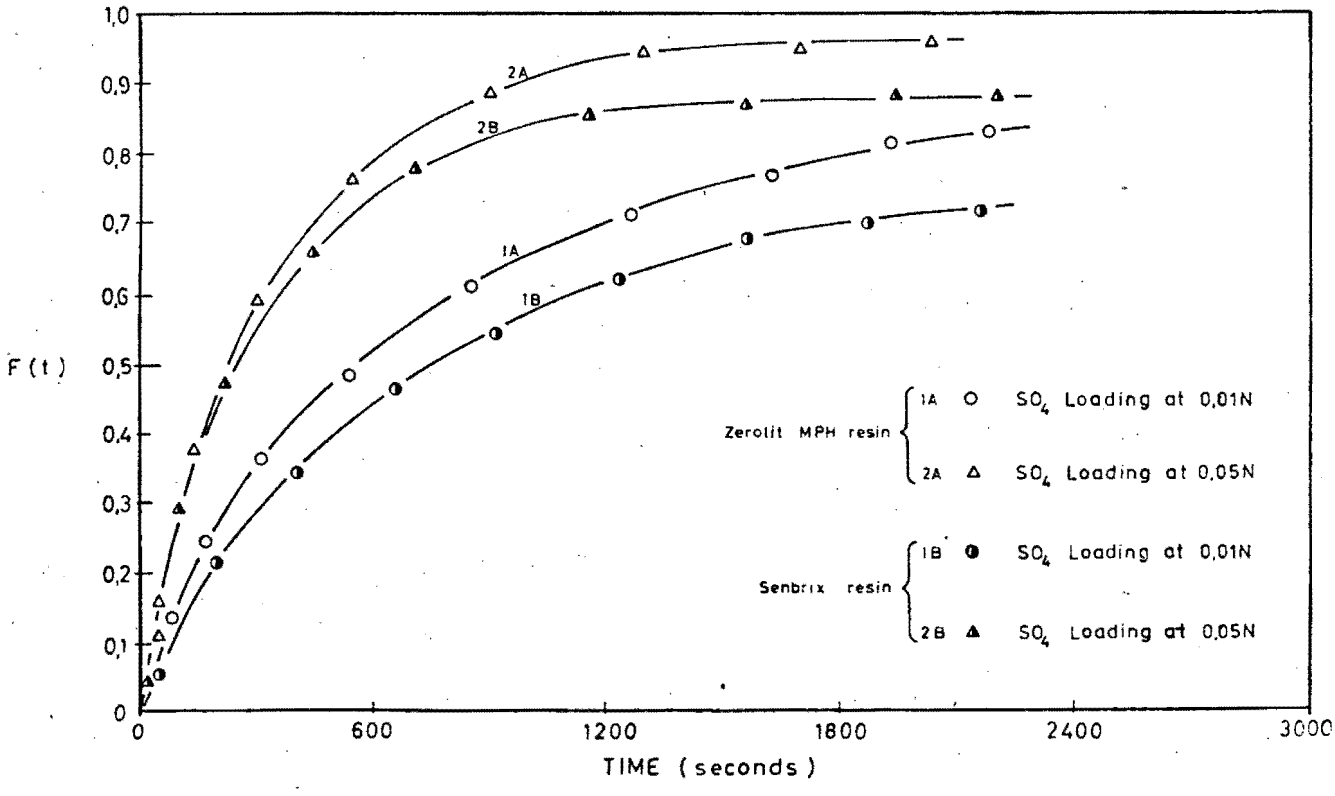

Fig. 6.24: Comparison Between SO_4^{2-} Loading at 0,01N and 0.05N Initial Concentrations on Free-base Zerolit MPH and Senbrix Resins

major difference between the two is, firstly, that the Cl^- kinetic curves are more widely spread than those of the SO_4^{2-} kinetics, and, secondly, whereas Zerolit MPH is more favourable for Cl^- loading, Senbrix is more favourable for SO_4^{2-} loading. Both of these observations can be explained by selectivity effects.

As discussed in Sections 6.3.2.2 and 6.2.2.3, both counter-ion mobility and resin selectivity affect the kinetic properties of these anion systems. Thus, the SO_4^{2-} kinetics would be expected to be slower than the equivalent Cl^- kinetics, but the greater resin selectivity for SO_4^{2-} counteracts this effect, resulting in a relative increase in the SO_4^{2-} kinetics. This tends to compress the curves at varying concentrations, since the selectivity increases with decreasing solution concentration, thus tending to increase the lower concentration curves (graphs 1A and 1B) to a greater extent than the higher concentration curves (graphs 2A and 2B). This results in a smaller spread of the F(t) curves in the SO_4^{2-} system compared with the Cl^- system.

The second observation is more difficult to explain, but could similarly be attributed to a selectivity effect. It is probable that the Senbrix resin has a greater selectivity for SO_4^{2-} than does the Zerolit MPH resin (no equilibrium data for Senbrix are available), and this could result in the divalent SO_4^{2-} kinetics of Senbrix being disproportionately boosted, compared with either the Senbrix Cl^- or Zerolit MPH kinetics. If this were the case, the Senbrix kinetics could become faster than the Zerolit MPH kinetics, particularly at the lower concentration (since selectivity increases with decreasing solution concentration), as is shown in Fig. 6.24, while, for the Cl^- kinetics, this reversal would not occur, and the kinetics would remain the original way round, as is shown in Fig. 6.23.

6.4.4 COD Kinetics

Both the loading kinetics of the three organic acids and

the loading of butyric acid at the three initial solution concentrations are compared for the two resin types.

6.4.4.1 Loading Kinetics of Different Monocarboxylic Acids

Fig. 6.25 shows the kinetics of formic acid, propionic acid and butyric acid loading on the two resins at 0,05N.

This figure very clearly shows the effect of the different pore size distribution on larger loading molecules (as discussed in Sections 6.4.1, 6.2.3.3 and 6.3.3.2). The formic acid molecule is small enough to be only minimally retarded by the smaller "pore fraction" of the resin, and thus the two resins have equal kinetics (graph 1). However, the propionic and butyric acids are too large to diffuse successfully into the "small pore fraction" of the macroreticular Zerolit MPH resin (which the more isoporous Senbrix resin does not possess), and thus these loading kinetics are depressed (graphs 2A and 3A) compared with the equivalent kinetics of the Senbrix resin (graphs 2B and 3B). These latter two curves are depressed only slightly, due to the reduced diffusivity (and thus mobility) of these successively larger acid molecules. This principle is discussed in more detail in Section 6.3.3.2.

6.4.4.2 Loading Kinetics of Butyric Acid at Different Concentrations

Fig. 6.26 shows the comparison between the loading kinetics of butyric acid on free-base Zerolit MPH and Senbrix resins at 0,05N, 0,025N and 0,0125N initial concentrations.

It shows that, because of the "small pore fraction" effect discussed in Section 6.4.4.1, the Senbrix resin exhibits faster loading kinetics for this large acid molecule, compared with the Zerolit MPH resin. It is clear, also, that the concentration decrease results in almost corresponding decreases in the kinetic rates. (The exceptions to this are the two Zerolit MPH kinetic graphs at 0,05N and 0,025N concentration (graphs 1A and 2A) - the reason for this is

discussed in Section 6.2.3.5.) This phenomenon is consistent with film diffusion theory, and thus, although pore effects do play a role, the diffusion through the Nernst film is the major rate determining step.

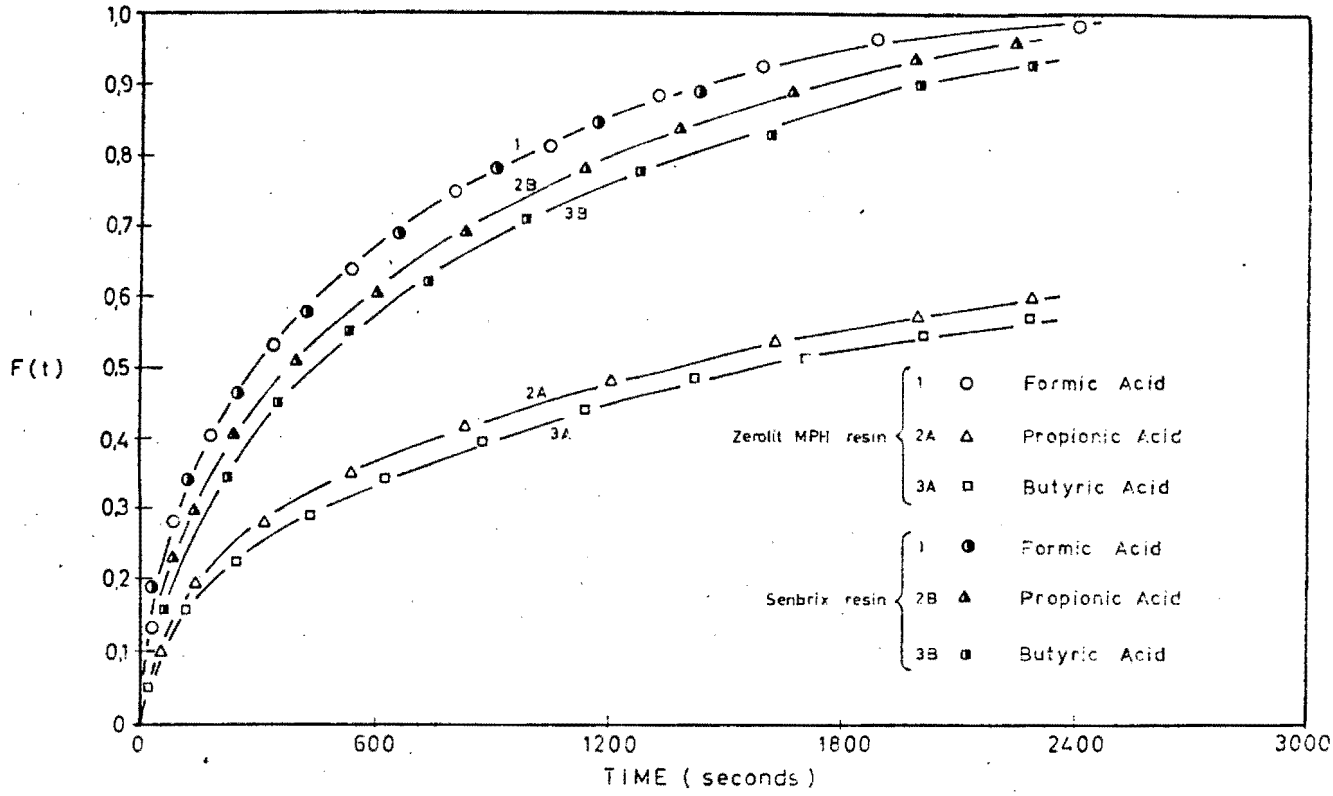

Fig. 6.25: Comparison Between Loading of Monocarboxylic Acids at 0,05N Initial Concentration on Free-base Zerolit MPH and Senbrix Resins

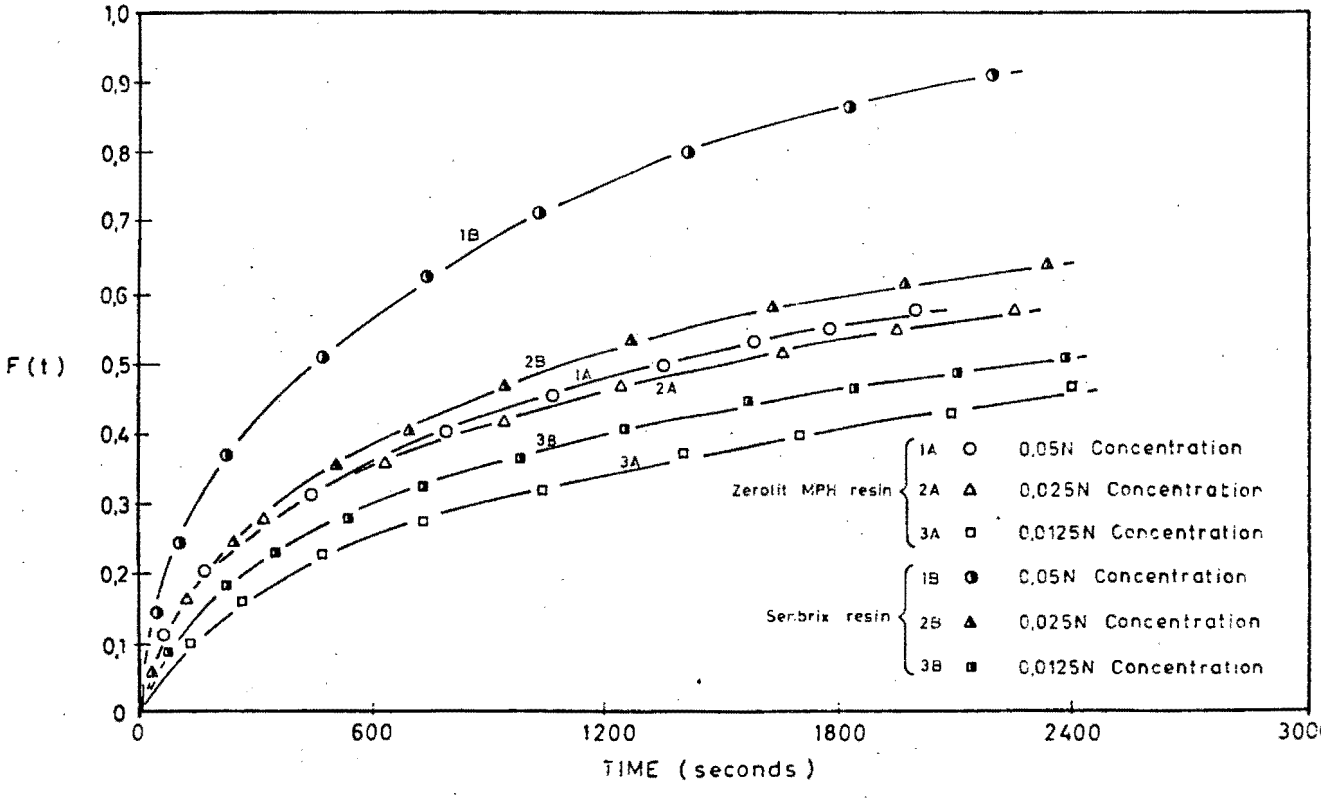

Fig. 6.26: Comparison Between Butyric Acid Loading at Three Different Initial Concentrations on Free-base Zerolit MPH and Senbrix Resins

CHAPTER 7

CONCLUSIONS, RECOMMENDATIONS AND RELEVANCE TO ION EXCHANGE DESIGN

The results of this work determine and compare the equilibrium and kinetic characteristics of two different cation and anion resins.

7.1 EQUILIBRIA

Both the macroporous and gel cation resins displayed a greater selectivity for Ca^{2+} than for Na^{+}, with both gel resin selectivity coefficients at 0,125N concentration marginally smaller than those of the macroporous resin. At 0,50N concentration there is no difference between the two resins' Ca^{2+} equilibria. Thus, within the concentration preference for ions of higher valency, there is a greater selectivity exhibited by the macroporous resin - an effect which increases at lower concentration.

Anion equilibrium studies showed an extreme selectivity for Cl^{-} on free-base forms of both high density and normal density resin.

7.2 KINETICS

7.2.1 Cation Kinetics

The gel resin's kinetics were found to be consistently faster than those of the macroporous resin, but both followed the same trends.

It was found that Ca^{2+} loaded onto the resin faster, and was stripped of the resin slower, than Na^{+}. This can be explained by the fact that all the kinetics are diffusion

controlled, and thus a more mobile ion will be able to diffuse faster than a less mobile one. Ca^{2+}, because of its double change, has a smaller hydrated radius than Na^{+}, and is thus more mobile.

The macroporous resin exhibited more pronounced film-diffusion controlled kinetics than the gel resin whose kinetics were pure pore-diffusion controlled for both 0,125N and 0,50N concentrations. This results in (i) the macroporous resin's kinetics being affected by solution concentration while those of the gel resin are not, and (ii) the loading and regeneration kinetics of the macroporous resin being similar while, for the gel resin, the loading kinetics are significantly faster than the loading kinetics.

Further, it was found that, generally, the most highly crosslinked gel resins exhibited slower kinetics.

In the ternary systems, the Na^{+} is stripped of the resin in preference to the Ca^{2+} which, consistent with the binary kinetic results, loads preferentially. The ionic mobility differences greatly affect the ternary kinetics, resulting in an "overshoot" of the Na^{+} beyond its equilibrium value. It is, however, the Ca^{2+} (being the least mobile ion) that consistently controls the overall kinetics. The same is true for the regeneration kinetics, except that no "overshoot" is observed. The resin type does not affect the final equilibrium value (i.e. the final, ionic fraction of each species), but does affect the time taken to reach this equilibrium. Also, the degree of overshoot is independent of resin type.

7.2.2 Anion Kinetics

The kinetics of both the gel and macroporous resins are dependent on the counter-ion mobility and on the selectivity of the resin for that particular ion. Since anion studies were conducted at low concentrations (0,01N and 0,05N), the kinetics are film-diffusion controlled. This is demonstrated by the Cl^{-} and SO_4^{2-} kinetics, where the concentration affects

REFERENCES

1. KUNIN, R., "Elements of Ion Exchange", R.E. Krieger Publishers, New York, 1971.
2. KITCHENER, J.A., "Ion Exchange Resins", John Wiley, New York, 1961.
3. KUNIN, R., "Ion Exchange Resins", 2nd edition, R.E. Krieger Publishers, 1972.
4. APPLEBAUM, S.B., "Demineralization by Ion Exchange", Academic Press, New York, 1968.
5. MILLAR, J.R., "Fundamentals of Ion Exchange", Chemistry and Industry, 5 May 1973, pp. 409-413.
6. DORFNER, K., "Ion Exchangers: Properties and Applications", ed. Andrée Fé Coers, Ann Arbor Science Publishers, 1972.
7. GODDARD, J.E., "Ion Exchange Processes in Effluent Treatment", The Theory and Practice of Ion Exchange, Proc. International Conference, University of Cambridge, July 1976, Published by Society of Chemical Industry, London.
8. PAULSON, C.F. and MINDLER, A.B., "Use of Ion Exchange in the Waste-Water Field", Chem. Eng. Prog. Symposium Series, Vol. 50, No. 14, 1954, pp. 93-96.
9. GIDDEY, T.B.S., "Ion Exchange in the 1980s in South Africa", Paper presented to the 3rd National Meeting of S.A. Inst. of Chem. Eng., Stellenbosch, April 1980.
10. GREGOR, H.P., "Using Ion Exchange Resins and Membranes", Chem. Eng., Vol. 68, No. 12, December 1961, pp. 73-75.
11. MARTINOLA, F., "Ion Exchangers and Adsorbents - Versatile Aids for the Chemical Industry", German Chemical Engineering, Vol. 3, No. 2, April 1980, pp. 79-88.
12. GRAESER, H.J., "Water Re-use: Resource of the Future", Journal of the American Waterworks Association, Vol. 66, No. 10, October 1974, pp. 575-578.
13. VASSILIOU, B. and DRANOFF, J.S., "The Kinetics of Ion Exclusion", AIChE Journal, Vol. 8, No. 2, May 1972, pp. 248-252.

14. HATTINGH, W.H.J., "Suggestions for Water Research with Regard to Health Aspects of Potable Water", NIWR and IofWPC (SA), Paper presented at "Health Aspects of Water Supply" Symposium, Pretoria, November 1979.

15. FRANZIDIS, J-P., "The Application of the Desal Process to a Typical Cape Town Waste Water", M.Sc. thesis, UCT, 1975.

16. ELIASSEN, R., WYCKOFF, B.M. and TONKIN, C.D., "Ion Exchange for Reclamation of Reusable Supplies", JAWWA, Vol. 57, No. 9, September 1965, pp. 1113-1122.

17. HEUNIS, B., "Regional Planning for Optimum Use and Re-use of Water in the Cape Peninsula", NIWR Report, 1976.

18. GIDDEY, T.B.S., "Report on the Research in the Treatment of Wastewater by Ion Exchange", WRC Contract, Ph.D. thesis, UCT, March 1979.

19. HATTINGH, W.H.J., "Health Aspects of Water Reclamation", Steering Committee for Technical Development Concerning Water Reclamation and Polution Control, NIWR and WRC Report, Vol. 4, September 1976.

20. KUNIN, R., "Two Decades of Macroreticular Ion Exchange Resins", Amber-hi-lites, No. 161, Rohm and Haas Company, 1979.

21. ARNOLD, D.R., "The Development of High Density Ion Exchangers for CIX Processes", Paper presented to the 3rd National Meeting of S.A. Inst. of Chem. Eng., Stellenbosch, April 1980.

22. BOYDEL, D.W., "The Recovery of Uranium from Solution by Continuous Ion Exchange", Paper presented to the 3rd National Meeting of S.A. Inst. of Chem. Eng., Stellenbosch, April 1980.

23. ANON., "Dowex: Ion Exchange", The Dow Chemical Co., Michigan, 1964.

24. GRAN, T., "The Synthesis of Nitrate Selective Resins", Ph.D. thesis, Kansas State University, 1973.

25. HELFFERICH, F., "Ion Exchange", McGraw-Hill, New York, 1962.

26. ANON., "Ion Exchange Resins", BDH Company, 5th edition, 3rd impression.

faster than those of the 12% resin) while the 6,5% DVB resin exhibits significantly faster kinetics.

These results are contrary to what would be expected from pure film-diffusion controlled systems [25]. Since, in such systems, the rate of exchange is controlled exclusively by the diffusion within the Nernst film surrounding the bead, the pore size and percentage swelling (which are affected by the degree of crosslinking) would not affect the exchange kinetics.

Thus it seems from the pattern of results plotted in Fig. 6.17 that these systems are partly pore-diffusion controlled, since the resin with the lowest degree of crosslinking (6,5% DVB) exhibits the fastest kinetics, while the 8% DVB and 12% DVB resins exhibit considerably slower kinetics, with the less crosslinked resin's kinetics marginally faster than those of the resin of higher crosslinking.

The large gap between the 6,5% DVB curve and the 8% DVB curve (graphs 1 and 2) compared with the much smaller gap between the 8% DVB and 12% DVB curves (graphs 2 and 3) suggests that this film-diffusion control effect pertains only to resins of low degree of crosslinking. The reason for this can probably be attributed to resin swelling and resultant pore size distribution.

6.3.2.5 Loading of Cl^- at 0,05N on Preloaded Resin

In order to determine the effect of the preloading of a similar ion on the kinetic rate of Cl^- loading, three runs were performed loading 0,05N HCl on Senbrix resin which was preloaded with approximately 25%, 50% and 75% Cl^-. The resin and liquid quantities used were calculated to give an initial R/L ratio of 0,5, based on the unloaded fraction of the resin (to remain consistent with the previous binary investigations). These quantities are tabulated in Table 6.11.

The resin samples were preloaded with calculated

quantities of 0,5N HCl solution and, before finally reacting them with 800 ml of 0,05N HCl solution, the percent preloading was checked by eluting each sample with 2N NaOH solution and analysing the elutant for Cl^-. These results are also presented in Table 6.11.

TABLE 6.11

DEGREE OF RESIN PRELOADING AND RESIN AND LIQUID QUANTITIES USED FOR SENBRIX PRELOADED RESIN KINETIC STUDIES

Theoretical % Cl^- Preloading	ml of Preloading 0,5N HCl	Actual % Preloading	Initial R/L	ml Resin	ml 0,05N HCl Solution
25	13,3	26	0,5	19,1	800
50	40	48	0,5	28,6	800
75	120	68	0,5	57,1	800

The detailed kinetic results are tabulated in Appendix D, Tables D-18 to D-20, and plotted, together with the straight Cl^- loading F(t) curve, in Fig. 6.18.

6.3.2.6 Discussion of Preloaded Resin Cl^- Loading Kinetics

Fig. 6.18 compares the Cl^- loading F(t) curves of the Senbrix resin with no preloading with the F(t) curves of the resin with 25%, 50% and 75% pre-loading. It is evident from this figure that the kinetics become faster as the degree of preloading increases.

This trend can be explained by the fact that, although all the experiments were performed at the same R/L (attained by varying the resin volume), in each separate case successively smaller fractions of resin were initially loaded at 0,05N concentration. Thus, in the situation where no preloading was present, the entire resin was loaded between

0,05N initial concentration and 0,025N final solution concentration, while, at increasing degrees of preloading successively smaller resin fractions had the benefit of the same concentration difference. Thus, since this is a film controlled system (see Section 6.3.2.2), this effective increase in the concentration driving force results in faster kinetics as the degree of preloading increases. Further, the type of counter-ion initially preloaded onto the resin should have no effect on the kinetics, provided that the resin had an equal (or greater) selectivity for it compared with the loading counter-ion. If this were not the case, the loading counter-ion would tend to replace some of the preloaded ions on the resin sites, resulting in an increase in the solution concentration of this initially preloaded ion. A similar result to the cation ternary loading kinetics would thus be expected in such a system (see Section 5.2.3.4).

6.3.3 COD Kinetics

As for the Zerolit MPH resin COD kinetic studies, the COD kinetics of Senbrix resin were investigated using similar artificial COD materials, namely formic, propionic and butyric acids. In addition, butyric acid loading at three different initial concentrations (0,05N, 0,025N and 0,0125N) as well as the kinetics of butyric acid regeneration at 0,05N were investigated.

6.3.3.1 COD Loading Kinetics

The loading kinetics of the three acids on Senbrix resin in the free-base form at 0,05N initial concentration were investigated. The resin and liquid quantities used in these runs are given in Table 6.12.

The detailed kinetic data are tabulated in Appendix D, Tables D-21 to D-23, and plotted in Fig. 6.19.

TABLE 6.12

RESIN AND LIQUID QUANTITIES FOR SENBRIX COD LOADING KINETIC STUDIES

Loading Acid Type	R/L	ml Resin	ml Acid
Formic	0,5	18,1	800
Propionic	0,5	18,1	800
Butyric	0,5	18,1	800

6.3.3.2 Discussion of Formic, Propionic and Butyric Acid Loading Kinetics at 0,05N

(a) Direct Comparisons:

Fig. 6.19 compares the kinetics of formic, propionic and butyric acid loading onto free-base Senbrix resin at 0,05N initial concentration.

As for the Zerolit MPH kinetics (see Section 6.2.3.3), the larger the organic molecule, the slower the kinetics become. This is again due to the relative diffusivities of the loading species - the larger the hydrated radius of the counter-ion, the slower it will be able to diffuse. Since this is a film-diffusion controlled system, the reduced mobility in the Nernst film surrounding the bead will result in slower loading kinetics. Fig. 6.19 shows this effect. It should also be noted that the percentage increase in molecular size between the three different acids is approximately equal, and this results in a similar reduction in their respective kinetics, indicating that only diffusivity effects are responsible for the change.

(b) Comparisons with Binary Kinetics:

Fig. 6.20 compares the formic acid loading kinetics with those of binary Cl^- and SO_4^{2-} loading.

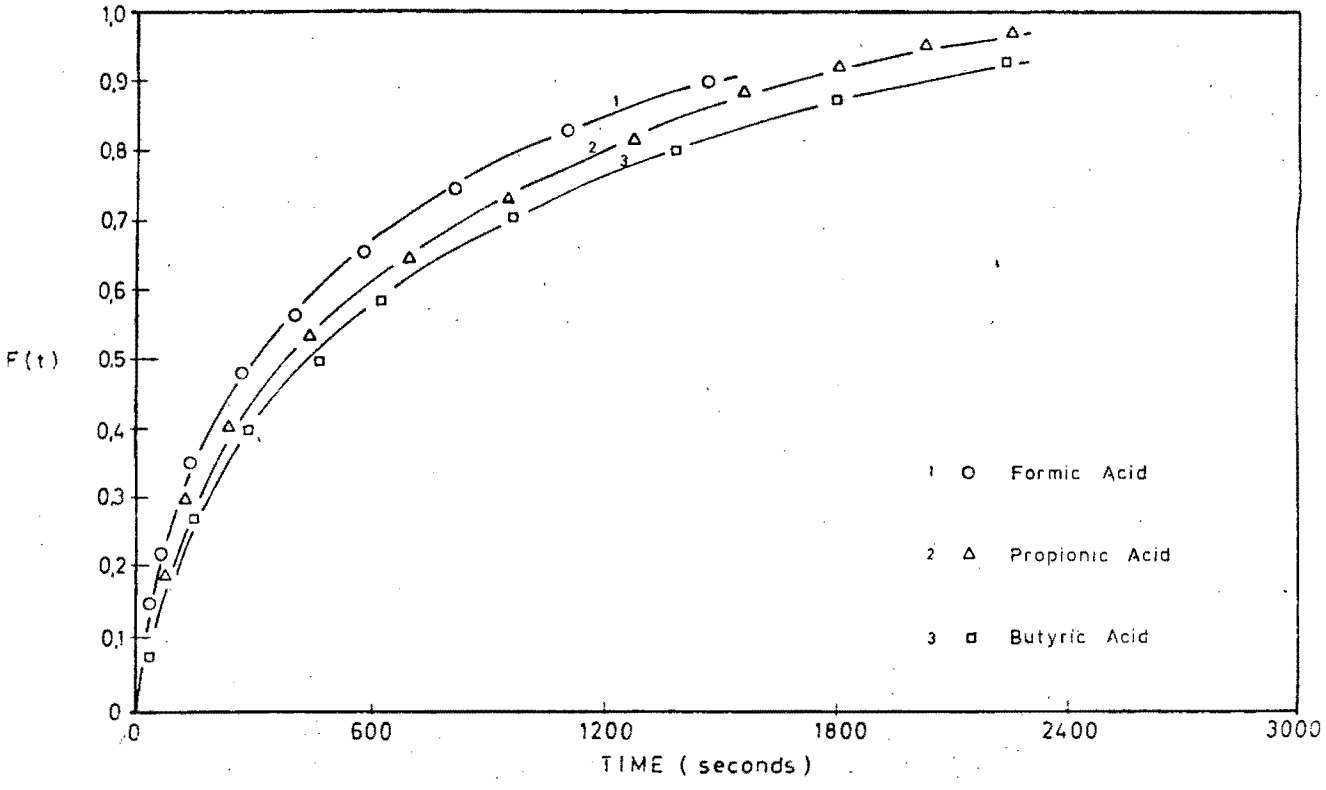

Fig. 6.19: Comparison of Three Different Artificial COD Materials Loaded at 0,05N Initial Concentration on Free-base Senbrix Resin

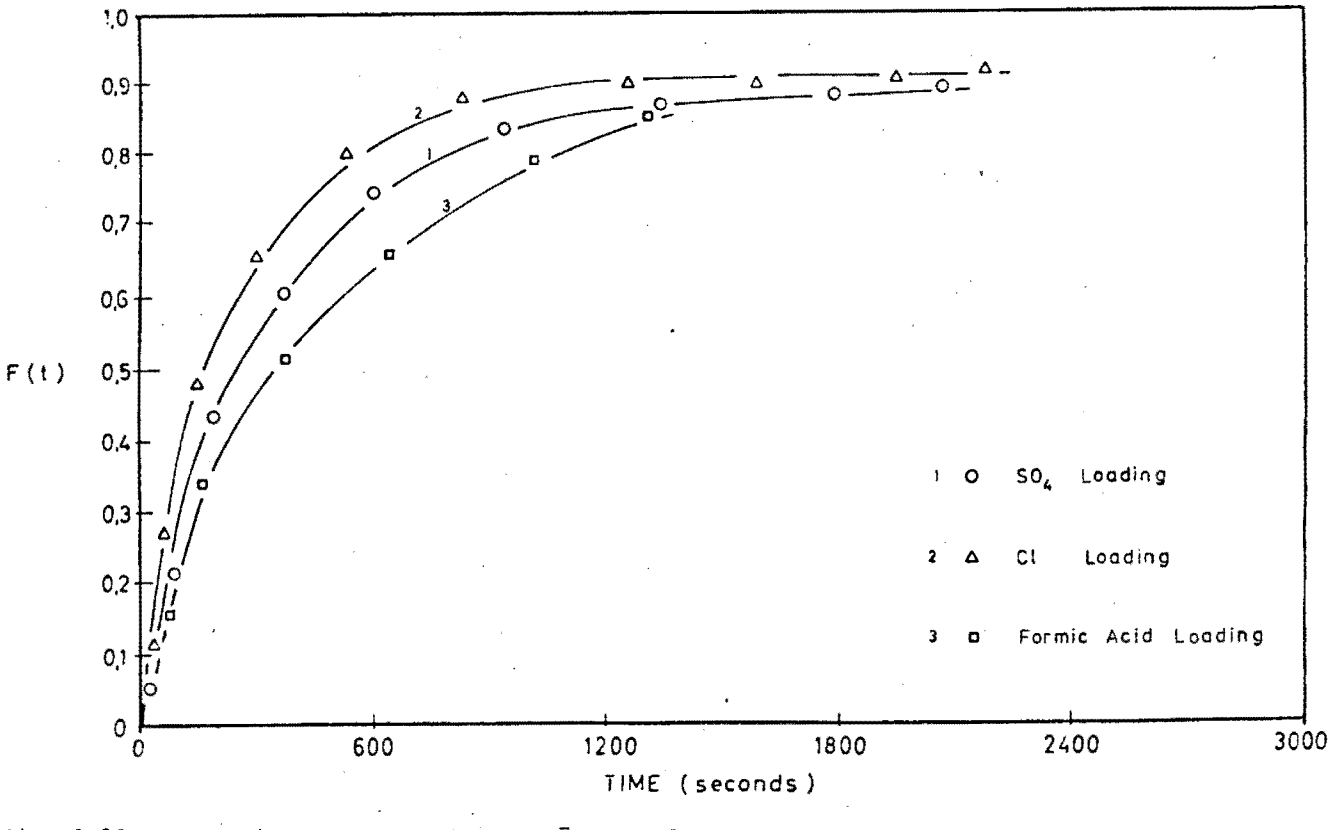

Fig. 6.20: Comparison Between Binary Cl^- and SO_4^{2-} Loading and Formic Acid Loading at 0,05N Initial Concentration on Free-base Senbrix Resin

When comparing these F(t) curves, in addition to mobility effects, selectivity effects should also be considered (see Section 6.2.3.3). As discussed in (a) above, the resin prefers the counter-ion with the highest charge density, and thus both the binary kinetic systems studied exhibit faster kinetics than the formic acid kinetics, even though the SO_4^{2-} counter-ion has a larger molecular weight than the formic acid molecule ($t_{\frac{1}{2}}$ for OH^-/Cl^- exchange = 150 seconds; $t_{\frac{1}{2}}$ for OH^-/SO_4^{2-} exchange = 220 seconds; and $t_{\frac{1}{2}}$ for OH^-/CH_3OH exchange = 300 seconds). The reason for the higher charge density of the Cl^- counter-ion compared with the CH_3OH molecule is that the organic molecule's structure results in a larger hydrated radius compared with the compact Cl^- ion, even though the latter has a larger molecular weight. For the SO_4^{2-} counter-ion this larger weight and size, compared with the acid molecule, is compensated for by the double charge (it is assumed that the acid molecules dissociate as $R - O^- H^+$, and are thus considered as monovalent ions).

6.3.3.3 Butyric Acid Loading at Different Concentrations

Similarly to the Zerolit MPH studies, free-base Senbrix resin was loaded with 0,025N and 0,0125N initial concentration butyric acid solutions in addition to the 0,05N butyric acid loading kinetics investigated in Section 6.3.3.1.

The liquid and resin quantities used in the above studies are given in Table 6.13.

The detailed kinetic data are tabulated in Appendix D, Tables D-24 and D-25, and plotted, together with the 0,05N kinetic results (presented in Section 6.3.3.1) in Fig. 6.21.

6.3.3.4 Discussion of Butyric Acid Loading Results at Different Concentrations

Fig. 6.21 compares the kinetic results of butyric acid loading onto free base form Senbrix resin at 0,05N, 0,025N and 0,0125N initial concentrations.

the kinetics both by a variation of the concentration gradient over the film and of the resin selectivity. Thus, for the macroporous Zerolit MPH resin, the SO_4^{2-} loading kinetics are faster than the corresponding Cl^- loading kinetics at both concentrations. However, for the more isoporous Senbrix resin, the Cl^- loading becomes faster than the SO_4^{2-} at 0,05N concentration. It is therefore necessary to take both concentration and selectivity effects into account for the prediction of film-diffusion controlled kinetics. Further, resins of very low DVB content (6%) were found to exhibit partial pore diffusion effects.

In the artificial COD studies for both resins, the smaller organic molecules loaded the fastest. Thus formic acid loaded faster than propionic acid which, in turn, loaded faster than butyric acid. However, a sudden "drop" in the macroporous resin's COD kinetics was noted between formic acid and propionic acid loading, which was not present in similar studies on the isoporous Senbrix resin. This "drop" was attributed to a hindrance by the "small pore fraction" of the macroporous resin, and thus, as the molecular size increases, a similar drop would be expected for the "large pore fraction" of the macroporous resin, and for the isoporous Senbrix resin. This is reinforced by the fact that the Cl^- and formic acid loading kinetics for the macroporous resin are similar, while, for the isoporous Senbrix resin, the Cl^- kinetics are faster. It was found also that the regeneration of butyric acid is pH dependent, and faster than the equivalent loading kinetics.

Loading runs performed on partially preloaded Senbrix resin showed that the higher the degree of preloading, the faster the kinetics became.

In general, Senbrix resin is superior for organic molecule loading and Cl^- loading at low concentrations, but Zerolit MPH is superior for Cl^- removal at higher concentrations and SO_4^{2-} removal at low concentrations.

7.3 RECOMMENDATIONS FOR FURTHER RESEARCH

More detailed comparisons between different resin types could be obtained by performing equilibrium and kinetic runs on additional counter-ion species. For effluent treatment systems in particular, the cations Mg^{2+} and K^{+} and the anions NO_3^- and PO_4^{2-} could be tested, as well as additional, high molecular weight organic compounds.

Both binary and ternary tests would furnish more detailed information as to the controlling diffusional process involved in these exchanges.

Further, the prediction of actual stage efficiencies in CCIX systems from kinetic and equilibrium data could be investigated. Such correlation data would facilitate the design of CCIX systems. (See Section 7.4 for the effect of resin properties on CIX system design.)

7.4 APPLICATION OF RESIN PROPERTIES TO CIX COLUMN DESIGN

The equilibrium and kinetic resin properties are fundamental to the engineering design of continuous counter-current ion exchange (CCIX) systems. Thus, the stepwise construction between the operating and equilibrium lines is used to determine the number of theoretical stages in a column, and this is then a function of the selectivity or equilibrium relationship. The kinetics are used to determine the efficiency of a stage. Thus the total number of actual stages required is determined by the kinetics of the system.

7.4.1 Equilibrium Effect on the Number of Theoretical Stages

A typical cation wastewater desalination system is taken as an illustrative example of a CCIX design. Fig. 7.1 shows stepwise construction for loading and regeneration of such a system, using two typical equilibrium curves - one of high selectivity (see Fig. 7.1 ① , corresponding to a typical

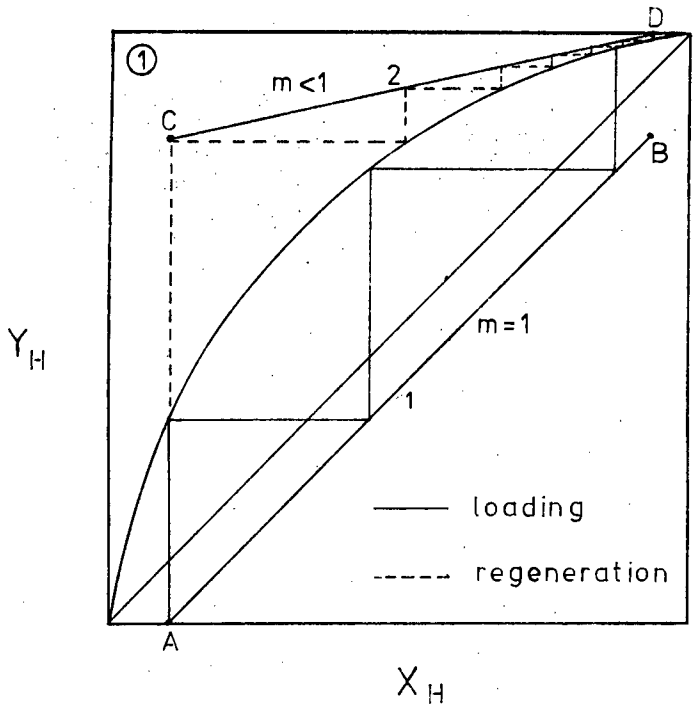

Operating point **A** = bottom of load column.

Operating point **B** = top of load column.

Operating point **C** = bottom of regeneration column.

Operating point **D** = top of regeneration column.

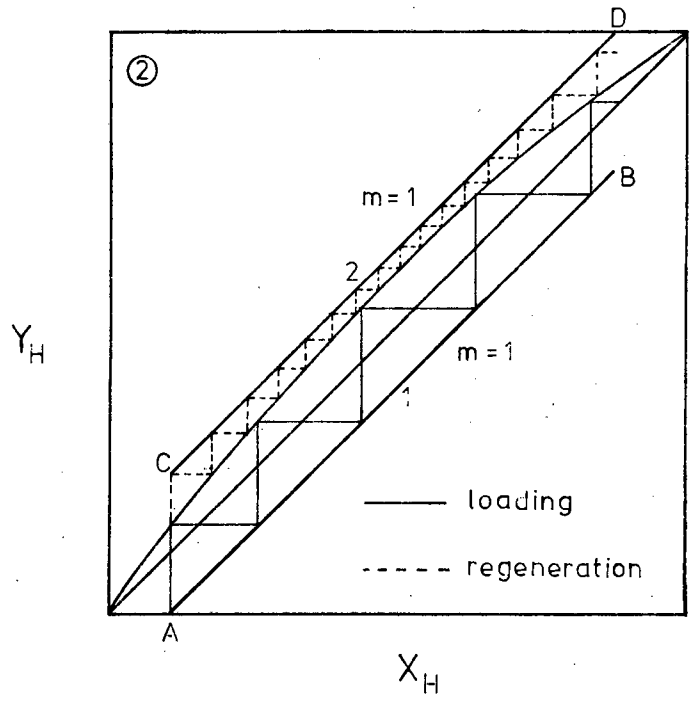

Fig. 7.1: Stepwise Stage Construction for CCIX Column Design

Ca^{2+}/H^{+} equilibrium), and one of low selectivity (see Fig. 7.1 ②, corresponding to a typical Na^{+}/H^{+} equilibrium). By definition, the loading operating line (1) lies below the equilibrium curve, and the regeneration operating line (2) above it.

The slope of the operating line (denoted by the symbol "m") is given by the stoichiometric (resin to liquid) ratio in the column (corresponding to the ratio of vapour to liquid in a distillation column or gas to liquid in an absorption column).

It can be seen from Fig. 7.1 that the resin selectivity (i.e. the distance the equilibrium isotherm lies from the diagonal) affects, firstly, the number of stages required in the loading and regeneration columns, and secondly, the allowable slope of the operating lines. It is usually desirable to have a resin to liquid (in meq/ml) ratio of 1 (or less, if possible) in the regeneration column, so that there is minimal waste of chemicals (which contribute the major running costs to any ion exchange process).

Fig. 7.1 ① depicts stepwise constructions for a typical highly selective equilibrium system (of which Ca^{2+}/H^{+} is an example). It is clear (in this example) that the regeneration column construction is the more sensitive to selectivity change - even a small change in the equilibrium isotherm will result in a large change in the number of regeneration steps, but a relatively small change in the number of loading stages (for the same conversion). Further, whereas a desired slope of 1 is able to be used for the loading operating line (1), a regeneration operating line (2) slope much less than 1 had to be used (with resultant waste of regenerant chemicals) because of a pinch point developing near point "D". If the slope of the regeneration column operating line was reduced still further, fewer stages would be required for the same conversion, but with resultant more chemical waste.

Fig. 7.1 ② depicts the stepwise construction for a much less selective equilibrium system (of which Na^{+}/H^{+} is an example).

In this system, a small change in the selectivity will again have a large effect on the number of regeneration stages required, but will, in addition, have a smaller but significant effect on the number of loading stages. Because of the less selective system, it is possible to use a slope of 1 for both the regeneration and loading operating lines. However, if the selectivity increases by any significant amount, a pinch point will develop where the equilibrium isotherm approaches the regeneration operating line (2). In such a case, the slope of this operating line would have to be reduced in order to achieve the required percent regeneration.

Similar effects are relevant to anion exchange systems.

7.4.2 Kinetic Effect on Stage Performance

Whereas the equilibrium determines the number of theoretical stages (assuming perfect exchange), the kinetics determine the contact time required for a given conversion, and it has been shown [18] that this affects the stage efficiency.

Batch kinetic curves (such as those derived during the course of this project) are equivalent to kinetic behaviour within a single stage. Thus, given the initial conditions similar to those within a stage, the contact time necessary for a given conversion can be determined from the batch test, and, using this value, the stage efficiency can be calculated. Thus the total number of real stages can be determined.

7.4.3 Effect of Other Resin Properties on Column Design

Besides the equilibrium and kinetic properties of resins, capacity, density and diameter are important characteristics which, indirectly, affect column design [21].

An increase in capacity results in longer possible cycle times, reducing the loss of resin by attrition and osmotic shock. An increase in density (such as is evident in the

Senbrix resin) will allow a reduction in the bead size (for the same fluidising velocity), resulting in faster kinetics due to improved surface area, as well as better fluidisation characteristics and higher liquid flow rates.

27. PANSWAS, T., "Ion Exchange Removal of Inorganic and Organic Wastewater Constituents", Ph.D. thesis, University of Colorado, 1975.

28. ANDERSON, R.E., "Contour Map of Anion Exchange Resin Properties", I & EC Research and Development, Vol. 3, No. 2, June 1964, pp. 85-89.

29. KUNIN, R., "Pore Structure of Macroreticular Ion Exchange Resins", Ion Exchange in Process Industries, Proc. of Conference held at Imperial College of Science and Technology, London, 16-18 July 1969, published by Society of Chem. Ind., London, 1970.

30. MIKES, J.A., "Pore Structure in Ion Exchange Materials", Ion Exchange in Process Industries, Proc. of Conference held at Imperial College of Science and Technology, London, 16-18 July 1969, published by Society of Chem. Ind., London, 1970.

31. KUNIN, R., MEITZNER, E. and BORTNICK, N., "Macroreticular Ion Exchange Resins", Analytical Chemistry, Vol. 84, No. 1, January 1962, pp. 305-306.

32. WALL, H.K. and WAKELIN, L.P., "Measurement of Rate of Anion Exchange and the Effect of Organic Fouling", Journal of Applied Chemical Biotechnology, Vol. 21, January 1971, pp. 1-4.

33. LAGOS, A.E. and KITCHENER, J.A., "Diffusion in Polystyrenesulphonic Acid Ion-Exchange Resins", Trans. Far. Soc., Vol. 56, 1960, pp. 1245-1251.

34. KUNIN, R. and MEYERS, R.J., "Ion Exchange Resins", John Wiley, 1950.

35. BAUMAN, W.C. and EICHHORN, J., "Fundamental Properties of Synthetic Cation Exchange Resins", Journal of the American Chemical Society, Vol. 69, No. 11, November 1947, pp. 2830-2836.

36. SMITH, R.P. and WOODBURN, E.T., "Prediction of Multicomponent Ion Exchange Equilibria for the Ternary System SO_4^{2-}, NO_3^-, Cl^- from Data of Binary Systems", AIChE Journal, Vol. 24, No. 4, July 1978, pp. 577-586.

37. COPELAND, J.P., HENDERSON, C.L. and MARCHELLO, J.M., "Influence of Resin Selectivity on Film Diffusion-Controlled Ion Exchange", AIChE Journal, Vol. 13, No. 3, May 1967, pp. 449-452.

38. HERING, B. and BLISS, H., "Diffusion in Ion Exchange Resins", AIChE Journal, Vol. 9, No. 4, July 1963, pp. 495-503.

39. SCHLOGL, R. and HELFFERICH, F., "Comment on the Significance of Diffusion Potentials in Ion Exchange Kinetics", Journal of Chemical Physics, Vol. 26, No. 1, 1957, pp. 5-7.

40. WEATHERLEY, L.R. and TURNER, J.C.R., "Ion Exchange Kinetics - Comparison Between a Macroporous and a Gel Resin", Trans. Inst. Chem. Eng., Vol. 54, No. 2, April 1976, pp. 89-93.

41. SMITH, T.G. and DRANOFF, J.S., "Film Diffusion-Controlled Kinetics in Binary Ion Exchange", I & EC Fund., Vol. 3, No. 3, August 1964, pp. 195-200.

42. REBHUN, M. and MANKA, J., "Classification of Organics in Secondary Effluents", Environmental Science and Technology, Vol. 5, No. 7, July 1971, pp. 606-609.

43. BOYD, G.E. and BUNZL, K., "The Donnan Equilibrium in Cross-linked Polystyrene Cation and Anion Exchangers", Journal of the American Chemical Society, Vol. 89, No. 8, April 1967, pp. 1776-1780.

44. SOLDATOV, V. and HÖGFELDT, E., "On the Properties of Solid and Liquid Ion Exchangers", Ion Exchange and Membranes, Vol. 2, No. 1, 1974.

45. REICHENBERG, D., "Ion-Exchange Selectivity", cited by MARINSKY, J.A., "Ion Exchange - A Series of Advances", Vol. 1, Marcel Dekker Inc., New York, 1966.

46. TOMBALAKIAN, A.S., "The Dependence of Cation Interchange Rate on the Association Constants of the Counterions Within the Ion-Exchange Membrane", The Canadian Journal of Chem. Eng., Vol. 57, No. 12, December 1979, pp. 768-769.

47. DRANOFF, S. and LAPIDUS, L., "Ion Exchange in Ternary Systems", Industrial and Engineering Chemistry, Vol. 53, No. 1, January 1961, pp. 71-76.

48. Zerolit Resin Manual, Permutit Co., Britain. Technical Publication No. 25-6-9.

49. SHARMA, H.D. and SUBRAMANIAN, N., "Determination of Water in Ion Exchange Resins: Anion Exchange Resins", Analytical Chemistry, Vol. 42, No. 11, September 1970, pp. 1287-1290.

50. COPELAND, J.P. and MARCHELLO, J.M., "Film Diffusion-Controlled Ion Exchange with a Selective Resin", Chem. Eng. Sci., Vol. 24, 1969, pp. 1471-1474.

51. PERRY, R.H. and CHILTON, C.H. (eds.), "Chemical Engineers' Handbook", 5th edition, McGraw-Hill, 1969.

52. WEAST, R.C. (ed.), "Handbook of Chemistry and Physics", 57th edition, CRC Press, 1976-1977.

53. MATĚJKA, Z. and ELIÁŠEK, J., "Kinetics of Sorption and Desorption of HCl and Low Molecular Weight Organic Acids by Styrene and Acrylic Weak Base Resins", Water Research, Vol. 14, No. 5, May 1980, pp. 467-470.

54. MANSFIELD, G.H., "The Assessment of Anion Exchange Resin Capacity With Respect to Fouling by Naturally Occurring Organic Metals", The Theory and Practice of Ion Exchange, Proc. International Conference, University of Cambridge, July 1976, Published by Society of Chemical Industry, London.

55. MILIS, E., "The Removal of Organic Waste Matter from Secondary Sewage Effluents by Chemical Coagulation", M.Sc. thesis, UCT, 1977.

56. KUNIN, R., "Organic Contamination of Anion Exchange Resins", Amber-hi-lites, No. 26, Rohm and Haas Company, 1954.

57. STANDER, G.J., "Micro-organic Compounds in the Water Environment and Their Impact on the Quality of Potable Water Supplies", Paper presented at the 26th Convention of the S.A. Chemical Institute, Port Elizabeth, January 1979.

58. VAN STEENDEREN, R.A., "Advances in the Measurement of Total Organic Carbon and Organic Halogens as Parameters for Water Quality Evaluation", NIWR and IofWPC (S.A.), Paper presented at Symposium on "Health Aspects of Water Supplies", Pretoria, November 1979.

59. BELFORT, G., "Pathogenic Viruses in Surface Waters: Do We Need to be Concerned About Them?", Quarterly Report of Ressselaer Polytechnic Institute, Vol. 9, No. 3, September 1979.

60. HART, O.O., "The Placing of the Disinfection Stage in a Reclamation Plant to Reduce Haloform Formation", Water S.A., Vol. 5, No. 4, October 1978, pp.178-179.

61. BUNCH, R.L., BARTH, E.F. and ETTINGER, M.B., "Organic Materials in Secondary Effluent", Journal of the Water Pollution Control Federation, Vol. 33, No. 2, February 1961, pp. 122-126.

62. McCREARY, J.J. and SNOEYKINK, V.L., "Characterisation and Activated Carbon Adsorption of Several Humic Substances", Water Research, Vol. 14, 1980, pp. 151-160.

63. "Standard Methods for the Examination of Water and Wastewater Including Bottom Sediments and Sludges", American Public Health Association et al., 12th edition, 1969.

64. BIEBER, H., STEIDLER, F.E. and SELKE, W.A., "Ion Exchange Rate Mechanism", Chem. Eng. Prog. Symp. Series, Vol. 50, No. 14, 1956, pp. 17-21.

65. ANON., "Analytical Methods for Flame Spectroscopy", Varion Techtron Company, Australia, 1972.

66. VOGEL, A.I., "Quantitative Inorganic Analysis", 3rd edition, Longmans, 1966.

67. "Handbook for Analytical Quality Control in Water and Wastewater Laboratories", for the U.S. Environmental Protection Agency, Technology Transfer, by Analytical Quality Control Laboratory, Ohio, 1972.

68. ANON., "Varian Techtron Models 1100 and 1200 Atomic Absorption Spectrophotometers Manual", Varian Techtron Company, Australia, 1972.

69. PARKER, C.R., "Water Analysis by Atomic Absorption Spectroscopy", Varian Techtron (Pty) Ltd., Australia, 1972.

70. "Analytical Guide Part 2 - Theoretical Aspects and Analytical Methods", CSIR, NIWR, 1974.

71. "Manual of Methods for Chemical Analysis of Water and Wastes", for U.S. Environmental Protection Agency, Technology Transfer, 1972.

APPENDICES

APPENDIX A : Apparatus.

APPENDIX B : Detailed Equilibrium Results.

APPENDIX C : Detailed Cation Kinetic Results.

APPENDIX D : Detailed Anion Kinetic Results.

APPENDIX E : Analytical Methods.

APPENDIX A

DETAILS OF APPARATUS

APPENDIX A

DETAILS OF APPARATUS

A.1 INTRODUCTION

A general description and photographs of the equipment are given in Chapter 3. In Section A.2 the timer unit is discussed in greater detail. A circuit diagram of the timer (Fig. A-1) and a scale drawing of the 3-way valve, sample tray and rotation system (Fig. A-2) are included in this Appendix.

A.2 THE MULTIPLE TIMER

The function of the multiple timer is to accurately set, and initiate, the sequences required for sampling on the fractional sampling apparatus. Since the comparative kinetic curves were drawn from the data obtained from the sampler, consistently accurate timing was required.

The timer requires a stabilised 12V DC input and has the capacity of variable, accurately set timing through the variable resistor R_1 (see Fig. A-1). This feature is necessary, since both anion and cation systems were studied on the device, the former requiring sampling at 5 or 10 second intervals, the latter at 30 or 60 second intervals. For the cation systems, an internal initial signal of one second frequency was required and obtained using a 100 KΩ set - point resistor trimmed to approximately 1% accuracy. For the anion systems, a 1 mΩ resistor was used, trimmed to produce a 6 second internal initial signal frequency (see Fig. A-3).

The total circuit consists of five integrated circuits (IC) chips (see Fig. A-1). IC1 produces the initial internal signal of the frequencies discussed earlier.

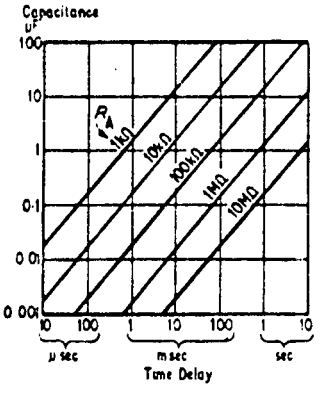

Fig. A-3: Values of Resistor R_1 Required to Give Various Time Delays.

IC2 divides this initial signal by a factor of either 5 or 10 (set by switch S2). The output of this IC triggers a short pulsed signal from IC3. This is amplified by transistor T1 and used to activate the tray rotation solenoid. The rotation solenoid may be continuously activated by means of S1, during which time the tray may easily be rotated to any position. IC4, triggered from the output of IC3, allows a time delay of approximately two seconds for the tray to rotate and a new sample cup to move into position. IC5 is activated at the end of the IC4 delay, and produces a 3 second signal, amplified through T3, which drives the 3-way valve solenoid allowing a sample to be taken. The cycle is then repeated. This entire sequence is best illustrated diagrammatically, as is shown in Fig. A-4.

Two LED's are displayed (see Fig. A-2). LED1 indicates the start of a sequence, i.e. the rotation of the tray to a new position. LED2 indicates when a sample is being taken. In addition, facilities are available for a solenoid activated recycle stream (in the sampler used, the recycle stream was activated by a spring), as well as a 12V DC motor for rotating the tray.

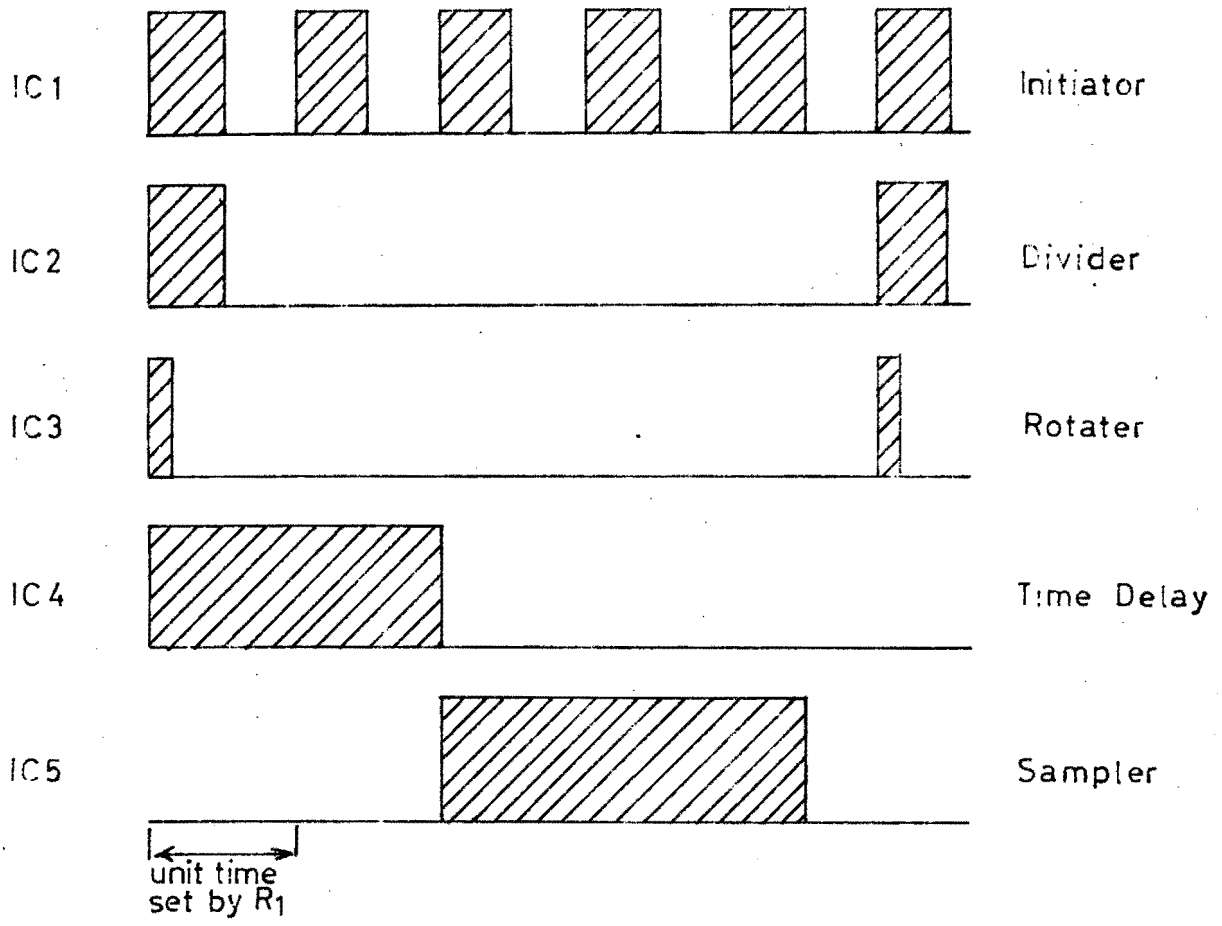

Fig. A-4: Diagrammatic Representation of Multiple Sampler Timing Sequences.

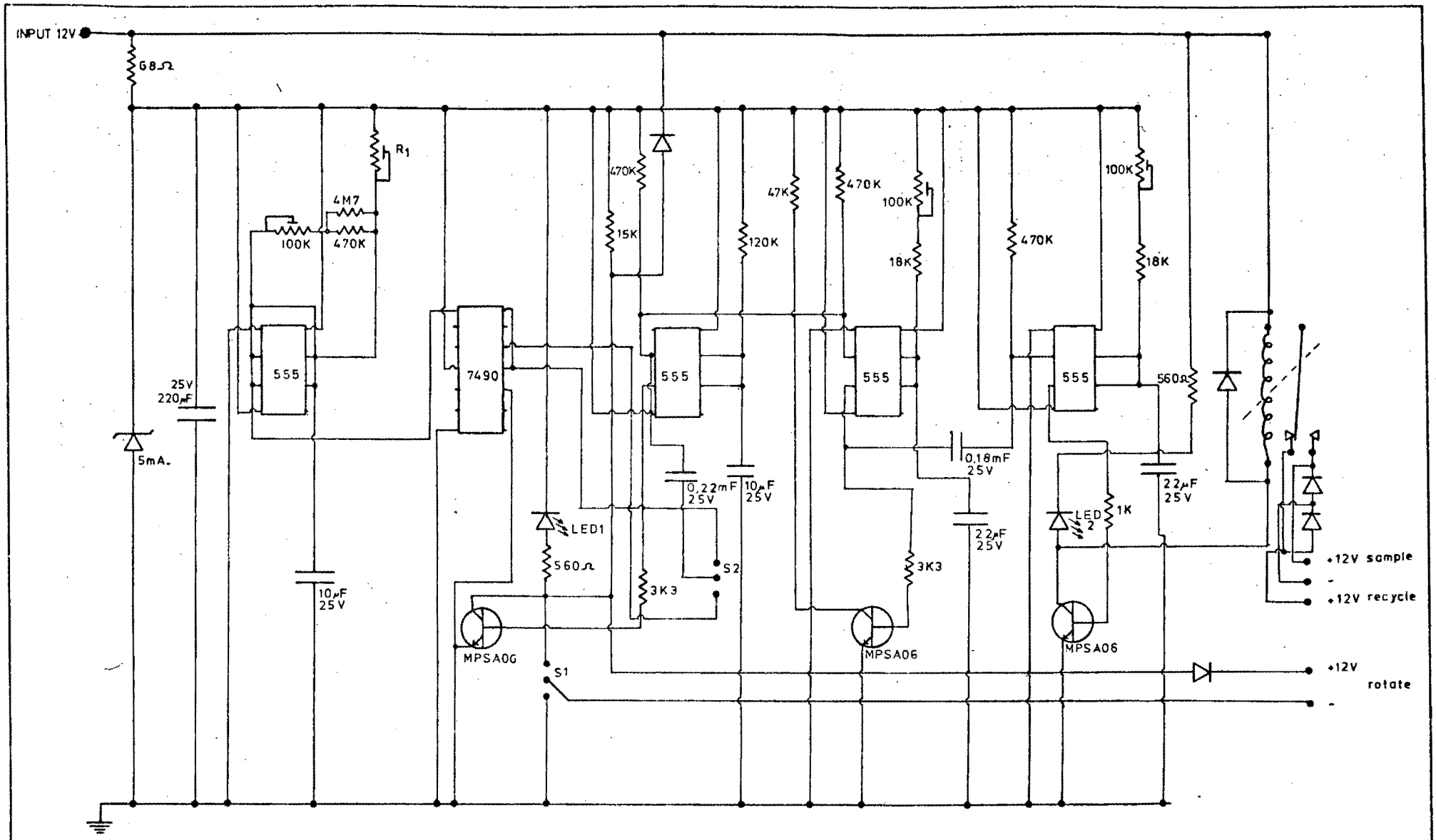

Not to Scale

FIG. A-1: FRACTIONAL SAMPLER TIMER CIRCUIT DIAGRAM

A4

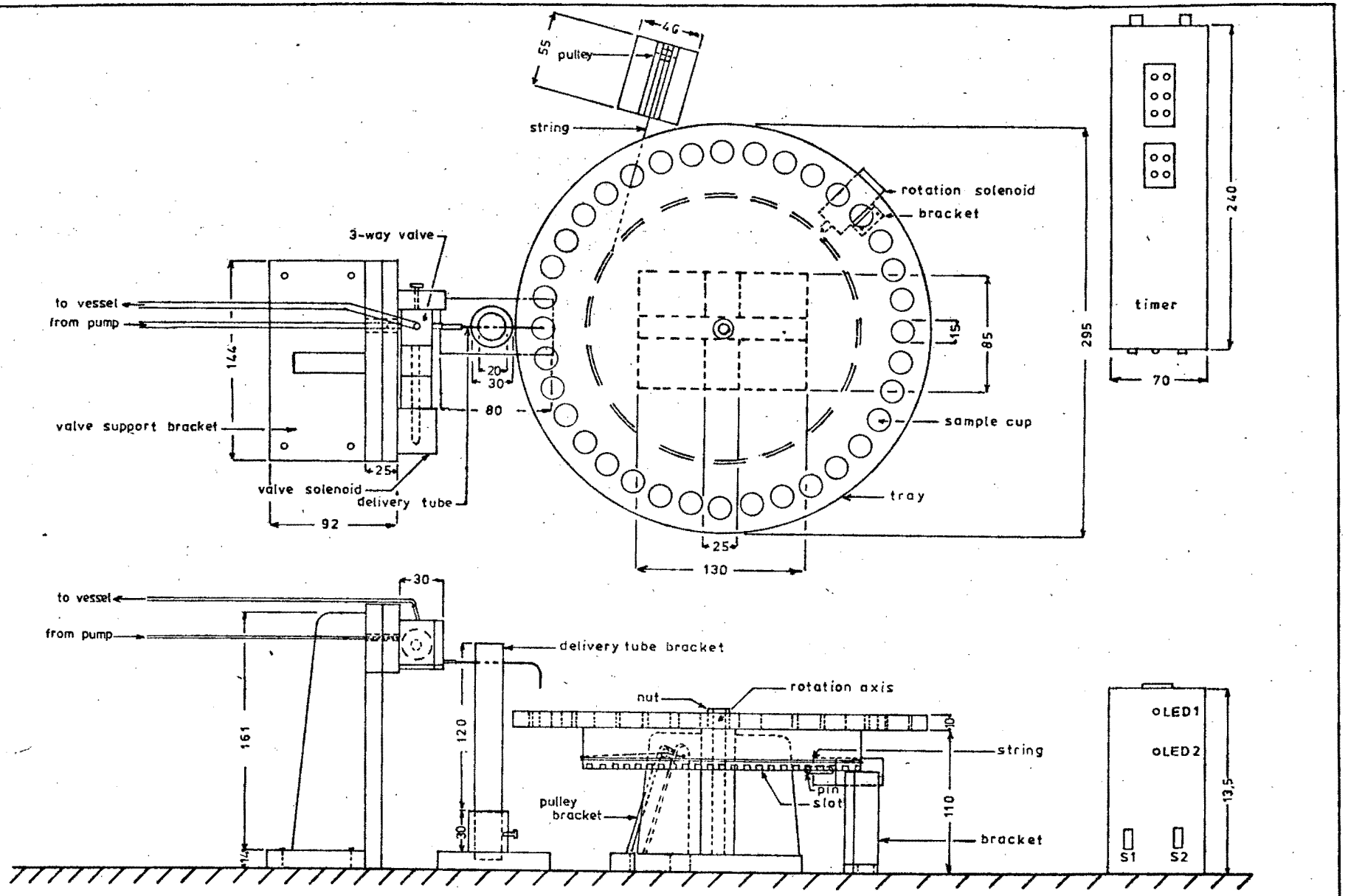

Scale: 3:100

FIG. A-2 : FRACTIONAL SAMPLING APPARATUS

TABLE B-1

RESULTS OF Na^+/H^+ EQUILIBRIUM AT 0,125N ON ZEROLIT 625

Liquid		Resin		y_H	y_{Na}	x_H	x_{Na}	$\alpha_{H^+}^{Na^+}$	$\alpha_{H^+}^{Na^+}$ Average
H^+ (meq)	Na^+ (meq)	H^+ (meq)	Na^+ (meq)						
28	91,57	16	83,30	0,23	0,77	0,16	0,84	1,57	1,64
37	87,43	21	83,30	0,30	0,70	0,20	0,80	1,71	
24	91,65	19	86,74	0,21	0,79	0,18	0,82	1,21	1,38
24	95,78	14	85,22	0,20	0,80	0,14	0,86	1,54	
74	32,65	52	47,17	0,68	0,32	0,52	0,48	1,96	1,89
74	32,65	51	44,13	0,68	0,32	0,54	0,46	1,81	
48	75,39	26	73,04	0,39	0,61	0,26	0,74	1,82	1,70
47	77,39	24	60,87	0,38	0,62	0,28	0,72	1,58	

$\alpha_{H^+}^{Na^+}{}_{ave.} = 1,65$

TABLE B-2

INITIAL RESULTS FOR Na^+/H^+ EQUILIBRIUM AT 0,5ON

y_H	x_H	$\alpha_{H^+}^{Na^+}$
0,20	0,18	1,14
0.50	0,40	1,50
0,80	0,70	1,71

$$\alpha_{H^+}^{Na^+}{}_{ave.} = 1,45$$

TABLE B-3

RESIN AND LIQUID QUANTITIES FOR Na^+/H^+ EQUILIBRIUM AT 0,5ON

$y_{H_{theor.}}$	ml Resin	ml 0,5ON HCl	ml 0,5O NaCl
0,25	14,65	100	266
0,50	14,65	200	153
0,80	14,65	300	28

TABLE B-4

RESULTS OF Na^+/H^+ EQUILIBRIUM AT 0,5ON ON ZEROLIT 625

Liquid		Resin		y_H	y_{Na}	x_H	x_{Na}	$\alpha_{H^+}^{Na^+}$	$\alpha_{H^+}^{Na^+}$ Average
H^+ (meq)	Na^+ (meq)	H^+ (meq)	Na^+ (meq)						
111	376,9	17	84,46	0,23	0,77	0,17	0,83	1,46	1,51
112	376,9	16	87,50	0,23	0,77	0,16	0,84	1,57	
242	248,9	36	64,00	0,49	0,51	0,36	0,67	1,79	1,79
244	239,3	36	64,01	0,50	0,50	0,36	0,67	1,79	
300	98,5	59	40,33	0,75	0,20	0,59	0,41	2,09	2,09
305	98,5	59	40,33	0,75	0,20	0,59	0,41	2,09	

$\alpha_{H^+}^{Na^+}{}_{ave.} = 1,80$

TABLE B-5

INITIAL EQUILIBRIUM DATA POINTS FOR Ca^{2+}/H^{+} SYSTEMS AT 0,125N AND 0,50N CONCENTRATIONS ON ZEROLIT 625

Concentration (N)	y_H	x_H	$\alpha_{H^+}^{Ca^{2+}}$
0,125	0,23	0,009	32
0,125	0,47	0,02	43
0,125	0,69	0,11	19
			$\alpha_{H^+}^{Ca^{2+}}$ ave. = 31
0,50	0,25	0,06	5,2
0,50	0,40	0,12	4,9
0,50	0,60	0,20	6,0
0,50	0,90	0,49	9,4
			$\alpha_{H^+}^{Ca^{2+}}$ ave. = 6,4

TABLE B-6

RESIN AND LIQUID QUANTITIES FOR Ca^{2+}/H^{+} SYSTEM AT 0,125N AND 0,50N CONCENTRATIONS ON ZEROLIT 625

Concentration (N)	$y_{H_{theor.}}$	ml resin (Ca^{2+} form)	ml HCl	ml NaCl
0,125	0,2	14,65	200	395
0,125	0,5	14,65	200	96
0,125	0,85	14,65	500	8,6
0,50	0,30	14,65	20	250
0,50	0,75	14,65	150	31,1
0,50	0,90	14,65	200	118

TABLE B-7

RESULTS OF Ca^{2+}/H^{+} EQUILIBRIUM AT 0,125N ON ZEROLIT 625

Liquid		Resin		y_H	y_{Ca}	x_H	x_{Ca}	$\alpha_{H^+}^{Ca^{2+}}$	$\alpha_{H^+}^{Ca^{2+}}$ Average
H^+ (meq)	Ca^{2+} (meq)	H^+ (meq)	Ca^{2+} (meq)						
25	89	10	99	0,22	0,78	0,01	0,99	28	27
23	87	1,1	109	0,21	0,79	0,01	0,99	26	
63	60	5,0	106	0,51	0,49	0,045	0,955	22	21,5
60	60	4,8	99	0,50	0,50	0,046	0,954	21	
89	17	21	79	0,84	0,16	0,21	0,79	20	20,5
91	16	19	72	0,85	0,15	0,21	0,79	21	

$$\alpha_{H^+}^{Ca^{2+}}{}_{ave.} = 23$$

TABLE B-8

RESULTS OF Ca^{2+}/H^{+} EQUILIBRIUM AT 0,5ON ON ZEROLIT 625

Liquid		Resin		y_H	y_{Ca}	x_H	x_{Ca}	$\alpha_{H^+}^{Ca^{2+}}$	$\alpha_{H^+}^{Ca^{2+}}$ Average
H^+ (meq)	Ca^{2+} (meq)	H^+ (meq)	Ca^{2+} (meq)						
140	347	3,5	80,7	0,32	0,68	0,04	0,96	11,3	11,12
140	346	3,5	82,9	0,31	0,68	0,04	0,96	10,9	
370	118	26	90	0,76	0,24	0,22	0,78	11,2	11,2
355	110	27	92	0,76	0,23	0,22	0,78	11,2	
430	48	50	66,6	0,90	0,10	0,43	0,57	11,9	12,1
440	46	51	62	0,91	0,09	0,45	0,55	12,3	

$\alpha_{H^+}^{Ca^{2+}}{}_{ave.} = 11,4$

TABLE B-9

RESIN AND LIQUID QUANTITIES FOR Na^+/H^+ SYSTEM AT 0,125N AND 0,50N CONCENTRATIONS ON GEL RESIN

Concentration (N)	$y_{H_{theor.}}$	ml resin (Na^+ form)	ml HCl	ml NaCl
0,125	0,2	14,65	50	102,4
0,125	0,4	14,65	100	39,0
0,125	0,6	14,65	200	9,1
0,125	0,8	14,65	700	24,0
0,125	0,95	14,65	1000	17,2
0,50	0,2	14,65	50	175,4
0,50	0,4	14,65	100	120,2
0,50	0,6	14,65	200	99,9
0,50	0,8	14,65	300	34,5
0,50	0,95	14,65	1000	6,9

TABLE B-10

RESULTS OF Na^+/H^+ EQUILIBRIUM AT 0,125N ON GEL RESIN

Liquid		Resin		y_H	y_{Na}	x_H	x_{Na}	$\alpha_{H^+}^{Na^+}$
H^+ (meq)	Na^+ (meq)	H^+ (meq)	Na^+ (meq)					
21	110	15,5	73,3	0,16	0,84	0,17	0,83	0,93
39	87	27,7	61,1	0,32	0,68	0,31	0,69	1,05
53	43	48,1	40,7	0,53	0,47	0,55	0,45	0,92
80	28	66,0	22,8	0,77	0,23	0,74	0,28	1,27
87	22	70,6	18,2	0,84	0,16	0,80	0,20	1,31

$$\alpha_{H^+}^{Na^+}{}_{ave.} = 1,10$$

TABLE B-11

RESULTS OF Na^+/H^+ EQUILIBRIUM AT 0,5ON ON GEL RESIN

Liquid		Resin		y_H	y_{Na}	x_H	x_{Na}	$\alpha_{H^+}^{Na^+}$	$\alpha_{H^+}^{Na^+}$ Average
H^+ (meq)	Na^+ (meq)	H^+ (meq)	Na^+ (meq)						
88,5	370	20,2	75,3	0,19	0,81	0,21	0,79	0,88	0,91
89,1	370	20,0	75,4	0,19	0,81	0,20	0,80	0,93	
183	289	36,8	58,7	0,39	0,61	0,38	0,52	0,88	0,88
182	291	36,5	59,0	0,38	0,62	0,37	0,53	0,88	
282	201	53,4	42,0	0,58	0,42	0,56	0,44	1,09	1,09
280	200	53,7	42,2	0,58	0,42	0,56	0,44	1,09	
385	101	71,6	23,9	0,79	0,21	0,75	0,35	1,75	1,72
379	101	72,9	22,6	0,79	0,21	0,76	0,34	1,69	
464	24,7	89,0	6,52	0,949	0,051	0,93	0,07	1,41	1,41
465	24,7	89,0	6,52	0,949	0,051	0,93	0,07	1,41	

$\alpha_{H^+}^{Na^+}$ ave. = 1,20

TABLE B-12

RESIN AND LIQUID QUANTITIES FOR Ca^{2+}/H^{+} SYSTEM AT 0,125N AND 0,50N CONCENTRATIONS ON GEL RESIN

Concentration (N)	$y_{H_{theor.}}$	ml resin (Ca^{2+} form)	ml HCl	ml NaCl
0,125	0,20	14,65	50	179,0
0,125	0,40	14,65	50	31,0
0,125	0,60	14,65	100	28,1
0,125	0,80	14,65	400	33,4
0,125	0,90	14,65	1000	22,3
0,50	0,20	14,65	50	173,7
0,50	0,40	14,65	100	120,2
0,50	0,60	14,65	200	99,0
0,50	0,80	14,65	300	34,4
0,50	0,95	14,65	1000	6,9

TABLE B-13

RESULTS OF Ca^{2+}/H^{+} EQUILIBRIUM AT 0,0125N ON GEL RESIN

Liquid		Resin		y_H	y_{Ca}	x_H	x_{Ca}	$\alpha_{H^+}^{Ca^+}$
H^+ (meq)	Ca^+ (meq)	H^+ (meq)	Ca^+ (meq)					
26,3	71	7,3	82,5	0,27	0,73	0,08	0,92	4,3
46,4	57	7,8	81	0,45	0,55	0,09	0,91	8,3
76,9	42	10,3	78,5	0,65	0,35	0,12	0,88	13,6
92	13,5	21,9	66,9	0,86	0,14	0,25	0,75	18,4
103	9,64	32,2	58,6	0,92	0,09	0,35	0,65	18,7

$$\alpha_{H^+}^{Ca^{2+}}{}_{ave.} = 13$$

TABLE B-14

RESULTS OF THE Ca^{2+}/H^{+} EQUILIBRIUM AT 0,5ON ON GEL RESIN

Liquid		Resin		y_H	y_{Ca}	x_H	x_{Ca}	$\alpha_{H^+}^{Ca^{2+}}$	$\alpha_{H^+}^{Ca^{2+}}$ Average
H^+ (meq)	Ca^{2+} (meq)	H^+ (meq)	Ca^{2+} (meq)						
121	324	2,6	86,5	0,24	0,76	0,03	0,97	10,2	13,3
100	296	2,0	87,1	0,25	0,75	0,02	0,98	16,3	
209	239	9,9	79,2	0,47	0,53	0,11	0,89	7,2	7,8
218	240	8,7	80,4	0,48	0,52	0,10	0,90	8,3	
313	95	20,2	68,9	0,77	0,23	0,23	0,77	11,2	13,3
319	95	15,9	73,2	0,77	0,23	0,18	0,82	15,3	
419	72	32,3	56,8	0,85	0,15	0,36	0,64	10,1	10,1
440	76	32,9	56,2	0,85	0,15	0,36	0,64	10,1	
479	19,2	57,95	31,15	0,96	0,04	0,65	0,35	12,9	12,1
494	20,1	61,3	27,85	0,96	0,04	0,68	0,32	11,3	

$\alpha_{H^+}^{Ca^{2+}}$ ave. = 11,3

TABLE B-15

RESIN AND LIQUID QUANTITIES FOR OH^-/Cl^- SYSTEM AT 0,05N ON ZEROLIT MPH

Y_{OH^-} theor.	ml resin (OH^- form)	ml 0,05N NaOH	ml 0,05N HCl
0,994	14,65	166	116
0,990	14,65	356	348
0,70	14,65	212	500
0,50	14,65	90,0	500
0,20	14,65	22,5	500

TABLE B-16

RESULTS OF OH^-/Cl^- EQUILIBRIUM AT 0,05N ON ZEROLIT MPH

Liquid		Resin		Y_{OH}	Y_{Cl}	x_{OH}	x_{Cl}	$\alpha^{Cl^-}_{OH^-}$
OH^- (meq)	Cl^- (meq)	OH^- (meq)	Cl^- (meq)					
49,7	0,30	7,2	2,8	0,994	0,006	0,72	0,28	64
49,5	0,50	2,4	12,6	0,990	0,010	0,16	0,84	520
35,6	15,2	0,04	19,46	0,70	0,30	0,002	0,998	1160
24,8	25,2	0,02	23,08	0,50	0,50	0,001	0,999	100
11	39,9	0,03	29,4	0,20	0,80	0,001	0,999	250

$$\alpha^{Cl^-}_{OH^-}{}_{ave.} = 420$$

APPENDIX C

DETAILED CATION KINETIC RESULTS

TABLE C-1

RESULTS OF REGENERATION AT 0,125N AND 0,50N OF Na^+ FORM ZEROLIT 625

Time (secs)	$C_{Na_1}(t)$ (ppm)	$C_{Na_2}(t)$ (ppm)	$F_{Na_1}(t)$	$F_{Na_2}(t)$	Time (secs)	$C_{Na_1}(t)$ (ppm)	$C_{Na_2}(t)$ (ppm)	$F_{Na_1}(t)$	$F_{Na_2}(t)$
0	13,8	30	0,016	0,010	80	652	2480	0,758	0,821
5	64	257	0,074	0,085	90	676	2547	0,786	0,843
10	152	710	0,177	0,235	100	691	2613	0,803	0,865
15	232	967	0,270	0,320	110	726	2658	0,844	0,880
20	298	1365	0,347	0,452	120	730	2725	0,849	0,902
25	349	1538	0,406	0,509	130	770	2749	0,895	0,910
30	392	1722	0,456	0,570	140	770	2764	0,895	0,915
35	435	1813	0,506	0,600	150	750	2810	0,872	0,930
40	478	1933	0,556	0,640	160	799	-	0,929	-
45	521	2063	0,606	0,683	170	-	2816	-	0,932
50	550	2145	0,640	0,710	180	804	-	0,935	-
55	574	2220	0,667	0,735	190	-	2858	-	0,946
60	579	2296	0,673	0,760	200	819	-	0,952	-
65	603	2341	0,701	0,775	210	-	2900	-	0,960
70	618	2371	0,719	0,785	280	829	2912	0,964	0,963

Subscripts : 1 indicates 0,125N concentration
2 indicates 0,50N concentration

$C_{Na_{1_0}}$ = 0,0 ppm $\quad C_{Na_{2_0}}$ = 0,0 ppm

$C_{Na_{1_\infty}}$ = 860 ppm $\quad C_{Na_{2_\infty}}$ = 3021 ppm

TABLE C-2

RESULTS OF REGENERATION AT 0,125N AND 0,50N OF Ca^{2+} FORM ZEROLIT 625

Time (secs)	$C_{Ca_1}(t)$ (ppm)	$C_{Ca_2}(t)$ (ppm)	$F_{Ca_1}(t)$	$F_{Ca_2}(t)$	Time (secs)	$C_{Ca_1}(t)$ (ppm)	$C_{Ca_2}(t)$ (ppm)	$F_{Ca_1}(t)$	$F_{Ca_2}(t)$
0	8,6	7,2	0,031	0,029	80	177	867	0,646	0,735
5	24,1	122	0,088	0,103	90	193	887	0,704	0,752
10	43	248	0,157	0,210	100	199	877	0,726	0,743
15	67	387	0,245	0,328	110	209	945	0,763	0,801
20	78	419	0,285	0,355	120	213	964	0,777	0,817
25	97	523	0,354	0,443	130	224	985	0,818	0,835
30	112	585	0,409	0,496	140	228	996	0,832	0,844
35	117	625	0,427	0,530	150	237	1005	0,865	0,852
40	-	-	-	-	160	234	1021	0,854	0,865
45	140	697	0,511	0,591	170	237	-	0,865	-
50	144	732	0,526	0,620	180	-	1038	-	0,880
55	154	759	0,562	0,643	190	246	-	0,898	-
60	161	779	0,588	0,660	200	-	1074	-	0,910
65	165	802	0,602	0,680	210	252	-	0,970	-
70	193	822	0,704	0,698	280	261	1151	0,973	0,975

Subscripts : 1 indicates 0,125N concentration
2 indicates 0,50N concentration

$C_{Ca_{1_o}}$ = 0,0 ppm $\quad C_{Ca_{2_o}}$ = 0,0 ppm

$C_{Ca_{1_\infty}}$ = 270 ppm $\quad C_{Ca_{2_\infty}}$ = 1180 ppm

TABLE C-3

RESULTS OF Na^+ AND Ca^{2+} LOADING AT 0,125N ON H^+ FORM OF ZEROLIT 625

Time (secs)	$C_{Na}(t)$ (ppm)	$C_{Ca}(t)$ (ppm)	$F_{Na}(t)$	$F_{Ca}(t)$	Time (secs)	$C_{Na}(t)$ (ppm)	$C_{Ca}(t)$ (ppm)	$F_{Na}(t)$	$F_{Ca}(t)$
0	2838	2723	0,000	0,000	80	2025	1715	0,783	0,728
5	2753	2720	0,081	0,010	90	1998	1700	0,814	0,739
10	2705	2505	0,120	0,158	100	1977	1724	0,829	0,722
15	2518	2478	0,313	0,173	110	1937	1705	0,868	0,737
20	2467	2267	0,345	0,329	120	1913	1654	0,891	0,772
25	2445	2215	0,377	0,357	130	1897	1640	0,907	0,783
30	2369	2159	0,448	0,407	140	1881	1589	0,922	0,819
35	2320	2139	0,503	0,425	150	1891	-	0,912	-
40	2289	2039	0,535	0,494	160	1881	-	0,922	-
45	2214	2014	0,605	0,512	170	1873	1576	0,930	0,829
50	2180	1940	0,628	0,568	180	-	-	-	-
55	2158	1989	0,659	0,530	190	1864	1539	0,939	0,855
60	2129	1891	0,683	0,601	200	-	-	-	-
65	2049	1862	0,760	0,622	210	1825	1490	0,976	0,891
70	2073	1833	0,737	0,643	280	1820	1419	0,981	0,940

C_{Na_o} = 2838 ppm C_{Ca_o} = 2723 ppm

C_{Na_∞} = 1800 ppm C_{Ca_∞} = 1339 ppm

TABLE C-5

RESULTS OF REGENERATION AT 0,125N OF 25% Na^+/75% Ca^{2+} PRELOADED ZEROLIT 625

Time (secs)	C(t)			F"(t)			F(t)		
	Na^+ (ppm)	Ca^{2+} (ppm)	H^+ (ppm)	Na^+	Ca^{2+}	H^+	Na^+	Ca^{2+}	H^+
0	53	3,8	122,5	0,02	0,000	0,98	0,12	0,05	0,11
10	123	22	119,0	0,04	0,010	0,95	0,28	0,28	0,27
20	176	32	116,0	0,06	0,013	0,93	0,41	0,41	0,40
30	218	41	113,0	0,08	0,016	0,90	0,50	0,53	0,53
40	241	45	112,0	0,08	0,018	0,89	0,55	0,58	0,58
50	267	52	111,0	0,09	0,021	0,89	0,61	0,67	0,62
70	289	61	109,4	0,10	0,024	0,87	0,67	0,78	0,71
90	309	68	108,2	0,11	0,028	0,86	0,71	0,91	0,78
110	326	71	107,3	0,11	0,028	0,86	0,75	0,91	0,78
130	360	76	105,6	0,13	0,030	0,85	0,83	0,97	0,86
150	363	76	105,4	0,13	0,030	0,84	0,84	0,97	0,87
170	380	82	104,4	0,13	0,033	0,83	0,87	1,00	0,81
190	382	81	104,4	0,13	0,032	0,84	0,88	1,00	0,81
220	373	84	107,7	0,14	0,034	0,86	0,89	1,00	0,76
250	399	80	103,7	0,14	0,032	0,83	0,92	1,00	0,94
280	405	80	103,4	0,14	0,032	0,83	0,93	1,00	0,96
340	414	80	103,0	0,14	0,032	0,82	0,95	1,00	0,97
410	418	86	102,5	0,15	0,034	0,82	0,96	1,00	1,00
470	420	82	102,6	0,15	0,033	0,82	0,97	1,00	0,99
530	420	82	102,6	0,15	0,033	0,82	0,97	1,00	0,99
590	427	-	-	-	-	-	-	-	-
710	437	76	102,2	0,15	0,030	0,82	1,00	0,97	1,00
830	430	76	102,5	0,15	0,030	0,82	0,99	0,98	1,00
950	426	86	102,1	0,15	0,034	0,82	0,98	1,01	1,00
1070	428	76	102,5	-	-	-	-	-	-
1190	432	78	102,3	-	-	-	-	-	-
1430	435	76	102,3	-	-	-	-	-	-
2750	435	78	104,4	0,15	0,031	0,82	1,00	1,00	1,00

C_{Na_o} = 0,00 ppm C_{Ca_o} = 0,00 ppm

C_{Na_∞} = 435 ppm C_{Ca_∞} = 78 ppm

TABLE C-6

RESULTS OF 50% Na^+/50% Ca^{2+} LOADING AT 0,125N ON H^+ FORM OF ZEROLIT 625

Time (secs)	C(t)			F'(t)			F(t)		
	Na^+ (ppm)	Ca^{2+} (ppm)	H^+ (ppm)	Na^+	Ca^{2+}	H^+	Na^+	Ca^{2+}	H^+
0	1412	1201	0,00	0,000	0,000	1,000	0,000	0,000	0,000
10	1365	1108	6,69	0,038	0,087	0,874	0,284	0,101	0,126
20	1284	1045	13,37	0,104	0,146	0,749	0,773	0,169	0,251
30	1262	975	17,87	0,122	0,212	0,665	0,907	0,245	0,335
40	1216	886	24,27	0,160	0,295	0,545	1,185	0,341	0,455
50	-	736	-	-	-	-	-	-	-
70	1180	740	30,05	0,189	0,382	0,428	1,403	0,441	0,572
90	1171	724	34,04	0,197	0,447	0,355	1,459	0,517	0,645
110	1148	674	37,09	0,216	0,494	0,289	1,598	0,571	0,711
130	1116	620	42,00	0,242	0,545	0,212	1,793	0,629	0,788
150	1134	600	42,02	0,227	0,564	0,208	1,682	0,651	0,792
170	1111	584	43,09	0,246	0,579	0,176	1,821	0,668	0,824
190	1148	540	44,05	0,216	0,620	0,165	1,598	0,716	0,835
220	1118	504	47,07	0,240	0,654	0,105	1,779	0,755	0,895
250	1097	476	49,09	0,257	0,680	0,064	1,904	0,785	0,936
280	1127	474	48,07	0,232	0,682	0,086	1,723	0,788	0,914
340	1090	428	52,07	0,262	0,725	0,011	1,946	0,837	0,989
410	1173	402	50,04	0,195	0,750	0,054	1,445	0,866	0,946
470	1180	392	50,06	0,189	0,759	0,051	1,403	0,876	0,949
530	1191	360	51,07	0,180	0,789	0,030	1,334	0,911	0,970
590	1203	354	51,04	0,171	0,795	0,036	1,264	0,918	0,964
710	1212	332	52,01	0,163	0,815	0,023	1,209	0,941	0,977
830	1219	324	52,03	0,157	0,823	0,019	1,167	0,950	0,981
950	1217	312	53,00	0,157	0,834	0,006	1,167	0,963	0,994
1070	1219	304	53,04	0,157	0,841	0,000	1,167	0,972	1,000
1190	1219	300	53,04	0,157	0,845	0,000	1,167	0,976	1,000
1430	1235	282	53,07	0,144	0,862	0,000	1,070	0,996	1,000
2750	1249	278	53,03	0,135	0,866	0,000	1,000	1,000	1,000

C_{Na_o} = 1412 ppm C_{Ca_o} = 1200 ppm

C_{Na_∞} = 1221 ppm C_{Ca_∞} = 278 ppm

TABLE C-7

RESULTS OF 25% Na^+/75% Ca^{2+} LOADING AT 0,125N ON H^+ FORM OF ZEROLIT 625

Time (secs)	C(t)			F'(t)			F(t)		
	Na^+ (ppm)	Ca^{2+} (ppm)	H^+ (ppm)	Na^+	Ca^{2+}	H^+	Na^+	Ca^{2+}	H^+
0	734	1886	0,0	0,00	0,00	1,00	0,05	0,00	0,00
10	692	1712	10,4	0,03	0,15	0,82	1,00	0,16	0,18
20	669	1572	18,4	0,04	0,27	0,68	1,11	0,28	0,32
30	649	1482	23,8	0,07	0,35	0,59	2,00	0,36	0,41
40	651	1450	25,3	0,06	0,38	0,56	1,95	0,39	0,44
50	633	1383	29,5	0,08	0,44	0,49	2,37	0,45	0,51
70	619	1316	33,4	0,09	0,50	0,42	2,68	0,51	0,58
90	614	1224	38,2	0,09	0,58	0,33	2,79	0,59	0,67
110	612	1166	41,3	0,09	0,63	0,28	2,84	0,65	0,72
130	603	1138	43,0	0,10	0,65	0,25	3,05	0,67	0,75
150	603	1098	45,0	0,10	0,69	0,22	3,05	0,71	0,78
170	598	1068	46,8	0,10	0,71	0,18	3,16	0,73	0,82
190	593	1032	48,7	0,11	0,74	0,15	3,26	0,77	0,85
220	596	992	50,6	0,11	0,78	0,12	3,21	0,80	0,88
250	582	984	51,6	0,12	0,79	0,10	3,53	0,81	0,90
280	575	-	-	-	-	-	-	-	-
340	607	944	52,5	0,10	0,82	0,09	2,95	0,85	0,91
410	623	862	55,9	0,09	0,89	0,03	2,58	0,92	0,97
470	635	862	55,5	0,08	0,89	0,03	2,32	0,92	0,97
530	644	826	56,9	0,07	0,92	0,01	2,11	0,95	0,99
590	642	-	-	-	-	-	-	-	-
710	649	804	57,7	0,07	0,94	0,00	2,00	0,97	1,00
830	653	792	58,2	0,06	0,95	0,00	1,89	0,98	1,00
950	656	782	58,5	0,06	0,96	0,00	1,84	0,99	1,00
1070	669	792	57,5	0,05	0,95	0,00	1,53	0,98	1,00
1190	672	774	58,2	0,05	0,97	0,00	1,47	1,00	1,00
1430	656	770	59,2	0,06	0,97	0,00	1,84	1,00	1,00
2750	697	770	57,4	0,03	0,97	0,00	1,00	1,00	1,00

C_{Na_o} = 734 ppm $\quad C_{Ca_o}$ = 1886 ppm

C_{Na_∞} = 697 ppm $\quad C_{Ca_\infty}$ = 770 ppm

TABLE C-8

RESULTS OF REGENERATION AT 0,125N AND 0,50N OF Na^+ FORM CATION FORT

Time (secs)	$C_{Na_1}(t)$ (ppm)	$C_{Na_2}(t)$ (ppm)	$F_{Na_1}(t)$	$F_{Na_2}(t)$	Time (secs)	$C_{Na_1}(t)$ (ppm)	$C_{Na_2}(t)$ (ppm)	$F_{Na_1}(t)$	$F_{Na_2}(t)$
0	0	0	0,000	0,000	180	746	3155	0,975	0,990
10	129	1063	0,169	0,334	190	762	3155	0,996	0,990
20	314	1921	0,403	0,604	200	760	3155	0,993	0,990
30	-	2594	-	0,814	210	751	3155	0,982	0,990
40	566	2784	0,740	0,874	220	751	3155	0,982	0,990
50	618	2899	0,808	0,910	230	736	3155	0,962	0,990
60	664	2976	0,858	0,934	240	736	3077	0,962	0,966
70	674	3015	0,881	0,946	250	736	2976	0,962	0,934
80	715	3015	0,935	0,946	260	736	3061	0,962	0,961
90	715	2861	0,935	0,878	270	746	3178	0,975	0,997
100	721	3000	0,942	0,945	280	746	3178	0,975	0,997
110	721	3040	0,942	0,954	290	746	3178	0,975	0,997
120	726	2861	0,948	0,898	300	746	3178	0,975	0,997
130	731	3131	0,956	0,983	310	746	3178	0,975	0,997
140	731	3131	0,956	0,983	320	746	3178	0,975	0,997
150	741	3131	0,969	0,983	330	746	3180	0,975	0,997
160	726	3131	0,948	0,983	340	746	3180	0,975	0,997
170	746	3131	0,975	0,983	350	746	3182	0,975	0,998

Subscripts : 1 indicates 0,125N concentration
2 indicates 0,50N concentration

$C_{Na_{1_o}}$ = 0,00 ppm $C_{Na_{2_o}}$ = 0,00 ppm

$C_{Na_{1_\infty}}$ = 765 ppm $C_{Na_{2_\infty}}$ = 3186 ppm

TABLE C-9

RESULTS OF REGENERATION AT 0,125N AND 0,50N OF Ca^{2+} FORM CATION FORT

Time (secs)	$C_{Ca_1}(t)$ (ppm)	$C_{Ca_2}(t)$ (ppm)	$F_{Ca_1}(t)$	$F_{Ca_2}(t)$	Time (secs)	$C_{Ca_1}(t)$ (ppm)	$C_{Ca_2}(t)$ (ppm)	$F_{Ca_1}(t)$	$F_{Ca_2}(t)$
0	0	0	0,000	0,000	115	293	1979	0,930	0,954
5	40	354	0,127	0,171	125	302	1939	0,959	0,934
10	91	721	0,289	0,347	135	300	2041	0,052	0,988
15	126	967	0,400	0,462	145	302	2089	0,959	0,998
20	166	1215	0,527	0,586	135	299	2051	0,949	0,988
25	171	1411	0,543	0,680	165	303	2051	0,962	0,988
30	185	1512	0,587	0,729	175	303	2014	0,962	0,971
35	-	1581	-	0,764	185	303	2014	0,962	0,971
40	218	1686	0,692	0,813	195	303	2014	0,962	0,971
45	229	1721	0,727	0,829	205	303	2014	0,962	0,971
50	241	1757	0,765	0,847	215	303	2014	0,962	0,971
55	258	1829	0,819	0,881	225	303	2051	0,962	0,988
60	233	1866	0,803	0,899	235	291	2051	0,924	0,988
65	265	1829	0,841	0,881	245	305	2051	0,967	0,988
75	271	1865	0,860	0,899	255	305	2051	0,967	0,988
85	277	1939	0,879	0,934	265	305	2051	0,967	0,988
95	283	1902	0,898	0,917	275	305	2051	0,967	0,988
105	293	1886	0,930	0,909	285	308	2051	0,978	0,988

Subscripts : 1 indicates 0,125N concentration
2 indicates 0,50N concentration

$C_{Ca_{1_0}}$ = 0,00 ppm $C_{Ca_{2_0}}$ = 0,00 ppm

$C_{Ca_{1_\infty}}$ = 315 ppm $C_{Ca_{2_\infty}}$ = 2055 ppm

TABLE C-10

RESULTS OF Na^+ LOADING AND REGENERATION AT 0,125N OF 7,5% DVB CATION FORT

Time (secs)	$C_{Na_1}(t)$ (ppm)	$C_{Na_2}(t)$ (ppm)	$F_{Na_1}(t)$	$F_{Na_2}(t)$	Time (secs)	$C_{Na_1}(t)$ (ppm)	$C_{Na_2}(t)$ (ppm)	$F_{Na_1}(t)$	$F_{Na_2}(t)$
0	22	2769	0,025	0,029	85	744	1789	0,833	0,949
5	108	2779	0,121	0,020	95	768	1850	0,860	0,892
10	210	2683	0,235	0,110	105	811	1745	0,908	0,989
15	312	2555	0,349	0,230	115	823	1814	0,922	0,926
20	385	2396	0,431	0,379	123	853	1808	0,955	0,931
25	439	2314	0,491	0,456	135	872	1784	0,976	0,954
30	499	2245	0,559	0,521	145	859	1826	0,962	0,915
35	555	2202	0,622	0,562	155	-	-	-	-
40	558	2047	0,625	0,707	165	-	1826	-	0,915
45	616	7979	0,690	0,771	175	-	1753	-	0,983
50	646	1887	0,723	0,857	185	-	-	-	-
55	663	1936	0,742	0,811	195	-	-	-	-
60	675	1929	0,756	0,818	205	-	-	-	-
65	687	1911	0,769	0,835	215	-	-	-	-
75	720	1789	0,806	0,949	285	887	1741	-	0,994

Subscripts : 1 indicates regeneration
2 indicates loading

$C_{Na_{1_0}}$ = 0,00 ppm $\quad C_{Na_{2_0}}$ = 2800 ppm

$C_{Na_{1_\infty}}$ = 893 ppm $\quad C_{Na_{2_\infty}}$ = 1735 ppm

TABLE C-11

RESULTS OF REGENERATION AT 0,125N OF Na^+ FORM OF 5,5% DVB CATION FORT

Time (secs)	$C_{Na}(t)$ (ppm)	F(t)	Time (secs)	$C_{Na}(t)$ (ppm)	F(t)
0	6,0	0,007	85	832	0,910
5	53	0,058	95	-	-
10	171	0,187	105	-	-
15	278	0,304	115	880	0,963
20	331	0,362	125	875	0,957
25	457	0,500	135	875	0,957
30	530	0,580	145	882	0,965
35	565	0,618	155	896	0,980
40	678	0,742	165	896	0,980
45	717	0,784	175	893	0,977
50	678	0,742	185	904	0,989
55	717	0,784	195	901	0,986
60	735	0,804	205	899	0,984
65	753	0,824	215	899	0,984
75	782	0,856	285	909	0,995

C_{Na_o} = 0,0 ppm C_{Na_∞} = 914 ppm

TABLE C-12

RESULTS OF REGENERATION AT 0,125N OF Na^+ FORM OF 7,6% DVB CATION FORT

Time (secs)	$C_{Na}(t)$ (ppm)	F(t)	Time (secs)	$C_{Na}(t)$ (ppm)	F(t)
0	11	0,012	85	766	0,825
5	47	0,051	95	808	0,872
10	126	0,136	105	816	0,879
15	258	0,278	115	845	0,911
20	361	0,389	125	864	0,931
25	408	0,440	135	867	0,934
30	465	0,501	145	874	0,942
35	543	0,585	155	880	0,948
40	581	0,626	165	893	0,962
45	619	0,667	175	893	0,962
50	642	0,692	185	915	0,986
55	665	0,717	195	896	0,966
60	699	0,753	205	904	0,974
65	733	0,790	215	909	0,980
75	740	0,797	285	923	0,995

C_{Na_o} = 0,0 ppm C_{Na_∞} = 928 ppm

TABLE C-13

RESULTS OF REGENERATION AT 0,125N OF Na^+ FORM OF 8,5% DVB CATION FORT

Time (secs)	$C_{Na}(t)$ (ppm)	F(t)	Time (secs)	$C_{Na}(t)$ (ppm)	F(t)
0	0	0,000	85	812	0,875
5	-	-	95	825	0,889
10	232	0,250	105	839	0,904
15	336	0,362	115	848	0,914
20	432	0,465	125	866	0,933
25	500	0,539	135	875	0,943
30	541	0,583	145	875	0,943
35	598	0,644	155	880	0,948
40	639	0,689	165	893	0,962
45	689	0,742	175	893	0,962
50	712	0,767	185	896	0,966
55	730	0,787	195	898	0,968
65	768	0,827	205	894	0,964
75	787	0,848	285	907	0,977

C_{Na_o} = 0,0 ppm C_{Na_∞} = 928 ppm

TABLE C-14

RESULTS OF REGENERATION AT 0,125N OF 50% Na^+/50% Ca^{2+} PRELOADED CATION FORT

Time (secs)	C(t)			F''(t)			F(t)		
	Na^+ (ppm)	Ca^{2+} (ppm)	H^+ (ppm)	Na^+	Ca^{2+}	H^+	Na^+	Ca^{2+}	H^+
0	22	56	124	0,01	0,000	0,99	0,03	0,12	0,03
10	197	11	116	0,07	0,000	0,93	0,31	0,28	0,31
20	322	22	110	0,11	0,010	0,88	0,51	0,55	0,51
30	400	25	106	0,14	0,010	0,85	0,65	0,62	0,65
40	446	30	104	0,16	0,012	0,83	0,71	0,75	0,71
50	474	31	103	0,17	0,012	0,82	0,75	0,78	0,75
70	524	33	101	0,18	0,013	0,81	0,83	0,83	0,82
90	547	35	99,0	0,19	0,014	0,79	0,87	0,89	0,88
110	575	37	98,4	0,20	0,015	0,78	0,91	0,92	0,92
130	589	-	-	-	-	-	-	-	-
150	591	37	97,0	0,21	0,015	0,78	0,94	0,94	0,95
170	609	38	96,6	0,21	0,015	0,77	0,97	0,95	0,97
180	614	37	96,5	0,21	0,015	0,77	0,97	0,94	0,97
200	612	33	96,8	0,21	0,013	0,77	0,97	0,82	0,96
230	612	36	96,7	0,21	0,014	0,77	0,97	0,89	0,96
260	614	-	-	-	-	-	-	-	-
290	614	38	96,4	0,21	0,015	0,77	0,97	0,95	0,97
380	614	40	96,3	0,21	0,016	0,77	0,97	1,00	0,98
440	628	40	95,7	0,22	0,016	0,77	0,99	0,99	0,99
500	623	38	96,0	0,22	0,015	0,77	0,99	0,96	0,99
560	621	45	95,8	0,22	0,018	0,77	0,99	1,14	0,99
650	630	39	95,6	0,22	0,016	0,77	1,00	0,99	1,00
770	621	41	95,9	0,22	0,016	0,77	0,99	1,00	0,99
890	621	-	-	-	-	-	-	-	-
1010	623	40	95,9	0,22	0,016	0,77	0,99	1,00	0,99
1130	628	39	95,7	0,22	0,016	0,77	1,00	0,99	0,99
1310	635	39	95,4	0,22	0,016	0,77	1,00	1,00	1,00
1430	628	40	95,7	0,22	0,016	0,77	1,00	1,00	1,00
2750	628	-	-	-	-	-	-	-	-

C_{Na_o} = 0,00 ppm $\quad C_{Ca_o}$ = 0,00 ppm

C_{Na_∞} = 630 ppm $\quad C_{Ca_\infty}$ = 40 ppm

TABLE C-15

RESULTS OF REGENERATION AT 0,125N OF 25% Na^+/75% Ca^{2+} PRELOADED CATION FORT

Time (secs)	C(t)			F''(t)			F(t)		
	Na^+ (ppm)	Ca^{2+} (ppm)	H^+ (ppm)	Na^+	Ca^{2+}	H^+	Na^+	Ca^{2+}	H^+
0	52	7,6	122,4	0,02	0,003	0,98	0,11	0,08	0,11
10	158	21	117,1	0,06	0,009	0,93	0,35	0,25	0,33
20	243	46	112,1	0,08	0,018	0,89	0,53	0,54	0,54
30	291	55	109,6	0,10	0,022	0,88	0,64	0,64	0,64
40	324	58	108,0	0,11	0,023	0,86	0,71	0,67	0,70
50	352	65	106,6	0,12	0,026	0,85	0,77	0,76	0,77
70	381	76	104,6	0,13	0,030	0,84	0,84	0,88	0,85
90	399	75	103,9	0,14	0,030	0,83	0,87	0,87	0,88
110	410	84	102,9	0,14	0,034	0,82	0,89	0,98	0,92
130	418	82	102,7	0,14	0,033	0,82	0,92	0,95	0,93
150	422	82	102,6	0,15	0,033	0,82	0,92	0,95	0,93
170	437	84	101,8	0,15	0,034	0,82	0,96	0,98	0,96
190	435	83	101,9	0,15	0,033	0,82	0,95	0,96	0,96
220	441	82	101,7	0,15	0,033	0,82	0,97	0,95	0,97
250	458	82	100,9	0,16	0,033	0,81	1,00	0,95	1,00
280	453	81	101,3	0,16	0,032	0,81	0,99	0,94	0,98
340	455	84	101,0	0,16	0,34	0,81	0,99	0,98	0,99
410	458	88	100,7	0,16	0,35	0,81	1,00	1,00	1,00
470	457	88	100,7	0,16	0,35	0,81	1,00	1,00	1,00
530	457	87	100,8	0,16	0,35	0,81	1,00	1,00	1,00
590	461	87	100,6	0,16	0,35	0,81	1,00	1,00	1,00
710	458	-	-	-	-	-	-	-	-
830	464	88	100,4	0,16	0,35	0,81	1,00	1,00	1,00
950	455	89	100,7	0,16	0,35	0,81	1,00	1,00	1,00
1070	457	84	100,9	0,16	0,35	0,81	1,00	1,00	1,00
1190	457	86	100,8	0,16	0,35	0,81	1,00	1,00	1,00

C_{Na_o} = 0,00 ppm C_{Ca_o} = 0,00 ppm

C_{Na_∞} = 458 ppm C_{Ca_∞} = 88 ppm

TABLE C-16

RESULTS OF 50% Na^+/50% Ca^{2+} LOADING AT 0,125N ON H^+ FORM OF CATION FORT

Time (secs)	C(t)			F'(t)			F(t)		
	Na^+ (ppm)	Ca^{2+} (ppm)	H^+ (ppm)	Na^+	Ca^{2+}	H^+	Na^+	Ca^{2+}	H^+
0	1444	1230	0,0	0,00	0,00	1,00	0,03	0,00	0,00
10	1304	1120	11,6	0,12	0,11	0,78	0,84	0,12	0,22
20	1394	962	15,7	0,05	0,26	0,70	0,32	0,30	0,30
30	1162	866	30,5	0,24	0,35	0,41	1,67	0,41	0,59
40	1132	778	36,2	0,27	0,44	0,30	1,84	0,51	0,70
50	1136	712	40,1	0,28	0,50	0,22	1,95	0,59	0,78
70	1136	594	45,2	0,26	0,62	0,13	1,81	0,72	0,87
90	1136	536	48,1	0,26	0,67	0,07	1,81	0,79	0,93
110	1194	500	47,5	0,21	0,71	0,08	1,48	0,83	0,92
130	1198	446	49,9	0,21	0,76	0,03	1,45	0,89	0,97
150	1219	436	49,6	0,19	0,77	0,04	1,33	0,90	0,96
170	1242	406	50,0	0,17	0,80	0,03	1,20	0,93	0,97
190	1256	386	50,3	0,16	0,82	0,03	1,12	0,96	0,97
220	1256	376	51,0	0,16	0,83	0,01	1,12	0,97	0,99
250	1274	366	50,6	0,15	0,84	0,02	1,01	0,98	0,98
280	1274	364	50,7	0,16	0,84	0,02	1,01	0,98	0,98
340	1256	348	52,4	0,16	0,85	0,00	1,12	1,00	1,00
410	1286	344	51,2	0,14	0,86	0,00	0,95	1,00	0,99
470	1281	348	51,3	0,14	0,85	0,01	0,97	1,00	0,99
530	1281	348	51,3	0,14	0,85	0,01	0,98	1,00	0,99
590	1274	340	51,9	0,15	0,86	0,00	1,00	1,00	1,00
710	1281	348	51,2	0,14	0,85	0,01	0,98	1,00	1,00
830	1267	350	51,7	0,15	0,85	0,00	1,05	1,00	1,00
950	1274	350	51,4	0,15	0,85	0,01	1,01	1,00	0,99
1070	1274	342	51,8	0,15	0,85	0,00	1,00	1,00	1,00
1190	1267	348	51,8	0,16	0,85	0,00	1,00	1,00	1,00
1430	1274	344	51,7	0,15	0,85	0,00	1,00	1,00	1,00
2750	1279	348	51,0	0,15	0,85	0,00	1,00	1,00	1,00

C_{Na_o} = 1444 ppm $\quad C_{Ca_o}$ = 1230 ppm

C_{Na_∞} = 1280 ppm $\quad C_{Ca_\infty}$ = 348 ppm

TABLE C-17

RESULTS OF 25% Na^+/75% Ca^{2+} LOADING AT 0,125N ON H^+ FORM OF CATION FORT

Time (secs)	C(t)			F'(t)			F(t)		
	Na^+ (ppm)	Ca^{2+} (ppm)	H^+ (ppm)	Na^+	Ca^{2+}	H^+	Na^+	Ca^{2+}	H^+
0	741	1886	0,0	0,00	0,00	1,00	0,00	0,00	0,00
10	683	1634	15,0	0,05	0,23	0,72	2,08	0,24	0,28
20	653	1492	23,4	0,07	0,36	0,57	3,17	0,37	0,43
30	626	1340	32,2	0,09	0,50	0,40	4,17	0,52	0,60
40	623	1224	28,2	0,09	0,61	0,29	4,25	0,63	0,71
50	614	1146	41,8	0,10	0,67	0,22	4,58	0,69	0,78
70	621	1072	46,0	0,10	0,75	0,14	4,33	0,78	0,86
90	653	878	54,1	0,07	0,93	0,00	3,17	0,96	1,00
110	669	966	49,0	0,06	0,85	0,09	2,58	0,88	0,91
130	672	-	-	-	-	-	-	-	-
150	683	884	52,5	0,05	0,93	0,02	2,08	0,96	0,98
170	688	862	53,6	0,04	0,95	0,01	1,92	0,98	0,99
190	692	880	52,4	0,04	0,93	0,03	1,76	0,96	0,97
220	699	856	53,3	0,03	0,95	0,01	1,50	0,98	0,99
250	699	874	52,4	0,03	0,93	0,03	1,50	0,97	0,97
280	704	838	54,0	0,03	0,97	0,00	1,33	1,00	1,00
340	708	820	54,6	0,03	0,97	0,00	1,17	1,00	1,00
410	713	838	53,6	0,02	0,97	0,00	1,00	1,00	1,00
470	704	838	54,0	0,03	0,97	0,00	1,33	1,00	1,00
530	706	844	53,6	0,03	0,96	0,00	1,17	1,00	1,00
590	713	856	52,7	0,02	0,95	0,02	1,00	0,98	0,98
710	708	838	53,7	0,02	0,98	0,00	1,08	1,00	1,00
830	708	838	53,7	0,03	0,97	0,00	1,17	1,00	1,00
950	704	832	54,3	0,03	0,97	0,00	1,33	1,00	1,00
1070	706	838	53,8	0,03	0,97	0,00	1,25	1,00	1,00
1190	708	832	54,0	0,03	0,97	0,00	1,10	1,00	1,00
1430	708	844	53,5	0,03	0,97	0,00	1,10	1,60	1,00
2750	713	832	53,9	0,02	0,98	0,00	1,60	1,00	1,00

C_{Na_o} = 741 ppm $\quad C_{Ca_o}$ = 1885 ppm

C_{Na_∞} = 710 ppm $\quad C_{Ca_\infty}$ = 840 ppm

APPENDIX D

DETAILED ANION KINETIC RESULTS

TABLE D-1

RESULTS OF Cl^- LOADING AT O,OlN ON OH^- FORM OF ZEROLIT MPH

Time (secs)	$C_{Cl}(t)$ (ppm)	F(t)	Time (secs)	$C_{Cl}(t)$ (ppm)	F(t)
0	364	0,000	900	306	0,319
30	363	0,005	960	305	0,319
60	352	0,066	1020	305	0,324
90	344	0,110	1080	305	0,324
120	343	0,115	1140	302	0,341
150	341	0,126	1200	299	0,357
180	337	0,148	1260	294	0,385
240	336	0,154	1320	294	0,379
300	335	0,159	1380	294	0,368
360	329	0,192	1440	293	0,390
420	325	0,214	1500	292	0,396
480	321	0,236	1560	290	0,407
540	378	0,253	1620	284	0,423
600	316	0,264	1680	284	0,423
660	313	0,280	1740	282	0,451
720	313	0,680	1800	284	0,440
780	311	0,291	1860	282	0,451
840	309	0,302	1920	282	0,451

C_{Cl_∞} = 364 ppm $\qquad$ C_{Cl_∞} = 280 ppm

TABLE D-2

RESULTS OF Cl^- LOADING AT 0,05N ON OH^- FORM OF ZEROLIT MPH

Time (secs)	$C_{Cl}(t)$ (ppm)	F(t)	Time (secs)	$C_{Cl}(t)$ (ppm)	F(t)
0	1766	0,000	900	1067	0,792
30	1642	0,140	960	1059	0,801
60	1547	0,248	1020	1047	0,814
90	1492	0,308	1080	1044	0,818
120	1445	0,364	1140	1016	0,849
150	1374	0,444	1200	1009	0,857
180	1366	0,453	1260	1025	0,839
240	1327	0,497	1320	1022	0,843
300	1296	0,532	1380	1019	0,846
360	1253	0,581	1440	1016	0,849
420	1218	0,621	1500	995	0,873
480	1202	0,639	1560	992	0,877
540	1163	0,683	1620	989	0,880
600	1152	0,695	1680	978	0,892
660	1121	0,730	1740	975	0,896
720	1105	0,749	1800	972	0,899
780	1094	0,761	1860	969	0,903
840	1086	0,770	1920	937	0,939

C_{Cl_o} = 1766 ppm C_{Cl_∞} = 883 ppm

TABLE D-3

RESULTS OF SO_4^{2-} LOADING AT 0,01N ON OH^- FORM OF ZEROLIT MPH

Time (secs)	$C_{SO_4}(t)$ (ppm)	F(t)	Time (secs)	$C_{SO_4}(t)$ (ppm)	F(t)
0	535	0,000	900	353	0,639
30	513	0,077	960	348	0,656
60	499	0,126	1020	328	0,726
90	487	0,168	1080	332	0,712
120	480	0,193	1140	-	-
150	469	0,232	1200	331	0,716
180	453	0,288	1260	327	0,730
240	445	0,316	1320	321	0,751
300	-	-	1380	319	0,758
360	-	-	1440	-	-
420	-	-	1500	316	0,768
480	396	0,488	1560	312	0,789
540	395	0,491	1620	310	0,789
600	387	0,519	1680	-	-
660	-	-	1740	308	0,796
720	-	-	1800	303	0,814
780	362	0,607	1860	302	0,818
840	356	0,628	1920	301	0,821

$C_{SO_4{}_o}$ = 535 ppm $C_{SO_4{}_\infty}$ = 250 ppm

TABLE D-4

RESULTS OF SO_4^{2-} LOADING AT 0,05N ON OH^- FORM OF ZEROLIT MPH

Time (secs)	$C_{SO_4}(t)$ (ppm)	F(t)	Time (secs)	$C_{SO_4}(t)$ (ppm)	F(t)
0	0	0,000	900	1335	0,880
30	2345	0,046	960	1312	0,907
60	2269	0,109	1020	1305	0,913
90	2153	0,206	1080	1310	0,908
120	2074	0,272	1140	1290	0,925
150	1998	0,336	1200	1254	0,925
180	1927	0,394	1260	-	-
240	1874	0,438	1320	1244	0,955
300	1747	0,544	1380	1269	0,963
360	1665	0,613	1400	1269	0,943
420	1609	0,659	1460	1272	0,943
460	1560	0,700	1520	1340	0,940
540	-	-	1580	1264	0,940
600	1464	0,780	1640	1325	0,947
660	1439	0,801	1700	1282	0,896
720	1393	0,839	1760	1310	0,932
780	1365	0,863	1820	1310	0,903
840	1395	0,671	1880	1287	0,908

$C_{SO_4}{}_o$ = 2400 ppm $C_{SO_4}{}_\infty$ = 1200 ppm

TABLE D-5

RESULTS OF Cl^- LOADING AT 0,05N ON FREE-BASE FORM OF SENBRIX USING BOTH FRACTIONAL SAMPLES AND CONDUCTIOMETRIC METHODS

Time (secs)	ppm Cl^-		F(t)		Time (secs)	ppm Cl^-		F(t)	
	Fractional Sample	Conductiometric Methods	Fractional Sample	Conductiometric Methods		Fractional Sample	Conductiometric Methods	Fractional Sample	Conductiometric Methods
0	1730	1825	0,000	0,000	500	1011	1061	0,835	0,838
30	1639	1660	0,105	0,171	600	1002	1049	0,842	0,851
60	1492	1543	0,275	0,309	680	982	1041	0,865	0,860
90	1354	1433	0,435	0,430	720	978	1033	0,869	0,868
120	1312	1365	0,483	0,504	780	959	1027	0,891	0,875
150	1253	1307	0,551	0,568	840	978	1023	0,869	0,879
180	1210	1267	0,601	0,612	900	970	1018	0,870	0,885
210	1167	1230	0,651	0,652	960	963	1014	0,887	0,889
240	1117	1202	0,709	0,683	1020	959	1011	0,891	0,893
300	1089	1156	0,741	0,734	1080	963	1010	0,887	0,894
360	1059	1122	0,776	0,771	1140	959	1007	0,891	0,897
420	1036	1098	0,802	0,797	1200	963	1007	0,876	0,897
480	1016	1078	0,825	0,819	1260	959	1005	0,891	0,900

$C_{Cl_0\ \text{frac. samp.}} = 1730$ ppm $\quad C_{Cl_0\ \text{conduc.}} = 1825$ ppm

$C_{Cl_\infty\ \text{frac. samp.}} = 865$ ppm $\quad C_{Cl_\infty\ \text{conduc.}} = 913$ ppm

TABLE D-6

RESULTS OF FORMIC ACID LOADING AT 0,05N ON FREE-BASE FORM OF ZEROLIT MPH

Time (secs)	$C_{Formic}(t)$ (ppm)	F(t)	Time (secs)	$C_{Formic}(t)$ (ppm)	F(t)
60	0	0,000	1080	495	0,808
120	683	0,248	1200	485	0,837
180	649	0,347	1320	474	0,869
240	629	0,418	1440	466	0,894
300	607	0,473	1560	460	0,911
360	592	0,518	1680	453	0,933
480	578	0,559	1800	447	0,948
600	555	0,629	1920	443	0,961
720	536	0,685	2040	439	0,974
840	520	0,733	2160	434	0,987
960	506	0,779	2280	430	0,988
			2400	-	-

C_{Formic_o} = 766 ppm C_{Formic_∞} = 430 ppm

TABLE D-7

RESULTS OF PROPIONIC ACID LOADING AT 0,05N ON FREE-BASE FORM OF ZEROLIT MPH

Time (secs)	$C_{Propionic}(t)$ (ppm)	F(t)	Time (secs)	$C_{Propionic}(t)$ (ppm)	F(t)
60	7400	0,000	1080	5686	0,442
120	7273	0,117	1200	5564	0,482
180	6995	0,175	1320	5464	0,461
240	6797	0,213	1440	5379	0,504
300	6649	0,244	1560	5303	0,519
360	6520	0,287	1680	5234	0,536
480	6403	0,294	1800	5173	0,548
600	6206	0,338	1920	5107	0,557
720	6047	0,368	2040	5054	0,571
840	5907	0,396	2160	4989	0,584
960	5778	0,421	2280	4220	0,596
			2400	4848	0,612

$C_{Propionic_o}$ = 7400 ppm $C_{Propionic_\infty}$ = 2950 ppm

TABLE D-8

RESULTS OF BUTYRIC ACID LOADING AT 0,05N ON FREE-BASE FORM OF ZEROLIT MPH

Time (secs)	$C_{Butyric}(t)$ (ppm)	F(t)	Time (secs)	$C_{Butyric}(t)$ (ppm)	F(t)
60	0	0,000	1080	6134	0,427
120	7397	0,127	1200	6039	0,450
180	7189	0,176	1320	5969	0,467
240	7022	0,216	1440	5900	0,483
300	6914	0,202	1560	5824	0,501
360	6807	0,267	1680	5778	0,512
480	6719	0,288	1800	5711	0,528
600	6546	0,329	1920	5667	0,539
720	6428	0,357	2040	5615	0,551
840	6312	0,385	2160	5557	0,565
960	6215	0,408	2280	5500	0,578
			2400	5429	0,595

$C_{Butyric_o}$ = 7930 ppm $C_{Butyric_\infty}$ = 3729 ppm

TABLE D-9

RESULTS OF BUTYRIC ACID LOADING AT 0,025N ON FREE-BASE FORM OF ZEROLIT MPH

Time (secs)	$C_{Butyric}(t)$ (ppm)	F(t)	Time (secs)	$C_{Butyric}(t)$ (ppm)	F(t)
60	3616	0,118	1080	2937	0,469
120	3509	0,173	1200	2904	0,486
180	3426	0,216	1320	2872	0,503
240	3369	0,245	1440	2840	0,519
300	3316	0,273	1560	2809	0,536
360	3267	0,298	1680	2781	0,550
480	3190	0,338	1800	2754	0,564
600	3124	0,372	1920	2725	0,579
720	3076	0,397	2040	-	-
840	3025	0,424	2160	-	-
960	2983	0,445	2280	-	-
			2400	-	-

$C_{Butyric_o}$ = 3843 ppm $C_{Butyric_\infty}$ = 1912 ppm

TABLE D-10

RESULTS OF BUTYRIC ACID LOADING AT 0,0125N ON FREE-BASE FORM OF ZEROLIT MPH

Time (secs)	$C_{Butyric}(t)$ (ppm)	F(t)	Time (secs)	$C_{Butyric}(t)$ (ppm)	F(t)
60	1863	0,063	1080	1657	0,337
120	1837	0,103	1200	1644	0,353
180	1812	0,132	1320	1632	0,370
240	1791	0,155	1440	1623	0,382
300	1777	0,180	1560	1614	0,394
360	1764	0,195	1680	1604	0,426
480	1741	0,226	1800	1594	0,418
600	1718	0,256	1920	1586	0,430
720	1700	0,280	2040	1580	0,438
840	1683	0,299	2160	1568	0,454
960	1671	0,318	2280	1561	0,464
			2400	1553	0,474

$C_{Butyric_o}$ = 1912 ppm $C_{Butyric_\infty}$ = 1155 ppm

TABLE D-11

RESULTS OF Cl^- LOADING AT 0,01N ON FREE-BASE FORM OF SENBRIX

Time (secs)	$C_{Cl}(t)$ (ppm)	F(t)	Time (secs)	$C_{Cl}(t)$ (ppm)	F(t)
0	373	0,000	900	284	0,477
30	373	0,600	960	281	0,493
60	364	0,048	1020	275	0,525
90	359	0,075	1080	275	0,525
120	352	0,113	1140	273	0,536
150	346	0,145	1200	272	0,542
180	342	0,166	1260	264	0,584
240	336	0,198	1320	270	0,552
300	327	0,247	1380	265	0,579
360	321	0,279	1440	264	0,584
420	314	0,316	1500	261	0,584
480	309	0,343	1560	264	0,584
540	303	0,375	1620	258	0,584
600	300	0,391	1680	258	0,638
660	297	0,408	1740	254	0,638
720	293	0,429	1800	254	0,638
780	291	0,440	1860	252	0,649
840	285	0,472	1920	252	0,649

C_{Cl_o} = 373 ppm $\quad$ C_{Cl_∞} = 186 ppm

TABLE D-12

RESULTS OF Cl^- LOADING AT 0,05N ON FREE-BASE FORM OF SENBRIX

Time (secs)	$C_{Cl}(t)$ (ppm)	F(t)	Time (secs)	$C_{Cl}(t)$ (ppm)	F(t)
0	1730	0,000	900	978	0,869
30	1639	0,105	960	970	0,879
60	1492	0,275	1020	963	0,887
90	1410	0,370	1080	959	0,891
120	1354	0,435	1140	963	0,887
150	1312	0,483	1200	959	0,891
180	1253	0,551	1260	972	0,876
240	1210	0,601	1320	992	0,853
300	1167	0,651	1380	992	0,853
360	1117	0,709	1440	987	0,859
420	1089	0,741	1500	981	0,866
480	1059	0,776	1560	978	0,869
540	1036	0,802	1620	975	0,873
600	1016	0,825	1680	976	0,872
660	1001	0,843	1740	972	0,876
720	982	0,865	1800	969	0,880
780	978	0,869	1880	992	0,852
840	959	0,891	1920	995	0,850

C_{Cl_o} = 1730 ppm C_{Cl_∞} = 865 ppm

TABLE D-13

RESULTS OF SO_4^{2-} LOADING AT 0,01N ON FREE-BASE FORM OF SENBRIX

Time (secs)	$C_{SO_4}(t)$ (ppm)	F(t)	Time (secs)	$C_{SO_4}(t)$ (ppm)	F(t)
0	535	0,000	900	380	0,544
30	523	0,042	960	-	-
60	519	0,056	1020	-	-
90	507	0,098	1080	374	0,565
120	502	0,116	1140	371	0,575
150	483	0,185	1200	365	0,596
180	476	0,207	1260	-	-
240	-	-	1320	352	0,642
300	-	-	1380	351	0,646
360	-	-	1440	347	0,660
420	462	0,256	1500	343	0,674
480	437	0,344	1560	340	0,684
540	-	-	1620	339	0,688
600	405	0,456	1680	337	0,695
660	399	0,477	1740	335	0,702
720	398	0,481	1800	333	0,709
780	392	0,502	1860	330	0,719
840	380	0,544	1920	330	0,719

$C_{SO_4 o}$ = 535 ppm $C_{SO_4 \infty}$ = 250 ppm

TABLE D-14

RESULTS OF SO_4^{2-} LOADING AT 0,05N ON FREE-BASE FORM OF SENBRIX

Time (secs)	$C_{SO_4}(t)$ (ppm)	F(t)	Time (secs)	$C_{SO_4}(t)$ (ppm)	F(t)
0	2350	0,000	900	1399	0,799
30	2293	0,048	960	1373	0,821
60	2222	0,108	1020	1381	0,814
90	2043	0,258	1080	1344	0,845
120	1943	0,342	1140	1344	0,845
150	1881	0,394	1200	-	-
180	-	-	1260	1359	0,833
240	-	-	1320	-	-
300	-	-	1380	1259	0,917
360	1699	0,547	1440	1318	0,867
420	1597	0,633	1500	-	-
480	1540	0,681	1560	-	-
540	-	-	1620	1342	0,847
600	-	-	1680	1317	0,868
660	1429	0,774	1740	1322	0,864
720	1438	0,766	1800	1322	0,864
780	-	-	1860	1316	0,869
840	-	-	1920	1320	0,866

$C_{SO_4}{}_o$ = 2350 ppm $C_{SO_4}{}_\infty$ = 1160 ppm

TABLE D-15

RESULTS OF Cl^- LOADING AT 0,05N ON FREE-BASE FORM OF 6,5% DVB SENBRIX

Time (secs)	$C_{Cl}(t)$ (ppm)	F(t)	Time (secs)	$C_{Cl}(t)$ (ppm)	F(t)
0	2067	0,000	870	960	0,899
20	1820	0,200	930	960	0,899
60	1700	0,298	990	891	0,955
90	1607	0,373	1050	855	0,984
120	1480	0,476	1110	867	0,974
150	1413	0,531	1170	864	0,976
180	1327	0,601	1230	856	0,983
210	1253	0,661	1290	847	0,990
270	1147	0,747	1350	873	0,969
330	1100	0,785	1410	873	0,969
390	987	0,877	1470	873	0,969
450	1000	0,866	1530	873	0,969
510	960	0,899	1590	873	0,969
570	920	0,931	1650	871	0,971
630	920	0,931	1710	867	0,974
690	893	0,953	1770	864	0,976
750	900	0,947	1830	860	0,980
810	887	0,958	1890	840	0,996

C_{Cl_o} = 2067 ppm $\quad C_{Cl_\infty}$ = 835 ppm

TABLE D-16

RESULTS OF Cl^- LOADING AT 0,05N ON FREE-BASE FORM OF 8% DVB SENBRIX

Time (secs)	$C_{Cl}(t)$ (ppm)	F(t)	Time (secs)	$C_{Cl}(t)$ (ppm)	F(t)
0	1813	0,000	900	1037	0,698
30	1720	0,085	960	1070	0,662
60	1615	0,178	1020	-	-
90	1520	0,267	1080	942	0,785
120	1469	0,308	1140	936	0,788
150	1440	0,332	1200	917	0,806
180	1400	0,374	1260	911	0,810
240	1347	0,417	1320	911	0,810
300	1267	0,492	1380	879	0,836
360	1240	0,515	1440	904	0,816
420	1200	0,551	1500	879	0,836
480	1200	0,551	1560	917	0,806
540	1188	0,566	1620	866	0,857
600	1182	0,567	1680	853	0,867
660	1164	0,586	1740	853	0,863
720	1127	0,620	1800	-	-
780	1057	0,672	1860	-	-
840	1019	0,713	1920	-	-

C_{Cl_o} = 1813 ppm $\quad C_{Cl_\infty}$ = 700 ppm

TABLE D-17

RESULTS OF Cl^- LOADING AT 0,05N ON FREE-BASE FORM OF 12% DVB SENBRIX.

Time (secs)	$C_{Cl}(t)$ (ppm)	F(t)	Time (secs)	$C_{Cl}(t)$ (ppm)	F(t)
0	1821	0,000	900	1172	0,618
30	1732	0,085	960	1159	0,630
60	1668	0,146	1020	1153	0,636
90	1630	0,182	1080	1134	0,654
120	1579	0,230	1140	1121	0,666
150	1541	0,266	1230	1095	0,691
180	1509	0,297	1260	1071	0,714
240	1496	0,309	1320	1032	0,751
300	1490	0,315	1380	1032	0,751
360	1426	0,376	1440	1044	0,739
420	1375	0,424	1500	1019	0,763
480	1337	0,461	1560	981	0,799
540	1223	0,569	1620	955	0,824
600	1210	0,581	1680	942	0,836
660	1210	0,581	1740	-	-
720	1197	0,594	1800	1032	0,751
780	1197	0,594	1860	960	0,819
840	1172	0,618	1920	952	0,827

C_{Cl_o} = 1821 ppm C_{Cl_∞} = 770 ppm

TABLE D-18

RESULTS OF Cl^- LOADING AT 0,05N ON 25% Cl^- PRELOADED SENBRIX

Time (secs)	$C_{Cl}(t)$ (ppm)	F(t)	Time (secs)	$C_{Cl}(t)$ (ppm)	F(t)
0	1750	0,000	900	1048	0,942
30	1625	0,168	960	1026	0,972
60	1619	0,176	1020	1057	0,930
90	1509	0,323	1080	1039	0,954
120	-	-	1140	-	-
150	1503	0,332	1200	1026	0,972
180	1413	0,451	1260	1026	0,972
240	1350	0,537	1320	1020	0,972
300	1185	0,758	1380	1051	0,938
360	1146	0,811	1440	1039	0,954
420	1143	0,815	1500	1039	0,954
480	1115	0,852	1560	1026	0,972
540	1112	0,856	1620	1048	0,942
600	1099	0,874	1680	-	-
660	1066	0,918	1740	1069	0,914
720	-	-	1800	1014	0,988
840	1051	0,938	1920	1014	0,988

C_{Cl_o} = 1750 ppm $\quad$ C_{Cl_∞} = 1005 ppm

TABLE D-19

RESULTS OF Cl^- LOADING AT 0,05N ON 50% Cl^- PRELOADED SENBRIX

Time (secs)	$C_{Cl}(t)$ (ppm)	F(t)	Time (secs)	$C_{Cl}(t)$ (ppm)	F(t)
0	1720	0,000	900	1094	0,936
30	1610	0,164	960	1106	0,918
60	1510	0,314	1020	1099	0,928
90	1448	0,407	1080	1081	0,955
120	1387	0,498	1140	1099	0,928
150	1326	0,589	1200	1075	0,964
180	1295	0,635	1260	1066	0,978
240	1234	0,726	1320	1072	0,969
300	1191	0,791	1380	1054	0,996
360	1161	0,836	1440	1069	0,973
420	1149	0,854	1500	1112	0,909
480	1146	0,858	1560	1069	0,973
540	1136	0,873	1620	1115	0,904
600	1143	0,862	1680	1161	0,836
660	1161	0,836	1740	1112	0,909
720	1081	0,955	1800	1088	0,945
780	1130	0,882	1860	1069	0,973
840	1088	0,945	1920	1081	0,955

C_{Cl_o} = 1720 ppm C_{Cl_∞} = 1051 ppm

TABLE D-20

RESULTS OF Cl^- LOADING AT 0,05N ON 75% Cl^- PRELOADED SENBRIX

Time (secs)	$C_{Cl}(t)$ (ppm)	F(t)	Time (secs)	$C_{Cl}(t)$ (ppm)	F(t)
0	1741	0,000	900	1089	0,972
30	1489	0,376	960	1098	0,958
60	1337	0,602	1020	1095	0,963
90	1228	0,765	1080	1080	0,985
120	1198	0,809	1140	1080	0,986
150	1185	0,829	1200	1077	0,990
180	1143	0,891	1260	1077	0,990
240	1137	0,900	1320	1077	0,990
300	1113	0,936	1380	1077	0,990
360	1113	0,936	1440	1077	0,990
420	1113	0,936	1500	1071	0,999
480	1107	0,945	1560	1089	0,972
540	1077	0,990	1620	-	-
600	1083	0,981	1680	1083	0,981
660	1095	0,963	1740	1077	0,990
720	1095	0,963	1800	1077	0,990
840	1110	0,940	1920	1085	0,978

C_{Cl_o} = 1741 ppm $\quad$ C_{Cl_∞} = 1070 ppm

TABLE D-21

RESULTS OF FORMIC ACID LOADING AT 0,05N ON FREE-BASE FORM OF SENBRIX

Time (secs)	$C_{Formic}(t)$ (ppm)	F(t)	Time (secs)	$C_{Formic}(t)$ (ppm)	F(t)
60	0	0,000	1080	5952	0,713
120	7239	0,156	1200	5884	0,742
180	7016	0,252	1320	5818	0,771
240	6878	0,312	1440	5752	0,799
300	6743	0,370	1560	5704	0,820
360	6629	0,419	1680	5655	0,841
480	6536	0,460	1800	5607	0,862
600	6380	0,527	1920	5568	0,879
720	6263	0,578	2040	5528	0,896
840	6158	0,624	2160	5481	0,916
960	6045	0,672	2280	5450	0,930
			2400	5434	0,936

C_{Formic_o} = 7598 ppm C_{Formic_∞} = 5288 ppm

TABLE D-22

RESULTS OF PROPIONIC ACID LOADING ON FREE-BASE FORM OF SENBRIX

Time (secs)	$C_{Propionic}(t)$ (ppm)	F(t)	Time (secs)	$C_{Propionic}(t)$ (ppm)	F(t)
60	0	0,000	1080	4364	0,733
120	5138	0,192	1200	4322	0,766
180	5004	0,289	1320	4240	0,825
240	4915	0,348	1440	4207	0,847
300	4839	0,409	1560	4180	0,865
360	4775	0,447	1680	4150	0,885
480	4718	0,488	1800	4130	0,901
600	4623	0,555	1920	4100	0,923
720	4551	0,609	2040	4071	0,943
840	4481	0,656	2160	4056	0,954
960	4417	0,700	2280	4042	0,966
			2400	4022	0,977

$C_{Propionic_o}$ = 5411 ppm $C_{Propionic_\infty}$ = 3990 ppm

TABLE D-23

RESULTS OF BUTYRIC ACID LOADING AT 0,05N ON FREE-BASE FORM OF SENBRIX

Time (secs)	$C_{Butyric}(t)$ (ppm)	F(t)	Time (secs)	$C_{Butyric}(t)$ (ppm)	F(t)
60	0	0,000	1080	467	0,799
120	647	0,218	1200	457	0,830
180	613	0,326	1320	449	0,858
240	592	0,395	1440	442	0,879
300	574	0,454	1560	436	0,899
360	558	0,503	1680	-	-
480	546	0,544	1800	-	-
600	524	0,616	1920	-	-
720	506	0,672	2040	-	-
840	491	0,722	2160	-	-
960	478	0,764	2280	-	-
			2400	-	-

$C_{Butyric_o}$ = 714 ppm $C_{Butyric_\infty}$ = 405 ppm

TABLE D-24

RESULTS OF BUTYRIC ACID LOADING AT 0,025N ON FREE-BASE FORM OF SENBRIX

Time (secs)	$C_{Butyric}(t)$ (ppm)	F(t)	Time (secs)	$C_{Butyric}(t)$ (ppm)	F(t)
60	0	0,000	1080	3284	0,479
120	3706	0,117	1200	3259	0,501
180	3640	0,174	1320	3229	0,526
240	3593	0,215	1440	3212	0,541
300	3551	0,251	1560	3192	0,559
360	3514	0,282	1680	3183	0,566
480	3491	0,302	1800	3155	0,590
600	3433	0,352	1920	3138	0,604
720	3389	0,390	2040	3122	0,618
840	3349	0,424	2160	3106	0,632
960	3314	0,453	2280	3094	0,643
			2400	3066	0,667

$C_{Butyric_o}$ = 3843 ppm $C_{Butyric_\infty}$ = 2677 ppm

TABLE D-25

RESULTS OF BUTYRIC ACID LOADING AT 0,0125N ON FREE-BASE FORM OF SENBRIX

Time (secs)	$C_{Butyric}(t)$ (ppm)	F(t)	Time (secs)	$C_{Butyric}(t)$ (ppm)	F(t)
0	0	0,000	1080	1654	0,388
60	1805	0,086	1200	1645	0,408
120	1784	0,123	1320	1639	0,419
180	1769	0,154	1440	1632	0,434
240	1757	0,179	1560	1629	0,439
300	1747	0,200	1680	1620	0,459
360	1731	0,233	1800	1614	0,476
480	1712	0,273	1920	1609	0,481
600	1697	0,301	2040	1603	0,492
720	1684	0,327	2160	1599	0,501
840	1687	0,322	2280	1595	0,509
960	1663	0,371	2400	1590	0,520

$C_{Butyric_o}$ = 1845 ppm $C_{Butyric_\infty}$ = 850 ppm

TABLE D-26

RESULTS OF REGENERATION AT 0,05N OF BUTYRIC ACID LOADED SENBRIX

Time (secs)	$C_{Butyric}(t)$ (ppm)	F(t)	Time (secs)	$C_{Butyric}(t)$ (ppm)	F(t)
0	0	0,000	1680	2097	0,995
60	807	0,383	1800	2098	0,995
120	1095	0,519	1920	2099	0,996
180	1287	0,611	2040	2099	0,996
240	1429	0,678	2160	2100	0,996
300	1538	0,729	2280	2100	0,996
360	1630	0,773	2400	2101	0,997
480	1764	0,837	2520	2105	0,998
600	1859	0,882	2640	2107	0,999
720	1925	0,913	2760	2107	0,999
840	1981	0,940	2880	2108	1,000
960	2014	0,955	3000	2108	1,000
1080	2042	0,969	3120	2108	1,000
1200	2060	0,977	3240	2108	1,000
1320	2070	0,982	3360	2108	1,000
1440	2083	0,988	3480	2108	1,000
1560	2095	0,994	3600	2108	1,000

$C_{Butyric_o}$ = 0 ppm $C_{Butyric_\infty}$ = 2108 ppm

APPENDIX E

ANALYTICAL METHODS

APPENDIX E

ANALYTICAL METHODS

E.1 CATIONS

Analyses for cations were performed on an atomic absorption spectrophotometer. This technique depends entirely on the absorption of energy liberated by valence electrons of ground state atoms (see Fig. E-1), and is so specific that elements may be detected at trace levels even in the presence of other elements at much higher concentrations [15,65].

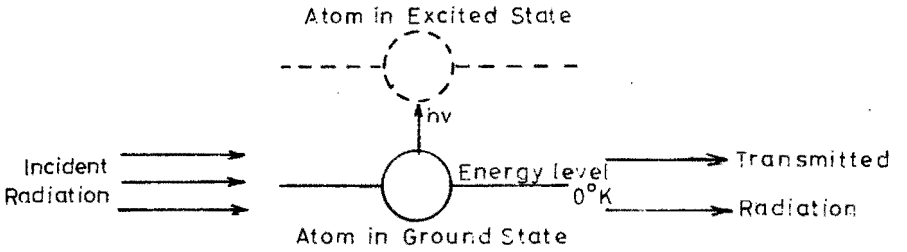

Fig. E-1: Illustration of Atomic Absorption Technique.

A liquid sample is atomised in a flame, and a light spectrum from a cathode ray preceding the atomiser passes through this flame which consists mainly of atoms in their ground state. Light of the specific resonance wavelength of the metal being analysed is absorbed by the metal in the flame, and detected by means of a monochromator. The degree of absorption is a function of the concentration of the metal in the sample. It is only necessary to compare the absorption of known standards with that of the sample and simply calculate, or graphically plot, the results in order to obtain the concentration of the sample [66,67].

During the course of the project a Varian Techtron 1100 atomic absorption spectrophotometer was used for the analysis of Na^{+} and Ca^{2+}. An air/acetylene flame was used in each case, being suitable for these cations [65,67,68].

The detailed experimental settings are summarised in Table E-1.

TABLE E-1

SETTINGS FOR CATION ANALYSIS BY ATOMIC ABSORPTION SPECTROSCOPY

Cation	Wavelength (nm)	Lamp Current (mA)	Slit Width (nm)
Na^+	589,0	5	0,2
Ca^{2+}	423,3	3	0,5

Because the accuracy of the readings directly affects the kinetic F(t) curves (see Chapter 5), tests were performed on both Na^+ and Ca^{2+} samples of different, known concentrations, and the percentage accuracy determined. These results are presented in Table E-2.

The "Standard Concentrations" for the Na^+ tests were only approximate - the accurate concentration is given under the "Actual Concentration" heading.

It is clear from these results that the maximum error obtained in either needle deviation or concentration differences was 3,12%. This was thus taken as the acceptable accuracy for the cation F(t) curves.

A Wang 2200 microcomputer system and a least squares correlation program were used to transfer the instrument readings into concentration data. The program required two sets of standard concentration data for the least squares correlation equation. A copy of the program is listed at the end of this Appendix.

TABLE E-2

ACCURACY CHECK ON ATOMIC ABSORPTION SPECTROPHOTOMETER

Cation	Standard Conc. (ppm)	Minimum Reading	Maximum Reading	% Difference	Average Analysed Conc.	Actual Conc.	% Resin
Na^+	50	6,8	7,0	2,94	46	45	2,17
Na^+	200	25,8	26,2	1,55	229	230	<1,0
Na^+	300	37,8	38,2	<1,0	284	287	1,06
Na^+	500	59,8	61,2	2,40	561	575	2,50
Ca^{2+}	5	8,0	8,1	1,25	4,9	5	2,00
Ca^{2+}	10	15,0	15,4	2,67	10,2	10	2,00
Ca^{2+}	20	32,1	33,1	3,12	19,7	20	1,50
Ca^{2+}	50	64,9	66,9	3,08	50,5	50	<1,0

E.2 ANIONS

Both Cl^- and SO_4^{2-} were analysed during the course of the project.

E.2.1 Chloride

Chloride was analysed by means of a Technicon Auto Analyser II. This automatic method of chloride determination depends on the liberation of thiocyanate ion (SCN) from mercuric thiocyanate, through sequestration of mercury by chloride, to form un-ionised mercuric chloride. In the presence of ferric ion, the liberated SCN forms highly coloured ferric thiocyanate; in concentration, proportional to the original concentration. This is detected by means of a colorimeter at 480 nm and recorded on a pen recorder [15,70,71].

E.2.2 Sulphate

Sulphate was also analysed on the Auto Analyser. The

method involves reaction with barium chloride to form barium sulphate (at a pH of 2,5 to 3,0). Excess barium reacts with methylthymol blue to form a blue-coloured chelate at a pH of 12,5 to 13,0. The amount of uncomplexed methylthymol blue, which is grey in colour, measured at 460 nm by a colorimeter, is equal to the sulphate present [15,71].

All anion concentration results were obtained from plotted peak heights, using the Wang 2200 system and the least squares correlation program.

E.3 CHEMICAL OXYGEN DEMAND (COD)

For the anion organic kinetic tests, COD determinations were performed on formic, propionic and butyric acid samples. The COD determination provides a measure of the oxygen equivalent of that portion of the organic matter in a sample that is susceptible to oxidation by a strong chemical oxidant. It involves the refluxing of a quantity of sample with potassium dichromate and sulphuric acid and the subsequent back titration of the excess dichromate with ferrous ammonium sulphate, which furnishes a measure of the oxygen equivalent

E.3.1 Procedure

(1) 0,4 gms of $HgSO_4$ is placed in a 250 ml erlenmeyer flask together with 20 ml of the sample and 10 ml of standard potassium dichromate titrant (see "Standard Methods" [63] for details of reagents). 30 ml of concentrated H_2SO_4 containing Ag_2SO_4 is carefully added, with mercury. Glass beads are added to prevent bumping.

(2) The flask is attached to a Liebigs condenser and refluxed for two hours.

(3) The mixture, once cool, is diluted to approximately 140 ml and the excess dichromate is titrated with standard ferrous ammonium sulphate solution using

ferroin indicator. The colour change is a sharp transition from blue-green to reddish-brown.

(4) In addition, a blank, consisting of 20 ml distilled water together with the other reagents, is refluxed and titrated in the same way as the samples above.

(5) Standardisation of the $Fe(NH_4)_2(SO_4)_2$ solution is performed by diluting 10 ml of standard potassium dichromate solution to about 100 ml, adding 30 ml concentrated H_2SO_4 and allowing to cool for two hours. This is also titrated with the ferrous ammonium sulphate titrant using 2 to 3 drops of ferroin indicator. The normality of the titrant is calculated using equation (E-1):

$$\text{Normality} = \frac{\text{ml } K_2Cr_2O_7 \times 0{,}25}{\text{ml } Fe(NH_4)_2(SO_4)_2} \quad . \qquad \text{(E-1)}$$

(6) The COD is calculated as mg/ℓ, using equation (E-2):

$$\text{mg}/\ell\,\text{COD} = \frac{(a-b)c \times 8000}{\text{ml sample}} \qquad \text{(E-2)}$$

where a = ml $Fe(NH_4)_2(SO_4)_2$ used for blank;
b = ml $Fe(NH_4)_2(SO_4)_2$ used for sample;
c = normality of $Fe(NH_4)_2(SO_4)_2$ solution.

More detailed procedure is described in "Standard Methods" [63].

"BASIC" PROGRAMME FOR WANG 2200 SYSTEM - DATA CORRELATION

```
1        10 DEFFN'1 'LISTS'
2        20 DEFFN'2 'RENUMBER 10,10,10'
3        30 PRINT'DATA CORRELATION PROGRAM':
4           PRINT'**************************':PRINT
5        40 REM FOR COMPUTING AA RESULTS
6        50 DIM A(3,3),B(3),C(3),D(3,3),X(50),Y(50),C$(4),K$(5),X2(50),Y2(50)
7        60 DATA 'COD','CL','SO4','NA','CA'
8        70 FOR I=1 TO 5:READ K$(1):NEXT I
9        80 PRINT'THIS PROGRAM COMPUTES THE AA REFERNCE LINE'
10       90 PRINT'KEY IN TWO SETS OF CALIBRATION DATA'
11      100 PRINT'KEY IN THE NUMBER OF REFERENCE DATA PAIRS,N,FOR BOTH SETS'
12      110 INPUT N:MAT A=ZER:MAT B=ZER:PRINTUSING 120,N
13      120 % NOW INPUT '##' PAIRS OF HEIGHT AND CONCENTRATION
14             FOR THE 1ST SET STARTING WITH THE LOWEST HEIGHT
15             FIRST AND ENDING WITH THE HIGHEST
16      130 PRINT'X,Y IN INCHES AND PPM ONE PAIR AT A TIME'
17      150 FOR J=1 TO N:INPUT X(J),Y(J):NEXT J
18      160 PRINTUSING 170,N
19      170 % NOW INPUT '##' PAIRS OF HEIGHT AND CONCENTRATION FOR 2ND SET
20      180 K=0
21      190 FOR J=1 TO N:INPUT X2(J),Y2(J):E=100*(X(J)-X2(J))/X(J):
22          IF ABS(E)>5.0 THEN 191:PRINT'POINTS -',X(J),X2(J),'ARE OKAY':
23          GOTO 210
24      191 IF ABS(X(J)-X2(J))>(0.05*X(N)) THEN 200
25      192 PRINT'POINTS -',X(J),X2(J),'ARE OKAY':GOTO 210
26      200 PRINT'POINTS -',X(J),X2(J),'EXCEED LIMIT':K=K+1
27      210 NEXT J:IF K<1 THEN 220:GOTO 690
28      220 FOR J= 1 TO N:X(J)=0.5*(X(J)+X2(J)):NEXT J
29      230 FOR J=1 TO N:A(1,2)=A(1,2)+X(J)
30      240 A(1,3)=A(1,3)+X(J)EXP2:A(2,3)=A(2,3)+X(J)EXP3
31      250 A(3,3)=A(3,3)+X(J)EXP4:B(1)=B(1)+Y(J):B(2)=B(2)+Y(J)*X(J)
32      260 B(3)=B(3)+Y(J)*X(J)EXP2:NEXT J:A(1,1)=N+1:A(2,1)=A(1,2)
33      270 A(2,2)=A(1,3):A(3,1)=A(1,3):A(3,2)=A(2,3)
34      280 MAT D=INV(A):MAT C=D*B:PRINT'THE REFERNCE LINE IS:'
35      290 MAT B=C:PRINTUSING 300,B(1),B(2),B(3)
36      300 % CONC. = #.####EXP4+ #.####EXP4 * HGT + #.###EXP4 * HGTEXP2
37      310 K=0
38      320 PRINT'AVG HEIGHT  ACT CONC.  PRED. CONC.  ERROR'
39      330 FOR J=1 TO N:YO=B(1)+B(2)*X(J)+B(3)*X(J)12:E=YO-Y(J):
40      340 FOR J=1 TO N:YO=B(1)+B(2)*X(J)+B(3)*X(J)12:E=YO-Y(J):
            Z=100*E/Y(J):IF ABS(Z)>5 THEN 331
42      331 IF ABS(E)>(0.05*Y(N)) THEN 370
43      340 PRINTUSING 350,X(J),Y(J),YO,E
44      350 % ##.###    ####.#    ####.#    ###.####
45      360 GOTO 400
46      370 PRINTUSING 380,X(J),Y(J),YO,E
47      380 % ##.###    ####.#    ####.#    ##.####    NOTE ERROR
48      390 K=K+1
49      400 NEXT J
50      410 IF K<1 THEN 420:GOTO 710
51      420 PRINT'KEY IN NUMBER OF ION SPECIES AND DILUTION FACTOR'
52      430 PRINT'PRINT ION NUMBER FROM 1 TO 12':INPUT I
53      450 PRINT'PRINT DILUTION FACTOR':INPUT F
```